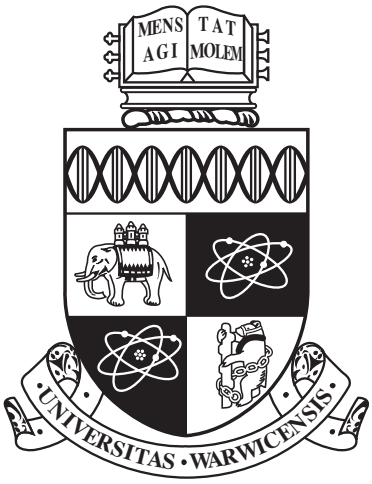

On the Host Galaxies of Superluminous Supernovae

by

Charlotte Rebecca Angus

Thesis

Submitted to the University of Warwick

for the degree of

Doctor of Philosophy

Department of Physics

September 2017

THE UNIVERSITY OF
WARWICK

Contents

List of Figures

Acknowledgments

I am especially grateful to my supervisor, Andrew Levan; whose expertise in the field of extragalactic transients is almost as impressive as his agility in the art of sarcasm. Without his guidance, support and verbal sparring matches, I would most certainly not be the astronomer I am today (whether or not this is a good thing, I leave for the reader to decide). I would also like to thank Elizabeth Stanway for her support and advice over the last three years, and my collaborators Joe Lyman, Nial Tanvir and Andy Fruchter for their comments and scientific input with all the projects I have worked upon.

To the Warwick Astronomy PhD students, who over the last 3 years have become the erratic, dysfunctional family I now know and love - thank you for making my time here so vibrant. Although it should be noted that without most of you, this thesis would have been written a damn sight more quickly.

In particular I give special thanks to; Greg as my transient-comrade-cum-therapist, you've been a constant source of support and bad disco music; Steph, for your ever insightful conversation and balanced outlook on life; Tom, for the caffeine fixes and outrageous chat; George, for getting my obscure pop-culture references; Kirk, for being my harshest baking critic; and finally Mark, for maintaining a true Swanson attitude to all things in life (and keeping the Knope in me subdued).

To my family, Rose and James, thank you for stopping my head from rising too far above the clouds - you've never ceased to remind me that deep down, I'm just a massive nerd. But above all, I am always grateful for Neil, who taught me my first back of the envelope calculation, and never stopped believing that I could accomplish anything. I wish you could have read this.

Declarations

This is a declaration of the extent of the original work within this thesis and of the work published/submitted for publication. This thesis has not been submitted in part or full to any other institution for any other qualification.

The work presented within Chapter 3 is based on a paper accepted for publication by the journal Monthly Notice of the Royal Astronomical Society (MNRAS), entitled "A Hubble Space Telescope Survey of the Host Galaxies of Superluminous Supernovae" (Angus et al., 2016, MNRAS, 458, 84). The Spectral Energy Distribution fitting results presented within Table 3.3 within this chapter, alongside the plots of these fits shown within Figure 3.7 were produced by collaborator Daniel Perley. All other analysis and work presented within the chapter were completed by the author. Comparison samples within this chapter were drawn from literature, primarily from the study of transient host galaxies performed by Svensson et. al 2010 (MNRAS, 405, 57). Any other literature results utilised within this chapter are declared within it. Collaborators for the work presented within this chapter include Andrew Levan, Joseph Lyman, Nial Tanvir, Elizabeth Stanway and Andrew Fruchter.

The computational implementation of the weighted fractional flux technique presented within Chapter 4 was aided by Joseph Lyman. All analysis for the work within this chapter was completed entirely by the author utilising publicly available data. Comparisons are once again drawn from prior literature studies, in particular the results presented within Blanchard et al. 2016 (ApJ, 817,144) and Habergham et al. 2014 (MNRAS, 441, 2230). Any other literature results used for comparison are declared within the chapter. Other collaborators for this chapter were Andrew

Levan and Joseph Lyman.

All work presented within Chapter 5 was performed by the author, with collaboration from Andrew Levan (who produced Figure 5.1).

Abstract

"There was a point to this thesis, but it has temporarily escaped the chronicler's mind"

—Douglas Adams, *So Long, and Thanks for All the Fish*
(adapted by C.R. Angus)

The nature of superluminous supernovae (SLSNe), supernovae whose radiated luminosities are a hundred times greater than normal core collapse supernova events, remains an outstanding question in the transient field. Many models for their production have been postulated, although placing constraints upon these models via the properties of the explosions themselves remains challenging. The potential to unlock their progenitor types may be contained within the properties of their host galaxies. Prior studies have shown SLSNe to preferentially occur within faint, star forming galaxies, highly suggestive of a strong connection between progenitor production and environment conditions. Within this thesis I study the photometric characteristics of a sample of SLSN host galaxies, with a particular focus upon their stellar masses, metallicities and star forming properties.

To do this I utilise high resolution imaging of a sample of SLSN host galaxies obtained with the Wide Field Camera 3 on the Hubble Space Telescope to study the global, and sub-galactic environments of SLSN events. By considering the photometric properties of these host galaxies within the near infrared and at rest-frame UV wavelengths, I am effectively able to probe the stellar mass and star forming properties of these environments. When compared to the host galaxies of other well known core collapse transients, such as long gamma ray bursts and core collapse

supernovae, constraints may be placed upon the likely progenitors of SLSNe relative to other transient progenitors. I show that on a global scale, the host galaxies of SLSNe are fainter, more compact, lower mass and less star forming than other core collapse transient host galaxies, which is highly indicative of low metallicity environments. I also highlight the diversity in environments exhibited between different spectral subclasses of SLSNe, which itself is reflective of the likely different progenitor routes for the two different subclasses of event. When considered on a sub-galactic scale, SLSNe events are associated with star forming regions within their galaxies, although at present it remains unclear whether these events are linked with the strongest regions of star formation (which would imply younger, more massive progenitors).

Finally, I consider the issue of progenitor metallicity threshold estimations, and the consequences of using both global spectroscopic measurements and mass-metallicity relation proxies to determine upper limits to progenitor chemical enrichment. I present a robust model for estimating this, incorporating the key sources of scatter in metallicity estimation which may be applied to a host galaxy populations to determine the presence of a threshold within the progenitor population.

Chapter 1

Introduction

"It is a truth universally acknowledged, that every star in possession of a large mass must undergo a collapse"

—Jane Austen, *Pride and Prejudice*
(adapted by C.R. Angus)

1.1 An Introduction to Massive Stars and Supernovae

It is perhaps somewhat ironic that we are able to glean a large fraction of our knowledge of a star's life in the fleeting moments of it's death. The relative juxtaposition of the stellar lifetime to the duration of it's termination; a few million years to just a few seconds, is so jarring that it seems nigh on impossible that astronomers have been able to study stellar deaths at all.

Although all stars begin life in the same manner, a collapsing cloud of cold interstellar gas, their end points can vary wildly, and it is ultimately the mass of a star which dictates the way in which it will pass through the final stages of it's life. As the internal pressure within the collapsing cloud of cool gas and dust becomes high enough to counteract the gravitational pull of the primordial stellar material completely, the centre of the star becomes hot enough for nuclear reactions to proceed, providing a source of energy to balance the continual leakage of radiation from the surface, creating a main sequence (MS) star [Shu et al., 1987]. Whilst all stars begin by fusing hydrogen to helium within their cores, the manner in which this occurs largely charts its evolutionary course, thus sealing it's fate.

The majority of stars (with masses typically less than $8\,M_{\odot}$which form the vast bulk of stellar material within any given galaxy), will fuse hydrogen (and poten-

tially helium) within their cores. All stars commence their MS life with the fusion of hydrogen into helium. In exceptionally low mass stars (stars of $\lesssim 1\,M_\odot$), fusion occurs solely through the proton-proton (or p-p chain), a short series of nuclear reactions which convert four protons into a single helium nucleus and positron, releasing energy (in the form of gamma rays) during the process [Bethe, 1939]. In slightly heavier stars, higher core pressures and temperatures allow further fusion of the build up of helium contained within the core via the triple alpha process to produce carbon and oxygen [Fynbo et al., 2005], with any remaining hydrogen continuing to fuse in a shell surrounding the core.

Within these lower mass stars the temperatures generated within the core never become hot enough to instigate the fusion of any of this new carbon or oxygen rich material. Thus these stars are no longer capable of generating energy within their cores, and with their final breaths, they will blow away their stellar envelopes in strong winds, surrounding the slowing cooling carbon-oxgyen core, a white dwarf (WD) with a nebula of recycled stellar material.

However, it is within stars more massive ($>8\,M_\odot$) than this that we concern ourselves here, for within these stars that we observe some of the most extreme physics within the Universe, which leads to some of the most dramatic stellar explosions at the moment of their termination.

1.1.1 Massive Stars

Massive stars are relatively rare. The fragmentation process when cool dust and gas collapses during star formation naturally results in a power law distribution of stellar masses within the newly formed cluster. The number of stars at the beginning of their main sequence lifetime contained within a given mass range, $\xi(M_*)dm$, takes the form of a power law distribution [Salpeter, 1955]. The relative fraction of the total stellar mass contained within stars of a given mass in the cluster is given by;

$$\xi(M_*) \propto \left(\frac{M_*}{M_\odot}\right)^{-\alpha} \tag{1.1}$$

More commonly known as the Initial Mass Function (IMF), the slope of this function (α) changes depending upon the mass range under consideration. For stars entering the main sequence in the mass range $M \geq 0.5\,M_\odot$, α is typically 2.3 [Kroupa, 2001], which as a result makes the fraction of the total cluster mass locked away within more massive stars very small, and thereby making very massive stars scarce.

In order to simply balance the self-gravitational pull of a massive star's bulk, the rate at which nuclear burning occurs within the core must increase dramatically from that which would normally occur in a lower mass star. As such, the main sequence life time of a star ($\tau_{\rm MS}$) scales broadly with mass ($\rm M_\star$) as $\tau_{MS} \approx M_\star^{-2}$ [Prialnik, 2000]. Thus the lifetimes of the most massive stars within the universe are brief (relatively speaking), blinking out of existence within a few million years.

Within stars $\gtrsim$1.3 $\rm M_\odot$[Schuler et al., 2009], hydrogen fusion begins to proceed not through the p-p chain, but through the carbon, nitrogen and oxygen (CNO) cycle, a series of reactions in which the nuclei of these elements act as catalysts to synthesise the fusion of hydrogen into helium. This fusion cycle becomes dominant at core temperatures $\gtrsim 1.7\times10^7$K [Schuler et al., 2009], and it's rate increases catastrophically with incremental increase in temperature, with an approximate dependence $\propto \rm T^{17}$ (notably stronger than the temperature dependence of the p-p chain, which is $\propto \rm T^4$). Consequently, massive stars begin to burn through their limited fuel supply at an expedited rate, with each subsequent increase in core temperature triggering more fusion reactions. Due to the steep temperature gradient this level of nuclear fusion invokes within the core, stars of $\sim$2-2.5 $\rm M_\odot$ are able to drive convection throughout the bulk of their cores, whilst maintaining a radiative outer envelope.

With rising temperature comes the ability to fuse heavier nuclei within the stellar core, however it is only within stellar cores at temperatures $> 5\times10^8$ K (corresponding to an initial stellar mass of 8 $\rm M_\odot$ and a carbon-oxgen core mass of 1.06 $\rm M_\odot$) that carbon fusion can be non-degenerately ignited. These stars begin to quickly burn through carbon, then neon, oxygen and finally silicon with increasing brevity. Each successive fusion stage leaves a series of lighter elements fusing in shells around the increasingly hotter core, producing an onion like stratification of fusion products within the stellar interior, increasing in nuclear mass towards the centre.

However silicon fusion, the final stage of stellar fusion, produces a particular isotope of iron, ^{56}Fe. This isotope has the highest binding energy per nucleon of all the elements within the periodic table (i.e. the nucleons within the nucleus are tightly bound), and thus any heavier elements will have lower binding energies. Thus the fusion of ^{56}Fe into heavier elements is very energetically unfavourable, as more energy will not be released through addition of extra nucleons, and thus the core becomes inert, simply growing in ^{56}Fe mass as more silicon fuses around it. We shall consider the consequences of a growing inactive core within the following section.

Evolutionary Effects in Massive Stars

Hot, luminous stars OB-type MS stars (zero age main sequence masses (ZAMS) of $M > 15\,M_\odot$) are subject to strong, radiation driven winds that gradually erode their outer layers, occasionally stripping the star of it's outer envelope all together. These winds are caused by strong interactions between photons and matter at frequencies corresponding to absorption lines in the stellar spectrum. As a consequence they are dependent upon the metallicity (Z) of the star (with an approximate theoretical dependence of $\dot{M} \propto Z^{0.7}$, Vink et al. [2001]). Within very massive stars ($M > 25\,M_\odot$) the hydrogen envelope is lost altogether to stellar winds at solar metallicity. As we extend to more extreme stellar masses, this mass loss begins to expose deeper and deeper layers within the star towards the core.

The affects of rotation in massive stars must also be taken into consideration. There is much observational and theoretical evidence that rotation crucially affects stellar structure and stellar evolution, as high spin rates may result in currents of stellar material moving from core to surface and back again. This creates mixing of material together from these regions and thus influences the rate of fusion within the core and surrounding layers [Heger et al., 2000]. Stellar rotation may also strongly influence mass loss within stars, as it may induce anisotropic mass loss at the poles and equator due to differences in effective gravity, temperature, and opacity. The influence of rotation at the end of the stellar lifetime is also important as the effects of angular momentum on the core at the point of collapse strongly influence the type of transient we observe.

1.1.2 The Physics of Core Collapse

Although the details of core collapse explosions remain an area of active research, the generally accepted model is described below.

Once the inert iron core has achieved a mass greater than $1.44\,M_\odot$ of ^{56}Fe , with no source of energy to maintain the pressure within the core, the careful balance between the outward gas pressure to the inward gravitational pull which has thus far kept the star in hydrostatic equilibrium becomes upset.

The core begins to collapse under its own weight, compressing the iron contained within it. As it does, the density increases to $\gtrsim 10^9$ g cm^{-3} [Janka et al., 2012], and the free electrons within the core become degenerate. However, unlike the inert cores of smaller stars, the electron degeneracy pressure which results from this is insufficient to support the core from continued collapse, and it continues to contract. As pressures continue to increase, some of the free electrons begin to be

captured by the heavy nuclei, which removes further support and accelerates the collapse [Janka et al., 2012].

Once the core reaches temperatures of $\sim 10^{10}$ K, conditions become sufficient for photodistintigration (the breaking up of heavier nuclei by energetic photons) to commence:

$$\begin{aligned} {}^{56}Fe + \gamma &\leftrightarrow 13\,{}^{4}He + 4n \\ {}^{4}He + \gamma &\leftrightarrow 2p^{+} + 2n \end{aligned} \tag{1.2}$$

It takes only a matter of seconds to unravel the evolutionary work of several million years. This process requires a relatively large amount of energy ($\sim$2 and 6 MeV per nucleon for ^{56}Fe and ^{4}He disintegration respectively). This energy is drawn from internal energy of the gas within the core, triggering a dramatic decrease in pressure and ultimately leaving the core in free-fall collapse.

With rapidly increasing pressure, soon electron capture once again recommences, as the soup of atomic particles is compressed further, forcing electrons to be captured by protons to form neutrons, releasing a torrent of neutrinos and removing yet more energy from the core.

$$p^{+} + e^{-} \longrightarrow n + \nu_e \tag{1.3}$$

The result of this exhaustive energy stripping is a core of highly neutron-rich matter, a proto-neturon star. What happens next once again relies upon the mass of the star in question; for stars with ZAMS masses in the range 25 to 40 $\mathrm{M}_{\odot}$, the neutron degeneracy pressure halts further collapse at pressures of $\sim 10^{18}$ kg m^{-3} [Stevenson, 2014]. Thus the core remains an incredibly dense ball of neutron rich material, merely a few kilometres in radius.

However for stars with a ZAMS mass[1] of $\gtrsim 40\,\mathrm{M}_{\odot}$, not even neutron degeneracy can save the neutron rich core from being pulled further in by it's own gravitational mass. Collapse continues to the point at which a gravitational singularity is achieved. This singularity, a black hole, contains the entire mass of the core, with a resulting gravitational field strong enough to prevent even light escaping it.

Whilst the core undergoes this rapid change in state, the outer layers of the star, suddenly lacking the support of the core, also fall inwards, their velocity increasing linearly with radius, eventually reaching supersonic speeds in the outermost layers. However as the inner, more slowly falling layers reach the now neutron rich

[1]The reader should note that these approximate ZAMS masses are for stellar evolution at approximately solar metallicity. Given the theoretical dependance of mass loss on metallicity, higher ZAMS masses would be required for a more metal enriched star (or vice versa for a metal poorer one) for the core to reach the required physical conditions.

inner core the increase in local pressure, combined with the Fermi nucleon-nucleon repulsion at short distances, make the innermost core incompressible, thus causing the inward falling material to rebound. It is this rebounding material which produces the observable explosion we know as a supernova (SN).

A flood of neutrinos are released during recombination, which effectively remove ∼99% of the remaining energy away from the core. However some of the energy removed by the shock wave is absorbed by another shock wave generated from the rebounding stellar material (around 10^{44} J). It is this intake of energy that prevents the outward moving shockwave from completely stalling due to loses in energy through dissociation of heavier elements closer to the core [Bethe and Wilson, 1985]. This shockwave transverses outward; sweeping up, compressing and heating material from the collapsing outer layers as it does. This generates violent nuclear reactions as neutrons and other atomic fragments punch through the surrounding layers, producing large amounts of radioactive ^{56}Fe , ^{56}Co and ^{56}Ni , whose subsequent radiative decay will drive the late time light curve of the explosion.

The first observable light from the supernova is a result of shock break out, which occurs when the optical depth of the shock wave exceeds that of the local material [Waxman and Katz, 2016]. At this point radiation from the SN becomes visible in a flash of hard UV or soft X-ray radiation, typically as the shockwave escapes the outermost layers of the stellar envelope at speeds of several 10^3 km s^{-1}, usually only minutes after the initial collapse (depending upon the extent of the envelope of the progenitor). Due to the prompt nature of this early emission, shock breakout has only recently been observed within the UV [Schawinski et al., 2008], X-ray [Li, 2007] and optical within Kepler observations [Garnavich et al., 2016].

The SN shock wave continues to move outwards, interacting with any interstellar material within it's path, whilst lagging behind it is a trail of expanding stellar debris. This shock-heated debris brightens as the surface area of the SN photosphere expands, increasing the luminosity of the observed SN, until the effects of cooling begin to offset those of expansion, causing the luminosity of the transient to fall at approximately 0.0098 mag day^{-1} [Woosley, 1988]. This reveals progressively deeper layers of the ejecta as the photosphere of the SN retreats, unveiling much of the inner architecture of the star.

1.1.3 Observational Classes of Supernovae

Although many of the physical principles outlined within the previous section are applicable across many (but not all) cases of stellar core collapse, the resulting SN explosions observed are exceptionally heterogeneous, and their properties are very

much tuned to the properties of the progenitor star. However, similar progenitor systems may be found through the grouping of observable SN characteristics. This is primarily conducted through through spectroscopic classification, although as we shall see, additional luminosity classes have become increasingly important in SN typing.

Spectroscopic Classes

The subdivision of SN is first performed based upon the presence of hydrogen within their spectra. Those without hydrogen are first classified as 'Type I' SNe, whilst those that show evidence of hydrogen emission lines are grouped as 'Type II' SNe [Minkowski, 1941].

Type I SNe can be further sub grouped based upon the presence (or lack of) additional lines within their spectra. Those which display strong silicon absorption lines, alongside those of iron group elements are classified as Type Ia SNe [Leibundgut, 2000]. SN-Ia are not actually associated with the collapse of massive stars, but originate from the remnants of much lower mass progenitors. They are the resulting thermonuclear detonation of a carbon-oxygen white dwarf which has exceeded the Chandrasekhar mass, above which electron degeneracy pressure can no longer support a white dwarf against gravitational collapse (recently confirmed through observations of the progenitor size, Nugent et al. 2011; Bloom et al. 2012). One consequence of this well defined upper mass limit is a strong (although not absolute) homogeneity in SN-Ia light curves (as each event involves the detonations of the same amount of carbon and oxygen), which when combined with their bright luminosities (typically peaking at $M_V \approx$ -19 to -20), make them excellent cosmological distance measures [Riess et al., 1998].

Other Type-I SN that exhibit broad helium absorption (but show no evidence of silicon absorption) are classified as Type Ib SNe, whilst those which do not display either of these absorption features are determined to be Type Ic SNe. These latter two spectral classes are thought to be associated with the deaths of exceptionally massive stars, as the lack of hydrogen within their spectra suggest more evolved, stripped progenitor stars which have likely lost their outer envelopes to strong stellar winds (such as those outlined within Section 1.1.1, Maeder 1981; Groh et al. 2013), although there are arguments for lower mass binary progenitor to produced an envelope stripped progenitor [Podsiadlowski et al., 1992; Wellstein and Langer, 1999; Eldridge et al., 2008; Yoon et al., 2010]. Lacking a direct progenitor detection, the true progenitor systems of SN-Ib/c events remain ambiguous.

For Type II SN events which do display hydrogen within their spectra, their

progenitor systems are thought to originate from stars with ZAMS masses distinctly less massive than those of Type Ib/c SNe (although at the point of collapse, they may be more massive, as these stars have retained their hydrogen envelopes). Although there are many finer ways of splitting this particular group of SNe, broadly speaking, they can be subclassed into either 'Plateau' (SN-IIP) or 'Linear' (SN-IIL) events, based upon the shape of the late time light curve. This division; whether the SN-II display a distinct plateau within their fading light or not, is the result of recombination of free electrons with hydrogen ions within the ejecta, forcing the photosphere to maintain nearly constant luminosity until the ejecta once again becomes optically thick, allowing light curve decay to continue [Stevenson, 2014]. This phase is prolonged in SN-IIP, which is thought to arise due to the extended hydrogen envelope of the progenitor star (likely a red or blue supergiant star). SN-IIL are thought to have distinctly smaller hydrogen envelopes, for which the level of recombination is not sufficient to prolong the decay of the SN light significantly.

Additional breakdown of these sub groups can be found by further splitting them based upon the width of the absorption lines; those with broad lines ('BL') and those with narrow lines ('n'). In general, SNe with narrow lines within their spectra are indicative of flash ionisation of a low density shell of gas surrounding the progenitor star by the SN shockwave, whilst broad spectral lines are a result of fast moving ejecta travelling in opposing directions.

Although, there are many additional subclasses of SNe (for instance SN-IIa; these are SN-Ia events which appear to show hydrogen absorption lines at late times), with an ever growing number of subclasses as wide field, high cadence transient surveys begin to increase the number of SN events available for follow up, they are beyond the scope of this thesis, and therefore need not be detailed here.

Luminosity Classes

The form of any given SN light curve is determined by two factors; the height (and width) of peak of the light curve achieved after the initial shock break out to the point at which the SN ejecta becomes opaque, and the rate of the light curve decline, as the bulk of the exploded star expands and the effective temperature of the photosphere begins to drop. The latter is a product of the density profile and opacity of the ejected material (which itself ultimately boils down to the progenitor mass, radius and explosion energy, Nakar and Sari [2010]).

The shock heating which occurs during core collapse fuses many intermediate mass elements (mostly silicon, sulphur, neon and magnesium) into radioactive ^{56}Ni . This isotope is particularly unstable, with a half life of 6.1 days [Nadyozhin, 1994].

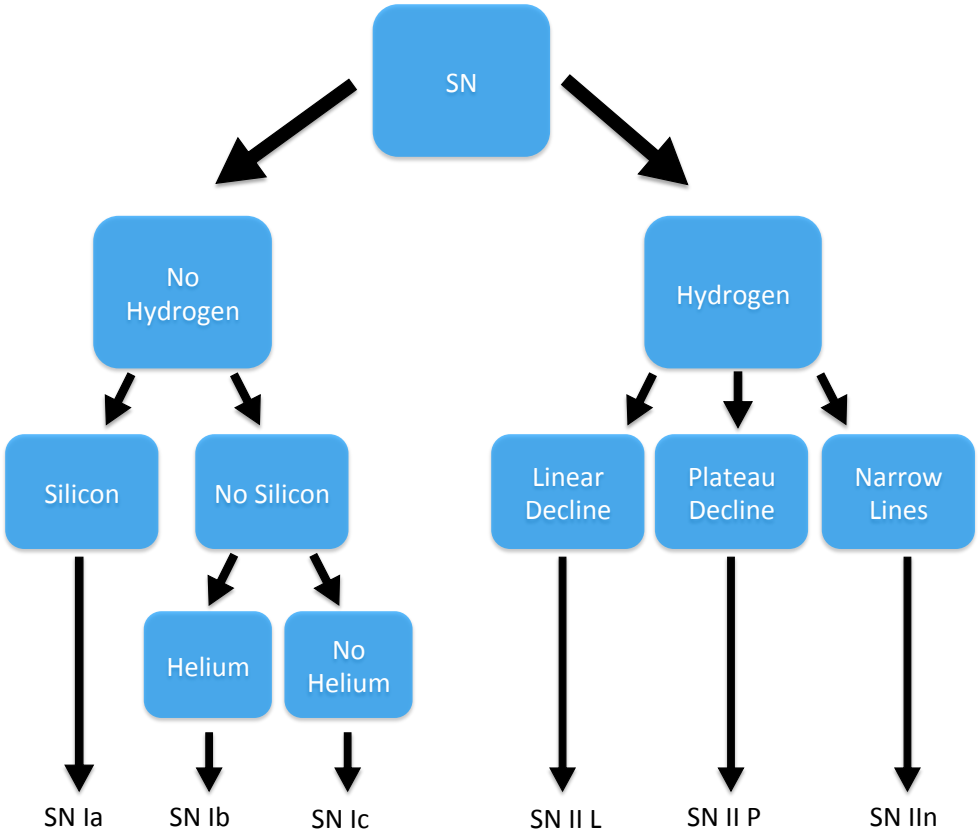

Figure 1.1: Simplified Classification of SN events based upon the presence or absence of key observed spectroscopic and photometric properties. Much diversity exits within each of these broad subclasses, with many further subclassifications likely arise as a result of wide field, all sky surveys.

The radioactive decay sequence of ^{56}Ni and the products of it's decay ultimately drives the light curve of the SN event, as the resulting gamma-rays from these decays become trapped within the expanding SN ejecta, re-heating it.

$$\begin{aligned} {}^{56}_{28}Ni &\longrightarrow {}^{56}_{27}Co + e^{+} + \nu_e + \gamma \qquad (\tau_{\frac{1}{2}} = 6.1 \text{ days}) \\ {}^{56}_{27}Co &\longrightarrow {}^{56}_{26}Fe + e^{+} + \nu_e + \gamma \quad (\tau_{\frac{1}{2}} = 77.12 \text{ days}) \end{aligned} \tag{1.4}$$

Simple light curve modelling has shown that the amplitude of the peak of the light curve is proportional to the amount of ^{56}Ni synthesised during the explosion [e.g. Arnett, 1982]. Thus for SN-Ia, in which a good proportion ($\sim$50%, 0.7 $M_{\odot}$) of the Chandrasekhar white dwarf mass is synthesised into ^{56}Ni during the explosion, are typically brighter ($M_B <$ -19 at peak) than other SNe which arise from the core collapse of a more massive progenitors.

Within core collapse events, the amount of ^{56}Ni formed during the explosion can be significantly smaller, with Type II-P SNe typically producing only 0.07 $M_{\odot}$of ^{56}Ni , whilst SN-Ib/c produce a $\sim$ few tenths of a solar mass during their explosions. Given the heterogenous nature of normal core collapse SNe progenitors, there is naturally some stratification of the peak luminosities of Type Ib/c and Type II SNe events, with Type II events typically peaking at around $M_B \approx$-17 – -19 and SN-Ib/c events peaking at a considerable $M_B \approx$ -18 [Richardson et al., 2002], although they still fall significantly fainter than SN-Ia events.

However, as mentioned previously, during the past decade, time resolved, wide field, transient surveys such as the Panoramic Survey Telescope And Rapid Response System (Pan-STARRS, Kaiser and Pan-STARRS Team 2005), the Palmomar Transient Factory (PTF, Law et al. 2009), the Catalina Real Time Survey (CRTS, Drake et al. 2009b) and the Dark Energy Survey (DES, The Dark Energy Survey Collaboration 2005), have revealed the extent of diversity amongst cosmic explosions showing that the optical transient sky exhibits a much broader range of events in both luminosity and duration than spanned by classical supernovae. These discoveries have largely been possible thanks to the unprecedented combination of depth, areal coverage and cadence of observations that are provided by such surveys, enabling order of magnitude increases in the number of transients recorded. This is combined with increasingly effective and sophisticated follow-up, that has allowed rare, hitherto unrecognised, populations of events to be uncovered, and sufficient numbers of events to be located to identify new populations, rather than just extreme outliers.

In particular, such surveys have unveiled a population of highly luminous,

but extremely rare SN, peaking at magnitudes of around or brighter than $M_V \sim$ -21, a factor of ∼100 times brighter than the majority of core collapse supernovae (e.g. SN-II's), and 10 times brighter at peak than SNe Ia. The achievement of such high luminosities during stellar collapse is likely a result of peculiar and poorly understood explosion mechanisms, through which we may shed light upon the exotic stars from which they originate. These have been named Superluminous Supernovae (SLSNe), and their extreme luminosities have made astronomers pause for thought, as they begin to question their current understanding of stellar core collapse. It is with these highly unusual transients that the work within this thesis is concerned.

1.2 Observational Properties of SLSNe

Although these exceptionally luminous events have been observed since at least the mid-1990's [Knop et al., 1999], it is only in the past few years that sufficient numbers of SLSN events with detailed follow-up have become available, enabling them to be identified as a new population of events [Quimby et al., 2011b]. SLSNe are characterised by absolute magnitudes[2] at maximum light of $M_V <$ -21 [Gal-Yam, 2012], although within recent years this limit has been relaxed somewhat by the transient community to include events generally $M_V <$ -20. For the purpose of work conducted within this thesis, when considering any individual event, I shall refer to those which do not strictly adhere to the $M_V <$ -21 limit as "luminous supernovae" (LSN) events, although currently there appears to be no strong distinction between the two subsets, other than their slightly different peak amplitudes.

Overall, SLSNe are exceptionally blue events, with the majority of their rest frame flux being emitted at near ultraviolet or very blue optical wavelengths. Their optical light remains visible for extensive periods of time, remaining optically detectable for 100's of days (see Figure 1.2). Observationally, this makes them appealing as cosmological probes, as their UV continuum emission can be detected at high redshifts in the near-infrared and optical (for instance, SN 2213-1745 and SN 1000+0216 identified at redshifts of 2.05 and 3.90, are the most distant supernovae ever located Cooke et al. 2012). Attempts have been made to standardise samples of SLSN events [Inserra and Smartt, 2014, for instance],although small sample

[2]It should be noted that this limit is somewhat arbitrary, derived from the work of Richardson et al. [2002], in which the absolute magnitudes of all SNe observed prior to 2002 were considered, and a "SN ridge line" was derived at M_B = -19.5 mag, corresponding to a flux of 1.2×10^{43} erg s^{-1} (the typical peak luminosity of a SN-Ia event). Events brighter than this ridge line were defined as "over luminous". For the review conducted by Gal-Yam [2012], it was useful to define a "lower-brightness limit" of $M_V <$ -21(applicable in any optical band) for SLSN events, in an attempt to avoid the inclusion of false events due to poorly constrained cosmological distances.

sizes currently hamper these efforts. Many have made predictions on the ability to constrain current cosmological parameters using SLSNe once large sample sizes are acquired [e.g. Wei et al., 2015; Scovacricchi et al., 2016]. Moreover, the detectability of SLSNe to high redshift also enables the star forming environments to be probed out to greater cosmological distances, whilst their high luminosities can be used to study the chemical enrichment of the host galaxy's interstellar medium (ISM) and the local intergalactic medium (IGM). Such extreme luminosities do initially hint at progenitors of very high ZAMS mass (many 100's of $M_{\odot}$), which in turn hints at the prospect of a group of Population-III like analog stars. However, like most CCSNe, SLSN events exhibit a large amount of internal diversity within their light curve and spectral properties, which makes understanding their progenitors non trivial.

SLSN events are intrinsically rare, with estimated volume-weighted rates of 91 SN Yr^{-1} Gpc^{-3} at a redshift of $z \approx 1$, approximately 0.0002% of the core collapse SN rate at the same redshift [Prajs et al., 2016]. Despite the currently modest collection of known events, there does appear to be several subgroups of SLSN event, based on their spectral properties and light curve evolution. Within the following sections I shall outline the various properties of these different classes of SLSNe.

1.2.1 Spectroscopic Classification

Like traditional SN events, SLSNe may also be classified according to their spectroscopic properties. However as we shall see, further distinction between the different subclasses can be found in the luminosity of SNe and the evolution of their light curves. Such differences may be indicative of different progenitor paths, as will be discussed within Section 1.3. Like normal SNe, all SLSNe can be broadly grouped into one of two spectroscopic classes; hydrogen-poor events or hydrogen-rich events (Type I and Type II respectively), although within each group there is additional diversity arising from duration of the transient, late time evolution of the lightcurve and presence/absence of narrow lines. A simplified classification tree of SLSNe is given within Figure 1.3.

Type I SLSNe

Type I SLSNe are perhaps the most well studied events, largely due to the challenges inherent to describing them physically, but also due to their more frequent discovery. Typically, close to maximum light their continua are bluer than hydrogen-rich SLSNe, peaking typically brighter than these events too (frequently observed

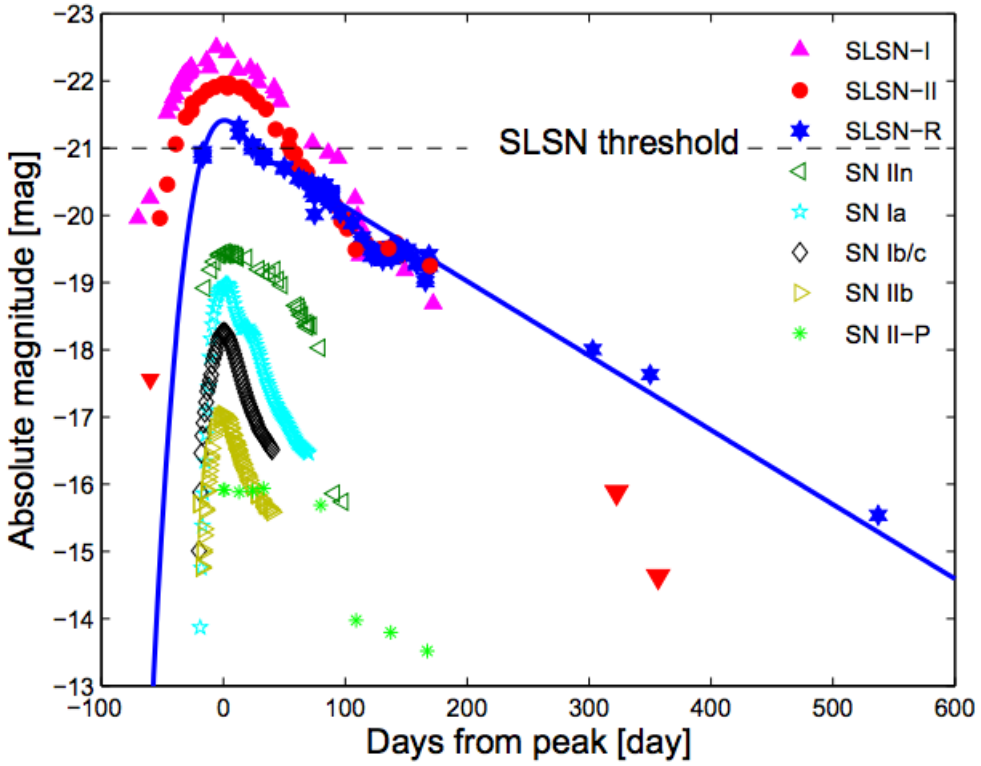

Figure 1.2: From Gal-Yam [2012], demonstrating the extreme luminosity of SLSN events when compared to normal core collapse SN (SN-Ib/c, SN-II) and thermonuclear (SN-Ia) events. Even the faintest SLSNe are ∼10 times brighter than Type Ia SNe

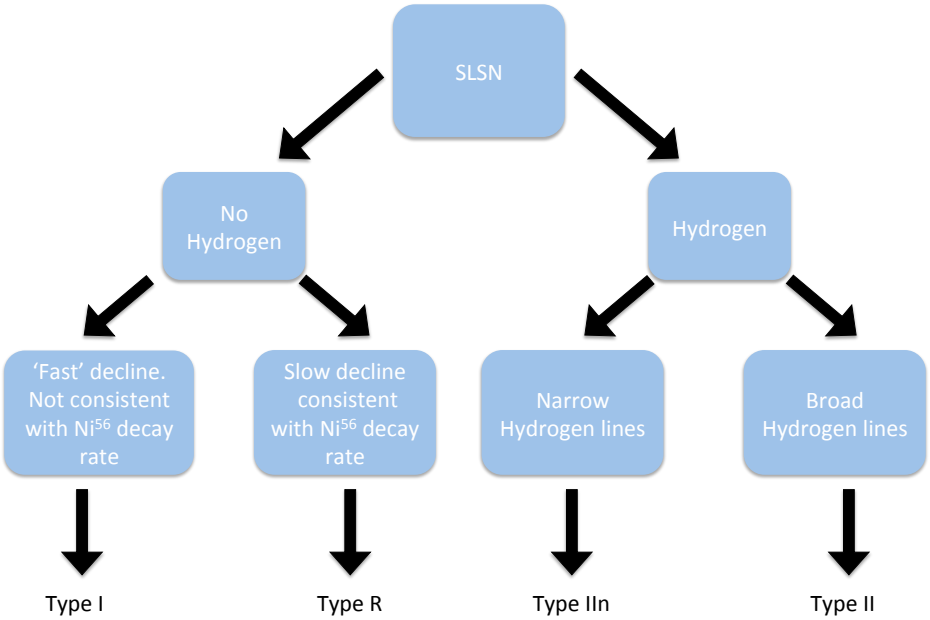

Figure 1.3: A classification tree of SLSN, based on their spectral behaviour and the evolution of their late time lightcurves. Initially classified like normal SNe by the presence of hydrogen within their spectra, additional subtypes are identified either through their behaviour at late times (e.g. Type R SLSNe) or through the width of hydrogen lines within their spectral (Type II and Type IIn SLSNe). It should be noted that examples of individual SLSNe developing spectral signatures of hydrogen at late times exist [both quickly and slowly evolving, see for instance Yan et al., 2017]. At present such SLSN are treated as Type II SLSN where the hydrogen shell is at extremely large radii, thus pushing the presence of narrow H lines to late times.

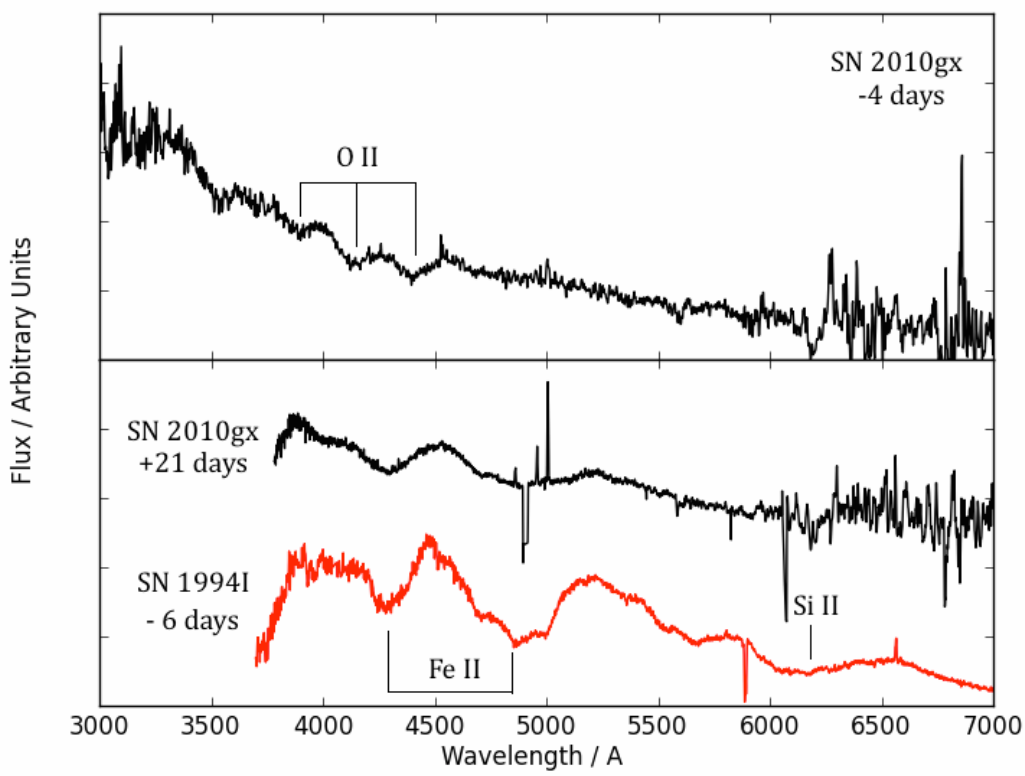

Figure 1.4: Spectra of Type I SLSN, SN 2010gx, observed at two different epochs (pre- and post-peak, spectra acquired from Pastorello et al. 2010). At 4 days before maximum light (upper panel), the spectrum is exceptionally blue but fairly featureless, marked only with the prominent 'W' shape from ionised oxygen. However, at later times (bottom panel) the spectrum has evolved significantly, now showing stronger SiII, FeII lines more typical of a SN-Ic event near peak. To demonstrate this, a SN-Ic event, SN 1994I, is shown for comparison (spectrum acquired from Modjaz et al. 2014).

at $M <$ -22 mag). During early epochs their spectra exhibit clear O II absorption features between rest-frame wavelengths of 4000-4500Å, which forms a distinct "W" feature, [Quimby et al., 2011b], with some events displaying additional SiIII, CII and MgII lines (see Figure 1.4). These features which persist for several weeks after the explosion are indicative of high photospheric temperatures and ejecta densities.

However at later times (typically ∼20 days after maximum light), the expanding and cooling ejecta causes their spectra evolve, developing broad CaII, MgII, FeII and SiII P-Cygni absorption profiles, which are characteristic of early SN Ic spectra [Pastorello et al., 2010] (although these SLSNe are evolving on a much longer timescale than normal SN-Ic events), which has lead to some SLSNe being labelled as SLSNe-Ic within the literature.

Of all of the known SLSN events, SLSNe-I evolve relatively quickly, with faster rise times to peak light (typically below 50 days)[3]. Following maximum light, their light curves decline at a rate substantially faster than radioactive cobalt decay (> 0.03 mag day^{-1}), making straightforward ^{56}Ni powered explosions difficult to reconcile [e.g. Pastorello et al., 2010; Quimby et al., 2011b; Chomiuk et al., 2011]. Combined with their spectral properties, this suggests that SLSN-I events require the deposition of significant amounts internal energy at large radii from the progenitor ($\sim 10^{15}$ cm, around ten times the radius of the largest known red supergiants), with hydrogen poor material expanding outwards at high velocities of 10^4 km s^{-1} [Pastorello et al., 2010; Quimby et al., 2011b].

Recent work has begun to highlight an additional feature within SLSN-I light curves; double bumps. Early photometry obtained $\sim$30 days prior to the peak of the SN has shown that some SLSNe possess quickly evolving initial peaks prior to the main peak of the SN light curve. First detected within the optical light curve of SN2006oz [Leloudas et al., 2012] and later within the light curves of LSQ14bdq [Nicholl and Smartt, 2016] and DES14X3taz [Smith et al., 2016], these early 'bumps' in the light curve last a few days in the rest frame and are typically $\sim$2 magnitudes fainter than the main peak of the SN in the same band. Their existence in hydrogen poor SLSNe which evolve both quickly and slowly (see the following section) is interesting, as it potentially indicates some underlying similarity in their explosion mechanism or progenitor systems. However, at present it is currently unclear if these bumps are ubiquitous to all hydrogen poor SLSNe. Many SLSN events are either too high redshift, or lack the high cadence survey coverage to detect any precursor peaks. To date, within the literature only 15 SLSN events have well-measured pre-explosion photometry [Nicholl et al., 2016; Smith et al., 2016], although of these SLSNe at least 30% do exhibit double peaks within their light curves [Smith et al., 2016]. With an ever expanding sample as new SLSNe are detected within ongoing high cadence surveys, time will tell whether the existence of double-peaked SLSN light curves is the norm, or if these events are actually representative of yet another sub-group of unusual SN events.

Type R SLSNe

This tentative subclass of hydrogen poor SLSN-I events, appear to have much longer decay timescales than those observed within other hydrogen poor events, with late

[3]Although it should be remembered that this is still considerably slower than most normal core collapse SNe events, which typically take 10-20 days [Taddia et al., 2015; González-Gaitán et al., 2015]

time light curves declining at a rate consistent with the radioactive decay rate of ^{56}Ni $\rightarrow$Co$^{56}\rightarrow$Fe^{56}, a fading of 0.0098 mag day^{-1} (earning this subgroup the 'R' suffix in their name). This radioactive decay releases energy more slowly via γ-ray and positron emission, which becomes thermalised and converted to optical radiation by the ejecta as it expands [Gal-Yam, 2012].

The rise to peak of SLSN-R events is much slower than normal SLSNe-I, usually >50 days. Their spectra are very blue, and remain so with significant flux shortwards of 3500Å. They also display prominent, broad CaII, MgII and FeII absorption lines at peak which form in an ejecta expanding at several 10^3 km s^{-1} [Gal-Yam et al., 2009].

Officially identified as a separate class of SLSN event within Gal-Yam [2012], the sample size of SLSNe-R remains small, with only a handful of candidate events. SLSN-R events are rare, even amongst SLSNe; with rates are estimated to be approximately one fifth of the rate of SLSN-I events [Gal-Yam, 2012] (the SLSNe-I rate is $\sim 10^{-17}$ SN Yr $^{-1}$ Gpc^{-3} at z$\sim$ 0.2; Quimby et al. [2011b]). Candidate events appear as early as 1999, with the detection of SN 1999as [Knop et al., 1999], although late time coverage of this object was somewhat lacking. Analysis of the spectra [Hatano et al., 2001] shows spectral properties (^{56}Ni mass, ejected masses and kinetic energy) which are similar to those of SN 2007bi, the first firm detection of a SLSN-R [Gal-Yam et al., 2009], with an estimated 5 $M_\odot$ of ^{56}Ni released during the explosion which would drive the late time light curve for >500 days.

The similarity to Co^{56} driven decay timescales has lead to the assumption that these particular events are driven only by the radioactive decay of ^{56}Ni produced by the explosion. In this case the peak of the light curve implies the synthesis of exceptional amounts of ^{56}Ni , typically of order $\sim$few solar masses per event. This immediately places restrictions upon the mass of the initial progenitor system and thus the way in which the star explodes (although there is much dispute over this matter, with suggestions that ^{56}Ni heating alone cannot produce the exceptionally blue spectra of SLSN-R events [Dessart et al., 2012], as shall be discussed further within Section 1.3).

Type II SLSNe

SLSN-II events show strong hydrogen emission features within their spectra, which implies that these SLSNe have retained some form of hydrogen rich envelope prior to the explosion. In many ways SLSNe-II are somewhat of an enigma, as whilst the retention of a hydrogen envelope makes them easier to pin down in relation to normal SN for which we have a better understanding, the study of these events

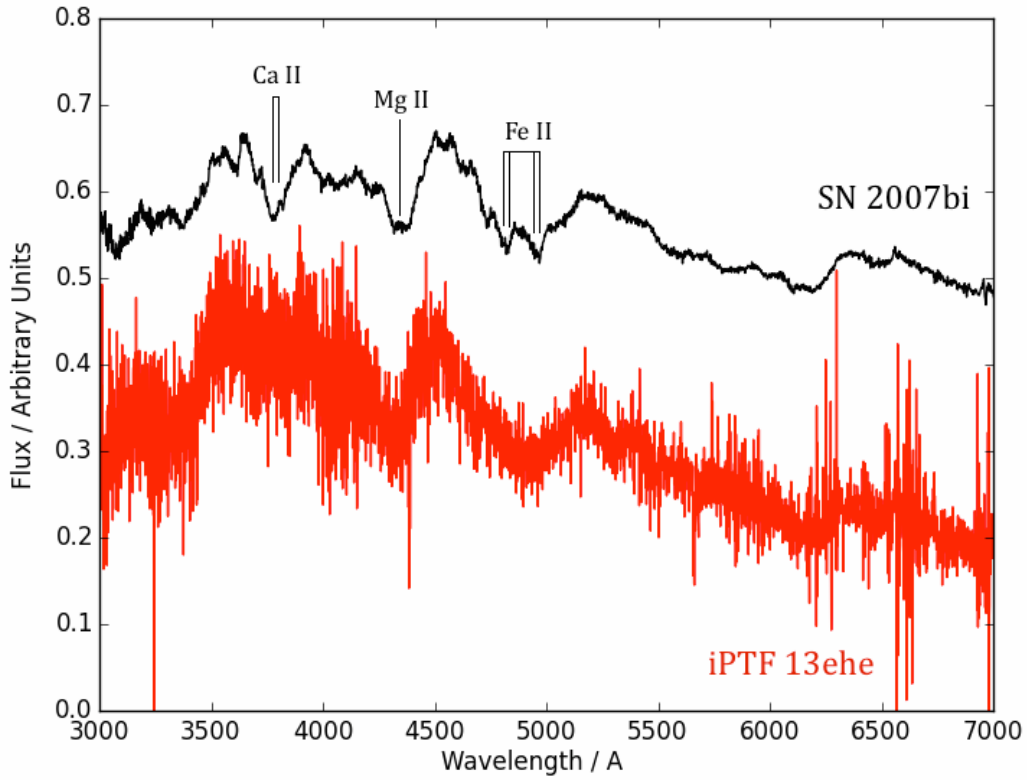

Figure 1.5: Spectra of the prototype Type R SLSN, SN 2007bi [spectrum sourced from Gal-Yam et al., 2009] alongside that of the relatively recent event iPTF13ehe [spectrum obtained from Yan et al., 2015]. The broad metal absorption lines are highlighted, which form within the quickly moving ejecta.

becomes complicated by the presence of this hydrogen due to the reprocessing of radiation by the envelope of material, losing much of the information from photons emitted from the core [Chugai et al., 2004].

Observationally the properties of SLSNe-II are particularly diverse, spanning the broadest range in peak brightness, from $M = -22.3$ (SN 2008fz, [Drake et al., 2010]) down to little brighter than $M \sim$ -20 [Gal-Yam, 2012]. Their light curve shapes vary more than other SLSN events, ranging from the rapidly rising PS15br (20 days to peak, Inserra et al. 2016), to a much steadier brightening such as that of SN 2006gy ($\sim$ 70 days, Ofek et al. [2007]; Smith et al. [2007]), with a variety of combinations of both rapidly rising and slowly declining events (e.g. SN 2008am, [Chatzopoulos et al., 2011]). .

Spectroscopically, SLSNe-II can further subdivided into two classes. The vast majority of SLSNe-II display narrow hydrogen Balmer lines, which arise from the shock photoionisation of dense hydrogen rich material as the shockwave from the explosion interacts with it, which subsequently recombines (making these events technically SLSNe-IIn). This hydrogen rich material is thought to have been thrown off from the progenitor during a prior evolutionary phase (the method in which this occurs will be discussed later).

However, a small sample of SLSNe-II have been observed with broader hydrogen emission during the photospheric phase of the SN (e.g. SN 2008es, SN 2013hx and PS15br [Inserra et al., 2016]), which lack the narrow features commonly associated with interacting SNe. The absence of these narrow lines suggests that these progenitor stars do not expel material from their outer layers for prolonged periods prior to exploding, with only intermittent mass loss [Miller et al., 2009]. The spectra and photometric evolution of these particular SLSNe-II is similar to "normal" bright SNe-II (or SNe-IIL), although at much higher luminosity and with more gradual evolution.

For the sake of completeness it should also be noted that some hydrogen-poor SLSN events have been observed with hydrogen lines present within their late-time spectra (for instance, iPTF13ehe, Yan et al. [2015]). Such events have been interpreted as the interaction of the SN ejecta with circumstellar hydrogen set at larger radii from the progenitor than those inferred for normal SLSN-II events (see Section 1.3.2 for further details).

1.2.2 Motivation for Study

The sheer luminosity of SLSN events suggests that their origins may lie within massive stars, with some having the potential to arise from some of the most massive

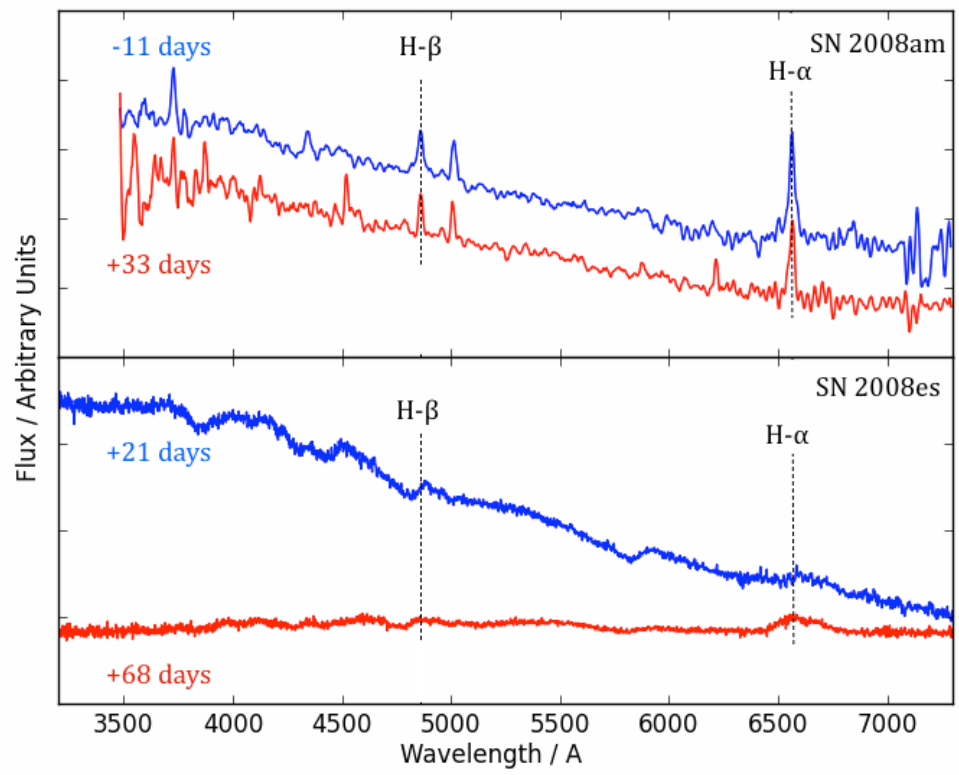

Figure 1.6: Spectra of Type II SLSNe, SN 2008am (upper panel) and SN 2008es (lower panel) observed at two different epochs [spectra obtained from Chatzopoulos et al., 2011; Gezari et al., 2009]. SN 2008am is an example of the far more common SLSN-IIn events, which display narrow hydrogen emission lines within their spectra, consistent with an interacting SN shock wave as seen within less luminous Type-IIn supernovae. SN 2008es represents the much rarer subclass of SLSNe-II which display broader hydrogen emission profiles at early and late times. It is yet unclear whether these two different groups of SNe are produced via similar progenitors, or if their differences in emission line profile are indicative of entirely different groups of SN event.

stars within the local Universe (i.e. if driven by ^{56}Ni , as suggested for SLSNe-R, then stars with initials masses of several 100 $M_{\odot}$ are required in order to produce the estimated amounts of ^{56}Ni ejecta). Thus their detectability at high redshift [e.g. Cooke et al., 2012] allows us to trace cosmic star formation history, as their rates should theoretically evolve with redshift as cosmic star formation rate does [Tanaka et al., 2012]. As such they also act as a tracer of any potential changes to the IMF (for instance, if it were to evolve to a more top-heavy form), whilst also providing additional information on the chemical composition of these distant stellar nurseries through absorption features imprinted in their otherwise smooth continua [e.g. Berger et al., 2012].

Although attempts at the standardisation of SLSNe are still somewhat in their infancy [e.g. Inserra and Smartt, 2014], as the potential of SLSNe literally outshines that of SNe-Ia, they may provide an suitable check for cosmological expectations of the Universe in the epoch of deceleration.

The key to unlocking the potential of SLSNe is to understand their progenitors. Through a more thorough comprehension of what creates a SLSN, we will not only understand the stellar populations these exceptional explosions trace through cosmic time, but we may also begin to standardise them, such that they may be utilised as cosmic beacons throughout the universe.

1.3 SLSN Progenitor Models

The enormous energies associated with SLSN explosions (typically radiating several 10^{51} ergs, as opposed to normal SNe, which only radiate only 1×10^{51} ergs), make it challenging to understand their energy production. These events are unlikely to be "scaled-up" versions of normal core collapse supernovae, which simply produce large amounts of ^{56}Ni during an energetic explosion, or that they originate from stars with large radii to explain the longevity of the events, as the inherent characteristics of the light curves (e.g. the rapid rise times of SLSNe-I) become difficult to replicate through standard core collapse mechanisms. Even for the SLSN-R events, whose light curves appear somewhat concurrent with the standard ^{56}Ni driven emission mechanism, the production of the required quantities of ^{56}Ni -rich material is non trival.

Even for SLSNe-II, for which the optical emission seems likely to be produced in a similar manner to normal Type II supernovae, the situation becomes complicated. In order to achieve the observed magnitudes and longevity of these events, either the stellar radius must be very large, or the star must become ex-

ceptionally bloated, stretching at least an order magnitude larger than the biggest red supergiants (which have radii ∼1,400 $R_\odot$, Wittkowski et al. 2012). Given the spectral signatures of these events, it may be more likely that these are the result of interaction of the SN shockwave with several shells of previously ejected material. Whilst physically, this may be somewhat easier to understand, how exactly such vast amounts of material are expelled in short periods of time prior to collapse is puzzling[4], and given the reprocessed nature of the light we detect from these SNe, whether the actual underlying explosion mechanism which produces the SN event is simply a more "normal" core collapse event, can only be guessed at.

It has become apparent that alternative sources of energy are required in order to drive the long lived light curves of these unusual SNe. Currently there are three competing models for the production of a SLSN event; Pair Instability Supernova, The Interaction Model and The Internal Engine Model. I will now outline the key concepts of each of these models, highlighting the expected physical characteristics of each before considering their application to observed SLSNe properties.

1.3.1 Pair Instability Supernovae

First theorised in the mid 1960's [Fowler and Hoyle, 1964], pair instability supernova (PISNe) have been searched for as ardently as the Loch Ness monster, with about the same level of success[5]. For stars within the mass range ∼130 to 260 $M_\odot$, the mass of the helium core is substantial ($> 60 \sim 130\,M_\odot$). Following the depletion of this central helium to form carbon, the contraction of the core which leads to the ignition of carbon burning is unstable. This is because as core temperatures reach $>\sim 10^9$K, the photons within the core have energies distributed according to Planck's law. This leaves some fraction of the photons in the high energy tail of this distribution, with energies in excess of the rest-mass energy of an electron-positron pair (0.511 MeV). This instigates intensive electron-positron pair creation, as energetic photons begin to interact, forming excess electrons and positrons within the core.

$$\gamma + \gamma \leftrightarrow e^+ + e^- \tag{1.5}$$

For every 10^{19} of these interactions, one electron positron pair will annihilate, producing a neutrino-anti neutrino pair:

[4]For instance see Kiewe et al. [2012] for mass loss rates and see Moriya and Tominaga [2012]; Ginzburg and Balberg [2012] for inferred circumstellar masses.

[5]For success rates, I refer the reader to Love, R. (1970), *"Sonar results from Loch Ness"*, Loch Ness Investigation, Annual Report

$$e^+ + e^- \rightarrow \nu_e + \bar{\nu_e} \tag{1.6}$$

As these neutrino pairs escape, they gradually erode away the internal energy of the core, which causes it to contract further[6]. In turn, this contraction raises core temperatures which increases the rate of pair production, thus accelerating the contraction and thereby causing temperatures to rocket higher. Very soon the pair production is not enough to counterbalance the loss of pressure within the core, and it begins to implode.

As it does so, temperatures rise to over 3 billion Kelvin, suddenly making conditions ideal for explosive nuclear burning of carbon and oxygen into iron. At some critical point, the energy released from this nuclear burning overcomes the implosion of the core. Inward motion ceases and instead drives a violent outward explosion which disrupts the star entirely, unbinding the stellar core and hurling the remaining envelope into space.

PISNe explosions have the potential to completely disrupt very massive stars, which as a consequence expels several tens of solar masses of synthesised heavy elements into the interstellar medium [Heger and Woosley, 2002; Kozyreva et al., 2014], greatly contributing to it's enrichment.

Theoretical modelling suggests that PISNe arising from sufficiently massive progenitors are capable of synthesising large amount of ^{56}Ni during the explosion (as much as $55\,M_\odot$, Heger and Woosley [2002]), with very little refinement to the underlying assumptions of the explosion physics. This produces a factor $\sim$100 more ^{56}Ni than that produced during a standard core collapse SN, and ten times more than the most energetic normal SN [Moriya et al., 2010].

While originally thought to be the final death throws of the exceptionally massive, metal poor stars of the early Universe (Population III stars), modelling has shown this instability to be possible within stars of higher metallicity if rotation is accounted for [Chatzopoulos and Wheeler, 2012a; Yusof et al., 2013; Marchant et al., 2016]. Their resulting light curves are capable of spanning a wide range of luminosities and durations, depending upon the initial composition and radius of the progenitor [Kasen et al., 2011], with more massive explosions capable of remaining bright for over 300 days. Due to the large amounts of optically thick ejecta associated with these events, PISNe are expected to have long ($>$ 100 days) rise-times and naturally a ^{56}Ni dominated late time decay.

Spectral modelling suggests that the early-time spectra of PISNe lack, or

[6]The neutrinos effectively strip energy away from the core as although core temperatures are high, they are not sufficiently so for the weak interaction of the neutrinos to become significant

show little evidence of metals lines, although these appear at later times as the photosphere recedes into the layers of burnt ejecta. In general, their spectra are expected to be remarkably similar to ordinary SNe, with P-Cygni line profiles superimposed over a pseudo black-body continuum. Their line velocities are moderate, despite the energy of the supernova, due to the large mass of the ejected material (as the entirety of the star is unbound during the explosion), which produces typical velocities of around 5000 km s^{-1}, about half that of a SN-Ia event, and significantly slower than SN-Ic associated with gamma ray burst events [Kasen et al., 2011; Modjaz et al., 2015].

There have been a few suggested candidate PISN events, particularly from the SLSN-R subset, whose slowly evolving light curves naturally match the expected slow decay rates of PISN predictions. SN 2007bi [Gal-Yam et al., 2009] was initially suggested to be the first recognised PISN event, as it possessed both the expected gradual light curve decay and it's nebular phase spectrum was consistent with several solar masses of ^{56}Ni being produced during the explosion. However, this assignment was received with some scepticism amongst the community, given the lack of available data prior to the SN peak, and alternate mechanisms have since been argued as the explosion route for SN 2007bi and other similar events [e.g. Inserra et al., 2013; Nicholl et al., 2013].

Currently the best observable match for a PISN event is the well monitored PS1-14jb [Lunnan et al., 2016], which displays the longest SN rise time to date (>125 days in the rest frame). Since such a long rise time is a key prediction of PISN models, this seems promising, and combined with its gradual fading of 0.01 mag day^{-1}, and an almost constant colour-temperature at very late times (which indicates sustained heating over long timescales), makes it a prime ^{56}Ni -powered PISN candidate. However, discrepancies to this model become apparent in the very late time observations (>400 days past peak), in which PISN models begin to under predict the light curve, which suggests that perhaps an alternative mechanism powers this transient at later times [Lunnan et al., 2016].

1.3.2 Circumstellar Interaction

In the case of hydrogen-rich SLSNe (especially those that show signs of narrow hydrogen lines within their spectra), perhaps the simplest way to explain their explosion properties is to build upon the already existing model of interaction between the SN shock wave and a shell of material lying away from the star, like normal Type IIn SNe (which although possess multiple velocity components, always have a strong narrow Hα profile). In normal SN-IIn this characteristic line profile is a result of

the collision of the SN blast wave with hydrogen-rich circumstellar material (CSM) surrounding the progenitor star.

Following the onset of the SN, rapidly expanding ejecta begins to plow into the CSM around the star, shock heating it as it goes and generating large quantities of X-rays as the material becomes shock ionised (around 10^{44}-10^{45} ergs s^{-1}, Pan et al. [2013]). The kinetic energy of the shock wave is efficiently converted through high energy collisions into blue visible light, which in turn slowly re-emits this energy through photons diffusing outwards. As the emission from the shock front heats the gas in the envelope, it becomes opaque, so the photosphere moves to the outer edge of the shell more quickly than the rest of the shock front. The SN achieves maximum light when the photosphere reaches this outermost radius. The speed of this rise to peak depends upon the mass of the CSM envelope, since more photons must be emitted from the shock to heat more massive envelopes.

With minor modification, this model can be applied to the much more luminous SLSN-II events. By extending the CSM which surrounds the star into a thicker shell, the collision process may be prolonged and thus the light curve stretched over a longer period of time [Smith and McCray, 2007]. If the density of this material is also increased the rise to peak in the light curve will become stretched, as the shock wave battles through this dense, slower moving material (see Figure 1.7).

However, whilst we may perhaps better understand the emission mechanism for SLSNe-IIn (and maybe all SLSNe-II, if you interpret the lack of narrow emission lines as interaction at very small distances away from the progenitor), it does not begin to explain the physical nature of these explosions (i.e. are they thermonuclear or core collapse?) and the fate of the stellar system within the CSM envelope (for instance, whether it is completely disrupted, or if some unseen remnant remains), as all this potential information is lost during reprocessing. A prime example of such information loss can be found in SN 1997cy. Originally classified as a SLSN-II event due to it's high luminosity and hydrogen dominated spectrum [Germany et al., 2000], signatures of the Fe and Fe features, characteristic of Type Ia events, later allowed this to be reclassified as a thermonuclear event rather than a core collapse one, taking place within a dense circumstellar shell, Deng et al. [2004].

The form that the SLSN light curve takes is predetermined by the density, structure and composition of the CSM material. Exactly how large quantities of material are pushed out from the progenitor to the very large ($> 10^{15}$ cm) inferred photospheric radii, is currently unclear. This process may take the form of a far reaching, very optically-thick massive stellar wind [Ofek et al., 2010; Chevalier and Irwin, 2011; Moriya and Tominaga, 2012], or vast quantities of material may be

expelled from the progenitor in brief, episodic bursts, perhaps similar to those observed within the luminous blue variable Eta Carinae (which expelled 12-20 $M_\odot$ of material within one outburst, Smith et al. [2003]). One such way to do this is through pulsational pair instability.

Pulsational Pair Instability

For stars slightly less massive than those discussed within Section 1.3.1 (typically 95-130 $M_\odot$), the instabilities inherent to high core temperatures described above still apply, and so these stellar cores too will begin to implode due to the spontaneous pair-production from energetic photons. However, with the onset of explosive fusion as the core begins to collapse, the energy released through these reactions is less than the binding energy of the star, and therefore it cannot be completely disrupted. In such cases, only a fraction of the envelope is ejected [Woosley et al., 2007; Woosley, 2016]. If this ejected mass is sufficient, the core stabilises, cooling via radiation or neutrino emission, until to much contraction causes the core to heat up again once again and instigate pair production, renewing the cycle. These dramatic episodes may go on for a few hours to ten's of thousands of years, keeping the star in this pulsating limbo until the mass of the helium/heavy metal remnant is eroded sufficiently to avoid pair production within the core (within the range 35-50 $M_\odot$). At this point, what remains of the ravaged star is free to continue it's evolution unimpeded by further pulsations, before finally collapsing to form a black hole.

Observationally, these events are diverse with total durations ranging from days to 10^4 years, and luminosities from 10^{41} to 10^{44} erg s^{-1} [Woosley, 2016]. Interesting transients in their own right, pulsational pair instability events may also provide the necessary method of mass removal required to produce dense shells of material at large radii from the progenitor, thus setting the stage for SLSN-II events [Woosley et al., 2007].

1.3.3 The Internal Engine Model

The assumed association of SLSN events with the deaths of massive stars naturally begins to draw parallels to better understood observations of massive stellar collapse; Long Gamma Ray Bursts (LGRBs). The current theory of LGRB production is that, within massive ($\gtrsim$40 $M_\odot$) stars, a core of $\sim 2\,M_\odot$ of ^{56}Fe will form, which will collapse to form a black hole during the final moments of core collapse [Stevenson, 2014]. If the progenitor star was rapidly spinning, the internal stellar envelope begins to form an accretion disc, which starting at the polar regions, feeds the new central

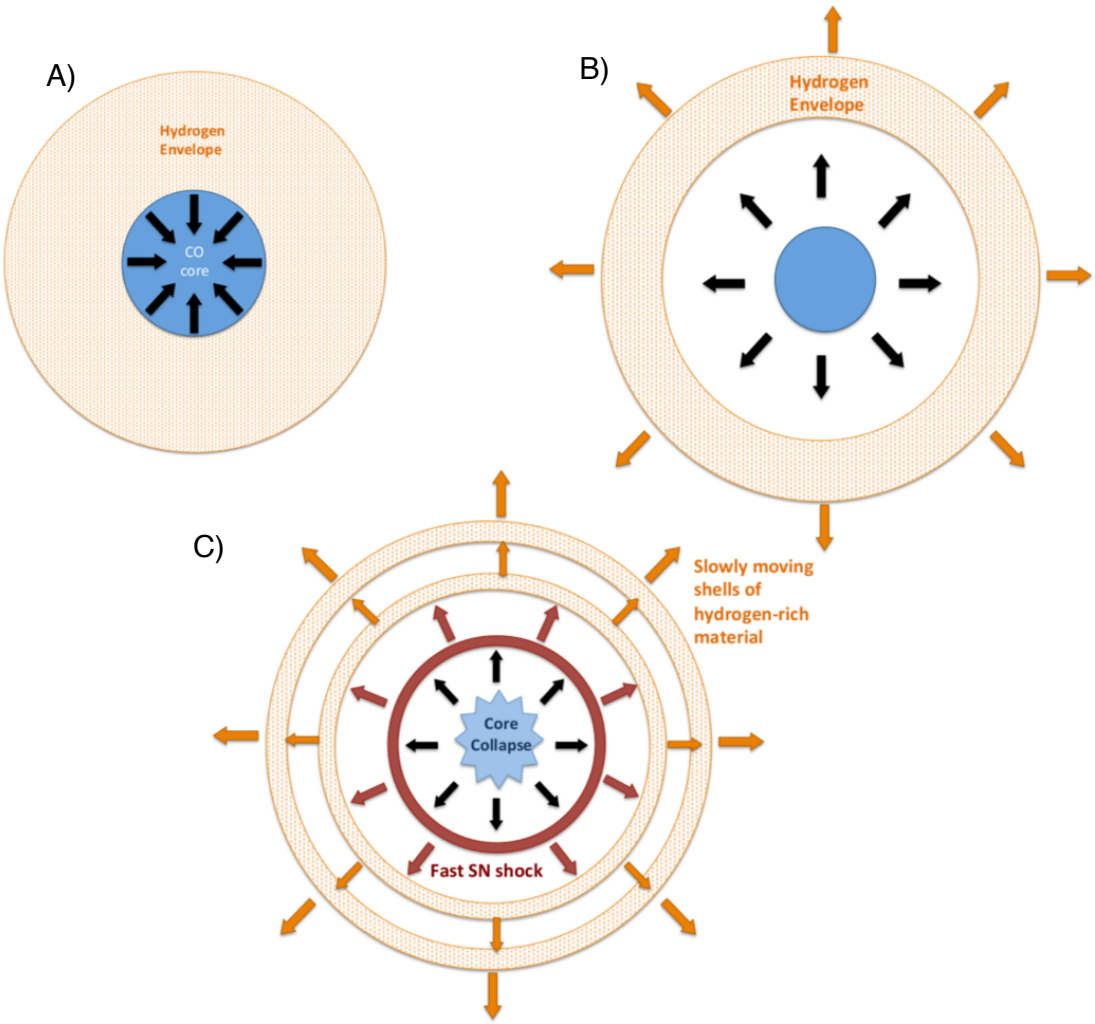

Figure 1.7: The pulsational pair instability CSM interaction model for SLSN production. Episodic mass loss is a result of an unstable CO core compressing (A) following spontaneous pair production, briefly igniting thermonuclear fusion within the core and releasing enough energy to expel a layer of hydrogen rich material from it's outer envelope. This shell of material travels slowly outwards from the core, which regains stability (B). This cycle may repeat several times, creating successive shells of material from the envelope at large radii from the core. When the core finally collapses, the fast SN shockwave catches up with these slowly moving shells, interacting with them and creating a more luminous event (C).

black hole. This configuration then launches ultra-relativistic bipolar jets along the rotational axis (although the precise mechanism for how this occurs is currently not fully understood), which break through the remaining stellar envelope and emerge as beams of high energy radiation. Collapses such as this which are viewed along the beaming axis are observed as LGRB events. This is more commonly known as the 'Collapsar Model' [Woosley, 1993; MacFadyen and Woosley, 1999].

If the stellar remnant is capable of driving large amounts of energy (which we observe as GRB jets), it is possible that this energy could be captured by the SN event, serving as an additional power source to drive its lightcurve. Energy released from the internal engine acts to re-energise the outgoing shockwave from the SN, which in turn prolongs the lifetime of the transient whilst simultaneously providing a substantial (factor $\sim$100) boost to the transient luminosity [Kasen and Bildsten, 2010; Dexter and Kasen, 2013].

This possibility of an internal engine formed by the remnant of the collapsed core has great appeal for SLSNe, given our much sounder knowledge of the formation of LGRB events and their association with massive stars. However, although the principle of the internal engine model is similar for LGRB and SLSN events (the observed transient is powered by an additional energy source to a standard core collapse), they differ primarily in the timescale over which this energy is deposited. Within a GRB event, the relatively brief observed burst of gamma rays observed is powered via rapid accretion onto the newly formed black hole, which occurs on a very short timescale [$\sim$10's of seconds, MacFadyen and Woosley, 1999]. Although adjustments to this model can be made by introducing a faster rotating progenitor (which in turn increased the fraction of the stellar envelope which may form a torus, which extends the period of accretion, Janiuk and Proga [2008]), the energy released is observed very shortly after the core collapse, delayed only by the time taken to break out of the stellar envelope [Bromberg et al., 2012].

In order for an internal engine to modify a SN event, the energy released must firstly occur at later times (as any energy released at early times is dissipated by the adiabatic expansion of the ejecta, [Kasen and Bildsten, 2010]), and be maintained over a much longer timescale (100's of days), in order to match the observed light curves of SLSNe. The engine succeeds by driving outflows of energy along the polar axis from the core, which accelerate through the envelope until it collides with the outward moving supernova shock wave. As it does so, the ejected material is heated up, increasing the luminosity of the event [Kasen and Bildsten, 2010; Stevenson, 2014]. This heating continues while ever the central engine remains active, thus prolonging the transient.

Such an internal engine has two proposed different forms; accretion onto a central compact object, or the spin down of a rapidly rotating neutron star.

Black Hole Accretion

This model builds upon the ground work laid down by the LGRB collapsar model. Here too a massive iron core collapses to form a black hole, and it's subsequent accretion launches jets along the polar axis [Woosley, 1993; MacFadyen and Woosley, 1999].

In this scenario, following core collapse some of the ejected material remains gravitationally bound to the core, and thus begins to fall inwards, until it encounters the newly formed black hole. This material is accreted at much later times (either because the progenitor has a particularly extended envelope, or because a reverse shock slows down the progress of inner ejecta layers Dexter and Kasen 2013), and unlike a GRB event, the outflows which result from this never break out through the stellar envelope. Instead they become trapped behind the SN ejecta, and thus begin to heat it up. This may potentially result in particularly luminous optical emission if the black hole releases significant energy on a long time scale (weeks-months), comparable to the photon diffusion time through the ejecta [Dexter and Kasen, 2013].

Magnetar Spin Down

If a rapidly rotating iron core collapses into a neutron star, angular momentum is conserved, such that the newly formed remnant is rotating with a period of milliseconds, inducing a strong magnetic field. Neutron stars with unusually strong magnetic fields ($>10^{14}$ Gauss), are more commonly known as magnetars.

The intense magnetic field begins to interact with the surrounding stellar material. This generates a powerful electric field within the hot gas, which in turn forms a counteracting magnetic field. These opposing fields effectively act as a brake to the magnetar spin period, and as it loses energy it begins to severely heat up the internal envelope, generating a rapidly expanding bubble of hot plasma. These plasma bubbles move out along the magnetic poles of the magnetar, moving more quickly than the expanding SN shock wave until it catches up with the outer shells of moving material. As the plasma bubbles collide with the outer moving material, they cause it to heat up, generating additional luminosity. In theory, this should produce a rebrightening 'bump' within the SN light curve.

It has been suggested that a GRB event could also be powered by magnetar

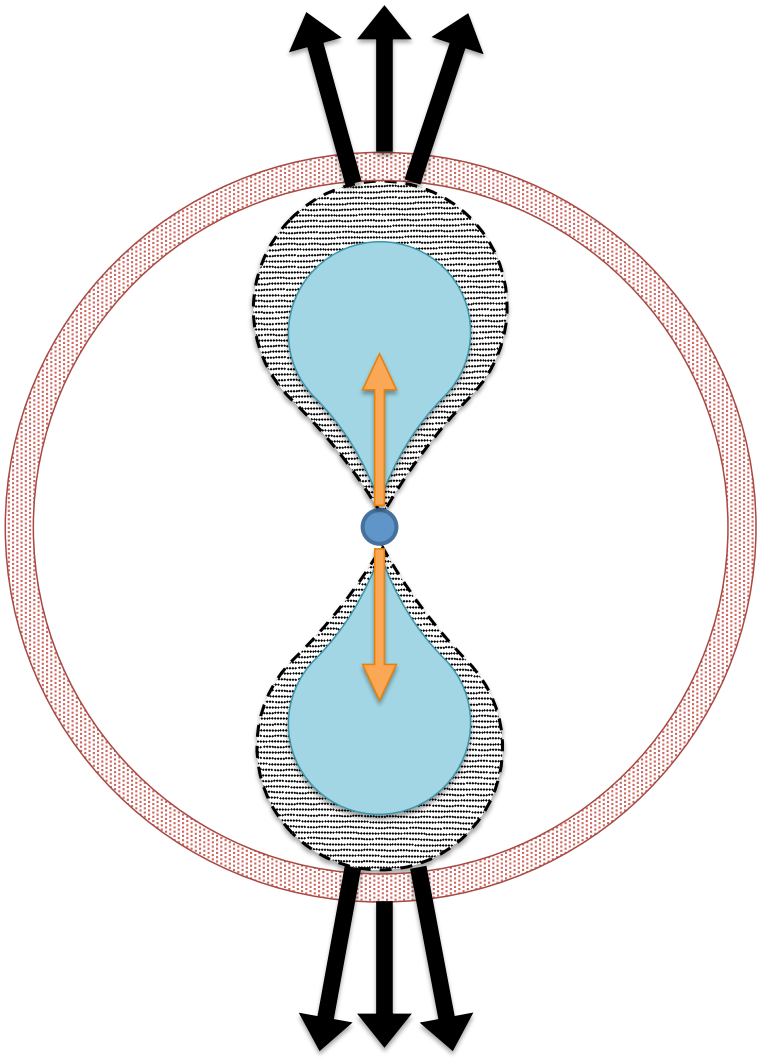

Figure 1.8: The magnetar internal engine model for SLSN production. The rapidly rotating central magnetar induces strong magnetic breaking as it's magnetic field interacts with the surrounding envelope. Lost angular momentum is converted into heat, which drives strong plumes of plasma out along the magnetic poles. When this plasma reaches the SN, it begins to heat up the ejected material, creating additional luminosity. As the magnetar continues to spin, it continues to drive these plasma bubbles, in turn generating a longer and brighter SN event.

spin down [Bucciantini et al., 2009], however the magnetars required to do so must have much stronger magnetic fields (10 - 100 times stronger than those required for SLSN events) and spin down quickly (within a few 100 seconds) so that the release of energy is much more rapid, which allows the jet of energy to break through the stellar envelope [Metzger et al., 2015].

The remnant left from such an event would be a slowly rotating magnetar with a period of only a few seconds, and although such magnetars have been observed within the Milky Way and nearby galaxies [e.g. Duncan and Thompson, 1992], the remnants left from GRB or SLSN events would be more luminous than these known Galactic magnetars, with longer spin periods [Rea et al., 2015], and as such appear to have different origins.

1.3.4 Modelling SLSN Events

The modelling of SLSN events using the explosion mechanisms outlined in the previous sections (or combinations thereof) has thus far proved challenging. As has been previously suggested, SLSN light curves are not aways well fit by simple ^{56}Ni driven power sources (as used within PISN). Typically, PISN models involve only three free parameters: the total mass of the ejecta, the mass of ^{56}Ni produced and time [e.g. Nicholl et al., 2013].

For normal SLSN-I events, a pair instability ^{56}Ni powered explosion is unable to re-produce the swift rise and decline of the peak, as within PISN models the SN rise time is firmly set by the diffusion timescale through the ejecta, which itself depends upon the kinetic energy of the explosion, the ejecta mass and its opacity. Thus this model is most relevant for slowly evolving SLSNe (SLSN-R events), whose rise times are typically more extended (>50 days).

However, given constraints pre-placed upon some SLSN-R explosions (e.g. the ejected ^{56}Ni mass inferred from spectroscopic observations), these predicted rise times are exceptionally slow (typically >100 days), when compared to the observed SLSN light curves. Thus pure ^{56}Ni powered events do not always provide adequate fits to the observed light curves of SLSN events [Inserra et al., 2013; Nicholl et al., 2013] (with the notable exception of PS1-14bj, for which the slow ∼125 day rise to peak is well replicated by PISN models [Lunnan et al., 2016]). However, recent PISN models involving very high mass progenitors (200-250 $M_\odot$) at moderate metallicity (0.001 $Z_\odot$) have shown significantly swifter rise and decline of the peak [Kozyreva et al., 2017], and therefore PISN models cannot be completely removed from progenitor considerations.

For many SLSN events, a magnetar powered internal engine has been found

to replicate the form of their light curves well [e.g. see Nicholl et al., 2013; Inserra et al., 2013; Dessart et al., 2012]. The greater flexibility afforded by these models (recreating a wider variety of light curve profiles) largely comes from breaking the degeneracy between the ejected mass of the explosion and the power source of the light curve. Within magnetar models, an explosion energy is usually assumed, leaving the amount and opacity of the ejected material, alongside the magnetar's spin period and magnetic field strength as free parameters [Kasen and Bildsten, 2010]. Such models agree with some of the observed SLSN light curves well, although it should be noted that the models are given more freedom by the number of free parameters involved.

Whilst it may seem apparent that the lack of (narrow) emission lines with hydrogen poor SLSN-I events naturally rules out a CSM interaction driven transient for these explosions, many plausible arguments have been made which allow for it. Conditions in which typical interaction features may be suppressed within the spectra of hydrogen-poor SLSNe, (such as the case of a rapidly expanding hydrogen-poor CSM) have been postulated [Chatzopoulos and Wheeler, 2012a], and their progenitor systems modelled [Chatzopoulos and Wheeler, 2012b], such that for some cases, pulsational pair instability may also potentially power a SLSN-I event, as well as hydrogen rich events.

The recent detection of pre-SN bumps within some SLSN light curves appear to have had a counter-productive effect upon constraining progenitors through light curve modelling, as these features have been interpreted in multiple ways. This could be cooling emission from a double-shelled CSM [Leloudas et al., 2012; Moriya and Tominaga, 2012] or originate from the extremely extended envelope of a stellar progenitor [Nicholl et al., 2015; Piro, 2015]. Alternatively they may represent a second shock breakout as a central engine interacts with expanding ejecta material [Kasen et al., 2016], or reheating of material following the initiation of this engine [Smith et al., 2016]. Once again it appears that larger sample sizes are required in order to confirm these theories.

Modelling of the spectra of SLSN events can provide an additional insight to SLSN progenitors - whilst analytical models of the light curves are able to estimate ejecta masses, they are often hampered by prior assumptions of opacities and explosion energies. However, within the SN spectra we are able to explore the composition of the progenitor system, as the expanding ejecta reveals successively deeper layers of the progenitor star [Mazzali et al., 2016]. Unfortunately current modelling of late time spectral properties of SLSNe does not always adequately distinguish between progenitor classes.

Given the observed degeneracies and lack of constraints apparent when using modelling to distinguish between the potential progenitors of SLSN events, the progenitors of SLSNe remain poorly understood. It is therefore clear that alternative approaches must be taken such that we may begin to constrain them.

1.4 Host Galaxy Studies

A powerful way of tackling this problem is to study the host galaxies of these extreme cosmic explosions, and infer progenitor properties from the properties of the stellar populations within the environments in which they form. As the majority of SLSNe lie out of reach of direct progenitor detection methods (i.e. through archival imaging of very local galaxies, [e.g. see Smartt, 2009]), host galaxy studies ultimately provide constraints upon transient progenitors through constraining the mass and age of the underlying stellar populations, usually through inference based upon the star forming properties and chemical composition of the environment. This method has been used effectively to constrain the properties of progenitors of other types of transient (e.g. LGRBs, Type-Ia SN and core collapse SNe, [for instance Fruchter et al., 2006; Kelly et al., 2008; Savaglio et al., 2009; Anderson et al., 2012; Perley et al., 2013]).

Host galaxies studies may be performed at one of two levels; either on a global scale, considering the properties of the galaxy as a whole, or by considering on the environment local to the position of the transient within it's host (the sub-galactic environment).

1.4.1 Global Environment Studies

The large scale environments of transients can be an easy first clue to the potential population from which the progenitor arises. For example, early differences between SNe Ia and SNe II could be inferred from the presence of the former in ancient elliptical galaxies [van den Bergh and Tammann, 1991; van den Bergh et al., 2005], while the latter arise exclusively in star forming hosts, which suggests that SN-II arise from a younger (and therefore more massive) population of stars. Given the high redshifts attributed to many transients (e.g. LGRBs, which are typically located at z>1, Tanvir and Jakobsson 2007; Jakobsson et al. 2012), the angular distances for many of the hosts are too small to resolve the hosts into many resolution elements using current detectors. Thus it becomes necessary to use global properties of the host as an indicator of the properties of the explosion site. When averaged over a large number of hosts such estimates should still provide robust statements

about transient environments.

For instance, the host galaxies of LGRBs have been frequently shown to be faint, blue, star-forming galaxies, which suggests low mass host galaxies with a newly formed young underlying population [Christensen et al., 2004; Kewley et al., 2007], unlike the host galaxies of core collapse SNe, which have been found to frequently occur within grand design spiral galaxies [Svensson et al., 2010].

The metallicities of host galaxies allow more specific constraints to be placed upon the chemical enrichment of the transient environment, and thus the likely underlying stellar populations. These measurements may be performed on a global or local ($\sim$ few pc to kpc, dependent on redshift) scale, and are either determined directly (through spectroscopic measurements of emission and absorption lines within the host spectrum), or indirectly through established relationships between the metallicity of the host and it's mass and luminosity.

Using a relatively local sample of host galaxies drawn from SDSS-DR4, Prieto et al. [2008] showed that the metallicities of SN-II, SN-Ia and SN-Ib/c are different. The rates of SNe events have also been considered as a function of host metallicity - with the rate of SN-Ib/c to SN-II events increases with increasing metallicity [Prieto et al., 2008; Kelly and Kirshner, 2012; Prantzos and Boissier, 2003; Arcavi et al., 2010].

However, it should be noted that global metallicity measurements do not always provide a direct indication of the metallicity of the progenitor, as these are typically representative of only the emission from the brightest regions within the host galaxy, which may be different at the location of the SN, given the significant metallicity gradients that may exist within galaxies.

One final consideration when performing global host galaxy studies is the possibility that the identified 'host' galaxy may not be the real site of the transient. Satellite galaxies nested within larger hosts are not always adequately resolved within ground based, and sometimes space-based observations, which may lead to misidentification of the host.

1.4.2 Sub-galactic Environment Studies

More recently, increasingly sophisticated approaches have been made to study both the luminosities and morphologies of the host galaxies of various transient types, along with their location within their hosts. Star formation within galaxies is a small scale process, and depending upon the intensity of the star formation, may take place in regions smaller than a single parsec [Portegies Zwart et al., 2010]. These are the natal regions where the youngest, most massive stars within the

galaxy are forming, and therefore most likely where the progenitors of massive stellar core collapse originate. The properties of these small star forming regions will provide direct information on the chemical enrichment of the progenitor, free from contamination of the rest of the host galaxy.

In practice, the resolution required to achieve this level of environment study can only be achieved using high resolution imaging and spectroscopy, which can only really be achieved through the use of adaptive optics or spaced based observations. Unfortunately, we are still limited by current technology; as the redshift of the transient increases, the resolution typically decreases, such that with a redshift z=1 at *HST* resolution (0.1 arcsec) the physical space probed by observations would be around ∼0.8 kpc. Even for exceptionally local events (z<0.1), the physical size of the resolution achieved only approaches ∼10pc.

However, even at limited resolution, sub galactic environments can still provide important information about the birth environments of transient progenitors. Several imaging studies have utilised the use of pixel statistics at the transient location to infer properties of the local underlying stellar population. Such techniques will be described with greater detail within Chapter 4, however in a nutshell they typically concern the use of high resolution images or multi fibre spectroscopy to estimate the photometric and spectroscopic properties at the transient site.

Such studies have been performed for the host galaxies of core collapse SNe. Through studies of the way in which these transients trace the blue light within their galaxies, there has emerged an apparent increasing mass spectrum from SN II → SN Ib → SN Ic [James and Anderson, 2006; Kelly et al., 2008; Leloudas et al., 2010; Kelly and Kirshner, 2012; Anderson et al., 2012]. Local spectroscopic studies have shown that SN Ib/c events arise from higher metallicity locations than SNe-II [Modjaz et al., 2011; Anderson et al., 2012], although this difference has been deemed tenuous and it seems likely that the metallicity of the natal environment is not a dominant factor in the production of the different normal SN types.

Of particular relevance to SLSNe have been the sub galactic environmental studies of the host galaxies of LGRBs. These events, the only stellar collapse events whose luminosities exceed those of SLSNe [Bloom et al., 2009; Racusin et al., 2009], have been shown to arise primarily from the brightest regions of low-mass mainly low metallicity hosts [e.g. Fruchter et al., 2006; Savaglio et al., 2009; Svensson et al., 2010; Perley et al., 2013]. Such results imply that they arise from massive > 40 $M_{\odot}$ low metallicity stars [e.g. Fruchter et al., 2006; Larsson et al., 2007; Raskin et al., 2008; Graham and Fruchter, 2013b].

1.4.3 SLSN Host Galaxy Constraints

Like other transients, the host galaxies of SLSNe may be studied to attempt to place constraints upon the progenitors systems through estimates of the properties of the underlying stellar populations, which may begin to discriminate between SLSN progenitor models. For instance PISN models predict that these events should be produced only by very massive stars, which based upon our current understanding of stellar evolution suggests that they should arise from low metallicity environments, such that a greater proportion of the original mass may be retained [Langer et al., 2008]. Whilst some models have been postulated in which PISN may be produced within higher metallicities [Kozyreva et al., 2017], these metallicities are still significantly different than those observed within normal star forming galaxies in the moderately local Universe.

The star forming properties of host galaxies may provide further clues to progenitor types - for instance host galaxies which show clear signs of intense, bursty type star formation are likely to have formed the progenitor during this starburst, which therefore places an upper age limit (and so, lower mass limit) upon the progenitor star, which may help to distinguish between PISN and internal engine models. Starbursting galaxies are more likely to produce dense stellar environments [e.g. M82 Lim et al., 2013], which increases the chance of dynamical interaction and mergers affecting the evolution of the progenitor [Portegies Zwart and van den Heuvel, 2007; Yungelson et al., 2008; Glebbeek et al., 2009; Pan et al., 2012].

On the other hand, the interaction model typically requires a rapidly rotating progenitor to produce either a central magnetar or an accreting black hole. In this case, for a single stellar model a lower metallicity environment may be more suitable, such that the progenitor star may retain more of it's initial angular momentum without losing it to winds. If these rapidly rotating progenitors are produced via spin up from a binary companion, it may be able to form across a wider range of environment chemical enrichments [e.g. see de Mink et al., 2008, for mass transfer scenarios with metallicity]. The similarity between the internal engine model and that of the collapsar model of LGRBs does suggest that it might not be unreasonable to expect to find SLSNe and LGRBs within similar environments (i.e. galaxies of typically low or intermediate metallicity), and therefore comparison of these types of host galaxy may prove valuable.

1.4.4 A History of SLSN Host Galaxy Studies

In recent years there have been several studies of the host galaxies of SLSNe. Several of these have been in depth studies of the properties of the host galaxies of individual SLSN events [e.g. Lunnan et al., 2013; Chen et al., 2013, 2015; Thöne et al., 2015], which have typically unveiled host galaxies with exceptionally high specific star formation rates and low metallicities, which the authors use as confirmation that at least some SLSN originate from young, low-metallicity populations. However whilst such studies may place stronger limits upon the constraining of progenitors for individual events, they are typically motivated by the accessibility of the host galaxy (i.e. it is of a sufficiently low redshift that spectroscopic observations are feasible). Studies of bulk populations provide evolutionary context of the state of the underlying populations, and allow better generalisations to be made about the progenitors of SLSNe as a whole

Within the following section I shall provide a brief overview of the work undertaken within this field and the key results and implications from these studies, such that the reader is provided with context for the motivation of the work undertaken within this thesis. It should be noted that the results provided within Perley et al. [2016] and Japelj et al. [2016] were published after the work within Chapter 3 was published.

Photometric Studies

The extreme nature of SLSN host galaxies was originally highlighted within Neill et al. [2011], who used GALEX and SDSS archival imaging to examine the properties of a small sample of 17 SLSN host galaxies, identified whilst the field of SLSNe was still relatively new. These hosts were found to be exceptionally faint and blue, especially when compared to a sample of field galaxies from SDSS. Their inferred star formation rates were moderately low, such that when considered alongside their low stellar masses, indicated high specific star formation rates. This preference for low-luminosity host galaxies to was initially used to infer a potential preference for lower metallicity environments. Unfortunately this early study was somewhat limited by the depth of the observations used (limits of $g' \sim 23$ and UV$\sim$23.5 for SDSS and GALAX MIS surveys respectively), which left the majority of the more recently discovered SLSNe from newer targeted surveys with only upper limits for their hosts in the UV and optical, as such host galaxies are more distant (although their SN events are better characterised).

Making comparisons between different types of host galaxies is important,

given our firmer understanding of the progenitors of other transients we may begin to place the progenitors of SLSNe within an evolutionary context (i.e. whether the progenitors are likely to be younger or older and more or less massive than other core collapse progenitors). Lunnan et al. [2014] were the first to carry out a survey of the photometric (and spectroscopic) properties of SLSN hosts and compare their properties with those of the host galaxies of other core collapse events such as "normal" CCSNe and LGRBs. The authors considered only the properties of hydrogen-poor Type-I SLSNe, given the proposed similarities between the explosion mechanism for these events and the collapsar model of LGRBs. Through SED fitting they determine the stellar masses and star forming properties for these host galaxies, from which they showed that the hosts of these SLSNe are less luminous than those of general SNe and LGRB population. However, based upon their few spectroscopic observations, they suggest the environments of SLSNe and LGRBs are comparable (at least in metallicity), which they use to advocate a similar progenitor path.

The majority of SLSN host galaxy samples studied within literature are a conglomeration of SLSN events discovered within a variety of different surveys [e.g. Leloudas et al., 2015, Chapters 3 and 4 of this thesis], and as a consequence may introduce non-trivial biases into the conclusions derived from their properties. However, other studies which have attempted to provide a stronger focus upon events discovered within Pan-STARRS (PS1) [Lunnan et al., 2014, e.g.], are subject to internal biases based upon the follow-up strategies invoked by the PS1 survey (for instance, the preferential follow up of "orphan" transients for which no obvious host can be found within archival imaging, highly biasing studies against the bright end of the host luminosity function). Perley et al. [2016] present a consistent sample of SLSN host galaxies discovered within the Palomar Transient Factory (PTF)[7]. The study uses a combination of ground based imaging and spectroscopy to determine the luminosities, star-formation rates, stellar masses, and gas-phase metallicities for both hydrogen poor and hydrogen rich SLSN hosts. Like previous studies, the authors find that SLSN-I hosts are typically faint, low mass star bursting galaxies which are metal poor, and suggest that the SLSNe-I rate becomes heavily suppressed within higher metallicity (>0.5 $Z_{\odot}$) galaxies, but do not find that the rate increases with further restriction to lower metallicities. This paper also confirms results shown within Chapter 3 (which were published prior to this publication), that hydrogen

[7]Although the spectroscopic follow up of PTF transients is a human decision process based on the available transient information, with some emphasis upon the follow up of transients from fainter/undetected host galaxies, examination of CCSNe followed up from PTF observations reveals no alarming fraction contained within exceptionally faint hosts, indicative of a fair sampling of SLSN events across the host galaxy luminosity function [Perley et al., 2016]

rich SLSNe-II are located within a much more varied range of host galaxy masses, suggestive that these events do not show any strong preference for environmental metallicity.

In a further attempt to refine the study of SLSN-I environments, [Japelj et al., 2016] consider the SLSN-I host galaxy properties available within the literature and compare their properties to a sample of LGRB host galaxies discovered within *Swift* BAT6 (as BAT6 LGRB events are selected by the luminosity of their prompt emission, and therefore should provide an unbiased sample of host galaxies). In order to reduce complications introduced through galaxy evolution with redshift, the authors consider only SLSN and GRB events within the redshift range $0.3<z<0.7$, and when doing so find that the two samples do not significantly differ in stellar mass, luminosity, star formation rate and metallicity. The authors suggest that within this range these galaxies lie on the fundamental plane of metallicity for low mass galaxies, and highlight the biases introduced in spectroscopic comparison of SLSNe and LGRBs given the differing spectral coverage of their hosts with redshift (there are relatively few LGRB hosts with spectra at low redshift, unlike SLSN hosts). The authors emphasise the need for a larger sample of SLSN hosts at higher redshift and LGRB hosts at lower redshift in order for further comparison to continue.

Spectroscopic Studies

The spectroscopic study of SLSN host galaxies has been somewhat limited, owing to the faint nature of the hosts, there are only a handful local and bright enough to make spectroscopic observations viable. Stoll et al. [2011] were the first to consider the spectroscopic properties of these hosts, comparing the gas phase oxygen abundances of two well studied SLSN host galaxies, and then considering these alongside the metallicities of a handful of local SLSN host galaxies from ground based surveys (e.g. SDSS). They found these hosts to lie at the low metallicity extreme of the distribution of star forming galaxies within the local universe, which the authors found to be comparable to the metallicities of LGRB environments, which lead to early suggestions that the metallicity of the star forming environment was a key parameter in the production of these events. Similar inferences have been made when considering hydrogen-poor SLSN hosts discovered within Pan-STARRS [Lunnan et al., 2014].

The study of absorption within SLSN spectra tells a very different story. Through high resolution spectroscopic observations of a few hydrogen-poor SLSN hosts, Vreeswijk et al. [2014] observed narrow metal absorption lines of MgI, MgII and FeII, which are associated with the cold interstellar medium (ISM) of the host

galaxy. The equivalent widths and column densities of these ISM metals were generally at the lower end of the ISM metal distribution, and much lower than those typically observed within the environments of LGRBs. This seems to suggest different progenitor paths for SLSN and LGRB events, due to the lower absorption strengths observed in SLSN environments than in GRB hosts.

These early studies were somewhat hampered by their limited sample sizes and the availability of spectroscopic data, which naturally produces samples which are somewhat discriminatory against the faint end of the SLSN host galaxy luminosity function. Even the spectral study of Pan-STARRS SLSN hosts within Lunnan et al. [2014] is limited by the availability of spectroscopic observations, which are restricted to lower redshifts. Thus these conclusions are somewhat tenuous based upon the availability of observations.

A more comprehensive spectroscopic study of the hosts of all spectral types of SLSNe was carried out by Leloudas et al. [2015]. The authors use spectroscopic observations obtained with 6-10m class telescopes to determine the strengths of strong star forming lines (Hα, Hβ, O[II], O[III], N[II]) to estimate the stellar masses, star forming properties and metallicities of these galaxies, before comparing them to those of LGRB hosts, and Extreme Emission Line Galaxies (EELGs). EELGs are dwarf, star bursting galaxies whose strong emission lines and equivalent widths represent phases of extreme star formation within the galaxy. As such, their populations are considered to be very young ($\sim$ 10's Myr old, Leitherer et al. 1999).

The authors show that the hosts of Type-I and Type-R events to possess extreme emission lines like EELGs, with broad equivalent widths and highly ionising radiation fields, as demonstrated within the different samples' cumulative distributions of metallicity, ionisation and Hα equivalent widths shown in Figure 1.9, from the work of Leloudas et al. [2015]. This is in contrast to the spectroscopic properties of SLSN-II hosts, which have comparatively softer radiation fields. These differing radiation fields have been used to support the notion of different progenitor systems for Type-I and Type-II events. The strong similarity between SLSN-I hosts and EELGs has been used to advocate a massive, potentially population III-like progenitor for H-poor SLSNe based upon the extremity of their emission lines, as such spectral signatures can only be produced by large numbers of very young, hot, massive stars. The implied upper age limits of <10 Myr upon the populations within these hosts pushes progenitor masses in excess of 40 $M_{\odot}$.

Spectroscopic studies of SLSN hosts so far have been somewhat contradictory. The results of Leloudas et al. [2015] seem to agree with that observed within the spectroscopic environment localised to the location of PTF12dam [Thöne et al.,

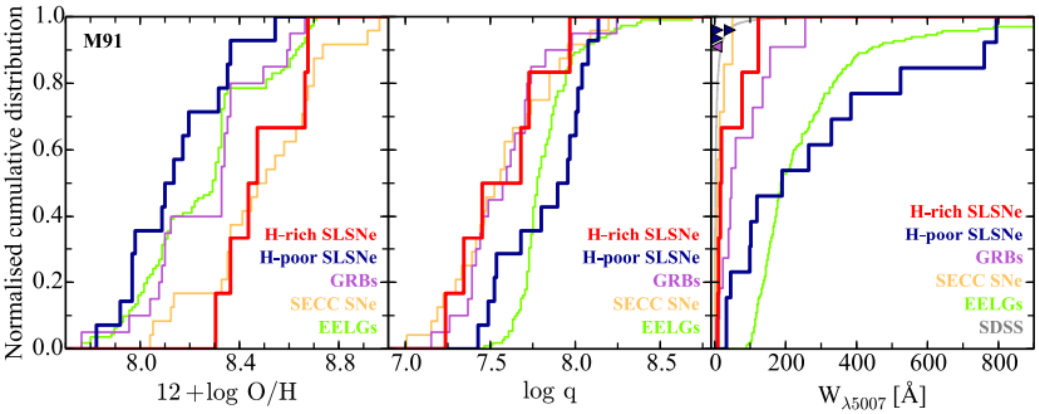

Figure 1.9: *Figure taken from Leloudas et al. [2015]*: Comparison of the spectroscopic properties of SLSNe host galaxies alongside LGRB hosts, Extreme Emission Line Galaxies (EELGs) and "standard" SDSS field galaxies. *Left panel:* Cumulative distributions of the galaxy metallicities as determined from strong emission line measurements. SLSNe and LGRBs are typically found within sub-solar ($12+\log(O/H)<8.7$) environments. The hosts of SLSNe are also shown to exhibit strongly ionising radiation fields, as seen through the distribution of the ionisation parameter, q *(centre panel)* with broad equivalent widths similar to those seen within EELGs *(right panel)*. The consistency of SLSN hosts with the spectroscopic properties of EELGs, who's populations are thought to be extremely young (<10 Myr, Leitherer et al. 1999), implies similarly young populations within these environments, and thus a more massive progenitor path for SLSN explosions.

2015], however they conflict with the findings those who subscribe to a LGRB-like internal engine or magnetar powered progenitor model [e.g. Lunnan et al., 2014; Inserra et al., 2013], for which a slightly less massive progenitor [>40$M_{\odot}$, Davies et al., 2009] would suffice. Although the samples presented by Lunnan et al. [2014] and Leloudas et al. [2015] have limited overlap, their distributions of metallicity are rather different, perhaps explaining the disparate conclusions.

Local Environment Studies

In some cases it has been possible to directly study the immediate environments of the SLSNe, and determine the stellar populations at the explosion sites. The relatively local SLSN PTF12dam has been studied in some detail, largely due to it's low redshift (z = 0.107) and well monitored late time follow up. The host galaxy of this hydrogen poor SLSN is notable for it's strong nebular emission lines, which have placed strong constraints upon it's metallicity [Chen et al., 2015]. However, as the galaxy is local, it's spatial extent is much larger than other detected SLSN hosts, which allows different regions of the host to be studied with greater detail. The galaxy has a "tadpole" morphology, and by obtaining two long slit spectra at perpendicular orientations, Thöne et al. [2015] were able to determine the local metallicity within 5 distinct regions of the host galaxy, localising to regions of ∼1kpc radius. They determined that the SN occurred within the star forming region at the 'head' of the tadpole, was a result of a recent star burst which was superimposed on the much older underlying stellar population comprising the other regions of the host. The authors estimate a local population age of 3 Myr at a metallicity of 12+log(O/H)=8.0, from which the authors infer a very young, massive progenitor of at least 60 $M_{\odot}$.

Lunnan et al. [2015] have used *HST* imaging of a sample of hydrogen-poor SLSN-I host galaxies to probe the local environments of these SN at ultraviolet wavelengths. This study focussed upon the fractional host light contained within locations of these SLSNe-I, once again comparing these locations to those of LGRB and CCSN events. The authors find that the locations of SLSNe-I to be correlated with star formation activity within their hosts, and slightly more concentrated on these regions within their hosts than CCSNe. However, they find these SLSN-I events to be less concentrated upon the bright light within their hosts than LGRBs events, (although statistically their sample is comparable to both comparison samples). The strong association of LGRBs with the brighter UV regions in their hosts has been used to tie them to the younger, more massive stellar populations (given the strong link between stellar mass, stellar luminosity, and stellar lifetime). Therefore

this more diluted preference for strongly star forming regions exhibited by these SLSN-I events could naturally be explained by longer lived, possibly lower mass progenitors for SLSNe-I.

These two local environment studies seem to directly contradict one another, as if SLSNe-I originate from very massive stars implied by their host galaxy irradiation, then their locations should be more strongly associated with the brightest UV pixels within their hosts. Lunnan et al. [2015] suggest that the mass of the progenitor is not the only deciding factor in the production of a SLSN-I event, and that this deciding factor may be metallicity (as LGRBs are typically situated on the brightest pixels of their hosts, this makes global metallicity measurements a fair estimate of the GRB progenitor metallicity. If SLSNe are not always situated within the peak of the light of their hosts, progenitor metallicities may not be truly represented by the global metallicity of the host).

1.4.5 The Objective of This Work

At a glance, it would appear the properties of SLSN host galaxies are highly conflicting. Although the consensus that the vast majority of SLSN hosts are intrinsically faint galaxies with low masses and star formation rates appears to hold, the conclusions drawn from spectroscopic and local environment studies differ wildly. Is the metallicity of the host environment a key factor in the production of a SLSN progenitor? Are global metallicity measurements a good approximation for the metallicity of the explosion site? Is there a strong dependance upon metallicity at all[8]?

Whilst the host galaxies of SLSNe-I have been studied at some length (again, likely owing to possible likeness to LGRB events), the environments of SLSNe-II have been relatively untouched. Although the mechanism for producing their light seems to be somewhat better understood than SLSNe-I, the progenitor systems are still somewhat of a mystery. If pulsational pair instability is the primary method of removing shells of stellar envelope prior to the explosion, then these stars are still likely to be very massive, which should be reflected within their environments.

Current spectroscopic studies of SLSN host galaxies omit >20% of hosts due to their exceptionally low luminosities ($M_V >$ -16.5), and a large fraction of SLSN at higher redshift discovered within ground based surveys lack deep enough imaging to recover their host galaxies. The work undertaken within this thesis will attempt to create a better understanding of the physical conditions necessary for the create of SLSN events through the use of high resolution imaging of SLSN hosts, particularly

[8]Given that the LGRB metallicity dependance is thought to be rather weak, somewhere between solar [e.g. Perley et al., 2015a; Krühler et al., 2015] and 1/3 solar [Graham and Fruchter, 2017]

including those which were previously undetected within ground based observations. By using *HST* observations, any biases due to the inherent brightness of the host sample are significantly reduced, with the advantage of being able to to easily probe these host galaxies in the ultraviolet such that their star forming properties may be better understood. These observations will cover the host galaxies of all spectral classes of SLSNe, such that they may be put into context.

Organisation of the Thesis

The remainder of this thesis shall be organised as follows; the photometric observations which form the basis of the analysis performed within Chapters 3 and 4 will be outlined within Chapter 2, alongside details of techniques used in the reduction of these images and any analysis common to both Chapters 3 and 4 (any analysis particular to any specific science chapter will be provided within it).

Within Chapter 3 I will explore the global photometric properties of SLSN host galaxies as imaged with *HST*, with particular emphasis upon the star forming properties and masses of these galaxies. I will show that in comparison with the properties of other core collapse transient hosts (CCSNe and LGRBs), these SLSN hosts are notably different, being fainter, lower mass galaxies with less star formation.

I will then proceed to explore the sub galactic environments of SLSN events imaged with *HST* in the ultraviolet within Chapter 4. The offsets, fractional flux values and surface brightnesses of these transient sites will be determined, and once again the properties of their locations will be compared to those of CCSNe and LGRBs explosion sites. I will show that although these locations trace star formation with SLSN hosts, when accounting of positional uncertainty of the transients, it is at present unclear whether they exhibit strong preference for highly star forming regions within their hosts, before considering the implications of these locations.

Within Chapter 5 I will attempt to place the results obtained within Chapter 3 into context, through modelling the likely range of host galaxies within which stars below a given metallicity restriction may be located. I consider the results of this model in light of the observed distributions of typical host galaxy masses before discussing the implications of using this model to infer the presence of a metallicity threshold in transient progenitor populations.

Chapter 2

Photometric Observations and Methods

"Though this be madness, yet there is method in't."
—William Shakespeare, *Hamlet*

Within this chapter I will outline the photometric observations and methods used mostly within Chapters 3 and 4 in this thesis, given the significant overlap in data used between the two chapters. I will first outline the overall sample of SLSN host galaxies common to this thesis, indicating which host galaxies are studied within each chapter. I will then provide details of the photometric observations used within both Chapters 3 and 4 before outlining any methods or analysis carried out common to both of these chapters. Any analysis particular to any specific science chapters will be provided within them.

2.1 SLSN Sample

Within Table 2.1 I present the combined SLSN host galaxy sample used for analysis at various points within this thesis, detailing locations, redshifts and discovery references for each object. I also indicate for which chapters within the thesis the host galaxies are used.

The majority of the sample of SLSN host galaxies used throughout this work were selected based upon the availability of high resolution *HST* imaging of the host galaxies at ultraviolet wavelengths. For the work within this thesis, an early[1] sample of SLSN host galaxies were identified from the work of Neill et al. [2011],

[1]relative to the study of SLSNe

and these host galaxies, supplemented with a few additional SLSN hosts whose SN discoveries had been published prior to early 2012, were targeted for *HST* imaging at rest frame ultraviolet and near infrared wavelengths within the program GO 13025 (PI: Levan). For the work contained within Chapter 3, only these host galaxies are considered (i.e. only targets observed within proposal GO-13025). However, for the work undertaken within Chapter 4, in order to include a larger sample of host galaxies for this analysis, additional SLSN hosts were sourced from other programs which had become publicly available following the publication of the work within 3. These additional *HST* rest-frame ultraviolet images comes from proposals GO-13022, GO-13026 and GO-13858, and are indicated within Table 2.1. Finally, to mitigate small number statistics when performing additional offset analysis within Chapter 4, an extra sample of SLSN-IIn hosts were sourced from Perley et al. [2016], which are detailed at the bottom of Table 2.1.

Table 2.1: SLSN host galaxies used throughout this thesis. References: [1] Richardson et al. [2002] (classification uncertain), [2] Hamuy et al. [2003], [3] Gal-Yam [2012], [4] Schmidt et al. [2000], [5] Quimby et al. [2007], [6] Smith et al. [2007], [7] Ofek et al. [2007], [8] Leloudas et al. [2012], [9] Barbary et al. [2009], [10] Gal-Yam et al. [2009], [11] Chatzopoulos et al. [2011], [12] Miller et al. [2009], [13] Gezari et al. [2009], [14] Drake et al. [2010], [15] Quimby et al. [2011c], [16] Inserra et al. [2013], [17] Quimby et al. [2010], [18] Quimby et al. [2011a]. [19] Nicholl et al. [2013], [20] Moriya et al. [2015], [21] Chomiuk et al. [2011], [22]McCrum et al. [2015], [23] Lunnan et al. [2014], [24] McCrum et al. [2014], [25] Perley et al. [2016]. Note that PTF10hgi and PTF11rks are also sometimes referred to by their IAU designations of SN 2010md and SN2011kg respectively. Hosts below dividing line are not covered by *HST* but are used for additional offset analysis within Chapter 4.

SLSN	$M_{\rm peak}$	Class[2]	RA J2000	Dec J2000	z	Ch.	Disc. Ref.
SN1995av	-20.87 (R)	LSN-IIn	02:01:41.34	+03:39:38.9	0.300	3,4	[1]
SN1997cy	-20.1 (R)	SN-Ia/IIn	04:32:54.86	- 61:42:57.5	0.063	3,4	[2]
SN1999as	-21.4 (V)	SLSN-R	09:16:30.86	+13:39:02.2	0.127	3,4	[3]
SN1999bd	-21.5 (V)	SLSN-IIn	09:30:29.17	+16:26:07.8	0.151	3,4	[3]
SN2000ei	-20.57 (R)	LSN-IIn	04:17:07.18	+05:45:53.1	0.600	3,4	[4]
SN2005ap	-22.7 (R)	SLSN-I	13:01:14.83	+27:43:31.4	0.283	3,4	[5]

[2]Here events which lie brighter than M_V<-21 are distinguished as SLSN events and those which fall fainter than M<-21 are identified as LSN events. Peak magnitudes and associated bands as reported within the discovery literature are provided.

SN2006gy	-22.0 (R)	SLSN-IIn	03:17:27.06	+41:24:19.5	0.019	3,4	[6,7]
SN2006oz	-21.5 (u)	SLSN-I	22:08:53.56	+00:53:50.4	0.286	3,4	[8]
SCP06F6	-22.5 (i)	SLSN-I	14:32:27.395	+33:32:24.83	1.189	3,4	[9]
SN2007bi	-21.3 (R)	SLSN-R	13:19:20.19	+08:55:44.3	0.128	3,4	[10]
SN2008am	-22.3 (z')	SLSN-IIn	12:28:36.30	+15:34:50.0	0.234	3,4	[11]
SN2008es	-22.2 (V)	SLSN-II	11:56:49.13	+54:27:25.7	0.202	3,4	[12,13]
SN2008fz	-22.3 (V)	SLSN-IIn	23:16:16.60	+11:42:47.5	0.133	3,4	[14]
SN2009jh	-22.0 (R)	SLSN-I	14:49:10.09	+29:25:10.4	0.349	3,4	[15]
PTF09atu	-22.5 (V)	SLSN-I	16:30:24.55	+23:38:25.0	0.501	3,4	[15]
PTF09cnd	-22.0 (V)	SLSN-I	16:12:08.96	+51:29:16.0	0.258	3,4	[15]
SN2010gx	-21.7 (R)	SLSN-I	11:25:46.71	-08:49:41.4	0.230	3,4	[8,15]
PTF10hgi	-20.3 (V)	LSN-I	16:37:47.00	+06:12:32.3	0.10	3,4	[16]
PTF10vqv	-22.5 (V)	SLSN-I	03:03:06.80	-01:32:34.9	0.45	3,4	[17]
SN2011kf	-21.73 (g)	SLSN-IIn	14:36:57.53	+16:30:56.7	0.245	3,4	[16]
SN2011ke	-21.42 (g)	SLSN-I	13:50:57.77	+26:16:42.8	0.385	3,4	[16]
PTF11dsf	-22.1 (V)	SLSN-IIn	16:11:33.55	+40:18:03.5	0.143	3,4	[18]
PTF11rks	-20.76 (V)	LSN-I	01:39:45.51	+29:55:27.0	0.190	3,4	[16]
SN2012il	-21.56 (V)	SLSN-I	09:46:12.91	+19:50:28.7	0.175	3,4	[16]
PTF12dam	-21.5 (V)	SLSN-R/I	14:24:46.20	+46:13:48.3	0.107	4	[18,19]
iPTF13ehe	-20.97 (g)	SLSN-R/I	06:53:21.50	+67:07:56.0	0.343	4	[20]
PS1-10awh	-21.59 (g)	SLSN-I	22:14:29.831	-00:04:03.62	0.908	4	[21]
PS1-10pm	-21.73 (g)	SLSN-I	12:12:42.200	+46:59:29.48	1.206	4	[22]
PS1-11afv	-21.91 (g)	SLSN-I	12:15:37.770	+48:10:48.62	1.407	4	[23]
PS1-11ap	-21.77 (g)	SLSN-I	10:48:27.73	+57:09:09.2	0.524	4	[24]
PS1-11tt	-21.27 (g)	SLSN-I	16:12:45.778	+54:04:16.96	1.283	4	[23]
PS1-12bmy	-22.64 (r)	SLSN-I	03:34:13.123	-26:31:17.21	1.572	4	[23]
PS1-12bqf	21.122 (r)	SLSN-I	02:24:54.621	-04:50:22.72	0.522	4	[23]
PTF10fel	<-20.5 (V)	LSN-IIn	16:27:31.103	+51:21:43.45	0.235	4	[25]
PTF10heh	-21.2 (V)	SLSN-IIn	12:48:52.05	+13:26:24.5	0.337	4	[25]
PTF10jwd	-21.4 (V)	SLSN-IIn	16:43:43.325	+44:31:43.8	0.477	4	[25]
PTF10qwu	-21.0 (V)	SLSN-IIn	16:51:10.572	+28:18:07.62	0.225	4	[25]
PTF10scc	-21.5 (V)	SLSN-IIn	23:28:10.495	+28:38:31.10	0.242	4	[25]
PTF10yyc	-21.0(V)	SLSN-IIn	04:39:17.297	-00:20:54.5	0.214	4	[25]
PTF12epg	-21.3 (V)	SLSN-IIn	12:55:36.596	+35:37:35.79	0.342	4	[25]
PTF12gwu	-21.4 (V)	SLSN-IIn	15:02:32.876	+08:03:49.47	0.275	4	[25]

2.2 Photometric Observations

I will first describe the observations which provide many of the key results for the work undertaken within this thesis, high resolution *HST* observations of SLSN host galaxies, before detailing additional photometric ground based observations used to supplement the work undertaken within Chapter 3. Finally, I will outline the SLSN discovery images used for astrometric purposes within the science chapters.

2.2.1 HST Observations

The unmatched sensitivity and resolution of the Hubble Space Telescope and Wide Field Camera 3 (WFC3) make it the ideal instrument to begin to unravel the mysteries of the faint and, in some cases, undetected host galaxies of SLSNe. *HST* WFC3 images were initially obtained for an early sample of 21 SLSN host galaxies, within program GO 13025 (PI: Levan). To explore the star forming properties of these host galaxies, observations were obtained in the rest-frame UV, probing the approximate rest-wavelength range of 2500 - 3500 Å, utilising the F275W ($z < 0.1$), F336W ($0.1 < z < 0.3$) and F390W ($0.3 < z < 0.6$) filters depending upon the redshift of the host in question.

In order for the stellar mass of the host galaxies to be studied, each orbit in the program also switched from the UV to nIR channel within WFC3, enabling short nIR exposures ($\sim$ 200s) to be obtained. Despite their brief duration, such observations are competitive with much longer ground based observations, reaching limits of $H_{AB} \sim 25$ (3σ). Within GO-13025, additional UV observations were obtained of the well studied SLSN, SCP 06F6 [Barbary et al., 2009; Gänsicke et al., 2009] at $z = 1.19$. For this particular event 3 orbits were used to obtained imaging using ACS/WFC in the F606W band (matching the rest frame UV wavelength of the host galaxy).

Some of the host galaxies observed within program GO 13025 were undetected in these exposures, implying that the underlying hosts possessed extremely faint absolute magnitudes ($M_{nIR} > -15$). A handful of these undetected hosts were also targeted by a second programme (GO-13480; PI Levan), which obtained much deeper optical observations ($\sim$ 5000 s) using ACS in F606W and WFC3 again in the nIR. A full log of all of these UV, nIR and optical observations are provided within Tables 2.2, 2.3 and 2.4 respectively. Inclusive of the deeper latter imaging, 18/21 of the original SLSN host sample imaged with *HST* were detected with the rest frame UV imaging, and 19/20 in the nIR imaging. The hosts of some of the undetected SLSNe in the initial observations were recovered in the deeper GO-13480

exposures. Hence, there are host detections in at least a single band for 96% of the *HST* observed sample (all SLSNe excluding PTF09atu).

For the study of sub galactic environments of SLSN events, additional observations of SLSN hosts at rest-frame UV wavelengths were sourced from publicly available studies GO-13022 (PI: Berger) and GO-13326 (PI: Lunnan). These programs targeted hydrogen poor SLSN host galaxies from within the PanSTARRS Medium Deep Survey (PS1/MDS) for rest-frame UV and rest-frame optical imaging, some of which were undetected in data from ground based surveys. Observations of two SLSN-R host galaxies were also obtained from program GO 13858 (PI: De Cia), a programme originally dedicated to targeting the locations of local PISN candidates at UV and optical wavelengths. I utilise only the UV observations from these programs, which are also described within Table 2.2.

2.2.2 Ground Based Observations

The *HST* data for several SLSNe within the original GO 13025 sample were supplemented additional optical observations obtained from the ground with the William Herschel Telescope (WHT) and the Very Large Telescope (VLT). These included a service mode programme using ACAM on the WHT (Program ID: SW2012b31, PI: Levan) to obtain relatively shallow optical imaging (∼1500 - 1800s in the sdss r′ band) for a small sample of SLSN hosts (namely SN 1995av, SN 2000ei, SN 2006oz, SN 2008es, PTF09atu, PTF09cnd, PTF10hgi, PTF10vqv, PTF11dsf and PTF11rks).

R-band imaging was also acquired for three galaxies from this sample (namely the hosts of SN 2005ap, SN 2008fz and SN 2009jh) using the FOcal Reducer and low dispersion Spectrograph [FORS2; Appenzeller et al., 1998] on the VLT during the nights of 2013-08-31, 2014-01-24 and 2014-02-01 (Program 092.D-0815(B), PI: Levan). For each host 239 second images were obtained within R-band. Faint unresolved detections of each host galaxy were recovered within these images.

The work within Chapter 3 also benefits from deep optical imaging of the two faintest targets in the low-z sample (SN 2008es and SN 2008fz) using the Low Resolution Imaging Spectrometer [Oke et al., 1995] on the the Keck I 10m telescope, during the night of 2013-12-04 (Program C247LA, PI: Perley, *private communication*). These deeper observations consisted of both B-band and R-band images, with exposure times detailed within Table 2.5. Once again faint, unresolved detections of the host galaxies of both targets in both filters were recovered within the images. All reduction and analysis for these Keck images was performed by Daniel Perley.

Table 2.2: SLSN host galaxies imaged with *HST* at rest frame UV wavelengths. The UV filter, exposure time and *HST* program ID are provided within this table. I identify host galaxy imaging used for analysis within Chapters 3 and 4 with a $\star$ and † symbols respectively.

SLSN	UV Filter	$T_{\rm exp}$ UV (s)	GO Program ID
SN1995av *	F390W	1808	13025
SN1997cy *	F275W	1832	13025
SN1999as *†	F336W	2032	13025
SN1999bd *†	F336W	2036	13025
SN2000ei *†	F390W	1808	13025
SN2005ap *†	F390W	1804	13025
SN2006gy *†	F390W	932	13025
	F275W	846	13025
SCP06F6 *†	F606W	8054	13025
SN2007bi *†	F336W	1808	13025
SN2008am *†	F336W	1808	13025
SN2008es *†	F336W	1824	13025
SN2008fz *†	F336W	2032	13025
SN2009jh *†	F390W	2044	13025
PTF09atu *	F390W	2036	13025
PTF09cnd *†	F390W	2224	13025
SN2010gx *†	F390W	1808	13025
SN2011kf *	F336W	2036	13025
SN2011ke *†	F336W	2044	13025
PTF11dsf *†	F390W	1832	13025
PTF11rks *†	F336W	1804	13025
SN2012il *†	F336W	2036	13025
PTF12dam†	F336W	984	13858
iPTF13ehe†	F625W	2545	13858
PS1-10awh†	F606W	680	13022
PS1-10pm†	F606W	1960	13022
PS1-11afv †	F606W	1960	13022
PS1-11ap †	F475W	2464	13226
PS1-11tt†	F606W	1960	13022
PS1-12bmy†	F814W	2224	13226
PS1-12bqf†	F475W	2200	13326

Table 2.3: SLSN host galaxies imaged in the nIR with *HST* used for analysis within chapters 3 and 4 in this thesis. The filter, exposure time and *HST* program ID for each set of observations is provided. All images are used within Chapter 3, but those also used within Chapter 4 for pixel statistics are highlighted with a † symbol.

SLSN	nIR Filter	$T_{\rm exp}$ nIR (s)	GO Program ID
SN1995av	F160W	206	13025
SN1997cy	F160W	206	13025
SN1999as†	F160W	206	13025
SN1999bd†	F160W	206	13025
SN2000ei†	F160W	206	13025
SN2005ap†	F160W	206	13025
SN2006gy†	F160W	206	13025
SN2007bi†	F160W	206	13025
SN2008am†	F160W	206	13025
SN2008es†	F160W	2812	13048
SN2008fz†	F160W	2612	13048
SN2009jh†	F160W	2612	13048
PTF09atu	F160W	206	13025
PTF09cnd†	F160W	206	13025
SN2010gx†	F160W	206	13025
SN2011kf	F160W	206	13025
SN2011ke†	F160W	206	13025
PTF11dsf†	F160W	206	13025
PTF11rks†	F160W	206	13025
SN2012il†	F160W	206	13025

Table 2.4: SLSN host galaxies with additional *HST* imaging in the nIR with *HST* used within Chapter 3 . The filter, exposure time and *HST* program ID for each of these observations is provided.

SLSN	Optical Filter	$T_{\rm exp}$ Optical (s)	GO Program ID
SN2008es†	F606W	5630	13048
SN2008fz†	F606W	5236	13048
SN2009jh†	F606W	5922	13048

Table 2.5: Additional ground based optical imaging used for SED fitting within Chapter 3. Images in the r' filter were obtained with the William Herschel Telescope (WHT), B and R band imaging using the Keck I 10m Telescope and additional R band imaging was obtained with Very Large Telescope (VLT).

SLSN	Optical Band	$T_{\rm exp}$ opt. (s)	Telescope/ Instrument	Program ID
SN1995av	r′	1500	WHT ACAM	SW2012b31
SN2000ei	r′	1500	WHT ACAM	SW2012b31
SN2005ap	R	240	VLT FORS2	092.D-0815(B)
SN2006oz	r'	300	WHT ACAM	SW2012b31
SN2008es	r′	1800	WHT ACAM	SW2012b31
	R	870	Keck LRIS	C247LA
	B	900	Keck LRIS	C247LA
SN2008fz	R	1290	VLT FORS2	092.D-0815(B)
	B	1475	Keck LRIS	C247LA
SN2009jh	R	240	VLT FORS2	092.D-0815(B)
PTF09atu	r′	1500	WHT ACAM	SW2012b31
PTF09cnd	r′	1500	WHT ACAM	SW2012b31
PTF10hgi	r′	1500	WHT ACAM	SW2012b31
PTF10vqv	r′	1500	WHT ACAM	SW2012b31
PTF11dsf	r′	900	WHT ACAM	SW2012b31
PTF11rks	r′	1800	WHT ACAM	SW2012b31

2.3 Analysis Techniques

2.3.1 Sub-pixel Sampling and Dithering

The major advantage to space based observations, such as those obtained with *HST*, is the removal of seeing affects due to turbulence in the Earth's atmosphere. This significantly improves the resolution of the point spread function (PSF) of the resulting image, transitioning from a seeing dominated case, to one in which space-bourne instruments may, in principle, reach the diffraction limited regime. Whilst this may sound like a significant improvement upon the quality of the incoming data, there are additional resolution restrictions enforced by the detectors used by space based instruments. Frequently the pixel scale of the primary science instrument's CCD under samples the width of the PSF.

One solution to this conundrum lies in the ability to accurately offset the telescope spatially by small increments. Dithering is the practice of shifting the detector such that sky coordinates within the field of view land on different detector co-ordinates, and is typically used to negate the effects of bad pixels and CCD defects. When these detector shifts are much smaller than the relative scale size of the detector pixels with non-integer deviations of the telescope pointing (i.e. dithering at a sub-pixel level), the target is moved through a number of different locations on the detector chip. This allows for the recovery of some of the information lost through undersampling the PSF, as each separate sub-dithered imaged now samples it. The dither pattern employed directs the level to which the PSF is sampled, with 4 dither pointings recovering the majority of the information contained within the image. Unfortunately, the final combination of these dithered images to produce a better sampled final PSF is a non-trivial task.

Drizzling

To some, this may merely suggest typical British weather conditions[3], however, to the astrophysical community, drizzling is a method of reconstructing sub-pixel dithered images.

Drizzling [Fruchter and et al., 2009] combines two different image reconstruction methods; "interlacing" and the "shift-and-add" method. Interlacing, as it's name suggests, alternates the placing of pixels from two or more input images within the CCD grid, such that the final output is a uniformly woven "mesh" of these input images. Whilst this technique naturally mitigates the affects of bad

[3]Or perhaps the practice of moistening sponge-based confectionary with slightly sweetened citrus juice

or hot pixels within the CCD chip, any small errors within the positioning of the telescope or any geometric distortion of the image by the telescope optics become apparent when combining images this way. The "shift-and-add" method on the other hand takes each input pixel from the dithered images and moves it into location within a finer sub-sampled grid on the final output image, simply summing the sub-pixel inputs to determine the value of each final output pixel. Whilst the absolute positions of the dither locations are less consequential using this method, the resulting image is still convolved to the scale of the original detector pixel.

Variable-pixel linear reconstruction, or more colloquially, "drizzling", attempts to alleviate the issues inherent to the previous two techniques. As with the "shift-and-add" technique, pixels from the original dithered images are mapped onto a subsampled output grid, in which the user may specify the final size of the output pixels. However, drizzle allows the user to shrink the size of the input pixels relative to the final output pixels. This parameter, known as the PIXFRAC, runs between 0 and 1, permitting the user to dictate the degree to which pixels are convolved with the PSF of the detector (although it should be noted that setting the PIXFRAC too small will result in some output pixels receiving no data from input pixels, [Gonzaga and et al., 2012]).

These shrunken pixels are then drizzled onto the output grid of pixels, accounting for any shifts or rotations in the input frames, and the optical distortion of the camera. The flux contained within each of the input pixels is proportionally divided between the output pixels depending upon the fractional overlap of the input pixel. Consequently, this introduces correlated noise to the final uncertainties of each pixel values, which is discussed later in this section.

Drizzling may be easily performed for *HST* images using AstroDrizzle software [Fruchter and Hook, 2002] within PyRAF, which I do for all of the *HST* images used within this thesis. Given the $\geq$4 dither positions employed for all of the WFC3/UVIS and ACS images used within this thesis, I drizzle these UV images to a final pixel scale of $0.025''$ pix^{-1}, whilst for the nIR images used I retain the native $0.13''$ pix^{-1} scale due to the lack of dithering.

Within the UV data set, images are subject to greater Charge Transfer Efficiency (CTE) losses, which arise due to inefficient transfer of charge between pixels during CCD readout, a consequence of cumulative radiation damage in a low Earth orbit environment [Bourque et al., 2013]. To mitigate against this, all early images taken under programme GO-13025 utilised a pre-flash to fill charge traps. In the latter observations of this program, and indeed for all of the UV observations taken within programs GO-13022 and GO-13026, sources were additionally relocated to

the corners of the UVIS chip to minimise the number of transfers employed before readout. The final individual images were then cleaned for CTE tails using the method of Anderson and Bedin [2010] prior to drizzling.

The UV images were also re-drizzled again to match the plate scale of the nIR imaging ($0.13''$ pix^{-1}). Though this lowers the resolution of the image, the technique allows for easier detection of low surface brightness features, and for a direct comparison between the nIR and UV imaging used within both Chapters 3 and 4.

Correlated Noise

A consequence of combining dithered images through drizzle is the correlation of noise between adjacent pixels due to the way in which the flux is spread over multiple output pixels. This not only produces an underestimate of the measurement of the noise in an object within the final drizzled image on the output pixel scale, but also creates uncertainty on the measurement on an individual pixel. As demonstrated within Figure 2.1, for any given input pixel, covering areas a,b,c,d etc within the final output pixel plane, the noise contained within the entirety of the input pixel is greater than the sum of that contained within the fractional areas in the output pixel, as the cross terms caused by the division of flux with neighbouring pixels cannot be incorporated in the error measurement of any one pixel (i.e. $(a^2+ b^2+ c^2+ d^2)\epsilon^2<\epsilon^2$).

The noise correlation ratio, R, depends upon the drizzle parameters chosen and the geometry and orientation and geometry of the dithered input images. The full derivation of this parameter is beyond the scope of this work, however it is useful to note that it may be simplified to the following expression:

$$\begin{aligned} R &= \frac{r}{1-\frac{1}{3r}} \quad \text{for } r \leq 1 \\ &= \frac{r}{1-\frac{r}{3}} \quad \text{for } r \geq 1 \end{aligned} \tag{2.1}$$

where r is the ratio of the pixfrac value used within drizzling and the pixel scale of the output image.

2.3.2 Photometry

Photometry throughout this thesis was performed using one of two different methods, dependant upon the appearance of the host galaxy within the observations. Where possible (i.e. for galaxies which are clearly detected within their images) I

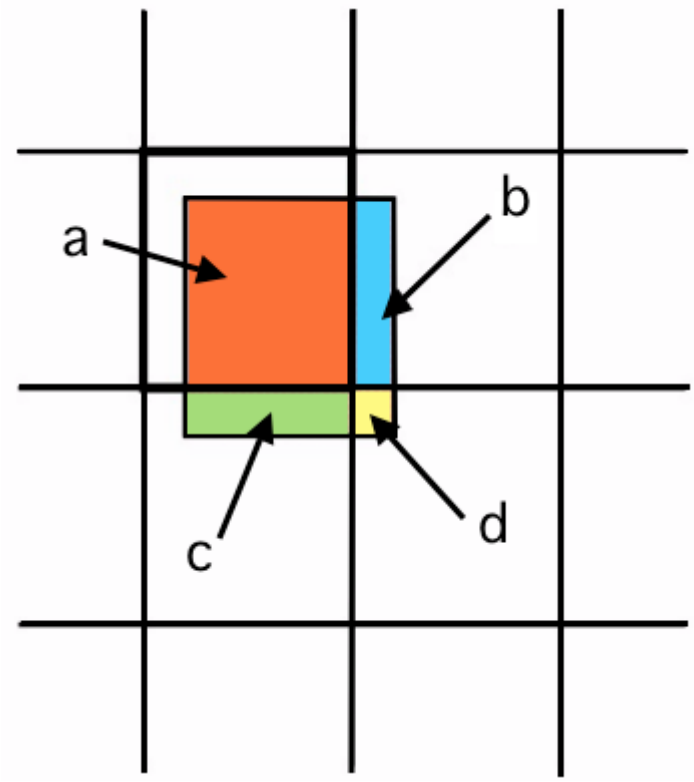

Figure 2.1: Adapted from Fruchter and et al. [2009], a representation of an input pixel being dropped into the output pixel frame. The regions a,b,c and d represent the overlapping regions of the input pixel with pixels in the output frame. This overlap causes an underestimation of the error associated with any one pixel, as the cross terms caused by the division of flux with neighbouring pixels cannot be incorporated.

used the automatic detection and extraction package, Source Extractor [here after SExtractor; Bertin and Arnouts, 1996]. The key advantage of using SExtractor for photometry is the ultimate production of a 'segmentation map', in which different groups of pixels are identified as belonging to different astronomical objects within the image. This is a particular bonus when considering diffuse objects, or to ensure the incorporation of low surface brightness features when performing photometric analysis.

The SExtractor process (outlined briefly here, for a more complete overview, see Bertin and Arnouts [1996]) first creates a background map from the input image, using iterative sigma clipping to estimate it's level and applying a median filter to account for any potential overestimations from bright sources in the field. Once background subtracted, the image is then convolved with an input PSF profile before object identification begins. A user-specified detection threshold (typically number of σ above the background) and limits on the number of adjoining pixels an object should have before triggering a detection are applied before object extraction.

For each object extracted from the image, the pixel group is passed through a deblending filter which attempts to separate any overlapping objects contained within it. It does so by creating a 2-dimensional brightness profile for the extracted object then, working from the brightest points downward, searches for 'saddles' between peaks in the brightness profile. At each saddle point the program determines whether the intensity contained within the peak above the saddle point is greater than a user-specified fraction of the total intensity of the composite object. If this is so, the peaks (and their surrounding pixels) are identified as two separate objects. The algorithm continues to move downwards through the brightness profile, searching for new saddle points (treating any identified objects individually). This is schematically represented within Figure 2.2.

Once de-blending has commenced, SExtractor will then determine the positional parameters (location of the peak, isophotal centre, barycentre, size, ellipticity etc.) of each of the identified objects before photometric measurements are performed. The user may specify whether they require isophotal magnitudes or aperture magnitudes, with the option for corrections to be applied if attempting to account for additional light which may be outside of the notional aperture.

Thus for each host galaxy the program parameters were adjusted accordingly to optimise its detection and extraction within the image, and since I was concerned with individual galaxies this means that blending decisions were made manually. For the *HST* data set I applied a surface brightness signal to noise cut of two per pixel for nIR images and one for UV images, in order to include faint surface brightness

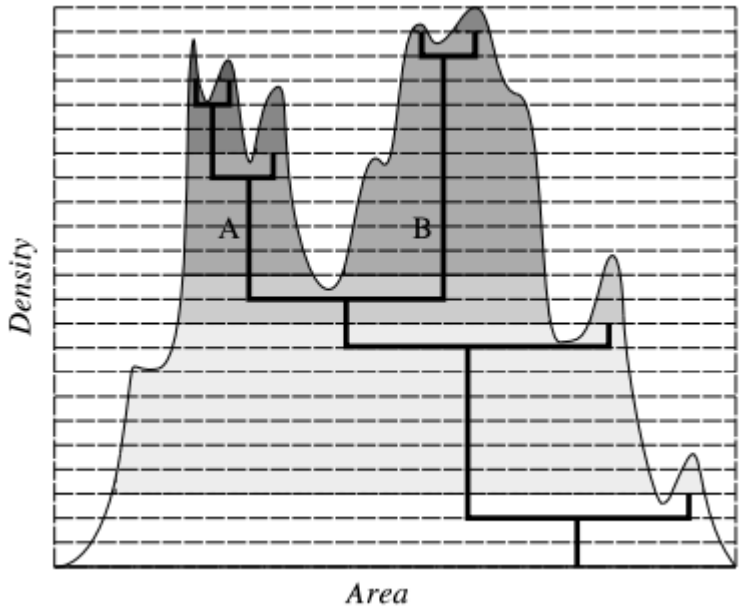

Figure 2.2: Figure taken from Bertin and Arnouts [1996]; a schematic representation of the method used to identify separate objects during the deblending process. The 2D brightness profile of the pixel group (smooth line) is analysed - the program works in a top-down fashion, searching for saddles in the brightness profile. If the integrated brightness of the peak above the saddle point in found to exceed a specified fraction of the total brightness of the input pixels, the peak (and neighbouring pixels) are regarded as separate from the rest of the profile. Here the input object has been broken into two separate objects, A and B.

features, measuring the host galaxy magnitudes using the `MAG_AUTO` feature, which provides are the most precise estimate an objects total magnitude using a flexible elliptical aperture around the object and measuring the flux contained within it [Kron, 1980]. For these *HST* images, zeropoints for each filter were taken from the STScI WFC3 handbook [Dressel, 2012].

It should be noted that some of the photometry produced within SExtractor provides extremely small photometric errors, occasionally as low as $\sim$1/1000 of a magnitude. Such unrealistic errors are a result of using "weight maps" for the extraction of sources from the science frame. A weight map is a combination of weight images from the individual dithered inputs containing information on the location of bad pixels within the image produced during the drizzle process, [Gonzaga and et al., 2012]. Whilst the use of weight maps for object extraction is beneficial for better photometric detection of faint sources, they produce problems with the way in which SExtractor computes photometric errors.

SExtractor takes the inverse of the drizzled weight map (which thus creates a lower significance for highly weighted pixels and vice versa) and then uses this map to scale the variance that the program itself measures within the science frame [Bertin and Arnouts, 1996]. Thus the resulting noise associated with most pixels is lower than it should be (as pixels of a high weighting become low in variance within SExtractor's error algorithm). This underestimation becomes more apparent in sources which have an intrinsically higher S/N. Whilst the side-effects of using a weight map for object extraction affects the photometric uncertainties of all SLSN within our sample, this should not significantly impact upon the conclusions drawn from the results presented within this thesis.

Several galaxies showed a light distribution dominated by individual bright knots in UV imaging, and the deblending parameters were adjusted for each host to ensure it was not broken into multiple components. Where possible, the nIR images were used to determine which UV components should be included in the analysis, as these bands are dominated by a smoother light profile arising from an older stellar population.

I also utilised straightforward aperture photometry, particularly for cases in which the host galaxy was either undetected within the image, or for cases in which the SExtractor deblending was insufficient to reconcile to the various components of a particularly diffuse host. When doing this, I typically set large apertures (>1.4 FWHM) to encompass the majority of the light of the galaxy, and determine the background via the use of a large number (>20) of sky apertures. This technique gave results consistent with those determined via SExtractor, and was used to obtain

3σ limits where necessary. In cases in which I employ aperture photometry, I apply aperture corrections determined by the estimated encircled energy curves of WFC3 detectors [Dressel, 2012]. In the event of a host detection in one *HST* band but no detection in another, the size of the aperture used to determine the upper limit was set equal to that used to measure the magnitude in the band where the source was detected.

Additional photometry of hosts imaged using the WHT and VLT in r' and Johnson-Morgan R bands respectively was carried out in a like manner to the *HST* images, applying a surface signal to noise cut off of one per pixel before extraction with SExtractor. Photometry of galaxies on ground based images was carried out relative to SDSS observations of the same field, and is given in the r' band.

For all photometric results here I perform a K-correction. This allows for the photometric comparison of objects at different redshifts which have been observed within a single bandpass (which will only cover a fraction of the total light emitted by the object). As objects move to higher redshifts, their spectral energy distribution becomes stretched by a factor of $1 + z$, such that as an object moves to higher redshifts, observations within the same photometric band will sample progressively bluer parts of the spectrum. A K-correction corrects for this by converting the flux measurement in the observer frame into an equivalent measurement of that flux in the rest frame of the object.

Normally filter-matching must also be performed, where a redder filter is selected which corresponds to the approximate wavelength coverage and sensitivity of the filter the observations were taken with, but in the rest frame wavelength of the observed object. If the Spectral Energy Distribution (SED) of the object is known (for instance, a blackbody spectrum), then a K-correction is determined in two stages: by integrating the redshifted SED over the redder bandpass and then by integrating the same SED as seen at zero redshift over the band passes of interest to the observer to produced two expected fluxes. The K-correction is thus computed as:

$$K = -2.5 \log \frac{F_{\mathrm{z}=0}}{F_{\mathrm{z}}}$$

Where $F_{\mathrm{z}=0}$ and F_{z} are the expected fluxes at zero redshift and at the redshift of the object. If multi-wavelength photometry of the object exists, then the observer fits this photometry to a model SED of choice, before following the above steps. However, if observations are obtained in the observer frame within a filter corresponding the the rest frame wavelength of interest, as there is no energy loss

due to redshifting then the K-correction simply becomes:

$$K = -2.5 \log (1 + z)$$

as the difference between the expected fluxes is diluted by a factor of $1 + z$.

All photometry within this thesis was also corrected for Galactic extinction using the Milky Way dust maps of Schlafly and Finkbeiner [2011] (via the NASA/IPAC Infrared Science Archive[4]) for the appropriate image filter and adheres to the AB magnitude system.

2.3.3 Astrometry

In order to identify the host and accurately pinpoint the location of the SLSN event within the galaxy for sub-galactic analysis within Chapter 4, where possible, I performed astrometry measurements using optical discovery imaging where the SNe are as close as possible to maximum light. The majority of SLSNe from the sample possess discovery locations such that the SN position lies on, or close to, an underlying host detected within the *HST* imaging.

The images used in this procedure are described in Table 2.6. Astrometric measurements were carried out by aligning the discovery images by WCS for an initial approximation, where possible. A geometric alignment was found between the discovery image and the *HST* images using common sources in the two fields. Using routine IRAF tasks (IMEXAM) I determined the [x,y] centres of multiple matching sources in both discovery and *HST* images, using point sources where available. Using IRAF tasks GEOMAP and GEOXYTRAN I then map and transform between co-ordinate systems for the two images, before transforming the [x,y] co-ordinates for the SN within the discovery image to the corresponding pixel within the *HST* imaging. This allows the SN position to be determined within the *HST* imaging.

Ideally, more than >8-10 matching sources are found between the two images before performing geometric mapping, to minimise the free parameters involved with the fitting of a geometric solution between the two coordinate systems. For some of the SLSN events, the discovery images did not provide a satisfactory number of matching point sources ($< \sim 8$), due to either the depth or field of view of the available within the discovery image. In these cases I reduce the fitting parameters by manually accounting for rotation. This was done by rotating the discovery image to match the orientation of the *HST* image (contained within the image header) before fitting only the scale and offset within the geometric transformation map.

[4] http://irsa.ipac.caltech.edu/applications/DUST/

Table 2.6: Images of the SN whilst visible used for carrying out astrometry and identifying the locations of the SLSN events within their host galaxies. Details for images taken from data archives and literature are outlined here; [1] ESO 59.A-9004(A), Service Mode, NTT , [2] NASA SkyMorph, [3] CADC, [4] Rezman Observatory ,[5] GO-10877, PI: Li ,[6] Barbary et al. [2009],[7] Gal-Yam et al. [2009] ,[8] Chatzopoulos et al. [2011] ,[9] ToO ESO ,[10] Service Mode, NTT ,[11] PTF data archive ,[12] ToO Gemini South, [13] ToO Gemini North, [14] *HST* DDT [15], ToO Keck

SLSN	Instrument	UV[a] X_{err} mas	UV[b] Y_{err} mas	IR X_{err} mas	IR Y_{err} mas	Ref.
SN1999as	ESO NTT	44.22	34.69	37.69	41.17	[1]
SN1999bd * [c]	NEAT/GOEDSS	221.36	52.59	75.65	17.97	[2]
SN2000ei	CFHT	51.84	69.11	45.05	60.06	[3]
SN2005ap* [d]	RezmanI	-	-	-	-	[4]
SN2006gy	HST	5.89	5.78	0.30	0.29	[5]
SCP06F6	*HST*	5.92	4.71	6.37	5.07	[6]
SN2007bi	ESO FORS2 VLT	60.90	32.53	18.10	9.67	[7]
SN2008am	Keck LRIS Blue	68.67	64.37	54.02	43.85	[8]
SN2008es*	ESO FORS2 VLT	29.77	63.15	-	-	[9]
SN2008fz*	ESO NTT	42.40	69.89	13.02	21.47	[10]
SN2009jh*	PTF/P48	55.26	36.46	35.42	23.37	[11]
PTF09cnd*	PTF/P48	66.72	75.37	134.47	137.89	[10]
SN2010gx	GMOS Gemini-S	49.41	45.53	23.60	21.75	[12]
SN2011ke	PTF/P48	47.00	53.74	32.06	36.67	[11]
PTF11dsf	PTF/P48	41.69	97.00	13.61	31.67	[11]
PTF11rks	PTF/P48	39.42	52.70	16.24	21.71	[11]
SN2012il	GMOS Gemini-N	22.04	26.87	27.43	19.55	[13]
PTF12dam	*HST* WFC3	31.56	19.63	12.85	7.99	[14]
iPTF13ehe	Keck LRIS Blue	75.69	56.72	76.80	57.56	[15]
PS1-10awh	GMOS Gemini-N	48.28	61.11	39.22	49.66	[12]
PS1-10pm	GMOS Gemini-N	54.84	73.94	47.33	63.81	[12]
PS1-11afv	GMOS Gemini-N	59.20	70.04	51.93	61.44	[13]
PS1-11ap	GMOS Gemini-N	61.08	62.17	47.99	62.49	[13]
PS1-11tt	GMOS Gemini-N	28.29	52.11	24.61	45.34	[13]
PS1-12bam	GMOS Gemini-S	54.70	51.95	48.73	46.28	[12]
PS1-12bmy	GMOS Gemini-S	57.04	58.22	50.24	51.29	[12]
PS1-12bqf	GMOS Gemini-S	19.28	37.81	12.52	24.55	[12]

[a]Total positional uncertainty in X direction: the star-matched geometric alignment and afterglow centroiding uncertainties added in quadrature.

[b]As above but for Y direction

[c]* = Candidate with <8 astrometric tie points

[d]SN2005ap: Whilst I was able to locate the transient within the *HST* image using this discovery image, image compression prevents the firm ascertain of positional uncertainties for this event. Whilst it may provide a transient location, it cannot be included within the later weighted F_L analysis.

Table 2.7: Table 2.6 continued. Discovery image references are as given in previously.

SLSN	Instrument	UV X_{err} mas	UV Y_{err} mas	IR X_{err} mas	IR Y_{err} mas	Ref.
PTF10fel	PTF/P48	147.03	144.66	-	-	[11]
PTF10heh	PTF/P48	473.80	1059.56	-	-	[11]
PTF10jwd	PTF/P48	186.78	167.79	-	-	[11]
PTF10qwu	PTF/P48	105.98	59.62	-	-	[11]
PTF10scc	PTF/P48	89.15	85.01	-	-	[11]
PTF10yyc	PTF/P48	209.30	119.74	-	-	[11]
PTF12epg	PTF/P48	133.52	77.84	-	-	[11]
PTF12gmu	PTF/P48	129.85	129.85	-	-	[11]

The orientation of both the *HST* and the ground based images are well known, and experience has shown that this approach provides reasonable astrometric fits. SN for which this is the case are highlighted within Table 2.6

In the eventuality that discovery images were not publicly available for any of the *HST* imaged hosts, I was only able to localise the SN position to the discovery RA and Dec, correcting for small offsets in *HST's* WCS solution by aligning it with 2MASS point sources.

Throughout this work I assume a standard ΛCDM cosmology with H_0=71 km s^{-1} Mpc $^{-1}$ and Ω_M=0.27 and Ω_{vac}=0.73 [Larson et al., 2011]. All reported magnitudes are given in the AB system and uncertainties are given at a 1σ confidence level, unless otherwise stated.

Chapter 3

A HST Study of Host Galaxies of SLSNe

"What light through yonder galaxy breaks?"
—William Shakespeare, *Romeo and Juliet, Scene II*
(adapted by C.R. Angus)

3.1 Introduction

As we have seen within Chapter 1, the progenitors of SLSN events are poorly constrained through modelling of their explosion parameters, thus the study of host galaxies provides a valuable route to accessing progenitor information.

The earliest study of the host galaxies of SLSNe by Neill et al. [2011] found them to be exceptionally faint and blue, compared to a sample of field galaxies, although this study was limited by the depth of the observations (GALEX and SDSS), with a large fraction (approximately ∼47%) of the more recently discovered, better characterised, but more distant SLSNe yielding only upper limits for their hosts in the UV and optical. With increasing numbers of these transients being detected within ongoing time resolved, wide field, transient surveys such as the Panoramic Survey Telescope And Rapid Response System (Pan-STARRS, Kaiser and Pan-STARRS Team 2005), Palomar Transient Factory (PTF, Law et al. 2009), and Catalina Real Time Survey (CRTS, Drake et al. 2009b), it has become clear that further observations of SLSN hosts are required in order to characterise these elusive transient environments.

There have been several studies of SLSN hosts prior to this work. Lunnan

et al. [2014] have shown that Type-I SLSN hosts, when compared to the host galaxies of other core collapse events such as "normal" CCSNe and LGRBs, are less luminous and less metal rich than those of the general SNe population, but do exhibit comparable metallicities to the hosts of LGRBs, suggestive of similarities of progenitor between these two classes of event. Alternatively, the study of Mg and Fe absorption lines in handful of SLSN hosts by Vreeswijk et al. [2014], seems to suggest different progenitor paths for SLSN and LGRB events, due to the lower absorption strengths observed in SLSNe environments than in GRB hosts. A spectroscopic study of the hosts of SLSNe carried out by Leloudas et al. [2015] has shown the hosts of Type-I and Type-R events to possess extreme emission lines (Extreme Emission Line Galaxies), in contrast to SLSN-II hosts, which have comparatively softer radiation fields. The authors use this to support the notion of different progenitor systems for Type-I and Type-II events, advocating a massive, population III-like progenitor for H-poor SLSNe. This is, however, contrary to the analysis of those who subscribe to a magnetar powered progenitor model [e.g. Lunnan et al., 2014; Inserra et al., 2013], for which a slightly less massive progenitor [$>40M_{\odot}$, Davies et al., 2009] would suffice. Although the samples presented by Lunnan et al. [2014] and Leloudas et al. [2015] have limited overlap, their distributions in metallicity are rather different, perhaps explaining the disparate conclusions.

By turning to high resolution imaging of SLSN hosts, particularly including those previously undetected within ground based observations, we may find a new insight into these environments and hence their underlying stellar populations. Through comparison of SLSN hosts with the hosts of LGRBs, we may begin to discriminate between SLSN progenitor models (e.g. if SLSN host galaxies and LGRB host galaxies are similar, then given the similarity of the Internal Engine model to the Collapsar model of LGRBs, this might favour this particular model for SLSN production). By doing this using *HST* observations, any biases due to the inherent brightness of the host sample are significantly reduced.

In this chapter I present results from our survey of the hosts of SLSNe with the *Hubble Space Telescope* (*HST*) in the UV and nIR, complemented by a modest ground based programme of optical observations. These observations, outlined within Chapter 2, provide a view of the ongoing star formation via deep rest-frame UV observations, as well as a handle on any older populations within the hosts, substantially expanding the wavelength baseline with respect to earlier surveys. In this chapter I will focus on the broadband photometric properties of the host galaxies, demonstrating their origin in extremely small, low mass, and likely metal poor, systems.

3.2 Sample

Here I use nIR and rest-frame UV observations of a sample of 21 SLSN host galaxies, identified within Table 2.1, within a redshift range of $0.019 < z < 1.19$ (SN 2006gy $\rightarrow$ SCP 06F6).

This *HST* sample (programme GO-13025; PI: Levan) comprised 21 targets, based on the sample of Neill et al. [2011], supplemented with luminous SNe from the literature (up to Jan 2012). This selection pre-dated more detailed sample work, such as that by Gal-Yam [2012] which introduced a cut at $M_V < -21$ for a SNe to be considered superluminous. In particular, several of the original sample, while significantly more luminous than typical SNe, were rather fainter than $M_V < -21$, based on the reported magnitudes and hence would be classed as luminous supernovae (LSNe) rather than SLSNe. However, it should be noted that early examples such as SN 1995av, SN 1997cy and SN 2000ei have extremely limited follow-up, and hence poorly know peak magnitudes, making their true nature uncertain. They are therefore conservatively assigned as LSN in the absence of a detection of the SNe at a magnitude of $M_V < -21$. Additionally, the nature of SN 1997cy remains debated, and it now seems likely that it is a Type Ia-SNe interacting with a hydrogen-rich shell of circumstellar material [see Hamuy et al., 2003]. Hence, SN 1997cy is removed from this sample of SLSNe for comparison with other populations. Other SNe that do not make the peak-luminosity threshold for SLSNe are classified as "LSN", while the unambiguous SLSN sample is then used for the analysis and conclusions within this chapter. This yields a sample of 17 SLSNe and 4 LSNe. Unsurprisingly given the small contamination, the conclusions are not significantly affected by the inclusion (or not) of LSNe.

Table 2.1 lists all of the SNe targets used within this chapter and the distribution of redshifts for this sample is shown in Figure 3.1. Figure 3.1 also shows the redshift distributions of host samples of core collapse SNe discovered in GOODS [see also Dahlen et al., 2003; Fruchter et al., 2006; Svensson et al., 2010] and of GRBs at $z \lesssim 1.5$ [Fruchter et al., 2006; Savaglio et al., 2009; Svensson et al., 2010] . I use these as a comparison sample of core collapse events that should represent both all core collapse systems creating a SNe (the GOODS CCSNe sample) and those occurring from only a restricted range of massive stars (probably those at low metallicity), represented by the GRBs. I also implement a redshift cut at $z \sim 1.5$ on the GRB sample, in order to cover a comparable redshift range to the SLSNe, but not include the many high-z GRBs whose host galaxies may differ because of the cosmological evolution of the galaxy population. Recent work within the field of

GRB hosts has now made it clear that low-z GRBs occur predominantly in smaller, lower-luminosity galaxies than the more distant bursts, probably due to their metallicity dependence, combined with the shifting mass-metallicity relation with redshift [Perley et al., 2013, 2015b; Schulze et al., 2015]. Although this bias manifests itself predominantly below $z \sim 1$ [Perley et al., 2015b] it is possible that should SLSNe and LGRBs both exhibit metallicity bias, but at a different critical metallicity, then we could confuse evolution in galaxy properties with differing environmental constraints. Indeed, the survey of SLSN-I host galaxies reported by Lunnan et al. [2014] does find some evidence for evolution, with lower-z SLSNe occurring in even smaller and lower luminosity galaxies. We note that within the pure SLSN sample, 90% of the SLSN hosts lie at $z < 0.4$. Restricting the comparison samples to these lower redshifts does not impact the nature of the conclusions drawn here, but given the much smaller sample sizes would impact the statistical significance.

Astrometry as detailed within Chapter 2 was performed to identify the hosts within the *HST* imaging. I present mosaics of the nIR and UV observations within in Figures 3.2 and Figure 3.3 (and the imaging of SN 2006gy in three bands shown within Figure 3.4) with the location of the SN marked in each case.[1]

In the case of three SLSNe from this sample, initial astrometric measurements create some ambiguity in the identification of the real host. For SN 2000ei the presence of two galaxies within $\sim 1''$ of the SN position precludes its unique identification. I test the chance probability of association (P_{chance}) that an unrelated galaxy of the same optical magnitude or brighter would be found within the given offset from the apparent host for SN 2000ei from each of these nearby galaxies, using the method outlined within Bloom et al. [2002]. We adopt the host to the south west of the SN location, which has the lowest P_{chance} value ($=4.0\text{x}10^{-3}$), as the true host to SN 2000ei.

Initial astrometric measurements for SN 2006gy suggest that the SN location is coincident with an unresolved "knot" of radiation approximately $\sim 1''$ from the centre of NGC 1260, suggestive of perhaps a much smaller host satellite to the larger galaxy or that the SN continues to contribute strongly, even 8 years after the SN detection (see Figure 3.4). To test this I perform relative astrometry compared to an archival image of the SN, taken in November 2008 using the Wide Field and Planetary Camera 2 (WFPC2) in the F450W band (GO-10877, PI: Li). The SN position was found to be consistent with the centre of the source seen in the F390W observations with a $0.08''$ error circle.

[1]For one of the *HST* hosts for which a discovery image was unavailable (namely SN 1997cy, SN 1999bd, the SN position can only be localised to the discovery RA and Dec, correcting for small offsets in HST's WCS solution by aligning it with 2MASS point sources.

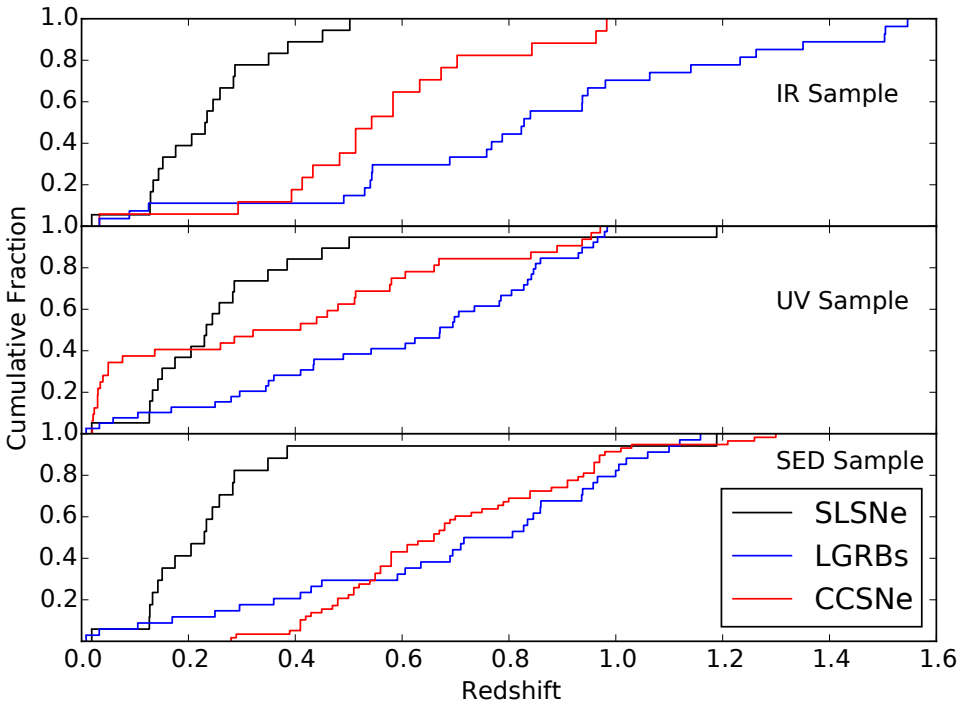

Figure 3.1: Redshift distribution of SLSN hosts used for comparisons in this work. I compare rest-frame IR (top) and UV (middle) properties, as well as masses and star formation rates derived from SED fitting (lower panel). Since these different diagnostics are available for only a fraction of each of the comparison samples the global redshift distribution is less appropriate. Hence the redshift distribution for each sample is shown separately. The SLSN host galaxies are typically at lower redshift ($z < 0.5$) than the GRBs, or than the GOODS CCSNe samples to which I wish to compare. The possible impacts of this selection, and consideration of alternatives are presented in section 5.

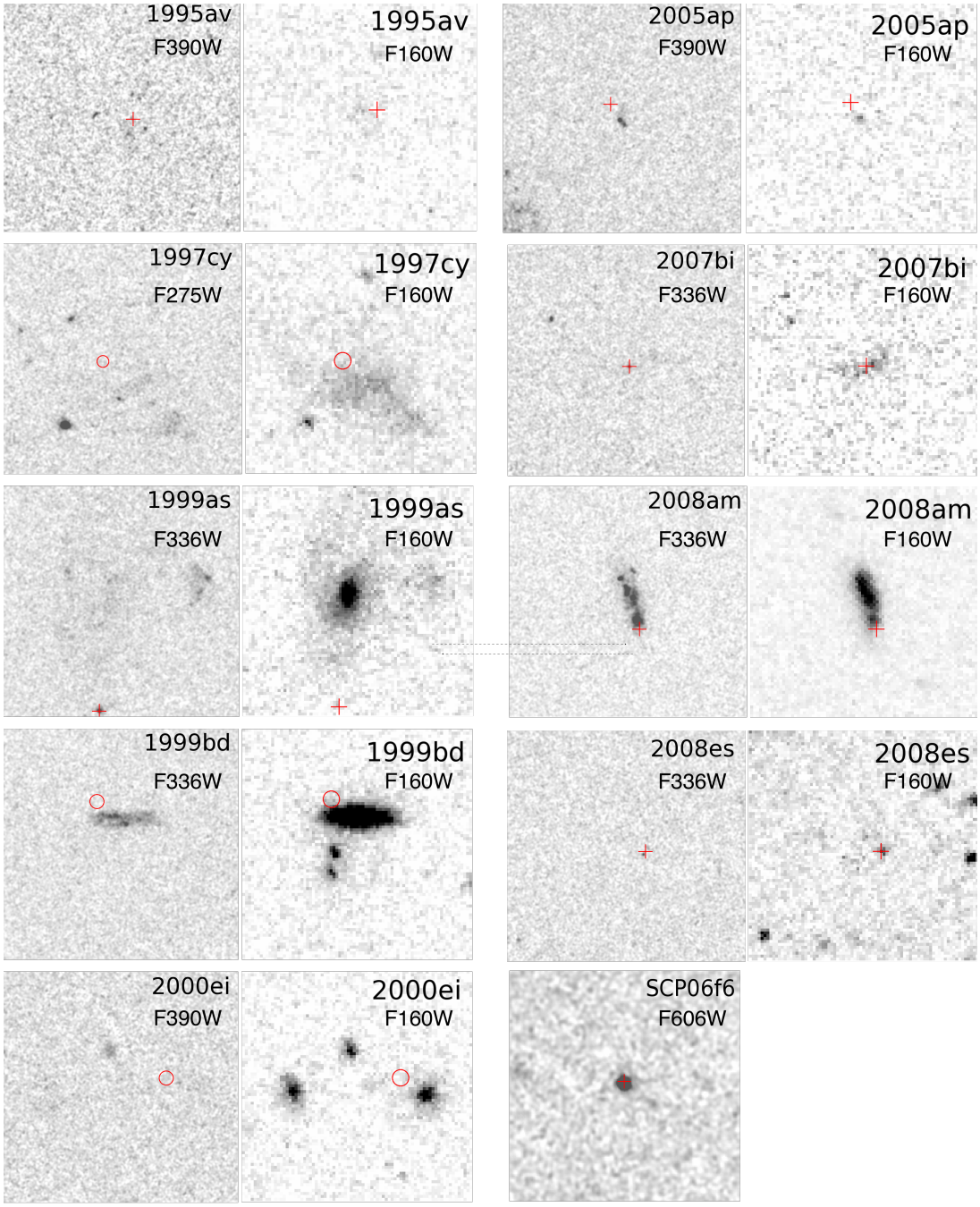

Figure 3.2: Host galaxies of SLSNe imaged in the rest frame UV and the nIR (left and right panels respectively for each object) within *HST* programs GO-13025 and GO-13480. Images (bar SN 2006gy - see Figure 3.4) are scaled to $10'' \times 10''$ and approximate SN positions are marked with red crosses where astrometry has been carried out, or circles located at the discovery co-ordinates of the SNe when discovery images were not available at the time of writing.

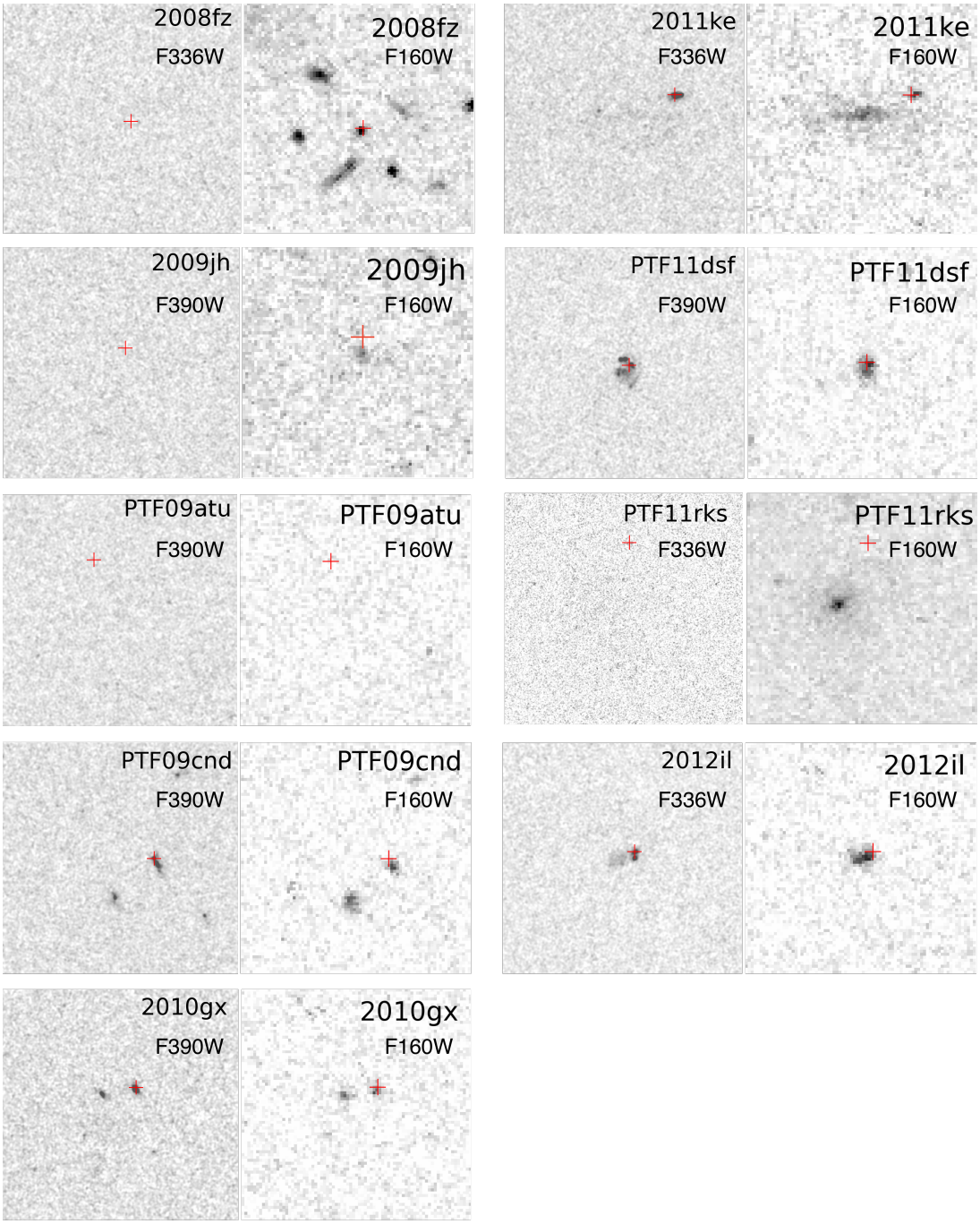

Figure 3.3: Host galaxies of SLSNe imaged in the rest frame UV and the nIR (left and right panels respectively for each object) within *HST* programs GO-13025 and GO-13480. Images (bar SN 2006gy - see Figure 3.4) are scaled to $10'' \times 10''$ and approximate SN positions are marked with red crosses where astrometry has been carried out, or circles located at the discovery co-ordinates of the SNe when discovery images were not available at the time of writing.

Subtraction of a point spread function reveals some possible features around the SN position, however, these could be faint features within the disc of NGC 1270, rather than extension of the source at the location of SN 2006gy. The source magnitude in the imaging of F390W(AB) = 22.6 ± 0.1 corresponds to an absolute magnitude of ~ -11.7, assuming that the source is unresolved (or at least the majority of the light arises from a very compact region) then the size is < 30pc. This size is typical of a globular cluster, but the magnitude in blue light is too bright [e.g. Harris, 1996]. If it were a dwarf galaxy it would be relatively faint [e.g. McConnachie, 2012], but unusually compact. In this case it may be an ultra-compact dwarf, a magnitude fainter than the densest known example, M85-HCC1 [Sandoval et al., 2015], but comparable in size. Given the astrometric coincidence with the SN position it is then perhaps more likely the light continues to be dominated by SN emission (see also Miller et al. [2010]; Fox et al. [2015]), although in this case the minimal fading over the course of several thousand days is puzzling and also requires unusual explanations [Fox et al., 2015]. Further observations will clearly be needed to distinguish between these possibilities. However, as the source is relatively faint, it does not significantly contribute to the photometric measurements of the host galaxy, and so does not impact our conclusions drawn for it.

In the case of SN 2009jh, the SN apparently lies to the North-East of the host detected in deeper nIR imaging. I determine the $P_{\rm chance}$ value of the apparent host of SN 2009jh, which I found to be 0.038 within an offset radius of $0.99''$ (from the host half light radius and the SN's projected offset from the host centroid), indicating that for optical depth reached within the ACS imaging, the probability of the event being associated with another galaxy is low, but not especially so. Indeed, averaged over 20 hosts, one might expect a chance alignment with a sample of this brightness. This nearby galaxy is assigned as the host of SN 2009jh.

It should be noted that although the inclusion or exclusion of hosts SN 2006gy and SN 2009jh does not dramatically impact the results presented here, the host of SN 2006gy is the most luminous host in this sample by some margin, and so assigning it to a fainter satellite would result in some changes to the range of the distribution of SLSNe-II host luminosities.

3.2.1 Comparison Samples

While the properties of the SLSN hosts themselves are of interest, they are most diagnostic when compared to other classes of extragalactic transient whose progenitors are better understood. To this end, I employ a comparison sample of LGRB

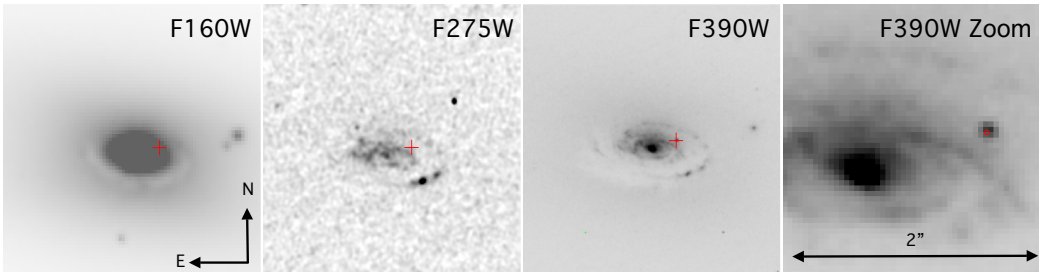

Figure 3.4: Host of SN 2006gy detected in F160W (first panel), F275W (second panel) and F390W (third panel). Images are scaled to $10'' \times 10''$. The SNe location, determined from astrometric measurements from late time imaging with WFPC2, is marked in red. Attention is drawn to a possible satellite to the larger host, coincident with the SNe location, revealed within our F390W imaging. This is highlighted within the 2 ” x 2 ” image zooming in on this region and the central bulge in the fourth panel, where the SNe position is marked by a 0.08” error circle

and CCSN[2] host galaxies. In principle, CCSNe should trace all core collapse events, although the mass function means they will be dominated by stars at the lower mass end (~ 8 M$_\odot$ to ~ 25 M$_\odot$). There also remains a possibility that some very massive stars can undergo core collapse without yielding a luminous supernovae [e.g. Smartt, 2009; Ugliano et al., 2012; Kochanek, 2014] such that CCSNe samples might only provide a census of lower mass core collapsing stars (e.g. $8 < M_* < 20$ M$_\odot$). Indeed, constraints from explosion parameters have shown the majority of CCSNe to be consistent with lower mass progenitors, as opposed to more massive Wolf Rayet stars [Cano, 2013; Lyman et al., 2014] GRBs likely represent a population with rather larger initial masses [Larsson et al., 2007; Raskin et al., 2008]. LGRBs are now known to be associated with the core collapse of massive stars, and broad line SN Ic are near ubiquitously associated with low-z events [where such signatures can be seen, Hjorth et al., 2012]. When compared to the hosts of CCSNe they are generally smaller and of lower luminosity, consistent with an origin in galaxies of lower metallicity [Fruchter et al., 2006; Svensson et al., 2010]. In relatively local examples, where spatially resolved gas phase metallicities can be obtained, these indeed appear to be lower for GRBs than for CCSNe, even in cases where the luminosity of the galaxy is relatively high (i.e. the GRB host galaxies lie off the mass-metallicity relation, Modjaz et al. 2008; Graham and Fruchter 2013b). Hence, comparing the hosts of SLSNe to these events provides a test of the large scale environments of SLSNe against those of the bulk core collapse population and a subset which ap-

[2]Here, CCSNe is used to define all core collapse events, including SN Ib, Ic, II and their various sub-types. Where appropriate and possible, I specify the SN type

pears to derive largely from massive stars at lower metallicity, although it should be noted that agreement on this matter is not complete [e.g. Podsiadlowski et al., 1992; Eldridge et al., 2008; Smartt, 2009; Drout et al., 2011]. By exploiting both LGRB and CCSN host samples it may be possible to ascertain if there is a strong metallicity dependence in SLSN production, and if this is more or less extreme than that observed in GRB hosts.

The observed samples are undoubtedly biased against highly dusty lines of sight such that the most dusty examples are missed. This effect has been well studied in GRBs [e.g. Jakobsson et al., 2006; Fynbo et al., 2009], and the inclusion of dusty sight lines does apparently extend the GRB host mass function to higher masses than if they are excluded [e.g. Perley et al., 2013]. However, the effect below $z \sim 1.2$, where these comparisons to SLSNe are conducted, is small, with very few dusty massive systems [Perley et al. 2015a,b, although see Stanway et al., 2015]. The impact on SNe detection may be even larger given their fainter peak magnitudes and uniquely optical selection.

Tables A.1, A.3, A.4 and A.5 list the names, locations and redshifts of the host galaxies used for direct photometric comparison. I make my own photometric measurements for CCSN hosts with available *HST* rest frame UV or nIR imaging, and draw from literature elsewhere. These photometric results are given within tables A.1, A.6 andA.7.

The LGRB host sample contains events at $z< \sim 1.2$ (for broad matching of the SLSNe redshift distribution, and comparable sample size). Rest frame UV observations are obtained from the literature [in particular utilising the GHostS project Savaglio et al., 2009, for other references see Table A.5]. nIR observations are obtained from GHosts, and also from a *HST* snapshot programme (GO-12307; PI Levan, Lyman et al. 2017), for which Joseph Lyman provided the nIR photometric measurements, performed in a similar manner to that carried out for the SLSN hosts.

The CCSNe host sample is based on that detected in the rolling SNe searches of the GOODS field [Dahlen et al., 2003; Fruchter et al., 2006; Riess et al., 2007; Svensson et al., 2010; Strolger et al., 2010]. These tiled the GOODS field repeatedly in the F850LP filter, with a cadence of ~ 45 days, primarily chosen to locate SNe Ia at $z > 1$. However, this search also provides an untargeted and highly sensitive moderate redshift ($0.1 < z< \sim 1$) survey for core-collapse events. Subsequently, the GOODS field has been observed in the nIR with both NICMOS and WFC3, and more recently in the blue using ACS and WFC. I use these images to obtain nIR magnitudes for the CCSN hosts, and for rest-frame UV magnitudes where field

coverage and redshifts allow, performing photometry as described above for the SLSN population.

Due to restrictions in field coverage and probed rest-frame wavelength from the GOODS UV field imaging, the CCSNe host comparison sample is supplemented with that of Sanders et al. [2012], which provides an untargeted, albeit typically low redshift, sample of stripped envelope SNe hosts. For these hosts literature values are drawn upon to determine their rest-frame UV brightness.

3.3 Analysis

3.4 Determining the Physical Parameters

As the redshifts of both the SLSN hosts and comparison galaxies are known, I can compare the physical properties of these galaxies. Of particular use can be a simple comparison of observed properties to physical properties over a similar redshift range, especially in cases for which Spectral Energy Distribution coverage is poor. In particular, the absolute magnitudes at UV and nIR wavelengths can be compared, using these as proxies for star formation rate and stellar mass respectively.

Spectral Energy Distribution fitting was applied to all of the SLSN host galaxies by Daniel Perley to constrain stellar masses, ages and star formation rates. I also measure the sizes of the host galaxies, specifically the radius within which 80% of their light is contained (following Fruchter et al. 2006; Svensson et al. 2010).

3.4.1 Spectral Energy Distribution Fitting

The available photometry ranges from rest-frame nIR to near UV in all cases, with an extension to the mid-IR for brighter hosts, which allows for the fitting of template spectral energy distributions. So that this may be done, I supplement the current *HST* photometric measurements with those from other public data and literature. I used Sloan Digital Sky Survey (SDSS) images [Ahn et al., 2012] to extract optical photometry for the SLSN hosts using the same techniques applied to the other ground based imaging within this work, in some cases this was supplemented with observations with Catalina Real-time Transient Survey [CRTS; Drake et al., 2009a], with additional mid-IR observations from WISE [Cutri and et al., 2013]. Finally, I also utilise published photometry of individual SLSN host galaxies from Germany et al. [2000]; Quimby et al. [2007]; Barbary et al. [2009]; Neill et al. [2011]; Hudelot et al. [2012]; Leloudas et al. [2012] and Lunnan et al. [2014] to complete the SEDs. For all photometry, I utilise the MAG_AUTO function within SExtractor, which

models and accounts through fitting Kron-like elliptical apertures to the source, in order to minimise any differences in the fraction of host light across different bands.

The acquisition of both nIR and UV data points allowed for simultaneous fitting of both masses and star formation rates, which when combined with the depth of the imaging provides better constraints upon the blue and red ends of spectra when fitting, achieving more realistic estimates of host properties than previous SED fitting attempts. The broad-band observations were fitted against the template model chosen to derive masses, ages and star formation rates for these hosts, a more detailed outline of which can be found within Perley et al. [2013]. The fitting assumed a mass-dependent metallicity and a host ionization parameter of $4{\times}10^7$, except in the case of SN 2011kf and SN 2011ke, as in both of these SED's there was an observable excess of flux within the filters corresponding to rest-frame O[III] or Hα lines when compared to a fit with no nebular emission. For these cases, this parameter was drawn from the previous spectroscopic studies of Lunnan et al. 2014 and Leloudas et al. [2015].

3.4.2 Luminosity Diagnostics

Whilst SED fitting allows the properties of host galaxies to be determined to a relatively high degree of precision, the constraints of an SED fit are strongly dependent upon the number and wavelength range of bands used to fit the template spectra. The properties derived are also highly sensitive to the star formation history adopted during the fitting procedure. For simplicity, and for direct comparison with previous work, I also consider nIR and UV rest frame luminosities as direct proxies for the stellar mass and star formation rate[3]. To do this I utilize the relations used in Savaglio et al. [2009] for stellar mass;

$$\log M_* = -0.467 M_{nIR} - 0.179 \tag{3.1}$$

The rest frame UV luminosities can also be directly converted into star formation rates as per Kennicutt [1998];

$$SFR(\mathrm{M}_\odot\ \mathrm{yr}^{-1}) = 1.4 \times 10^{-28} L_\nu \tag{3.2}$$

where L_ν is in cgs units of erg s^{-1} Hz^{-1} in the rest-frame wavelength range from 2500-3500Å, a region in which all of these UV observations lie. This relation assumes a

[3]In figures in which the main x-axis shows an observed absolute magnitude, the upper axis therefore shows the mass/star formation rate inferred from these proxies, while figures showing physical parameters are those derived from SED fits

constant star formation over a 100 Myr period with a specified initial mass function. Utilizing both mass and SFR the specific star formation rate, $\Phi = \frac{SFR}{M_*}$ can also be calculated. These values generally give results comparable to those from the direct SED fitting.

Finally, in addition to straight forward photometry, SExtractor also can be used to ascertain the fractional light radii of host galaxies using the `FRAC_LIGHT` parameter [Bertin and Arnouts, 1996], which fits an isophotal profile to a source then measures the relative size of the source in pixels, later converted into kiloparsecs using the plate scale. I use the common LGRB host diagnostic of radii containing 80% of the total flux from the host (r_{80}) within the nIR F160W images.

Errors for the SExtractor measurement of r_{80} in pixels for the hosts were estimated by modelling the capability of SExtractor to detect the full radial profile of a source at given magnitude and redshift as a function the image noise. An artificial field of objects was generated using IRAF routines within ARTDATA, with artificial galaxies specified to span a similar apparent magnitude and surface brightness range to our host galaxies in the F160W band. The discrepancy between specified object size and that measured by SExtractor was measured, with different levels of simulated noise, suggesting that significant errors can arise for sources close to the noise limit. These errors are provided in Table 3.2, alongside the r_{80} measurements.

3.5 Results

Below I first present the measured nIR and UV luminosities of the host galaxies, and consider the implications these results have when treated as proxies for stellar mass and SFR, respectively, before evaluating the derived SED properties of the SLSN hosts, and their physical sizes. I then compare these to the comparison samples. In the majority of cases it is apparent that the SLSN hosts bear little similarity with any other core collapse host population, being both fainter and smaller, the implications of which I consider within section 3.6.

The photometric UV, optical and nIR magnitudes of the LSN and SLSN host sample considered within this chapter are presented in Tables 3.1 and 3.2, and the derived UV and nIR host properties from SED fitting of these hosts are presented in Table 3.3. The direct photometric measurements and derived properties of the chosen LGRB and CCSN comparison samples are presented for nIR and UV observations within Tables A.1, A.3, A.6 and A.7 respectively.

In Figure 4.13, I present the cumulative distribution of the absolute nIR

Table 3.1: Apparent and absolute magnitudes of SLSN hosts observed with rest-frame UV (F275W, F336W or F390W) and optical bands. Optical photometric properties of a subset of this sample as observed with [a] WHT (r'), [b] VLT (R band) and [c] *HST* ACS (F606W). Optical imaging key: [a] r′ band, [b] R band, [c] B band. Uncertainties presented here are smaller than expected as a result of the way in which errors are computed within the SExtractor program. However, these errors do not impact the results presented in this thesis.

SLSN	m_{UV} AB mag	M_{UV} AB mag	$m_{optical}$ AB mag	$M_{optical}$ AB mag
SN1995av	24.97 ± 0.32	-15.82 ± 0.32	23.77 ± 0.19 [a]	-16.96 ± 0.19 [a]
SN1997cy	21.14 ± 0.21	-16.17 ± 0.21	-	-
SN1999as	21.15 ± 0.10	-17.70 ± 0.10	-	-
SN1999bd	21.85 ± 0.06	-17.40 ± 0.06	-	-
SN2000ei	23.81 ± 0.21	-19.29 ± 0.21	22.67 ± 0.14 [a]	-20.07 ± 0.14 [a]
SN2005ap	24.32 ± 0.09	-16.24 ± 0.09	23.64 ± 0.27 [a]	-16.90 ± 0.27 [a]
SN2006gy	19.86 ± 0.01	-15.55 ± 0.01	-	-
SN2006oz	-	-	24.09 ± 0.26 [a]	-16.56 ± 0.26 [a]
SCP06F6	27.88 ± 0.20	-15.88 ± 0.20	-	-
SN2007bi	23.83 ± 0.28	-15.03 ± 0.28	-	-
SN2008am	21.20 ± 0.026	-19.00 ± 0.026	-	-
SN2008es	>25.32	>-14.526	25.96 ± 0.20 [b]	-13.86 ± 0.20 [b]
			26.96 ± 0.25 [c]	-12.85 ± 0.25 [c]
SN2008fz	26.73 ± 0.55	-12.28 ± 0.55	25.58 ± 0.19 [b]	-13.33 ± 0.19 [b]
			26.17 ± 0.22 [c]	-12.81 ± 0.22[c]
SN2009jh	>25.92	>-15.139	25.46 ± 0.07 [b]	-15.59 ± 0.07 [b]
SN2010gx	23.96 ± 0.04	-16.24 ± 0.04	-	-
PTF09atu	>25.47	>-16.533	>23.14 [a]	>-18.79
PTF09cnd	24.01 ± 0.05	-16.40 ± 0.05	23.60 ± 0.04 [a]	-16.768 ± 0.04 [a]
PTF10hgi	-	-	22.05 ± 0.06 [a]	-16.329 ± 0.06 [a]
PTF10vqv	-	-	23.33 ± 0.12 [a]	-18.392 ± 0.12 [a]
SN2011kf	24.51 ± 0.38	-15.78 ± 0.38	-	-
SN2011ke	23.12 ± 0.03	-15.92 ± 0.03	-	-
PTF11dsf	22.88 ± 0.04	-18.38 ± 0.04	22.04 ± 0.11 [a]	-19.204 ± 0.11 [a]
PTF11rks	22.43 ± 0.16	-17.38 ± 0.16	20.95 ± 0.25 [a]	-18.77 ± 0.25 [a]
SN2012il	22.78 ± 0.06	-16.75 ± 0.06	-	-

Table 3.2: Apparent and absolute magnitudes of SLSN hosts observed with *HST* in nIR (F160W). I also present apparent r_{80} sizes of the *HST* SLSN hosts as detected within WFC3 F160W imaging. Again underestmated uncertainties are produced within SExtractor, but do not impact the overall conclusions of this chapter.

SLSN	m_{nIR} AB mag	M_{nIR} AB mag	r_{80} (kpc)	r_{80} (arcsec)
SN1995av	23.17 ± 0.27	-17.51 ± 0.27	10.66 ± 3.07	2.41 ± 0.69
SN1997cy	20.19 ± 0.03	-16.98 ± 0.03	3.29 ± 1.10	2.75 ± 0.91
SN1999as	19.19 ± 0.03	-19.55 ± 0.03	6.81 ± 2.39	3.03 ± 1.07
SN1999bd	18.779 ± 0.003	-20.349 ± 0.003	2.95 ± 1.02	1.13 ± 0.39
SN2000ei	20.90 ± 0.03	-21.44 ± 0.03	6.55 ± 2.00	0.98 ± 0.30
SN2005ap	23.48 ± 0.36	-17.05 ± 0.36	3.23 ± 0.85	0.76 ± 0.20
SN2006gy	11.951 ± 0.001	-22.661 ± 0.001	3.69 ± 2.11	9.70 ± 5.56
SN2006oz	-	-	-	-
SCP06F6	-	-	-	-
SN2007bi	22.07 ± 0.18	-16.68 ± 0.18	2.62 ± 0.77	1.16 ± 0.34
SN2008am	19.48 ± 0.006	-20.63 ± 0.006	4.31 ± 1.44	1.17 ± 0.39
SN2008es	26.85 ± 0.40	-12.95 ± 0.40	1.19 ± 0.23	0.36 ± 0.07
SN2008fz	25.18 ± 0.06	-13.66 ± 0.06	0.87 ± 0.18	0.37 ± 0.08
SN2009jh	25.30 ± 0.15	-15.71 ± 0.15	2.71 ± 0.63	0.55 ± 0.13
SN2010gx	23.17 ± 0.15	-16.90 ± 0.15	1.84 ± 0.46	0.51 ± 0.13
PTF09atu [a]	>23.39	>-18.452	-	-
PTF09cnd	22.56 ± 0.12	-17.76 ± 0.12	3.11 ± 0.89	0.78 ± 0.22
PTF10hgi	-	-	-	-
PTF10vqv	-	-	-	-
SN2011kf	24.06 ± 0.40	-16.14 ± 0.40	1.24 ± 0.27	0.33 ± 0.07
SN2011ke	23.21 ± 0.14	-15.78 ± 0.14	5.17 ± 1.48	2.08 ± 0.60
PTF11dsf	21.81 ± 0.07	-19.41 ± 0.07	3.48 ± 0.98	0.67 ± 0.19
PTF11rks	20.69 ± 0.06	-18.96 ± 0.06	5.55 ± 1.77	1.77 ± 0.57
SN2012il	21.82 ± 0.06	-17.63 ± 0.06	1.89 ± 0.53	0.64 ± 0.18

magnitudes of the SLSN hosts against those of the LGRBs and a subsample of GOODS CCSN hosts for which parallel photometric measurements were carried out. It can be seen here that SLSN hosts are in most cases much fainter than either LGRB hosts or CCSN hosts over the redshift range considered. Breaking down by SLSN sub-type, the most extreme examples (ignoring the small sample size of SLSNe-R) are the SLSN-I hosts, which are inconsistent with any other population of transient hosts. In contrast the SLSN-II hosts extend to magnitudes much fainter than CCSN host galaxies but at the brighter end of their distribution are comparable to the luminosities of LGRB hosts. In addition to the observed populations I also show as a solid cyan line the expected distribution of host magnitudes should they be drawn from the field population in proportion to the total nIR luminosity density (i.e. uniformly from the luminosity weighted luminosity function, Cirasuolo et al. 2007b), demonstrating that all transient types arise from fainter galaxies than expected in this scenario. This is not surprising since weighting the luminosity function by the nIR is approximately equivalent to weighting by galaxy mass, and as such there is a significant contribution from massive, but largely quiescent galaxies which will not host core collapse events.

Figure 4.7 shows the same analysis for the UV luminosity distribution of the SLSN sample. Again, the SLSNe are markedly fainter (hence possess lower star formation rates) than the GRBs or CCSNe. However, since they are also faint in the nIR their inferred specific star formation rates (SFR/M), do not suggest that they are forming stars at a rate unusually low for their mass, and they would still class as actively star forming galaxies. Interestingly in this UV range the CCSN and LGRB hosts appear to be more similar, although it should be noted that due to the paucity of UV observations of CCSNe in GOODS, this CCSNe host sample is different from the one used for the nIR comparison. The similarity of LGRB and CCSNe hosts in the UV, and the differences in the nIR could also be explained by the typically higher specific star formation rates of GRB hosts [Castro Cerón et al., 2006; Svensson et al., 2010].

To formalise the significance of these differences I perform both Kolmogorov-Smirnov (KS) and Anderson-Darling (AD) tests of each population (including a separate tests for our SLSNe and combined (SLSNe+LSNe) samples). The AD test provides a sample comparison more sensitive to the ends of the distribution, which in light of the extremely faint nature of some of the hosts within the sample, may provide a more apt test statistic than the KS test. Hence I refer to the AD statistic throughout the rest of this chapter, although the conclusions would be unaffected by the use of the KS-test. The probabilities of an underlying association between

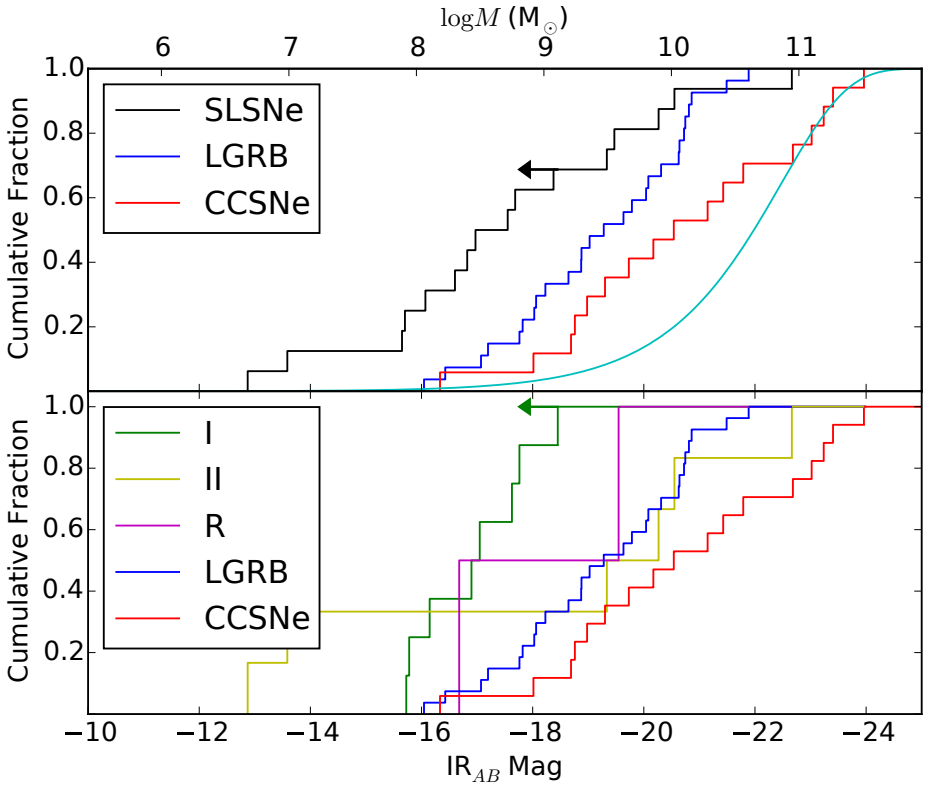

Figure 3.5: Upper panel: Cumulative frequency distribution of the absolute nIR magnitudes of core collapse event host galaxies. Arrows represent cases in which no host was detected and the 3σ limiting magnitude is used to place an upper limit upon the brightness of these hosts. The difference between the distributions of the SLSN and other core collapse hosts is statistically significant, with probabilities of 0.008 and 0.0017 of the SLSN hosts being drawn from the same population as LGRB and CCSN hosts respectively. I also display the NIR galaxy luminosity function for galaxies within this brightness range (cyan line) [Cirasuolo et al., 2007a]. Using nIR brightness as a proxy for mass (top x-axis), it is to be expected that the SLSN hosts are significantly less massive too. Lower panel: I present the same distributions with the hosts of SLSNe broken down by classification. Here the SLSN classes appear indistinguishable from one another in brightness, but this is likely due to small number statistics. I perform AD testing between the different subclasses and both core collapse comparison groups, and find SLSN-I hosts to be inconsistent with this sample of core collapse transients, although there is a stronger association for SLSN-II, due to the much broader distribution in brightness it exhibits.

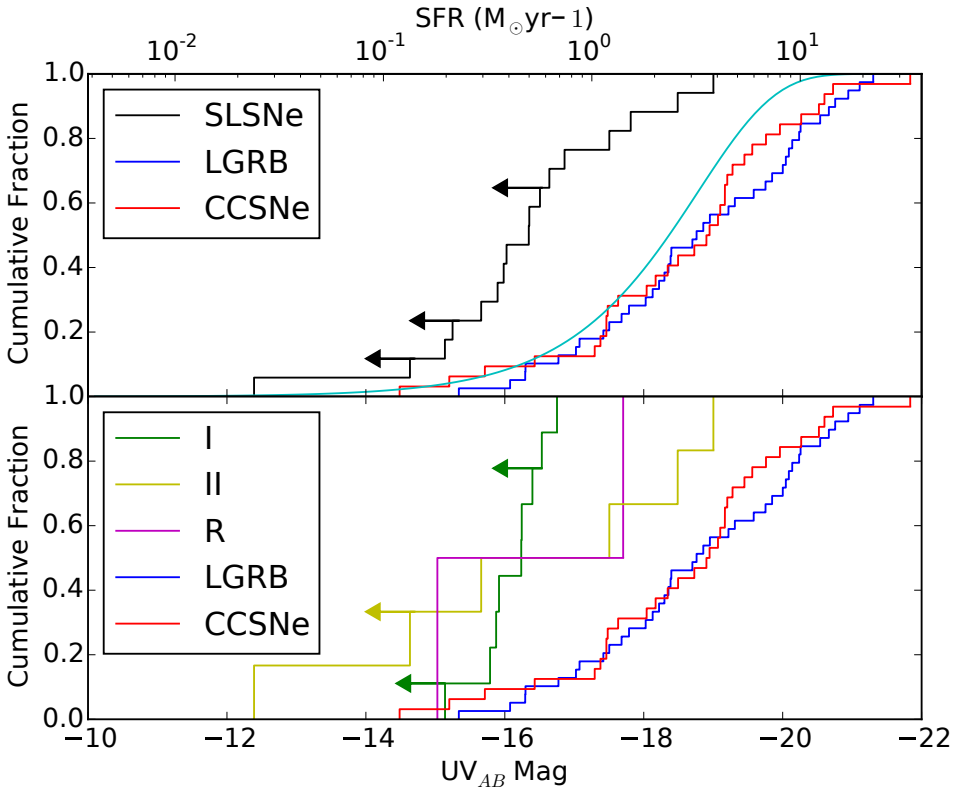

Figure 3.6: Cumulative distribution of the UV luminosities of SLSN, LGRB and CCSN host galaxies (upper panel). Anderson-Darling results show that SLSN hosts are not drawn from the same distribution of hosts at a high confidence (p=2.7x10^{-5} and p=5.4x10^{-5} for LGRBs and CCSNe respectively). I also display the Baldry et al. 2005 UV galaxy luminosity function for galaxies within our brightness range (cyan line). Using UV brightness as a proxy for SFR (top x-axis), one might expect these hosts to be substantially less star forming than the comparison samples too. Breaking this down by SLSN type (lower panel) shows little distinction between the subclasses, although again small number statistics are likely to be an influence here. AD testing between subclasses proves a strong inconsistency between the all classes of SLSN hosts and the comparison samples in M_{UV}.

different distributions are presented in Table 3.4, and the results indicate that the probability of the SLSN host sample and the hosts of LGRBs and CCSNe being drawn from the same pool of galaxies is low. As expected the differentiation is strongest for the SLSN-I hosts, which rejects the hypothesis that they arise from hosts with similar absolute magnitudes to either CCSN or GRB host galaxies, in both cases indicating that the host galaxies are significantly less luminous, with further implications for their masses and star formation rates (see below).

The SLSN-II hosts have low to modest probabilities of being drawn from the same underlying host population as both the LGRBs ($P = 0.01, 0.23$ for UV and nIR respectively) and the CCSNe ($P = 0.008, 0.29$ for UV and nIR). However, as previously noted the most striking feature of the SLSN-II hosts is their presence over a wide range of luminosity from our brightest host (SN 2006gy, $M_{nIR} \sim$ -22.5) to the faintest two (SN 2008es, SN 2008fz, $M_{nIR} \sim -13$). Should these galaxies be drawn from some star formation (or mass) weighted distribution, the chance of obtaining any such faint hosts within a small sample would be very small. For example, the expected number based on the extrapolation of a luminosity function is $<<1$. Indeed, KS and AD tests suffer from a lack of sensitivity to such extremes since they measure the maximum offset between two distributions, and are insensitive to these extremes. Despite the small number statistics, the presence of two SLSNe-II in such faint host suggests than unusual mechanisms may be at play in at least some of these events.

I present the SED fits to all of the SLSN targets in Figure 3.7, and their derived properties in Table 3.3. I compare these stellar masses and star formation rates to those found through proxies from the nIR and UV luminosities, which provides a model independent check upon the SED fit values, and find them to be generally of the same order of magnitude. Using the properties derived from the SED fitting, I present the distribution of masses and SFRs for the sample in Figures 3.8 and 3.9 respectively, alongside those properties which have been derived from SED fitting for LGRB and CCSN hosts from Fruchter et al. [2006] and Svensson et al. [2010]. As suggested by proxies, SLSN hosts are less massive and possess lower SFRs than CCSN and LGRB hosts, to a high level of significance, as show in Table 3.4.

A comparison of the measured r_{80} values from the nIR observations is presented in Figure 3.10, combined with the masses to provide an indication of the relative evolution of size with luminosity for our core collapse transient host sample. The compact and low mass nature of the SLSN hosts is clearly visible, as they occupy a distinct region of parameter space from other core collapse hosts of simi-

Table 3.3: Properties of SLSN hosts derived from SED fitting performed by Daniel Perley. Uncertainties presented here are those associated with photometric errors only and do not include systematic uncertainties related to the fitted SED models. Objects marked * are detected within only one band. Mass errors provided for these objects represent the upper and lower bound that can be placed upon these hosts. Note that the mass reported for SCP06F6 is an assumed fixed mass used within SED fitting.

SLSN	SFR ($M_\odot$ yr $^{-1}$)	M_* ($\times 10^9$ $M_\odot$)
SN1995av	$0.201\ ^{+0.063}_{-0.077}$	$0.578\ ^{+0.270}_{-0.192}$
SN1997cy	$0.170\ ^{+0.207}_{-0.030}$	$0.255\ ^{+0.042}_{-0.216}$
SN1999as	$0.610\ ^{+0.014}_{-0.006}$	$2.197\ ^{+0.396}_{-0.000}$
SN1999bd	$0.412\ ^{+1.030}_{-0.259}$	$10.494\ ^{+1.339}_{-2.073}$
SN2000ei	$9.597\ ^{+3.511}_{-0.000}$	$0.863\ ^{+0.175}_{-0.000}$
SN2005ap	$0.090\ ^{+0.017}_{-0.016}$	$0.287\ ^{+0.107}_{-0.097}$
SN2006gy	$0.000\ ^{+0.000}_{-0.000}$	$153.280\ ^{+6.251}_{-6.463}$
SN2006oz	$0.013\ ^{+0.025}_{-0.013}$	$0.466\ ^{+0.113}_{-0.038}$
SCP06F6*	$0.136\ ^{+0.028}_{-0.025}$	$0.010\ ^{+0.000}_{-0.000}$
SN2007bi	$0.048\ ^{+0.006}_{-0.009}$	$0.136\ ^{+0.097}_{-0.053}$
SN2008am	$2.018\ ^{+0.001}_{-0.002}$	$5.637\ ^{+0.018}_{-0.047}$
SN2008es	$0.007\ ^{+0.001}_{-0.001}$	$0.006\ ^{+0.005}_{-0.005}$
SN2008fz	$0.009\ ^{+0.001}_{-0.001}$	$0.017\ ^{+0.001}_{-0.001}$
SN2009jh*	$0.030\ ^{+0.000}_{-0.000}$	$0.068\ ^{+0.041}_{-0.000}$
PTF09cnd	$0.162\ ^{+0.035}_{-0.019}$	$0.673\ ^{+0.100}_{-0.185}$
SN2010gx	$0.340\ ^{+0.015}_{-0.018}$	$0.349\ ^{+0.055}_{-0.046}$
PTF10hgi	$0.003\ ^{+0.008}_{-0.003}$	$0.351\ ^{+0.020}_{-0.016}$
SN2011kf	$0.174\ ^{+0.061}_{-0.015}$	$0.124\ ^{+0.077}_{-0.090}$
SN2011ke	$0.177\ ^{+0.009}_{-0.007}$	$0.070\ ^{+0.016}_{-0.017}$
PTF11dsf	$0.924\ ^{+1.849}_{-0.076}$	$2.651\ ^{+0.188}_{-1.368}$
PTF11rks	$0.602\ ^{+0.029}_{-0.000}$	$0.773\ ^{+0.080}_{-0.000}$
SN2012il	$0.212\ ^{+0.057}_{-0.009}$	$0.284\ ^{+0.177}_{-0.112}$

Table 3.4: Two sample Anderson-Darling and Kolmogorov-Smirnov probability results between samples, including testing for the pure SLSN sample and the combined LSN+SLSN sample. Probabilities $\lesssim \times 10^{-6}$ are given 0.0

		SLSNe Sample		Combined Sample[a]	
Data Set	Host Connection	KS	AD	KS	AD
	Connection	Stat.	Stat.	Stat.	Stat.
	SLSNe - LGRB	0.013	0.008	0.022	0.020
nIR Magnitude	SLSNe - CCSNe	0.005	0.0017	0.009	0.003
	SLSNe-I - LGRB	$8.1\text{x}10^{-4}$	$8.1\text{x}10^{-5}$	$1.5\text{x}10^{-4}$	$8.7\text{x}10^{-5}$
	SLSNe-I - CCSNe	$1.5\text{x}10^{-5}$	$6.8\text{x}10^{-5}$	$4.4\text{x}10^{-5}$	$6.8\text{x}10^{-5}$
	SLSNe-II - LGRB	0.55	0.23	0.77	0.33
	SLSNe-II - CCSNe	0.61	0.29	0.56	0.27
	LGRB - CCSNe	0.05	0.04	-	-
	SLSNe - LGRBs	$4.5\text{x}10^{-5}$	$2.7\text{x}10^{-5}$	$3.2\text{x}10^{-5}$	$3.1\text{x}10^{-5}$
UV Magnitude	SLSNe - CCSNe	$1.4\text{x}10^{-5}$	$5.4\text{x}10^{-5}$	$1.0\text{x}10^{-5}$	$6.5\text{x}10^{-5}$
	SLSNe-I - LGRB	$1.0\text{x}10^{-6}$	$1.9\text{x}10^{-6}$	$1.0\text{x}10^{-6}$	$1.4\text{x}10^{-5}$
	SLSNe-I - CCSNe	$1.7\text{x}10^{-6}$	$5.0\text{x}10^{-5}$	0.0	$2.7\text{x}10^{-5}$
	SLSNe-II - LGRB	0.12	0.01	0.07	0.009
	SLSNe-II - CCSNe	0.06	0.008	0.053	0.011
	LGRB - CCSNe	0.85	0.84	-	-
	SLSNe - LGRB	0.0	0.09	0.0	0.14
Masses	SLSNe - CCSNe	0.0	0.015	0.0	0.0019
	SLSNe-I - LGRB	0.002	$1.2\text{x}10^{-5}$	$8.6\text{x}10^{-4}$	0.0
	SLSNe-I - CCSNe	$8.9\text{x}10^{-5}$	0.0	$2.6\text{x}10^{-5}$	0.0
	SLSNe-II - LGRB	0.64	$3.3\text{x}10^{-5}$	0.84	$1.5\text{x}10^{-5}$
	SLSNe-II - CCSNe	0.49	$1.32\text{x}10^{-5}$	0.70	0.0
	LGRB - CCSNe	0.48	0.12	-	-
	SLSNe-LGRB	$6.7\text{x}10^{-5}$	$6.9\text{x}10^{-5}$	$5.5\text{x}10^{-5}$	$9.9\text{x}10^{-5}$
SFRs	SLSNe - CCSNe	0.0	0.0	0.0	0.0
	SLSNe-I - LGRB	$8.3\text{x}10^{-5}$	$2.6\text{x}10^{-4}$	$9.1\text{x}10^{-5}$	$1.5\text{x}10^{-5}$
	SLSNe-I - CCSNe	0.0	$1.34\text{x}10^{-5}$	0.0	$1.1\text{x}10^{-5}$
	SLSNe-II - LGRB	0.065	0.065	0.09	0.02
	SLSNe-II - CCSNe	0.016	0.0013	0.04	0.002
	LGRB - CCSNe	0.11	0.06	-	-
r_{80}	SLSNe - LGRB	0.0	$1.0\text{x}10^{-5}$	0.0	$1.5\text{x}10^{-5}$
	SLSNe - CCSNe	$1.4\text{x}10^{-4}$	$1.1\text{x}10^{-4}$	$7.3\text{x}10^{-4}$	$3.6\text{x}10^{-4}$
	LGRB - CCSNe	0.15	0.09	-	-

[a]Excluding SN 1997cy

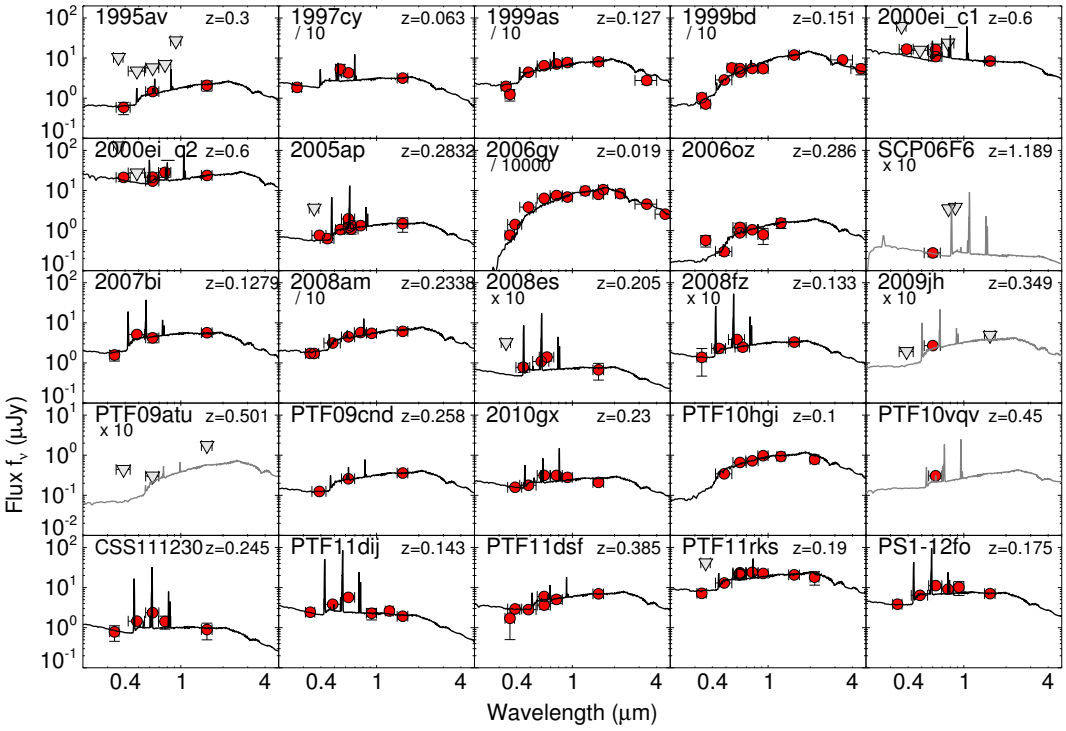

Figure 3.7: [*Figure produced by Daniel Perley*] SED fits of SLSN hosts as carried out in a similar manner to Perley et al. 2013, using photometric results from the *HST* programmes and ground based WHT and VLT images described within Chapter 2, with additional photometric results drawn from the literature and public SDSS images. Arrows indicate upper limits to photometry.

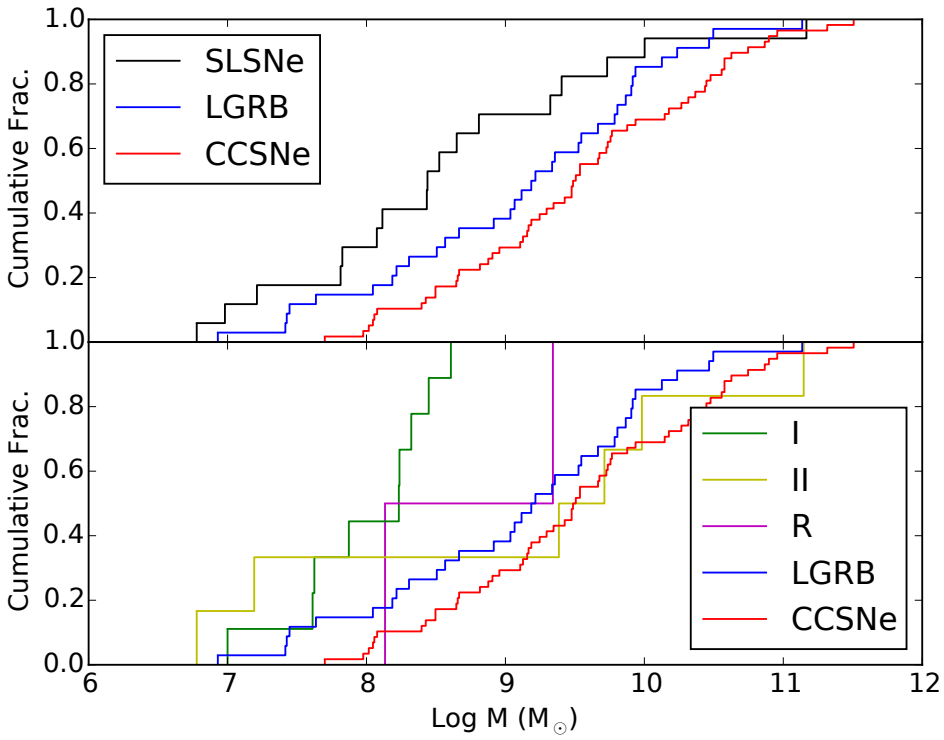

Figure 3.8: Masses of transient hosts as determined by SED fits. SLSN hosts are significantly less massive than CCSNe host galaxies, and show a 1σ difference to LGRB hosts. Splitting by subtype little similarity is found between the subclasses of SLSN hosts and the comparison samples

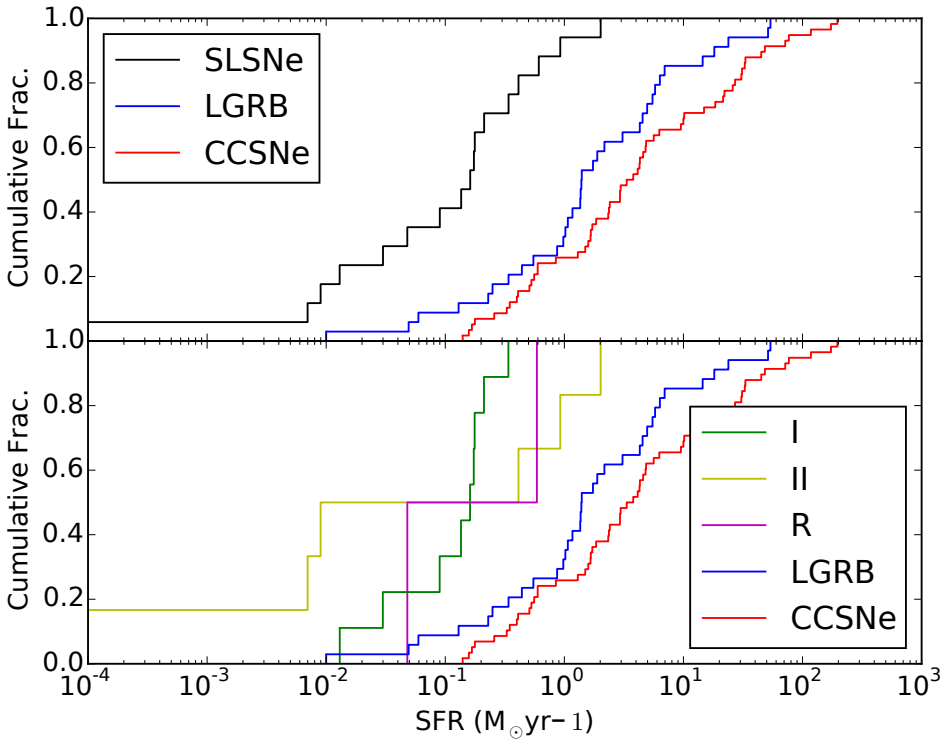

Figure 3.9: Star formation rate for transient hosts determined by SED fitting. SLSN hosts appear to not be as strongly star forming as CCSNe or LGRB host galaxies, with very low probabilities of the distributions being drawn from the same underlying population. Again, splitting by subtype shows little deviation from this result for the hosts of SLSNe-I, however for those of SLSNe-II, there appears to be slight overlap between it and the LGRB hosts distribution (p=0.08). However, the evolution exhibited within the average SFR of LGRB hosts over low redshift Perley et al. 2013, 2015b; Schulze et al. 2015, may somewhat bias these results.

lar brightness. It should be noted that CCSN hosts are in turn more compact than SDSS galaxies [e.g. Kelly et al., 2010], whose size distribution peaks well above of the range of sizes presented within this work. Again, AD tests between the *HST* SLSNe and comparison samples give little probability that they are drawn from the same underlying population. Although the reader should bear in mind that the nIR observations used within this work are frequently (although not exclusively) rather short (∼200s), so low surface brightness features could be missed in comparison to deeper observations of the GRB hosts and GOODS SNe. To evaluate the probability of this, I used the IRAF package ARTDATA to model galaxies at a variety of host sizes, apparent magnitudes and exposure times to estimate the expected recovery rate. I found that even if SLSN hosts were to lie at the upper extrema of their error bars (i.e. if there were a systematic shift of each point by 1σ larger) the result would still be statistically significant to $1\text{x}10^{-4}$ and 0.014 for LGRBs and CCSNe respectively.

Given that the redshift distributions of these classes of transient exhibit somewhat different functional forms it is reasonable to ask if the observed differences in the properties of the population are due to redshift evolution in the host galaxies, rather than the properties of the progenitor stars themselves.

Ideally it may be beneficial to conduct tests considering only low-z SLSNe (e.g. $z<0.4$) and with comparison samples at the same redshift. However, the comparison samples utilised within this chapter become very small at these low-redshifts, frequently with $< 4-8$ objects for comparison (see Figure 1). These small sample sizes lack the statistical power to make strong statements about redshift evolution within the SLSN sample in comparison to those of others. Given that there is some evidence for evolution in LGRB properties with redshift, albeit occurring predominantly around $z \sim 1$ [Perley et al., 2015b] it is possible that some apparent differences between SLSNe and other transient populations are amplified, or damped, by evolution in the host properties themselves. I will discuss this further within section 3.6.

I also determine specific SFRs (sSFRs) for the SLSN hosts, which I present within Figure 3.11. When compared alongside those of LGRBs and CCSNe from Svensson et al. [2010], they appear to fall within a similar range of sSFR as other core collapse transients. Although, when compared to a wider sample of galaxies, as carried out by Castro Cerón et al. [2006] (ref. their figure 2) and Svensson et al. [2010] (ref. their figure 7), such as distant red galaxies (DRGs), submillimeter galaxies (SMGs) and Lyman break galaxies (LBGs), the sSFRs of the core collapse transients lie at lower masses for a given sSFR than DRGs, SMGs and LBGs.

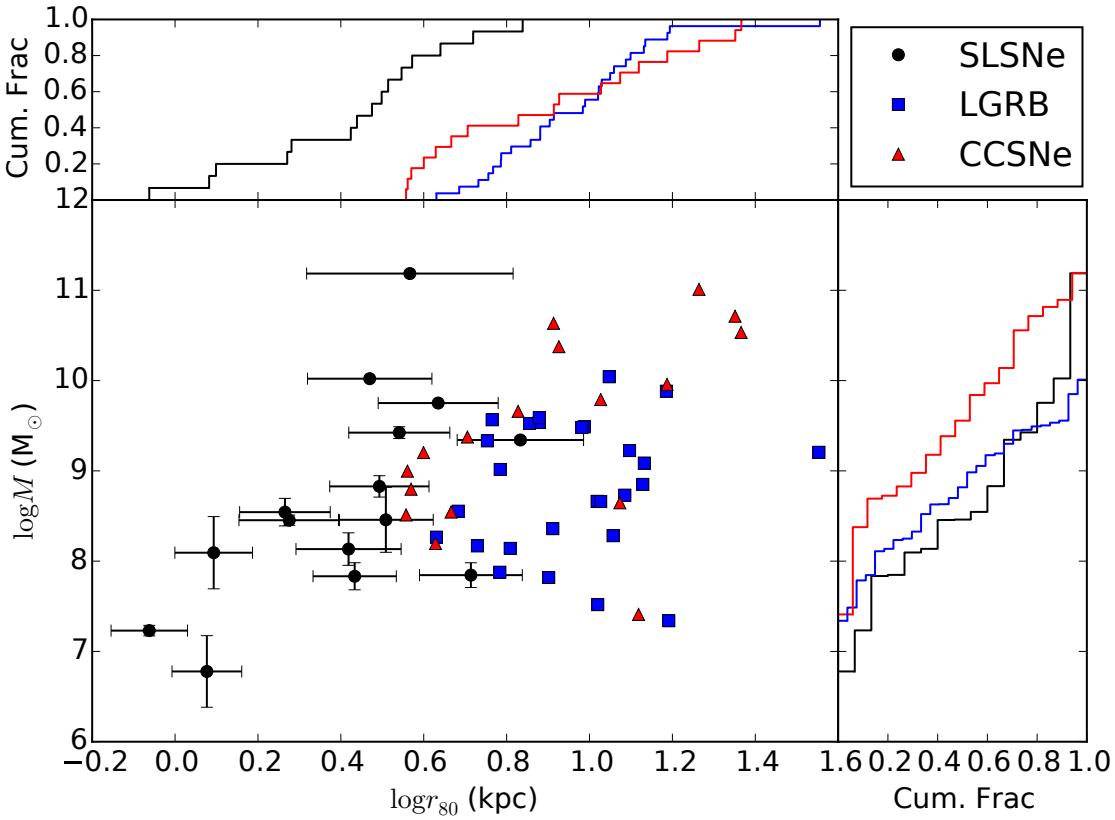

Figure 3.10: r_{80} light profiles measured in the *HST* F160W band of core collapse hosts against their mass as derived from SED fitting. Error bars are indicative of SExtractors ability to detect the edge of a galaxy at given brightness for a given redshift. The compact nature of SLSN hosts is apparent here.

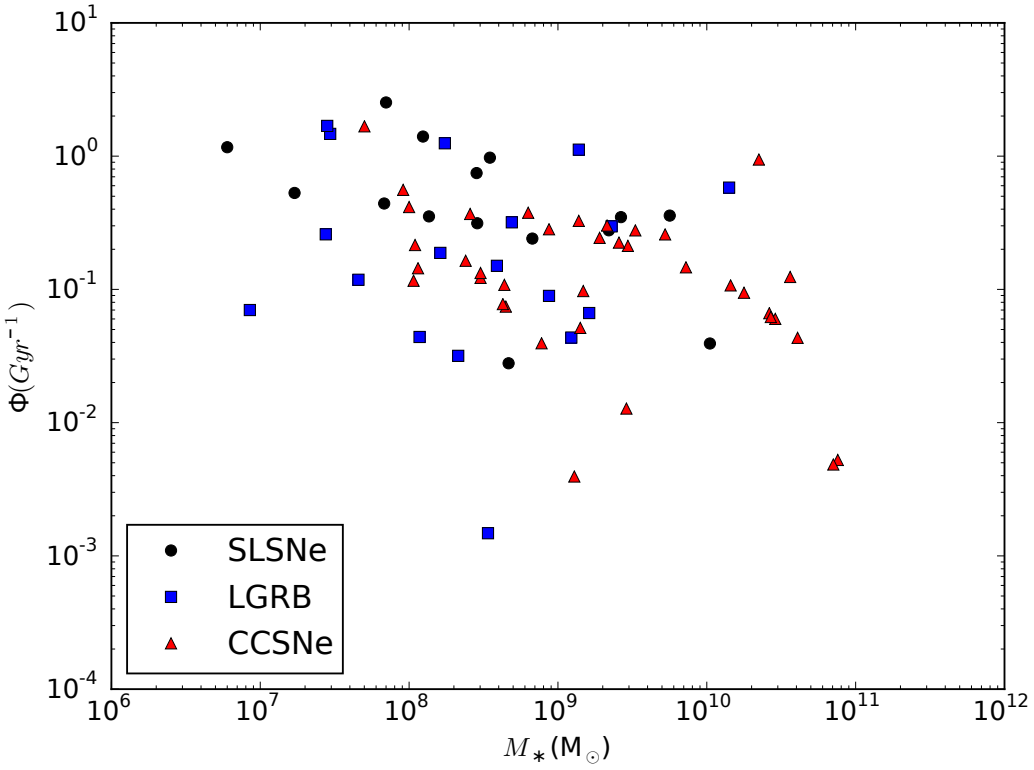

Figure 3.11: sSFR values for SLSN, CCSN and LGRB hosts against their respective stellar masses. Overall, the hosts of SLSNe appear to occupy a similar range of sSFR values as CCSN and LGRB host galaxies. Note that the host of SN 2006gy is not included here, due to it's poorly constrained star formation rate from SED fitting.

3.6 Discussion

3.6.1 General Properties

The results presented within this chapter highlight the extreme nature of the SLSN host population. A significant fraction arise in galaxies of exceptionally low luminosity, both in the UV and nIR. These galaxies are extreme even when compared to other populations of core collapse hosts, or even to GRBs, whose host galaxies are already set well apart from a typical field sample. Given that the UV and IR naturally provide a probe of both star formation and stellar mass, these differences are indicative of extremely low mass star forming hosts for SLSNe. Indeed, studies of SDSS galaxies indicate that there is little contribution to the global star formation rate in the local Universe from galaxies with $M_{UV} > -17$ [Blanton et al., 2005; Graham and Fruchter, 2013b], where I have shown the majority of the SLSN hosts within this sample lie. This result also holds in comparison to the host galaxies of CCSNe and LGRBs, the latter of which have been suggested to arise predominantly, if not exclusively from stars of low to moderate metallicity [e.g. Fruchter et al., 2006; Graham and Fruchter, 2013b; Perley et al., 2015a].

The host galaxies are also typically small, but exhibit surface star formation densities, and specific star formation rates that are more in keeping with those of other transient populations (i.e. they lie at the low end of most physical parameters compared to other core collapse transient hosts, such that any additional parameter derived with reference to two of more of SFR, mass and size, does not provide a strong distinction between the hosts of SLSNe and other star forming galaxies). The majority of these SLSN hosts exhibit high star formation surface densities, higher than those seen in the hosts of SNe-Ib/c and SNe-II, more akin to broad line SN-Ic and GRB hosts [Kelly et al., 2014], in agreement with the results of Lunnan et al. [2015].

However, these broad conclusions based on all SLSNe fail to consider the diversity of SLSN types. In splitting the sample by type (utilising the classification system of Gal-Yam 2012), small number statistics prevent strong conclusions from being drawn about differences *between* SLSN subtypes, although it does appear that SLSNe-I arise from predominantly fainter host galaxies than SLSNe-II on average. The larger differences between SLSNe and other classes of transient (compared to the differences between classes of SLSNe), do allow stronger conclusions to be made when comparing the host galaxies of SLSNe-I and SLSNe-II to the hosts of LGRBs and CCSNe.

3.6.2 SLSN-I

The SLSN-I hosts are much fainter than the hosts of either CCSNe or LGRBs. Since the LGRBs are frequently explained as arising from low metallicity systems, the logical conclusion might be to assign SLSNe-I to progenitors of even lower metallicity. This however is problematic; spectroscopic observations of the hosts of SLSNe [Lunnan et al., 2014; Leloudas et al., 2015] generally show modest metallicities, and indeed Lunnan et al. [2014] conclude the metallicities of SLSNe-I are consistent with those of GRB hosts. There are multiple possible origins for this discrepancy.

Firstly, it may be that rapid evolution in the properties of LGRBs hosts with redshift magnifies what is in fact a small difference between the metallicity cuts for SLSNe and LGRBs. Although small sample sizes prevent me from testing this reliably, it is not unlikely that evolution within the LGRB host population below $z \sim 1$ may accentuate the apparent differences between themselves and SLSN hosts. Work carried out by Japelj et al. [2016] following the publication of the study contained within this chapter, utilised a "complete" sample of LGRB host galaxies from *Swift*/BAT6 for comparison with a larger sample of SLSNe drawn from this work, and that of Lunnan et al. [2014] and Perley et al. [2016], found that with firmer redshift restrictions, the properties of SLSN-I and LGRB hosts appear more similar than reported with this sample, perhaps due to these evolutionary effects. Additionally it should be noted that the samples utilised by Lunnan et al. [2014], Leloudas et al. [2015] and this work, while containing some overlap are also significantly different. Small number statistics may then represent a potential concern.

Selection effects could also hinder such work. For example, many SLSNe have been found by searches targeting orphan transients (those without visible hosts in the survey images), since the SLSN so effectively outshines its host galaxy. This may immediately remove SLSNe in higher metallicity, more luminous hosts, causing the remaining sample to be biased towards a lower metallicity. I attempt to address this by adopting the PanSTARRS limiting magnitude cut of R$\sim$23.5 for host galaxy detection across all of the host samples (SLSNe, CCSNe and GRBs), such that I include *only* hosts fainter than this limit (it should be noted that this is the most conservative approach since the limiting magnitudes of the other surveys finding SLSNe are typically significantly brighter). Using this approach 8/21 hosts from the *HST* SLSN sample would be recovered. Within this limit the SLSN host sample appears fainter and less massive than the CCSNe and LGRB host samples. Although such small comparison samples would be once again dominated by small number statistics, it suggests that the differences between the differing populations are not created by the selection mechanisms of the transient surveys. The impact

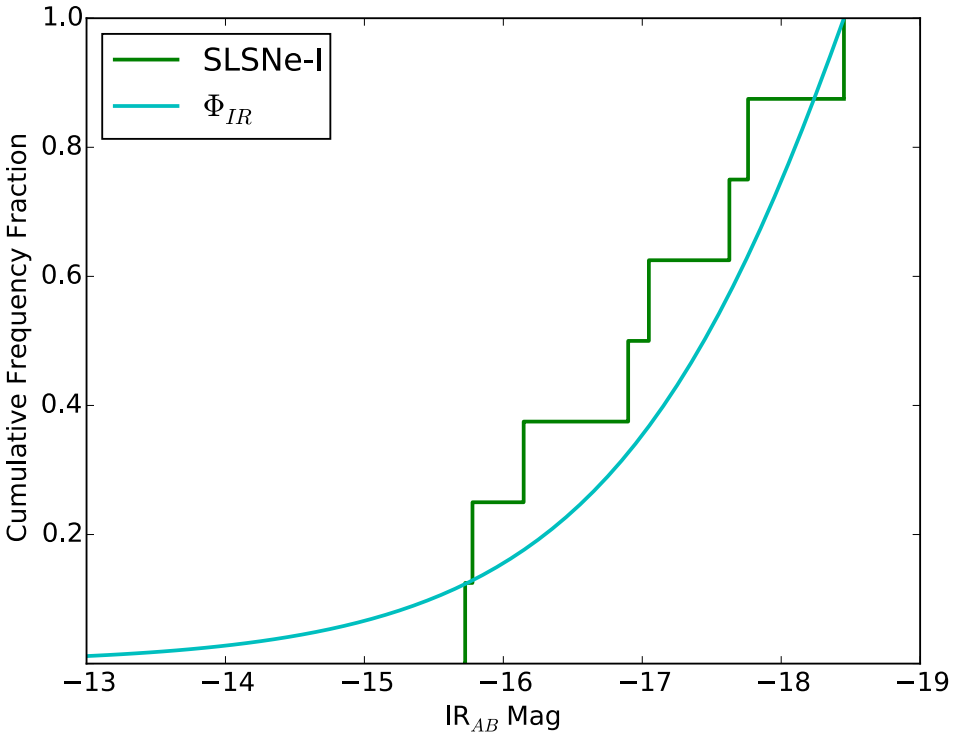

Figure 3.12: The nIR distribution of SLSN-I host galaxy luminosities compared to the nIR luminosity function once truncated to the absolute magnitude of the brightest SLSN-I host galaxy within this work. Here the observed distribution of SLSNe-I agrees well with expectation from the truncated luminosity function. Such behaviour may suggest that if SLSN hosts did follow a standard L-Z relation, their rate may be suppressed within host galaxies brighter than this limit.

of the faintest galaxies may operate in the opposite direction, very faint galaxies are difficult to obtain metallicities for, and so if these are omitted it may bias the observed metallicity distribution towards higher levels.

Finally, it is relevant to consider if astrophysical effects could be at play. Mass (or luminosity) metallicity relations have been used to infer the metallicities of GRB host galaxies, and this could be extended to SLSN hosts. In this case one might infer a metallicity threshold based on the most luminous observed SLSN host galaxy, and could then test the consistency of the distribution of fainter (and using an L-Z relation, lower metallicity) galaxies. To demonstrate this, in Figure 3.12 I show SLSN-I nIR distribution alongside the nIR luminosity function truncated to the brightest SLSN-I host galaxy within this work. In this case the observed distribution of SLSNe-I would be broadly in keeping with expectations, and if SLSN hosts did follow a standard L-Z relation, this may suggest that SLSN-I hosts are

suppressed within host galaxies brighter than this limit (corresponding to a mass cut at around $10^8\,M_\odot$and a metallicity cut at $\sim$0.75 $Z_\odot$). However, this approach is imperfect and shall be further expanded in Chapter 5. For the UV luminosity function of Baldry et al. [2005], truncated at $M_{UV} \sim -16.8$ (the most luminous SLSN-I host within this sample), one would expect $\sim 60\%$ of the UV-light (hence SFR, or equivalent number of SNe) to arise from galaxies within 1-magnitude of this luminosity. This would match well the relatively narrow range of luminosities observed for the host galaxies of SLSNe-I, while the 2 upper limits (of 9 SNe) are consistent with the fainter fraction of the hosts. To this end, metallicity may appear an good description of the observed luminosity distribution. However, it is clear such relations between luminosity or mass and metallicity are crude at best; often GRB hosts are found to have low metallicity, even when in relatively luminous hosts (see e.g. figure 10 in Graham and Fruchter [2013b]). If SLSN hosts lie systematically low in metallicity when compared to mass in the mass metallicity relationship then it would not be surprising that they could appear very different from LGRBs in mass, but rather more similar in metallicity. It is also possible that an apparent discrepancy in interpretation may arise due to the different locations of SLSNe and GRBs on their host galaxy light distributions. GRBs are preferentially concentrated on the brightest regions of their host galaxies. In these situations the global metallicity of the host galaxy (which comes from "most" of the light) might be a reasonable proxy for the metallicity in the GRB region (although see e.g. Hammer et al. [2006] for some caveats). As we shall see within Chapter 4, in the case of SLSNe, the concentration is not so strong [see also Lunnan et al., 2015], and indeed some events (e.g. SN2009jh) lie apparently off their host galaxy light. In these scenarios it is more likely that the global host metallicity is not indicative of the metallicity at the location of the SNe, and so spatially resolved measurements are urgently needed.

Progenitor models of SLSN-I

Theoretically, there are good reasons to favour similarities between the environments of LGRBs and SLSNe-I. It is known that LGRBs arise from central engines [Woosley, 1993], and there is growing consensus that this is also the case for SLSNe-I [Kasen and Bildsten, 2010; Dexter and Kasen, 2013], which become active during the collapse of very massive stars. Observations of both classes of event provide evidence favouring this model (for SLSNe [Levan et al., 2013; Nicholl et al., 2013, 2015], for LGRBs e.g. [Metzger et al., 2011], although for association with luminous SNe, see [Mazzali et al., 2014]). If this is the case then we might expect the pro-

duction of these engines to be favoured in similar environments. However, there are differences in the necessary engine properties to create LGRBs or SLSNe. In particular, in LGRBs, the bulk of the energy must be released extremely early ($\sim 10^3$s) to power the ultra-relativistic outflow, this energy is then deposited into the ejecta close to the engine. In contrast, for SLSNe the engine must act to re-engerise the outflow on timescales of weeks to months after the initial core collapse. In the case of black hole engines this means the accretion timescales must vary by many orders of magnitude, while for magnetars the crucial spin down parameter must also be different.

Relative numbers of magnetars observed within the Milky Way, when placed in context with the galactic CCSN rate, requires that $\sim$10% of these events result in the birth of a magnetar [Mereghetti et al., 2015]. This rate is far higher than any suggested for SLSNe and suggests that the magnetars we observe in the Galaxy today have little connection to those that may be created in luminous SNe explosions. Rotation is a logical difference between those systems creating "normal" magnetars, and those which are powerful enough to re-energize explosions, and this may in turn provide an natural explanation for environmental biases. At higher metallicities the line driven winds will dramatically brake the rotation of the star prior to a supernova explosion, and hence conservation of magnetic flux and angular momentum upon core collapse may create a magnetar with a longer rotation period than needed to explain either GRBs or SLSNe. Hence we might expect to observe both LGRBs and SLSNe in relatively metal poor environments. Indeed, since the spin periods for the GRB magnetars are shorter than for those creating SLSNe (or they have higher magnetic fields) one might naively assume that GRBs could favour even lower metallicity. In this regard it is valuable to note the recent example of GRB 111209A, an ultra-long GRB in a low metallicity galaxy [Levan et al., 2014b] in which a magnetar may have produced both the GRB and luminous SNe [Greiner et al., 2015].

3.6.3 SLSN-R

There are only two SLSNe-R within this sample, and so we can say little about the properties of their hosts in comparison to other samples, aside from noting that their luminosity is generally in keeping with those of SLSNe-I, which some authors have suggested is their correct assignment. Interestingly, in both cases the SLSNe-R appear to originate from bright UV regions within their hosts, something that is not the case for all SLSNe-I, but given the small sample size and the available data it is not possible to investigate if they may arise from young, massive stellar populations

in metal poor regions, more so than the environments of SLSNe-I. It is also relevant to note that recent calculations suggest that stars at modest metallicity and mass can create pair instability SNe [Yusof et al., 2013] and so the environment alone may not ultimately provide as strong a means of discrimination between models as had previously been hoped.

3.6.4 SLSN-II

Less attention has been paid to the host galaxies of SLSNe-II, partly as the interaction model for their origin appears a more natural explanation given the likely presence of recently ejected hydrogen envelopes in Type-IIn SNe (and most SLSNe-II are of the IIn variety). However, their hosts span a very wide range of luminosity, including two host galaxies that are fainter than any SLSNe-I, LGRB or CCSN host in our sample. Recent work by Perley et al. [2016], in which the host galaxies of SLSNe discovered within PTF are considered, confirms this apparently varied nature of SLSN-II host galaxies, and identifies an additional two SLSN-II host galaxies of exceptional faintness; namely the hosts of PTF10scc and PTF12mkp, both of which lie below M_g<-14. Indeed, while a handful of SNe Ia have been found in comparably faint systems [e.g. Strolger et al., 2002] the presence of any type of core collapse SNe in galaxies fainter than $M_B \sim -14$ is extremely rare (for example, none in the cross correlation of the SAI catalog with SDSS [Prieto et al., 2008]). Although this may in part be due to a lack of follow-up, in practice at these modest redshifts essentially no SNe would be expected, even with the metallicity cuts used to explain the GRB population [Graham and Fruchter, 2013b]. The presence of two host galaxies in such low luminosity galaxies is then puzzling; whatever mechanism is at play must be able to produce supernovae across this wide range of galaxy types. Metallicity dependence here seems a less likely scenario, unless those SLSNe-II apparently born in the most luminous hosts are in fact born in lower mass dwarf galaxies within their halos (although in this case it would be odd that some SLSNe-I were not also seen in similar environments). However, other possible mechanisms may provide a viable alternative. For example, if SLSNe-II were formed only from very massive stars then they may exist only in very special locations.

Progenitors of SLSN-II

If the core mass prior to supernova is the dominant factor then indeed low metallicity will preserve core masses much better than at higher metallicity due to far lower radiative mass loss rates, and a possible bias to a more top heavy initial mass

function at lower metallicity. However, if SLSNe-II are in fact best explained by a strong interaction model then large scale mass loss is necessary at some point. In this case, the conditions necessary to form a SLSNe-II may be a combination of both relatively high core mass and still significant mass loss, meaning the initial (i.e. total) mass could play a more important role. In this regard it is interesting to note that the formation of very massive stars is potentially affected by stochastic processes even without changes in metallicity or to the underlying IMF. Small star forming regions, following a typical initial mass function, have a lower probability of building most massive stars, because there is insufficient mass. For example, if a star forming region will form only a few hundred solar masses of stars the probability of it forming any stars with greater than ~ 100 $M_{\odot}$ is extremely small, stochastic sampling assumes that masses are picked at random from the IMF, but that the star can only be formed should sufficient mass remain in the cluster. Hence, once a few stars have been formed, forming extremely massive stars in low mass clusters becomes unlikely.

Stochastic sampling effects have been observed in relatively local open clusters, and appear to be very important below cluster masses of $\sim 10^4$ $M_{\odot}$ [Piskunov et al., 2009]. Indeed, the most massive star in a cluster is thought to scale roughly as $0.39{M_{\rm cluster}}^{2/3}$ [Bonnell et al., 2001; Weidner et al., 2010], meaning that clusters with initial masses of $\sim 10^4$ $M_{\odot}$ are needed to form stars with masses $> 200M_{\odot}$. The most massive stars would then be formed in locations where either there was a large scale starburst (e.g. the very massive stars located in 30 Dor, or at a handful of locations within the Milky Way [Rauw and De Becker, 2004; De Becker et al., 2006; Crowther et al., 2010; Gvaramadze et al., 2013; Hainich et al., 2014]), or in places where the IMF was biased towards the creation of high mass stars (i.e. was top heavy relative to the local IMF). Indeed, it is interesting to note that the relative number of high mass clusters (scaled by star formation rate) does appear to be higher in dwarf galaxies, or in starbursts [e.g. Bastian, 2008], such that massive clusters, and hence the most massive stars may be found in relatively greater numbers in these galaxies, compared to relatively quiescent spirals such as the Milky Way. Qualitatively this model may have some appeal in explaining the unexpectedly large range of properties in the SLSN-II host population, although the lack of knowledge about variations in the IMF, even in the relatively local universe precludes more detailed work.

Finally, it is also possible that multiple progenitor routes are at play in the creation of the SLSNe-II population, meaning that some exhibit strong metallicity biases while others are formed at more typical metallicities, perhaps via binary

interactions which may eject large mass reservoirs quickly during common envelopes etc.

3.7 Conclusion

I have utilised the unparalleled UV and nIR sensitivity of *HST* to provide rest-frame UV and nIR observations of a sample of SLSNe. The hosts of SLSNe-I were shown to be consistently fainter than other core collapse hosts (CCSNe and LGRBs), by extension this should be indicative of a low mass, star formation rate and metallicity. This is despite apparently similar metallicities observed between LGRBs and SLSNe-I from optical spectroscopy of SLSN hosts (including some hosts for which nIR and UV observations are presented here, Lunnan et al. 2014). This discrepancy may be explained by a combination of small sample sizes and the absence of the faintest host galaxies from spectroscopic samples, although despite the similarities in the favoured progenitors for LGRBs and SLSNe-I there are also good astrophysical motivations (for example the timescales required in energy breakout and potentially the spin-down rate of any magnetar driven engines) as to why their environments may not be identical.

SLSNe-II appear to arise from galaxies spanning a surprisingly large range in absolute magnitude (and hence in star formation rate and stellar mass). This is difficult to explain from sampling the underlying star forming galaxy population subject to a simple metallicity bias, as has been attempted for LGRBs and SLSNe-I, but may be due to the preferential production of very massive stars in certain environments (either massive star formation regions, or at low metallicity). Equally, it could be a reflection that the current classification system has failed to adequately capture the true diversity of progenitor routes for SLSNe-II.

Nevertheless it is clear that studies of SLSN environments may still offer a powerful route to clues to their progenitor characteristics, in much the same way as they have for other classes of astrophysical transients. Such work will rely on a continuing stream of these very rare events, coupled with detailed follow-up across the electromagnetic spectrum. Through this detailed study of the environments we may hope to elucidate the progenitors of SLSNe, and how they fit in to the growing diversity now being discovered in the transient optical sky.

Chapter 4

On the Sub-galactic Environments of SLSNe

"It has long been an axiom of mine that the little things are infinitely the most important"

—Arthur Conan Doyle, *The Memoirs of Sherlock Holmes*

4.1 Introduction

As we have already seen, using the properties of the environments of transient explosions provides a complementary route to progenitor determination. Through various photometric and spectroscopic observations of SLSN hosts, they have been shown to be faint, low mass, compact galaxies of typically low metallicity and little star formation [Lunnan et al., 2014; Leloudas et al., 2015; Perley et al., 2016, and the work within Chapter 3]. However, whilst the global properties of a host galaxy can provide a rough estimate of the underlying stellar populations based upon these parameters, these numbers really only represent the galaxy's likely *overall* population, failing to account for potential variations in environmental conditions *within* the host. Such internal fluctuations in environment properties are not thought to be uncommon; the distribution of small scale (∼kpc) star forming regions within galaxies has shown to be asymmetric and clumpy [Hodge, 1969], which means the global star formations inferred may not reflect the star forming properties local to the site of a transient explosion. Furthermore observations of the Milky Way and nearby galaxies have shown considerable metallicity dispersion within the galaxy [e.g. Rolleston et al., 2000, 2002], whilst IFU observations regularly show spreads in

star formation region metallicities of ∼0.3-0.4 dex across nearby SN hosts [Christensen et al., 2008, Joseph Lyman, private communication]. Indeed, modelling of global inhomogeneity within LGRB hosts by Niino [2011] suggests that the overall host metallicities may trace a distribution which is systematically metal-richer than that traced by the metallicities of the local birth environments. These do suggest that some of the properties which we infer for the progenitors within such systems may be misleading, if such systematic differences in star formation and chemical enrichment are typical. Although it has been shown many SLSN host galaxies possess irregular morphologies or are compact in nature [Lunnan et al., 2015; Perley et al., 2016, the work within Chapter 3], and thereby gradients in metallicity observed within well-formed disk galaxies (which affect the local star formation and thus distribution of stellar mass) are unlikely to have strong influence within these particular SLSN hosting galaxies, a notable sample of SLSN-II events have been observed to occur within more massive, spatially extended hosts [e.g. see Chapter 3, Perley et al., 2016]. These galaxies may be subject to more observable small scale environmental variations in metallicity, or in star formation intensity. For instance, a pocket of small scale star formation within a massive galaxy with a typically older stellar population will only result in a very low global specific star formation rate, regardless of whether the SN was associated with this burst of star formation or not.

A neat solution to this issue may be found by looking at the sub-galactic environments of the explosions. The use of pixel statistics as a method of progenitor probing has been employed to great effect within the hosts of other core collapse transients, such as LGRBs and CCSNe. First independently implemented by Fruchter et al. [2006] and James and Anderson [2006], the fractional flux, a measurement of the brightness of the transient site within the brightness distribution of all regions of the galaxy, provides an excellent tool for estimating the stellar population immediate to the transient, free from morphological constraints that make features such as the offset from the host nucleus challenging in faint irregular systems. This allows for the identification of statistical trends within a sample of transient events such that preferences for brighter or fainter pixels may indicate properties of the underlying progenitor populations. When applied at multiple wavelength regimes, different stellar populations are thus examined and therefore a more accurate picture of the transient's local stellar population may be drawn. Previous studies covering the host galaxies of LGRBs and Type Ic SNe have shown them to be strongly correlated with the brightest star forming regions within their hosts, thus tying these transient events to the deaths of young, massive stars [Fruchter et al., 2006; James

and Anderson, 2006; Kelly et al., 2008; Svensson et al., 2010; Anderson et al., 2012], distinguishing them from Type II SNe, whose locations are less strongly correlated with star formation and therefore indicative of older progenitors [Kelly et al., 2008; Anderson et al., 2012]. Thus by studying the locations of SLSNe within their host galaxies, we may obtain a deeper insight into their progenitor channels.

An initial study of the sub-galactic environments of hydrogen-poor, SLSN-I hosts was carried out by Lunnan et al. [2015], finding the SLSN-I events to proportionally trace star formation within their host galaxies, although their locations are statistically less concentrated on star forming regions than observed for LGRB events. However, to date, no such approach has been taken to study the local environments of hydrogen-rich SLSN-II. As previously shown, the host galaxies of SLSN-II appear to be somewhat different from those of their hydrogen poor cousins, spanning an appreciably broad range of host luminosities, star formation rates and stellar masses [e.g. work within Chapter 3, Perley et al., 2016], which are globally more metal rich [Leloudas et al., 2015]. Indeed, amongst local ($z< \sim 0.5$) SLSNe-II, almost 30% appear[1] to have occurred within host galaxies of $>10^{10} M_{\odot}$. Given that it is thought that these events are more likely to originate from circumstellar interaction of the SN shock wave [Chevalier and Irwin, 2011], it would be beneficial to determine if the sub-galactic environments of these transients are as diverse as those observed for normal interacting SNe-IIn [e.g Habergham et al., 2014], or conversely, if these events occur within small scale environments of similar stellar properties replicated across this diverse range of galaxies. Therefore studies of SLSNe-II on a sub-galactic scale are vital, with particular inclusion of those host galaxies which appear to be spatially extended, such that we may place their natal progenitor environments into context.

Within this Chapter I will present analysis of the locations and offsets of both SLSN-I and SLSN-II events within high resolution, *HST* imaging of their host galaxies. I compare these SLSNe sub-galactic locations with those of other core collapse transient host galaxies, maintaining a like-for-like comparison in both UV coverage and redshift range. The sample selection for this chapter is described within section 4.2 along with the comparison samples, and a discussion of the observations and reduction can be found within Chapter 2. Section 4.4 describes the astrometric measurements of the transient locations and statistical analysis of the light distribution within the hosts. I present these results within section 4.5 and discuss their implications within section 4.6.

[1] Based upon the SLSN-II samples presented within the work of Chapter 3, Leloudas et al. [2015] and Perley et al. [2016]

4.2 Sample

Here I use nIR and rest frame UV observations of a sample of 27 SLSN host galaxies identified within Table 2.1, within the redshift range $0.019<z<1.57$. For pixel statistic methods to be used optimally as progenitor proxies, high spatial resolution imaging of the host galaxy is required, which can only be achieved via the use of adaptive optics, or from space-based instrumentation. I thus select a sample of SLSN host galaxies for which both *HST* imaging at rest frame UV wavelengths (such that the observations are more sensitive to younger, massive stellar populations) and SN discovery images (such that I may locate the transients), are publicly available.

The majority of the targets used within this chapter were initially targeted with *HST* programme GO-13025 (PI: Levan). However, given the limited number of SLSN host galaxies with *HST* coverage, I chose to also include targets from *HST* programmes GO-13858, GO-13022 and GO-13226, for which *HST* imaging at rest frame UV wavelengths is also publicly available. Full details of these observations can be found within Table 2.1.

Unlike SLSN-I events, current coverage of hydrogen rich SLSN-II host galaxies with high resolution imaging is poor. Indeed, even amongst the sample with *HST* imaging, many of the host galaxies are exceptionally faint or diffuse (see Chapter 3 for particular examples), making the study of the sub-galactic environments for these events particularly challenging. Therefore I supplement the SLSN-II sample within events drawn from the PTF survey published within the recent work of Perley et al. [2016]. Whilst these particular host galaxies are currently not imaged at high enough resolution to make comparable pixel statistic analysis with the original host sample, I utilise these additional hosts for offset measurements. This supplementary sample is also detailed in Table 2.1.

4.2.1 Comparison Samples

Transients which typically prefer brighter star forming regions within their hosts and are likely to originate from younger, more massive stars, as has been previously shown for LGRB events [Fruchter et al., 2006; Svensson et al., 2010]. Through comparison of the locations of SLSN events with those of other core collapse transients, an insight into the local underlying populations may be gained. To select an appropriate sample for comparison, it is required that the host galaxies are also imaged at high resolution (i.e. adaptive optics or space based observations), in bands covering rest frame UV wavelengths such that a direct comparison to the SLSN hosts used within this Chapter can be made. In order to reduce biases from galaxy evolution at

higher redshifts, it is also required that the comparison samples cover a comparable redshift range and distribution to the SLSNe sample utilised ($\sim$0.02 <z<$\sim$1.6) as demonstrated within Figure 4.1.

The somewhat different redshift ranges shown within Figure 4.1 arise from the heterogeneous nature of the samples used within this Chapter. The original sample of SLSN identified during the infancy of SLSN studies is largely at low redshift (due largely to the shallow depth of the surveys in which such events were usually serendipitously discovered). When this sample is supplemented with events from the PanSTARRS MDS survey, who's depth and design is capable of finding SLSN out to higher redshifts, the redshift distribution becomes broadened.

Whilst the overall redshift ranges of these samples are similar (all within $\sim$ 0.02<z< $\sim$ 1.6), the various photometric depths achieved within different transient surveys which are sensitive over a range of wavelengths, often results in each survey having volume at rather dissimilar redshifts. For instance, the GOODS survey is capable of reaching fairly deep 5σ limiting magnitudes of m_{AB} = 27 - 28 in the B,V,i,z filters [Dickinson et al., 2003], but as core collapse SNe typically peak at absolute magnitudes between M_V $\sim$-17 to -18, it is typically below redshifts of $\sim$ 1 that these SNe may be confidently detected within the *HST* *A*CS imaging. On the other hand, the intrinsically higher luminosities of SLSNe means that they are capable of being detected out to much higher redshifts within much shallower ground based surveys (i.e. out z $\sim$1.5 within the PanSTARRS MDS survey which reaches limits of $m_r$$\sim$23.5). Such effects can create radically different distributions between samples within the same redshift range, as seen within Figure 4.1. As this work requires rest frame UV imaging, here additional redshift limitations arise from the availability of rest frame UV imaging of the host environment (for instance, the UV mapping of the GOODS SN fields is ongoing and as such not all SNe within the GOODS sample have coverage at present).

Such differences in redshift range leave the conclusions about the subgalactic environments subject to the effects of galaxy evolution with cosmic time (i.e. at lower redshifts galaxies tend to be more metal rich), so two transients populations at different redshifts with locations strongly linked to star forming regions within their hosts do not necessarily have similar progenitor populations, if one sample is on the whole, more chemically enriched. Whilst at higher redshifts, where the vast majority of transient hosts are unresolved, we are unable to differentiate between the natal environment of the progenitor and the location of it's final explosion, this assumption becomes unsteady at lower redshifts, where (especially within late-type host galaxies) the progenitor may have moved significantly from it's birth

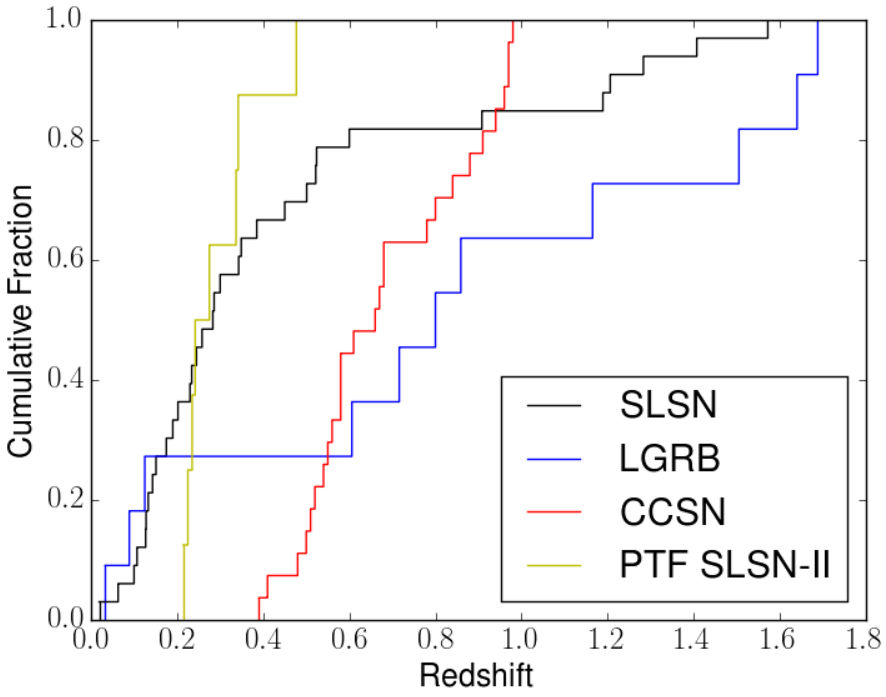

Figure 4.1: The redshift distribution of SLSNe and comparison LGRB and CC-SNe events used for sub-galactic environment analysis within this chapter. Ground based observations used to increase the SLSNe-II offset sample are shown separately. Whilst there is approximate matching of the SLSN and LGRB distributions, limitations in available data due to the ongoing mapping of the GOODS fields with WFC3 restricts the available redshift distribution of CCSN events from GOODS.

environment within it's lifetime (for instance, if a massive stars lifetime is $\sim$ Myr whilst its host's rotational period is of order a few 10-100 Myr). Such biases may lead to incorrect assumptions about the local environment of transient populations when compared to events at higher redshift.

I compare the pixel statistics of the SLSNe sample with the host galaxies of CCSN and LGRBs from the previous works detailed below.

Core Collapse Supernovae

I draw the CCSN comparison sample from the Great Observatories Origins Deep Survey (GOODS). This is a multi-epoch deep survey using the Advanced Camera for Surveys (ACS) imaging in F450W, F606W, F814W and F850LP bands provides a sample of CCSN host galaxies independent of their luminosity, and therefore an ideal untargeted survey sample. A further advantage of utilising this particular sample

for this study is that all SNe within the sample were discovered using *HST* images. As such, localisation of the transients within their hosts is exceptionally good ($\sim<1$ pixel).

A legacy program to map the star-forming properties of galaxies at $z\sim0.5$ - 2 in the CANDELS Deep fields in GOODS North and South is currently being undertaken using deep WFC3/UVIS imaging (GO-13872, PI: Oesch). GOODS SNe hosts covered within the data set provide the ideal comparison sample for pixel statistic analysis. I therefore draw a CCSN host galaxy comparison sample (based upon the original sample presented within Svensson et al. [2010]) of hosts which currently have UV imaging within this program[2]. This sample is restricted to include only those SNe covered at rest-frame UV wavelengths (shortwards of 4000Å), and the images for these hosts are all treated in an analogous manner to the UVIS SLSN host imaging discussed within Section 4.3.

One drawback with using this particular sample is the lack of spectral typing of the GOODS CCSNe, as any similarities the sub-galactic environments of hydrogen-poor or hydrogen-rich SNe and SLSNe may indicate likeness in their progenitors. Given the similarities between SLSN-II and "normal" SN-IIn events in their narrow hydrogen emission spectra, I also compare the sub-galactic environments of the SLSN-II sample to a sample of "normal" interacting type IIn SNe from Habergham et al. [2014], a study in which the locations of low redshift (recession velocities < 6000 km s^{-1}) interacting transients (SN-IIn and SN impostors), were compared with those with SN-IIP and SN-Ic events. In particular the authors looked at the fractional flux parameters for these transient hosts in H-α and near UV (NUV) emission, finding these interacting SNe to be less concentrated on star forming regions within their host galaxies than SN-IIP and SN-Ic events. I therefore utilise the NUV fractional flux results of the SN-IIn obtained from GALEX imaging from Habergham et al. [2014] for comparison with the SLSN-II fractional fluxes. As this sample of host galaxies is low redshift ($z<0.02$), the spatial resolution per pixel achieved within the GALEX images is comparable to that achieved for the SLSN-II hosts imaged with *HST* at redshift range $0.019<z<0.6$.

Long Gamma Ray Bursts

The locations of LGRBs have been intensely studied, and repeatedly shown to favour the brightest star forming regions within their host galaxies, linking them the deaths of young, massive stellar progenitors [Fruchter et al., 2006; Svensson et al., 2010]. Therefore by comparing the locations of SLSN with those of LGRBs, it may be as-

[2]Sample with imaging at the time of thesis production

certained whether the SLSN are also associated with a massive stellar population. I draw the comparison LGRB sample from the recent work of Blanchard et al. [2016], who present uniform fractional flux analysis for 100 LGRBs imaged with *HST* at UV and optical wavelengths. As the majority of LGRBs within the sample were discovered with *Swift*, potential biases which may have been introduced by including many targets drawn from multiple surveys (with varying observing strategies) are negated (although this sample is still subject to additional biases from the availability of afterglow imaging and reliable redshift estimations).

For this work, I strip the Blanchard et al. [2016] sample down to include only those LGRBs with measured redshifts which match the redshift range of the SLSN sample and CCSN sample ($z \lesssim 1.6$), and utilise only those hosts with *HST* imaging at rest frame UV wavelengths (<4000Å). Additionally, many of the LGRBs within the Blanchard et al. [2016] sample have poor localisations within their hosts (in some cases the astrometric error radius is factor several greater than the measured size of the host). In order to ensure a representative sample of LGRB fractional fluxes, I also remove any remaining objects within the sample for which the ratio of astrometric error radius to host galaxy size (here I use the radius in which 50% of the host light is contained, r_{50}, for consistency with other works) is >0.3, with a sample median ratio of 0.17, approximate to the average relative astrometric precision of the SLSN host sample.

4.3 Observations

Data for the SLSN host sample used within this work were taken from *HST* programmes with publicly available data, outlined within Chapter 2. These programmes imaged SLSN hosts at wavelengths corresponding approximately rest frame UV wavelengths for the given redshift of the host (see Table 2.1 for a full breakdown of used filters used for each target).

The images obtained for the hosts within this sample all used a dither pattern of 4 points or higher, thus allowing for good sampling of the PSF. All images were processed within AstroDrizzle software as described within Chapter 2. For the WFC3/UVIS and ACS images (for SLSNe and GOODS CCSNe imaging), as these images all have >4 point dithers, I drizzle these images to a final pixel scale of $0.025''$ pixel^{-1} such that an the spatial information may be improved, meaning a linear resolution of 0.11 kpc at the median redshift (z=0.3) of the sample. For the subsample of hosts with nIR images, due to fewer dither pointings than the UV, these images were kept at the native pixel scale of $0.13''$ pixel^{-1}.

For additional SLSN-II candidates not imaged with *HST* but used for additional offset analysis as described within Section 4.2, I obtained SDSS u or g band imaging of the host galaxies, dependant upon redshift of the SLSN, for astrometric matching with the PTF discovery images of these SLSN events for offset analysis. Details of these hosts are provided within Table 2.1.

For the LGRB comparison sample drawn from Blanchard et al. [2016], the fractional flux values were determined for these hosts using images drizzled to half the native pixel scale of the *HST* detector used, which given the fraction of hosts imaged with ACS whose native pixel size is $0.049''$, provides a good match for the optimal spatial resolution achieved within the SLSN sample.

4.4 Analysis

4.4.1 Astrometry

To determine the locations of the SNe within the *HST* imaging of their host galaxies, I obtained archival images taken whilst the SN was visible where publicly available. Where possible, I used images which had been obtained close to maximum light to maximise the S/N of the detection and thus improve the localisation of the centre of the SN's PSF. Table 2.6 lists the telescopes and instruments from which the bright SN images were obtained.

To precisely locate the SLSN events within the host's *HST* image I performed relative astrometry through identifying common point (or point like) sources between the discovery and host images, as described within Chapter 2. Positional errors (σ_x,σ_y) were determined for these astrometric solutions by estimating from the error associated with the centroiding of the SN within the discovery image and from the X,Y RMS of the astrometric solution. I present the astrometric uncertainties for the UV and nIR locations within Table 2.6, highlighting those hosts for which only a reduced number of point sources (<8) were able to be identified, and for which I account for the rotation of the image before astrometric matching, to reduce the number of free parameters involved with astrometric mapping (as described within Chapter 2).

4.4.2 Fractional Flux

The fractional flux (hereafter, F_L) provides a morphology-independent method of determining the degree to which any transient event traces the light distribution of it's host galaxy at any given wavelength. F_L is an estimate of the fraction of light

contained within pixels of the galaxy of a lower surface brightness than that in which the transient was deemed to occur. This technique provides valuable information about the potential progenitors on both an individual and bulk population scale. Given that the relative lifetimes of massive stars ($\sim$ few Myr) are significantly shorter than the time scales involved in star formation ($\sim$ Gyr), very young progenitors will be seen at the locations of young (and presumably bright) star forming regions within their hosts. Transients which track star forming regions within their hosts, such as normal CCSN, will as a population, follow a roughly linear distribution. Alternatively, transients perhaps originating from the more massive stars (e.g. Type-Ibc SNe and LGRBs) will trend as a population towards the brightest UV pixels within their host galaxies, where the most recent star formation is likely to have occurred (and therefore represents a younger, more massive population of stars).

The F_L parameter was calculated as follows: the pixels associated with the host galaxy are first detected using Source Extractor [SExtractor, Bertin and Arnouts, 1996], applying a 3×3 Gaussian convolution filter and requiring that all detections have N_{pix} >10 pixels detected above the background threshold. The de-blending parameters are adjusted manually for each host galaxy to ensure optimum detection of the host environment. I then use the segmentation output from SExtractor to determine which pixels are associated with the host galaxy, and create an image mask such that only these pixels are analysed. This pixel array is then processed using standard routines within PYTHON to rank these pixels in order of their brightness. The ranked position of the pixel within which the transient is located is identified. The fractional flux parameter is then computed as the cumulative sum of the brightnesses of the pixels of lower rank, normalised by the total brightness of the host galaxy's pixels.

Weighted F_L

In cases for which the positional uncertainty of the transient location is large (i.e. typically greater than ∼10% of the projected host galaxy size), the F_L parameter may vary largely within the error radius (depending upon its location). This is of particular concern for SLSN and LGRB hosts, many of which are compact, or possess irregular morphologies [Lunnan et al., 2015; Perley et al., 2016, , work with Chapter 3]. Such host galaxy morphologies often result in large pixel-to-pixel variations across the length of the host; as either the majority of the compact host's light is concentrated upon a few pixels, or for irregular hosts, pixels across the error region may have high contrast due to clumpy internal structure. Previous F_L studies of transient hosts often take the location of the transient as given, and account for

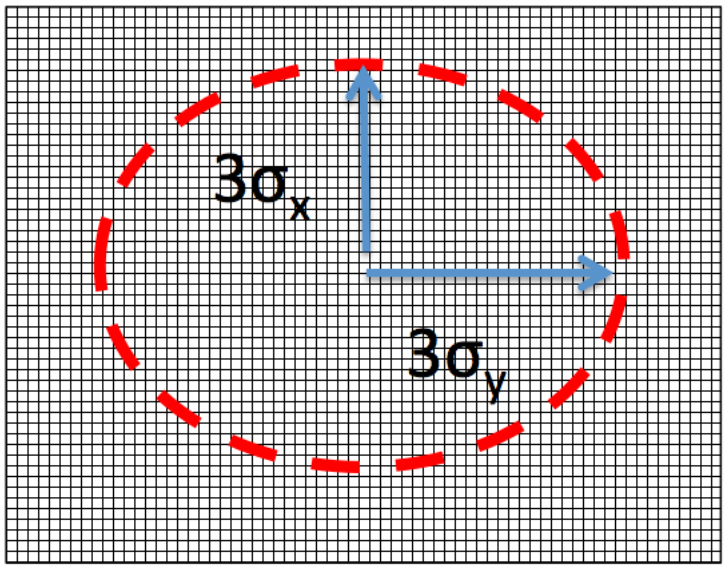

Figure 4.2: Demonstration of the error ellipse marked out when computing the weighted F_L , which accounts for poorer astrometric fitting in one direction, if required. Each pixel contained within this error ellipse will have a probability of association with the transient calculated for it. When combined with the intrinsic F_L value of these pixels, a distribution of probable F_L values can be found. Note that the scale of the error ellipse to the pixel grid is exaggerated here for the purpose of demonstration.

large positional uncertainties by convolving the host image to either the uncertainty radius or the PSF of the discovery image.

Here I present an alternative approach to F_L analysis which more accurately accounts for the locational uncertainties. This is done through creation of an 'error map'; an array of probabilities for each pixel's association with the transient location. I do this by superimposing a two-dimensional Gaussian (whose form is based upon the SN position and associated uncertainty) over the *HST* image, such that each pixel may be assigned an individual probability of being associated with the SN event. This is performed for each pixel contained within a 3σ error radius in the x and y directions of the transient location, as demonstrated within Figure 4.2.

For each SN event, I determine the x and y normal probability density distributions based upon the determined transient position within the *HST* image and it's associated Δx and Δy positional uncertainty (where $\Delta x, y = 3\sigma_{x,y}$). I then integrate these distributions between the upper and lower boundaries of each pixel within the $\Delta x, y$ range to determine the specific x and y transient probabilities for these pixels. The final locational probability is simply the product of these two liklihoods.

$$P(x,y) = \int_{x-0.5}^{x+0.5} P_x dx \times \int_{y-0.5}^{y+0.5} P_y dy \tag{4.1}$$

Therefore the F_L value of each pixel is weighted by it's final locational probability, allowing the distribution of likely F_L values to be examined (on an individual event basis or collectively, if these distributions are collected and normalised).

Whilst this method may account for locational uncertainties when considering pixel statistics within transient host galaxies, one potential drawback which must be considered given the large locational constraints of the SLSN sample under consideration, is the inclusion of additional pixels not associated with the galaxy light within a large error ellipse. Unless there is a clear offset between the transient and the proposed host galaxy (i.e. if an assessment of a "chance alignment" [Bloom et al., 2002] were performed, it would yield a very high probability of it being so), the transient most likely originates from the galaxy in question. Whilst it cannot be confidently ruled out that a nearby location off the galaxy light may simply be indicative of very low surface brightness features below the detection threshold of the image, a more plausible argument can be made for origin from detected UV regions, if an association with massive stellar core collapse is assumed.

As such, it may be prudent to apply an additional weight, which evaluates the probability of transient association with UV luminous pixels more highly than those which contain little/no UV light from the galaxy. This additional weighting is simply determined by the fraction of light contained within each pixel relative to all the pixels within the error ellipse, normalised to the total of of UV light contained within the error region (the $F_{\mathrm{UV}(x,y)}$).

$$P(SN_{UV}) = P(x,y) \times F_{\mathrm{UV}(x,y)} \tag{4.2}$$

The original locational probabilities for pixels within the error region are now weighted by this additional probability of UV-association. Whilst this weighting will naturally pull the distribution towards higher F_L values, it provide some indication of the strength to which SLSNe locations are tied to the star forming regions within their host galaxies.

By utilising each of these weighted fractional fluxes, the effects of localisation upon F_L values may be explored. I demonstrate these two techniques for two different location scenarios within Figure 4.3. Through combining the probable F_L distributions for all of the transient events within this sample from both weighted techniques, I may assess from the overall likely distribution of F_L values the likely behaviour of a normal F_L distribution given the locational constraints.

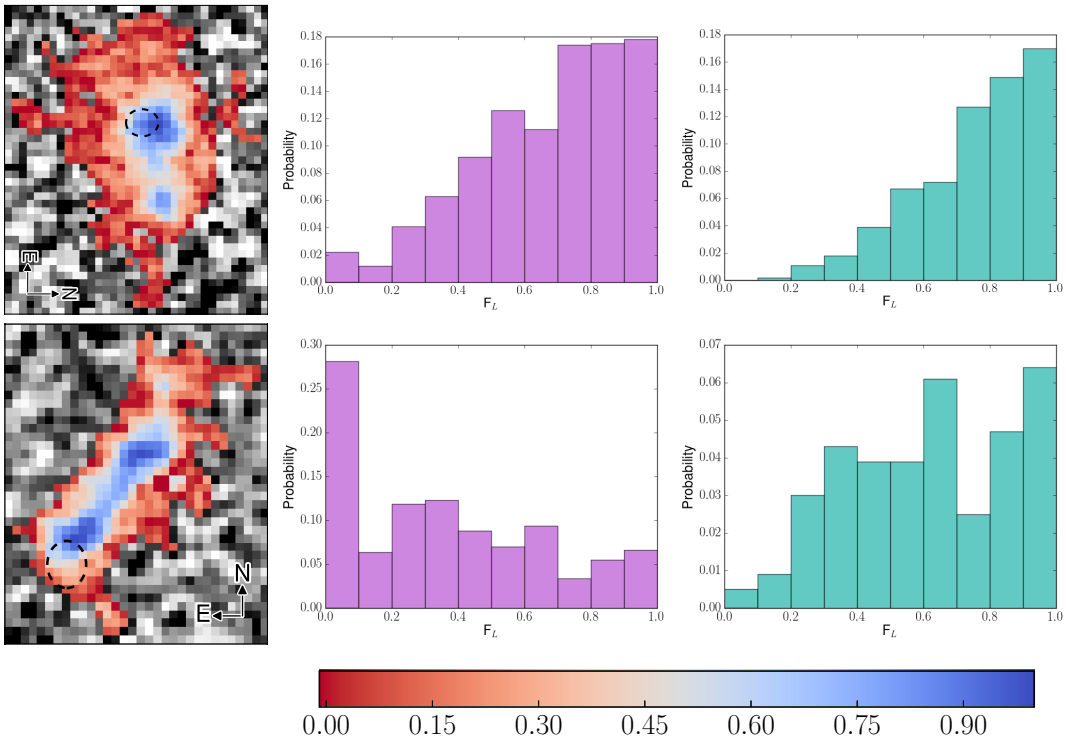

Figure 4.3: Demonstration of the weighted F_L techniques for the host galaxies of PTF11dij (upper row) and PS1-11afv (lower row). The left panels show the fractional flux "maps" of the host galaxies within their *HST* images, where red pixels represent low F_L values and blue represent higher F_L values (colour bar shown below). Here the 1σ locational uncertainty of the transient is marked with a dashed circle. Within the central panels (purple histograms), the distribution of probable fractional flux values contained within a 3σ error radius of the transient location and determined on a non-luminosity weighted basis are displayed. The far right panels (teal histograms) demonstrate this again, but with distributions for UV-luminosity weighted fractional flux values. For the better localised PTF11dij, whose location is more coincident with stronger star forming regions, the non-weighted flight does not drastically change the form of the likely distribution, whereas for PS1-11afv, weighting the probabilities shows a clearer shift towards higher F_L values.

4.4.3 Offsets

Another useful diagnostic when considering the local environments of transient events are the relative offsets of the explosion locations to the centres of their host galaxies. This has been most notably demonstrated by Bloom et al. [2002], who used the distribution of offsets of LGRBs to show that their locations were in agreement with an exponential disk distribution, which modelled the location of collapsars and promptly bursting binaries within galaxies. This provided strong evidence that they were associated with regions of massive star formation.

A handful of SLSN have been localised to regions significantly outside of the extent of the light from their hosts [c.f. the work within Chapter 3, Lunnan et al., 2014; Perley et al., 2016, for individual examples]. This may indicate that either these SLSN originate from exceptionally faint underlying host galaxies (typically fainter than $m_v{\sim}27$ for the majority of deep surveys), or that their progenitors are produced within relatively "faint" regions of the host galaxy where the surface brightness falls below the necessary detection limit, even with *HST*. Comparing the distribution of SLSN explosion offsets relative to their hosts with those of other core collapse transients provides additional constraints upon their likely progenitor populations (i.e. if SLSN have similar offsets to LGRB events, they may also follow the exponential disk model, which tells us something about the likely local populations).

To calculate the offset from the SLSN locations relative to their host galaxies, I first define the centre of each galaxy as the centre of the flux-weighted galaxy centroid as determined by SExtractor. From this I am able to determine the relative radial offset of the SLSN location to its host centre from it's x,y location within the *HST* image.

Differences in the centre and the brightest points of the host galaxy become increasingly apparent within galaxies of irregular structure and morphology, with multiple peaks or bumps within the galaxy's light profile with radius. These have important implications for the weighted probability distribution of fractional flux values (i.e. those located close to the brightest regions within their hosts are likely to exhibit a stronger preference for high fractional fluxes, given the priors assumed within this calculation). Therefore it is appropriate to measure the offsets of SLSN events from these regions too. Given the already highlighted irregular nature of some SLSN hosts, this method may provide a more morphology independent estimate of the offsets of the transients from regions of strong star formation within their hosts.

The coordinates of the brightest pixel can be determined using SExtractor, and thus the offset of the transient from these coordinates can be computed. I normalise all of the offset measurements by the size of the host galaxy, using the

radius in which 50% of the host light is contained (the r_{50} parameter), such that the results are in keeping with those of calculated for the LGRB comparison sample from [Blanchard et al., 2016].

Absolute Surface Brightness of SN Location

Finally, I also determine the surface brightness of the pixels in which our SLSNe are located. This is simply given by:

$$L_{\text{Surface}} = \frac{L/L_{\odot}}{A_{\text{pix}}}. \tag{4.3}$$

where A_{pix} is the physical size of the pixel in kpc^2. By determining the surface brightness of the transient location pixels, direct comparisons can be made between the luminosities of the populations local to SLSNe transients and those of LGRB and CCSNe events. As the luminosity of a given star is roughly proportional to the cube of its mass, this provides a mass (and hence age) sensitive method of directly comparing the underlying stellar populations which produced the events. This method has been used previously within Svensson et al. [2010] to show that LGRBs typically occur in regions of higher absolute surface luminosity than CCSNe, and was taken as confirmation that they originate from a typically younger stellar population. Despite differences in redshift distribution, the majority of the host images probe similar physical scales ($\sim$ few 0.1kpc per pix), which reduces the risk of transients which appear to originate from more luminous regions actually being the result of averaging small scale variations over a larger surface area.

4.5 Results

Within section 4.5.1 I present the measured properties of the sub-galactic environments of SLSNe within the UV. Figures 4.4, 4.5 and 4.6 provide a visual display of the F_L parameter mapped out for each galaxy within it's *HST* image, alongside it's locational uncertainty. I first inspect the standard fractional flux values (in which the location of the transient is taken as lying in the pixel with the highest probability) for the SLSN host galaxies within this sample alongside the surface brightnesses of the pixels in which the transient occurred, and consider the implications of these results when compared to the properties of the comparison sample transient locations. The use of the locational and UV-luminosity weighted fractional flux approach over the transient uncertainty region is explored before finally examining the distribution of offsets of SLSN events within their host galaxies both from

the projected galactic centres and from the brightest UV regions. Throughout this analysis I break down SLSN events into hydrogen poor SLSN-I and hydrogen rich SLSN-II events, (in which SLSN-I are inclusive of any SLSN-R events within the sample used within this chapter). As an aside I also consider the NIR F_L properties of the SLSNe sample within Section 4.5.2. The combined implications of these results will be considered in light of the underlying stellar populations which produce SLSN progenitors within section 4.6.

4.5.1 UV Results

The astrometrically determined locational uncertainties of the SLSN hosts considered within this work are presented within Table 2.6, whilst the measured fractional flux UV and IR values, pixel luminosities and locational offsets are presented within Table 4.1. The astrometric uncertainties for the GOODS CCSNe locations are presented within Appendix Table A.8 and the properties of their locations are given within Table A.9. I present the cumulative distribution of UV F_L values for the SLSN hosts within Figure 4.7, against those of the CCSNe and LGRB comparison samples at similar redshift range outlined within Section 4.2.1. To guide the eye, I also show a uniform distribution of fractional fluxes. Such an observed distribution would indicate the tracing of UV light across the host sample in a linear manner.

Looking at Figure 4.7 it is clear that SLSN events trace a distribution of generally brighter UV regions than CCSN (which themselves trace an almost linear distribution) but fainter than those occupied by LGRB hosts. To test the significance of the apparent differences observed between these transient host populations, I perform both two sample Kolmogorov-Smirnov (KS) and Anderson-Darling (AD) tests between each population for both our fractional flux and offset distributions. The results of these parametric tests are given within Table 4.2. This parametric testing suggests that the sub-galactic environments of SLSN cannot be statistically distinguished from those of CCSN and LGRB environments, despite the apparent visual sequence of increasing concentration towards bright UV regions of CCSN→SLSN→LGRB events.

Once broken down by spectral subtype, as shown within the lower panel of Figure 4.7, the sub-galactic environments of hydrogen-poor and hydrogen-rich SLSN events appear to differ. SLSN-I events seem to occupy much of the same parameter space as previously occupied by the entire sample of SLSN (which given that they comprise ∼80% of our sample, is hardly surprising), following a fractional flux distribution more concentrated than CCSN events and less so than LGRB ones, although once again this is statistically unsupported (this may be clarified at a later

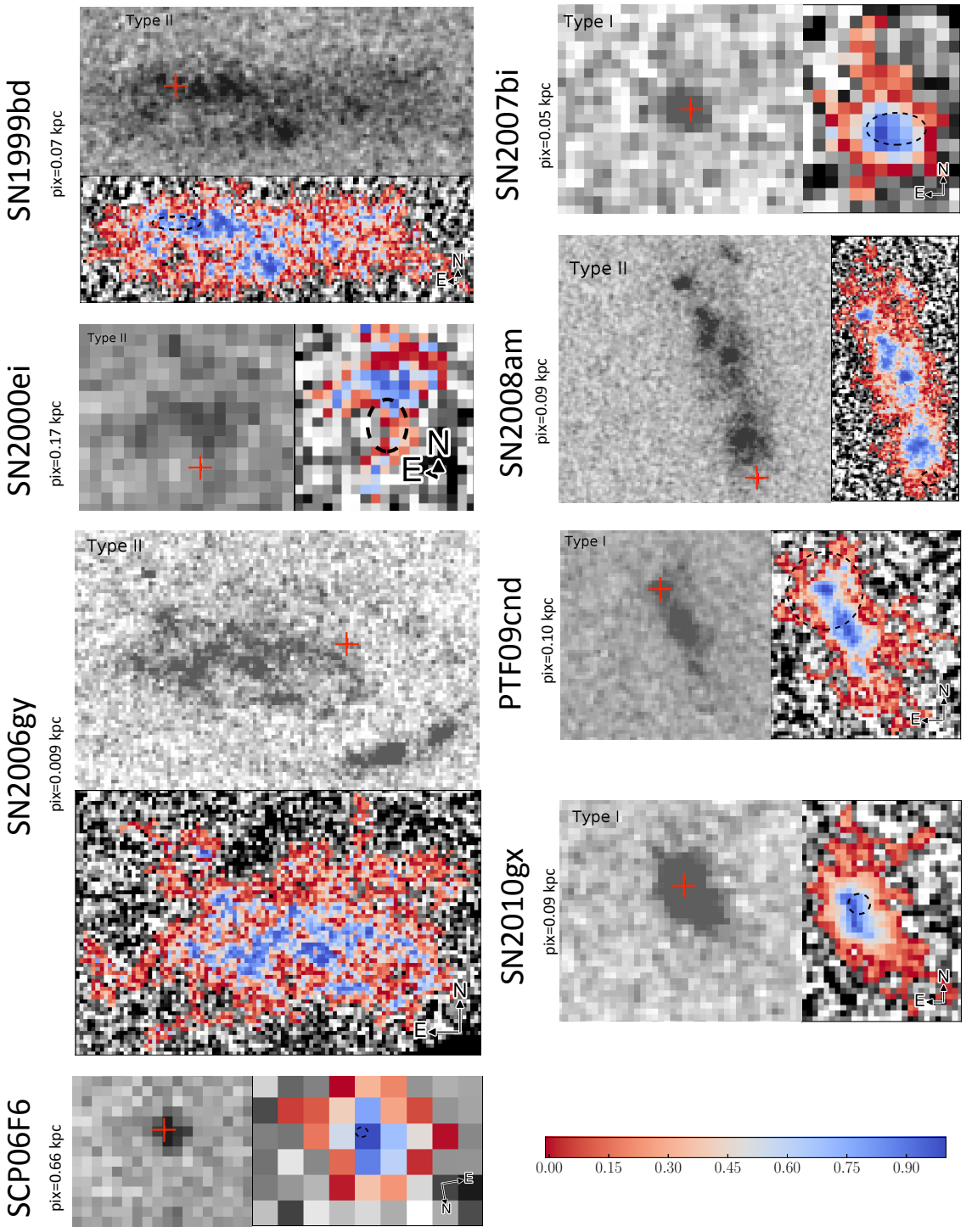

Figure 4.4: *HST* imaging of SLSN host galaxies used for location analysis alongside the fractional flux heat maps of these hosts in terms of each pixel's assigned F_L value. Dashed lines encompass the 1σ error ellipses associated with the locational uncertainty of the transient. SLSN spectral classes are provided for reference.

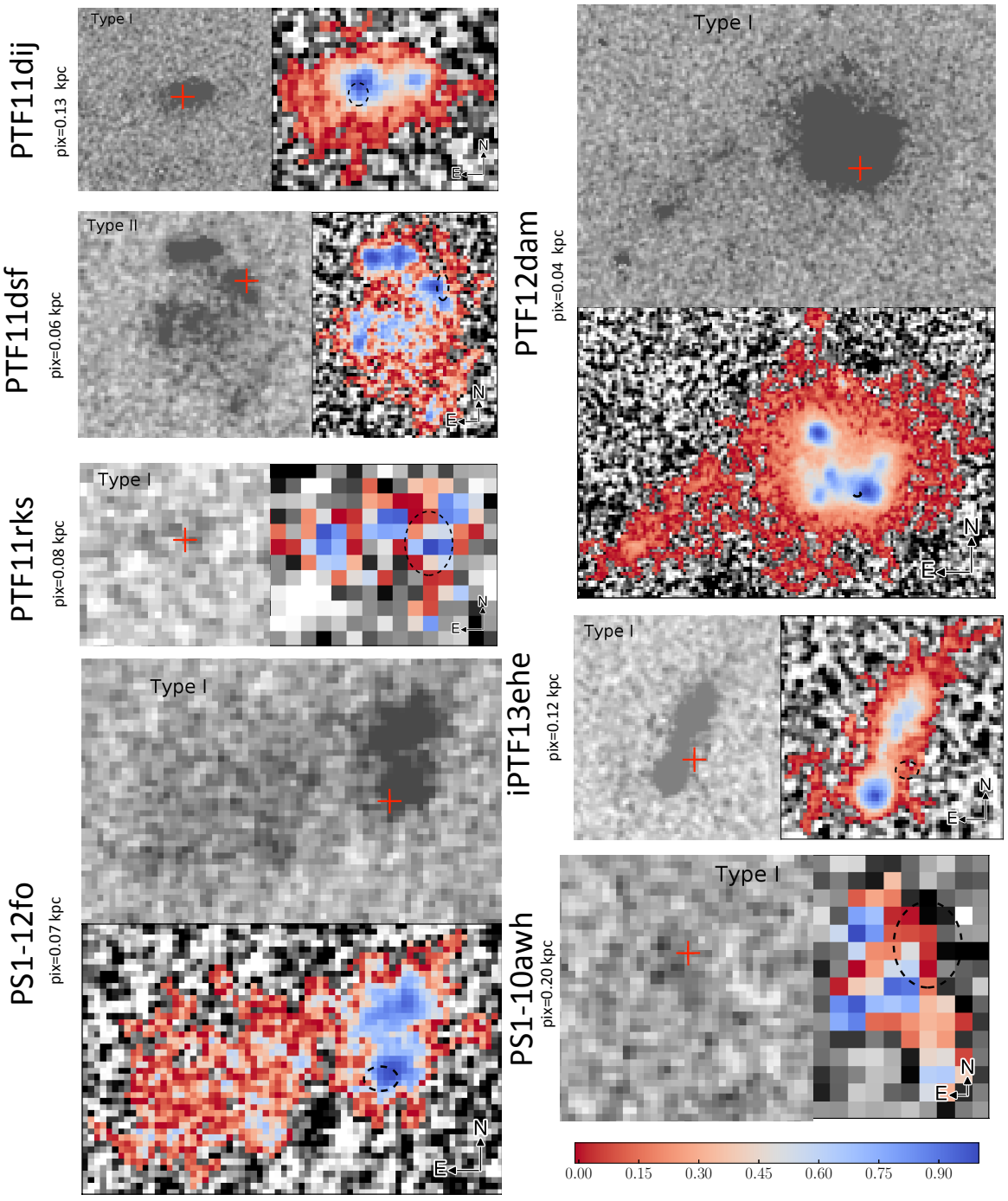

Figure 4.5: More *HST* imaging of SLSN host galaxies alongside their fractional flux heat maps displaying the estimated transient locational uncertainty.

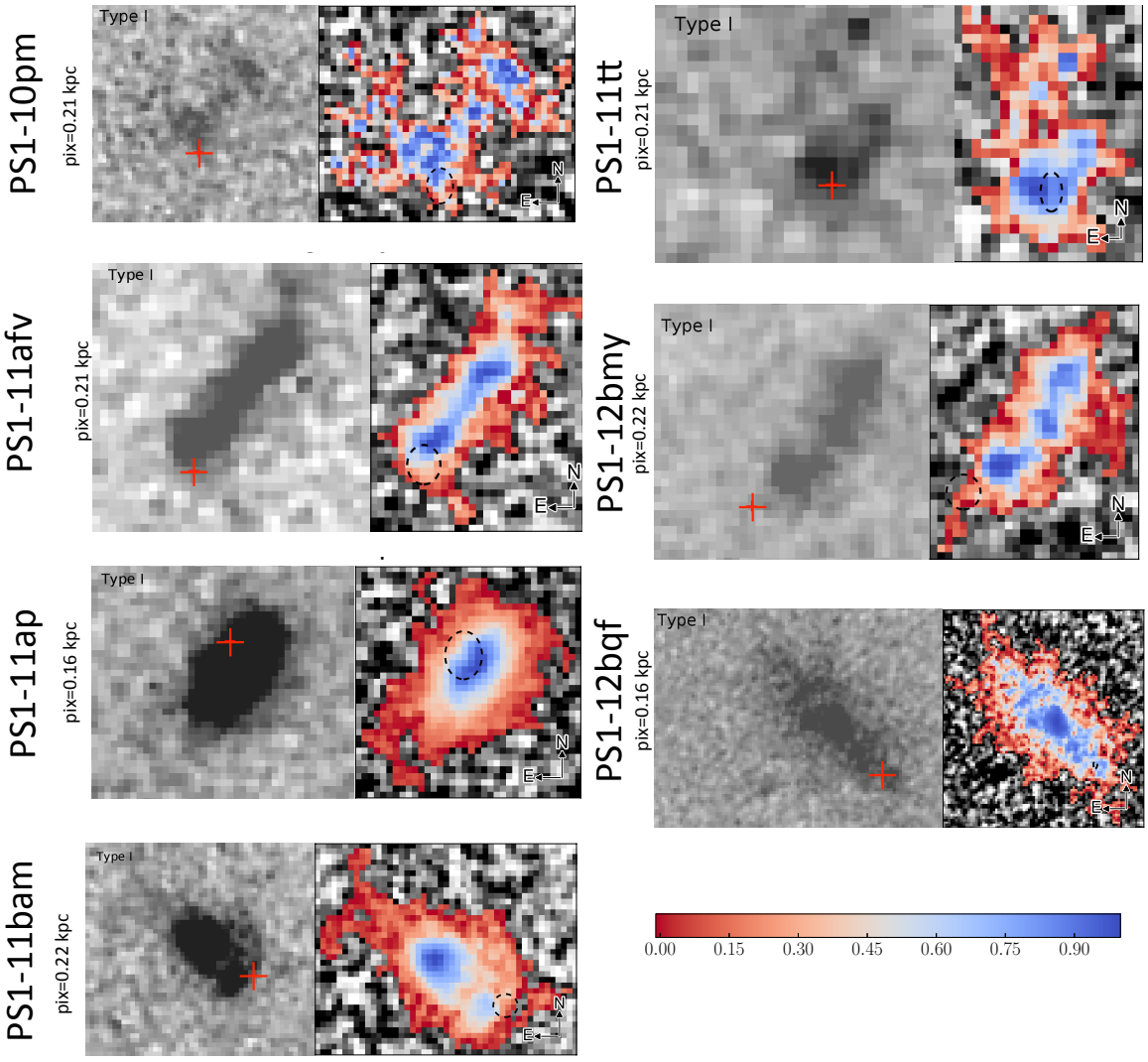

Figure 4.6: More *HST* imaging of SLSN host galaxies alongside their fractional flux heat maps displaying the estimated transient locational uncertainty.

Table 4.1: Properties of the locations of SLSN event sites presented within this chapter, including the fractional flux estimates (in UV and nIR where available), the surface brightness and the relative offsets of the explosion sites from the host centre and from the brightest UV region.

SLSN	F_L UV	F_L nIR	UV r_{50} (kpc)	UV Host Offset (kpc)	UV Bright Pix. Offset (kpc)	Offset Err (kpc)	Log L $L_{\odot}kpc^{-2}$
SN1999as	0.76	0.53	-	11.65	0.08	1.80	8.51
SN1999bd	0.63	0.46	1.74	1.95	2.53	2.33	8.01
SN2000ei	0.07	0.47	0.33	1.51	0.77	1.41	7.11
SN2005ap[3]	-	-	0.64	3.54	-	-	-
SN2006gy	0.02	0.88	0.25	0.17	0.30	0.03	7.69
SCP06F6	1.00	-	0.35	0.11	0.06	0.14	8.73
SN2007bi	0.84	0.77	0.21	0.10	0.08	0.66	8.37
SN2008am	0.05	0.29	2.46	4.59	5.14	1.75	6.09
SN2008es	-	0.95	-	-	-	-	-
SN2008fz	-	0.84	-	-	-	-	-
PTF09cnd	0.98	0.04	0.93	1.00	0.06	4.68	8.25
SN2010gx	0.76	0.92	0.40	0.17	0.18	0.81	8.38
SN2011ke	0.89	0.91	0.69	0.38	0.29	1.03	7.89
PTF11dsf	0.66	1.00	1.04	0.88	1.39	1.06	7.67
PTF11rks	1.00	-	0.22	0.1	0.55	0.74	8.12
SN2012il	0.96	1.00	0.94	0.57	0.16	0.95	8.66
PTF12dam	0.84	-	0.65	0.50	0.19	0.33	9.42
iPTF13ehe	0.11	-	1.32	0.75	1.27	1.32	7.49
PS1-10awh	0.51	-	0.56	0.79	0.82	1.23	8.05
PS1-10pm	0.49	-	1.35	1.36	2.25	1.50	8.04
PS1-11afv	0.38	-	0.98	0.83	0.54	1.51	8.39
PS1-11ap	0.98	-	0.68	0.46	0.33	1.71	8.54
PS1-11bam	0.15	-	0.91	3.09	2.63	1.25	8.61
PS1-11tt	0.85	-	0.69	0.25	0.31	0.97	8.46
PS1-12bmy	0.18	-	1.17	2.79	1.03	1.34	8.29
PS1-12bqf	0.15	-	2.14	3.63	2.91	0.60	7.81
PTF10fel	-	-	5.05	0.91	0.69	0.15	-
PTF10heh	-	-	1.46	0.16	0.09	0.93	-
PTF10jwd	-	-	7.04	0.11	0.13	0.22	-
PTF10qwu	-	-	1.60	0.31	0.24	0.08	-
PTF10scc	-	-	0.00	169.11	135.29	0.09	-
PTF10yyc	-	-	5.02	0.28	0.26	0.16	-
PTF12epg	-	-	4.76	0.08	0.03	0.12	-

Table 4.2: Two sample Anderson-Darling probability and Kolmogorov-Smirnov test results between the properties of the locations of SLSN events and of the properties of the core collapse comparison sample locations within their hosts. Probabilities less than 10^{-5} are presented as <0.00

Parameter	Host Connection	KS Stat.	AD Stat.
UV F_L	SLSNe - LGRB	0.195	0.095
	SLSNe - CCSNe	0.07	0.101
	SLSNe-I - LGRB	0.425	0.279
	SLSNe-I - CCSNe	0.343	0.018
	SLSNe-I - Uniform Dist.	0.044	0.026
	SLSNe-II - LGRB	0.032	0.008
	SLSNe-II - CCSNe	0.298	0.340
	SLSNe-II - SN IIn	0.477	0.734
	SLSNe-II - Uniform Dist.	0.073	0.065
	SLSNe-I - SLSNe-II	0.062	0.010
Centre Pixel Offsets	SLSNe - LGRBs	0.781	0.768
	SLSNe - CCSNe	0.055	<0.00
	SLSNe-I - LGRB	0.540	0.318
	SLSNe-I - CCSNe	0.0018	<0.00
	SLSNe-II - LGRB	0.047	0.095
	SLSNe-II - CCSNe	0.399	<0.00
Log L	SLSNe - LGRBs	0.094	0.168
	SLSNe - CCSNe	0.433	0.400
	SLSNe-I - LGRB	0.501	0.605
	SLSNe-I - CCSNe	0.109	0.051
	SLSNe-II - LGRB	0.001	0.001
	SLSNe-II - CCSNe	0.148	0.189
	SLSNe-I - SLSNe-II	0.007	0.011

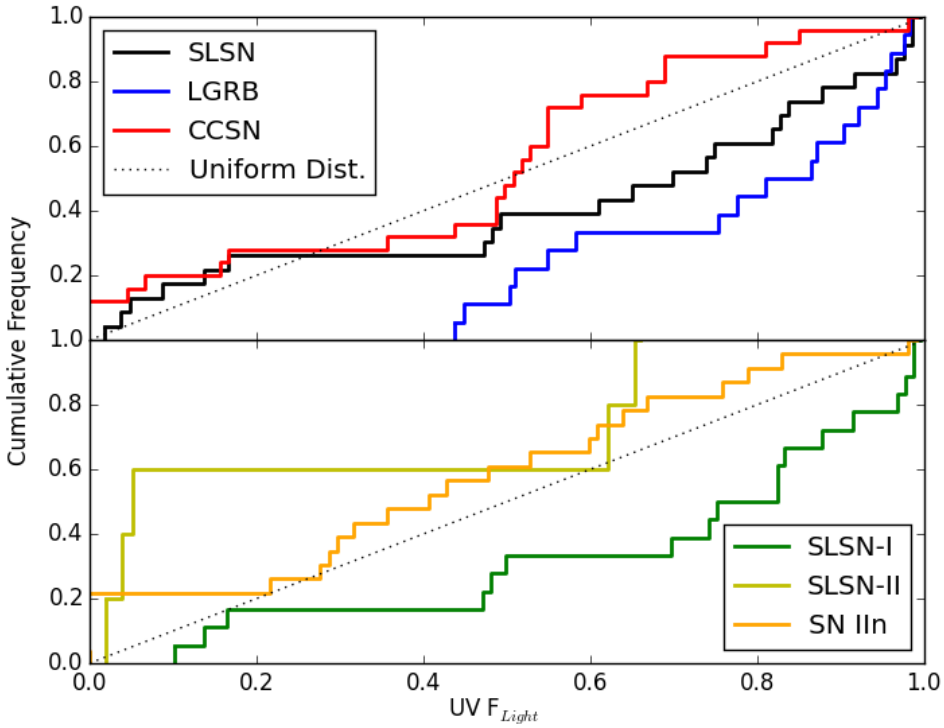

Figure 4.7: The cumulative distributions of UV F_L parameters for SLSN, GOODS CCSN and LGRB host galaxies from Blanchard et al. 2016 (upper panel) and the SLSN host broken down by spectral subclass (lower panel). The dotted line represents a uniform distribution of F_L . The SLSN distribution appears to trace a light distribution intermediate to the light traced by CCSNe and LGRB hosts. Although there is an apparent trend to more concentrated distributions, the small sample size means the differences in these distributions are not statistically supported.

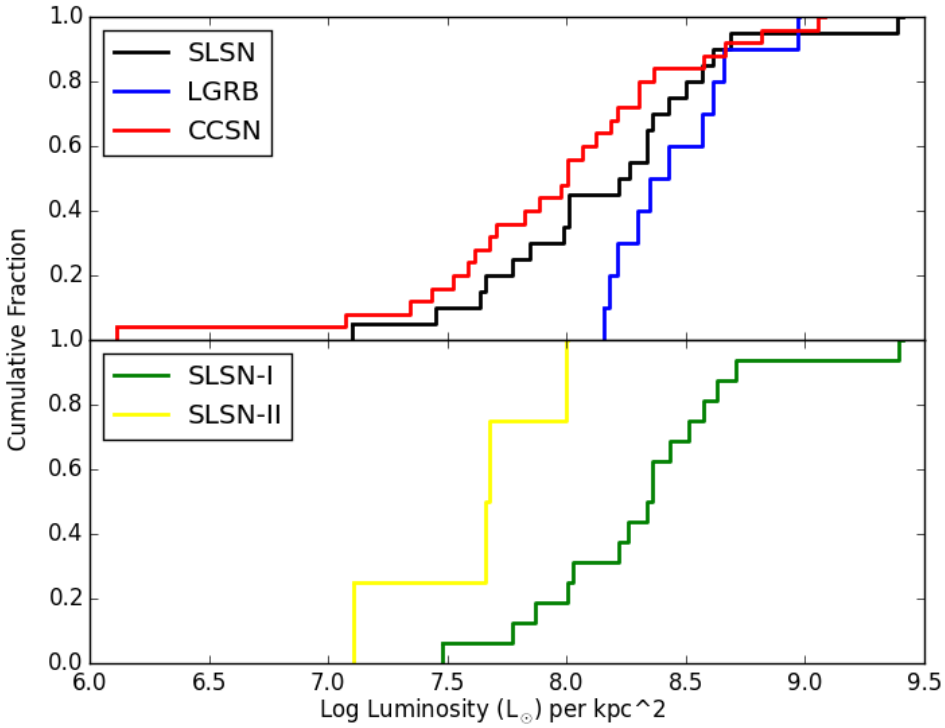

Figure 4.8: Top panel: The absolute surface luminosities of SLSN locations compared to those of LGRB and CCSN events from Svensson et al. 2010. In general SLSN occupy lower luminosity pixels than LGRB events, but comparable to those of CCSNe (p=0.87,0.78 for KS and AD statistics respectively). Lower panel: The situation changes once broken down by subclass, SLSN-I occupy pixels of moderate luminosity which are statistically indistinguishable from either of our comparison populations, whilst SLSN-II are located within much fainter pixels.

date with larger sample sizes).

Nonetheless, SLSN-I events are clearly tied to ongoing star formation within their host galaxies, although the strength of this connection (are they more strongly connected with recent/massive star formation?) has yet to be seen. On the other hand, the few SLSN-II for which F_L estimates have been obtained appear to strongly prefer fainter pixels within their hosts, with 3/5 of this sample originating from pixels with F_L values <0.1, whilst none of the 12 SLSN-I events originate from pixels with an F_L value this low. I compare the distribution of these SLSN-II F_L values with the F_L distribution of SN-IIn events from Habergham et al. [2014], who found SN-IIn environments to also exhibit an aversion to very bright UV pixels within their hosts. Although statistically, these two samples appear to be similar, producing high p-values for AD and KS tests which suggests some similarity in the two distributions, given the very small sample size of SLSN-II with fractional flux estimates, this result is likely to be affected by small number statistics, and should be reassessed once the sample size is increased. Despite this small sample size, there remains a clear statistical difference between the two spectral subclasses of SLSN event.

The surface luminosities for the sub-galactic environments of SLSNe are presented within Figure 4.8, and I compare them to those of the GOODS CCSN sample presented previously and for LGRBs events (which for this parameter are drawn from from Svensson et al. [2010], due to want of prior study[4]) . This allows us to assess if the differences observed within the F_L distributions are truly due to differences in the absolute brightnesses of the underlying galaxy regions. Overall, SLSN are located within pixels of a lower surface brightness than LGRB events, but brighter than those of CCSNe events, as suggested by the fractional flux distributions (although once again, as shown within Table 4.2, there are no statistically significant differences between these distributions). Interestingly, once broken down by SLSN subtype, it appears that SLSN-II are systematically located within pixels of fainter surface brightness than SLSN-I, with all events occupying pixels of $L_{\rm Surface} < 10^8$ $L_\odot$ kpc^{-2}.

As a check that the distribution of normal measured fractional flux value is not biased at any extremity by larger error radii (for instance that fainter F_L values are not simply a bias introduced via larger location uncertainties), the spread of F_L values with error radii in pixels, (as the localisation is relative to the individual host) are shown within Figure 4.9. For SLSN-I events, the degree of locational uncertainty shows some shallow decrease towards higher F_L values, with a spearman's

[4]Consistency in redshift and rest-frame UV coverage is maintained within this comparison sample as with previous comparison samples

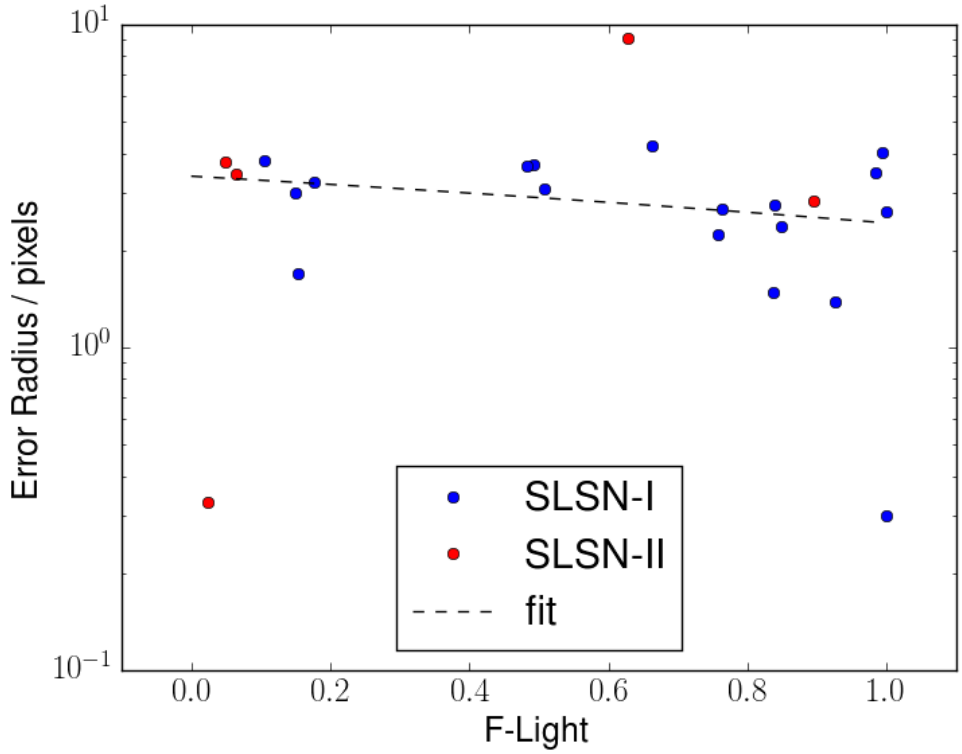

Figure 4.9: The scatter of F_L values with error radii (in pixels) for SLSN locations within their hosts. SLSN-I (blue) and SLSN-II (red) events are shown separately for consideration of the impact upon their individual distributions. In general, there is some shallow evolution of the error radius with F_L value, such that events with higher F_L values are have better constrained localisations.

rank correlation of -0.348 (with a significance of p=0.157). This linear regression fit does imply that towards fainter F_L values the larger locational uncertainties act to scatter the value of F_L measured, and thus suggest that the observed F_L distribution is less constrained towards the faint end.

To assess the variation of the F_L parameter within the individual SLSN uncertainty regions, I first perform a weighted fractional flux assessment for each SLSNe in this sample, weighting the resulting F_L distribution only by the probability of the transient being coincident with the pixels under consideration. These distributions are stacked and presented within Figure 4.10. This resulting cumulative distribution is compared to the normal distribution of F_L values and a uniform distribution. Within this figure I also display a 'location + UV luminosity' weighted F_L distribution. Here the purely location weighted distribution inhabits lower fractional flux values than normally measured, a result of the inclusion of fainter pixels

within a typical uncertainty region (for instance, see the error ellipses within Figures 4.4, 4.5 and 4.6). Whilst this acts to dilute the observed F_L distribution, the form of the location weighted distribution is still fairly similar to that observed without location weighting, which suggests that even under large locational uncertainties, SLSNe still trace bright UV regions within their host galaxies, but not in a manner stronger than that of CCSNe

Naturally, when additional weighting from the UV luminosities is applied, higher F_L values become more common. The form of the original F_L is recovered remarkably well for high F_L values (>0.5), which given their marginally better locational constraints, may not be particularly surprising (as being better constrained to these bright pixels will naturally provide them with a higher weighting). At the faint end of the F_L distribution, the additional weighting slightly overestimates the form of the distribution, which again is to be expected given their typically bigger uncertainty regions, as these will act to scatter the value of F_L obtained through normal measurements towards lower values. If the assumption of association with star forming regions is correct, this location and UV luminosity weighted F_L distribution may be indicative of the real underlying distribution of locations.

Within Figures 4.11 and 4.12 I display the cumulative distributions of normalised offsets from the host centre and brightest pixel within the host respectively, using an increased sample of SLSN-II hosts including those drawn from Perley et al. [2016]. Upon examination of Figure 4.11 it is immediately apparent that there exists a strong similarity between the SLSN and LGRB host offsets, both of which are clearly distinct from those of CCSNe, which are located at much wider offsets from their host centres. Most notably, when breaking down the SLSN by spectral type (lower panel of Figure 4.11), two distinct populations are observed, with SLSN-II covering a larger range of offsets from the centres of their hosts than SLSN-I, which themselves are more similar to the normalised offsets observed within LGRB hosts (an AD p-statistic of 0.318). For clarity, the offsets of those SLSN-II measured within *HST* imaging are also displayed separately from the combined [Perley et al., 2016] and *HST* sample. Here the combined SLSNe-II offset distribution is more consistent with those of SLSNe-I, whilst the sample with *HST* imaging remain at larger offsets within their hosts.

Of interest when considering how the normal and weighted F_L techniques may be impacted by the SLSN location, are the offsets of the events from the brightest pixels within their host galaxies. I measure such offsets and present these within Figure 4.12. When considering the larger combined sample of SLSN-II hosts, the offsets appear to be similar to those of SLSN-I, however when accounting only

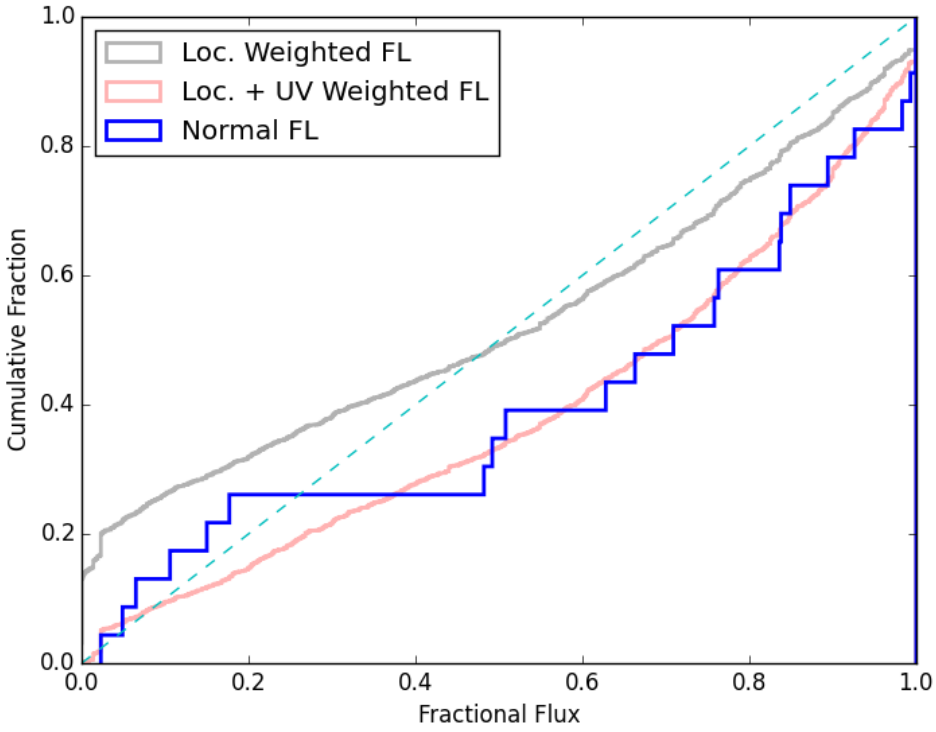

Figure 4.10: Here the cumulative distribution of the error weighted F_L distributions for the SLSNe sample are presented, displaying weighted by location (grey) and by location and UV preference (red). The measured normal F_L distribution is shown in blue. The location weighted F_L has similar form to the normal F_L distribution, but is diluted by the inclusion of fainter pixels with large location uncertainties. When additional weighting from the UV is applied, bright F_L values are recovered, whilst fainter ones appear to be overestimated, a likely result of the introduction of scatter towards the faint end of the normal F_L distribution with larger error regions.

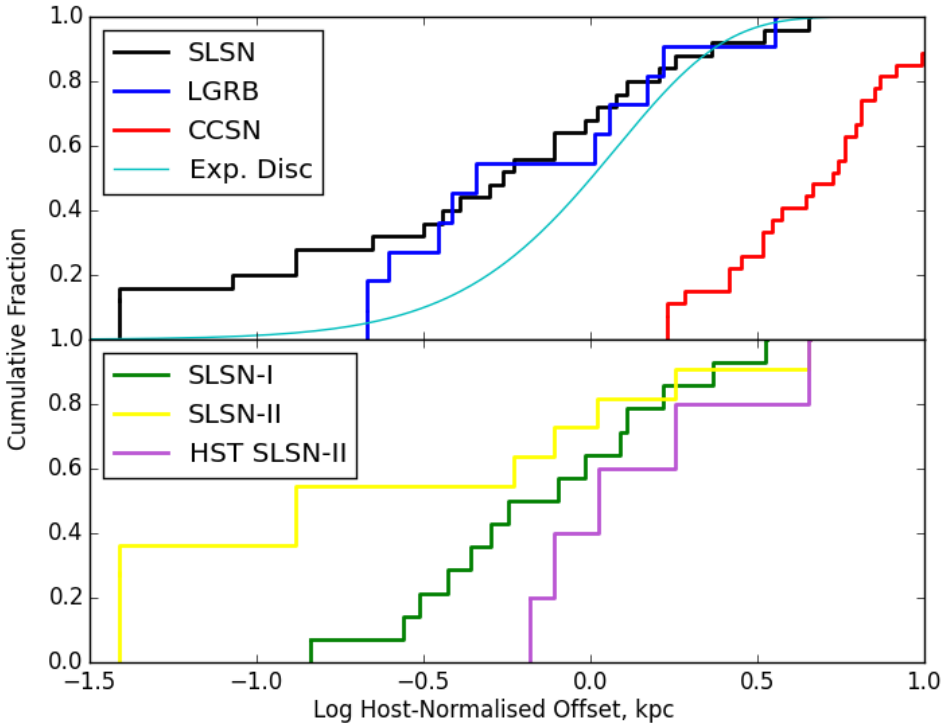

Figure 4.11: Upper panel: Here I present the offsets of SLSN, LGRB and CCSN events from the centres of their hosts, normalised by the host r_{50} size. Lower panel: The normalised offsets of SLSN hosts broken down by spectral subclass. Including SLSN-II hosts detected within ground based imaging from PTF, it can be seen that that SLSN-II events occupy a broader range of offsets from their host centres than SLSN-I, suggestive that perhaps their production is less dependant upon their environment within the host.

for those imaged with *HST*, these offsets appear to be wider and more consistent with SLSN-II arising from pixels of a lower F_L value. However, the poorer resolution of ground based imaging which is incapable of recovering the level of detail in host morphology that *HST* images achieve, may be the cause of this discrepancy.

4.5.2 NIR Results

For those SLSN hosts with *HST* imaging in the near infrared (nIR), I also determine the F_L values for these galaxies. Although less indicative in terms of the stellar populations probed than when conducted in the UV, it nonetheless may provide valuable information with regard to the density of stellar populations local to the transient. I measure nIR F_L values for SLSN within the sample with *HST* nIR

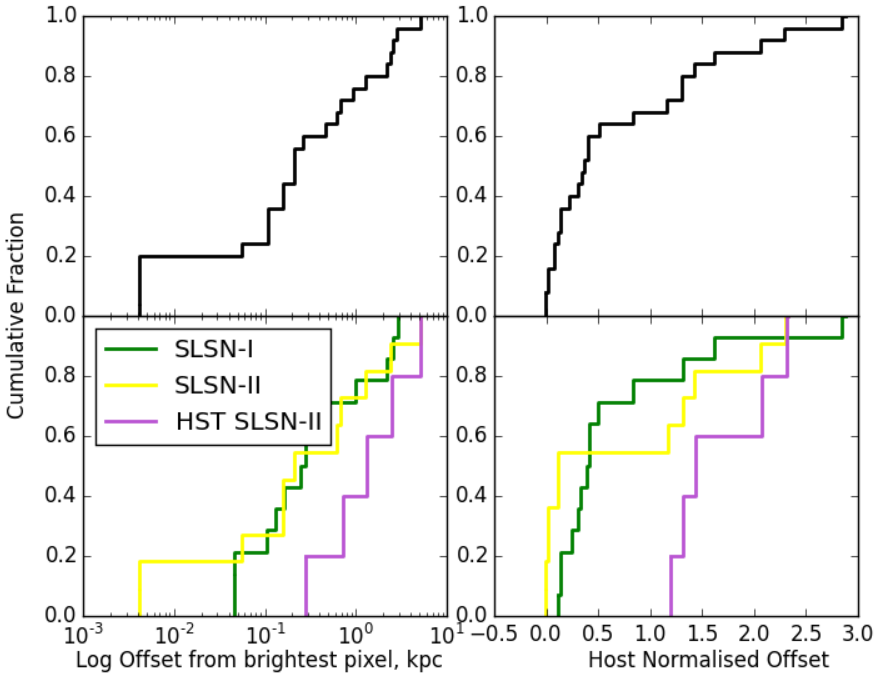

Figure 4.12: Left side: the offsets of SLSN events from brightest UV pixels within their hosts (upper panel) and broken down by SLSN subclass (lower panel). Right side: bright pixel offsets for the same sample normalised by the host r_{50} size. Upon the inclusion of additional SLSN-II locations from the sample within Perley et al. [2016], there appears to be no strong distinction between SLSN-I and SLSN-II event in respect to their association with the strongest star forming regions within their hosts, however those SLSN-II locations imaged with *HST* show larger offsets from bright star forming regions, more inline with the F_L distribution they exhibit.

imaging and also for LGRBs over similar redshift drawn from a SNAPSHOT survey of LGRB hosts (see Lyman et al. [2017] for further details of this sample), and present the results within Figure 4.13.

Here a strong bias is observed towards brighter nIR regions for both SLSN and LGRB host galaxies. KS and AD testing of these two distributions implies that the null hypothesis that these two samples are drawn from the same underlying distribution cannot be rejected, with p=0.72 and 0.63 for AD and KS statistics respectively. The SLSN subclass distributions shown in the lower panel of Figure 4.13 offer little distinction between them. These numbers when considered with respect to the relative size of both SLSN and LGRB host galaxies (shown within previous studies to be exceptionally small, [c.f. Chapter 3; Svensson et al., 2010; Lunnan et al., 2015], are most likely another comment upon the compactness of these particular transient host galaxies. For these hosts, the probability of being located on the brighter nIR pixels given that the transient is located within the host is high. To test this, for the subset of SLSN events covered at both UV and nIR wavelengths, I re-drizzle the *HST* UV images to the resolution of the nIR imaging ($0.13''$ per pixel) and perform F_L measurements upon these redrizzled images. Once drizzled to this larger pixel scale, it is apparent that the F_L values are consistently higher than those obtained at smaller pixel scale, and are similar to the nIR distributions. Therefore it seems likely that the nIR F_L results are strongly affected by the combination of the poorer resolution of the nIR detector, and the typical compactness of SLSN host galaxies.

4.6 Discussion

Although the field of SLSN is still somewhat in its infancy, the growing number of identified transients belonging to this class in recent years has allowed for group statistical analysis. Studies covering the hosts of both spectral classes of SLSN [e.g. Chapter 3, Leloudas et al., 2015; Perley et al., 2016], have begun to highlight the observed differences between the two subclasses in their host's masses, metallicities and star formation rates. The results presented within this Chapter are the first to call attention to the observed differences in the sub-galactic environment properties of hydrogen poor and hydrogen rich SLSN.

4.6.1 Locations of SLSN-I

I have shown that hydrogen poor SLSN are generally located within bright UV regions of their hosts, with modest local surface luminosities (typically 10^{8-9} $L_{\odot}kpc^{-2}$).

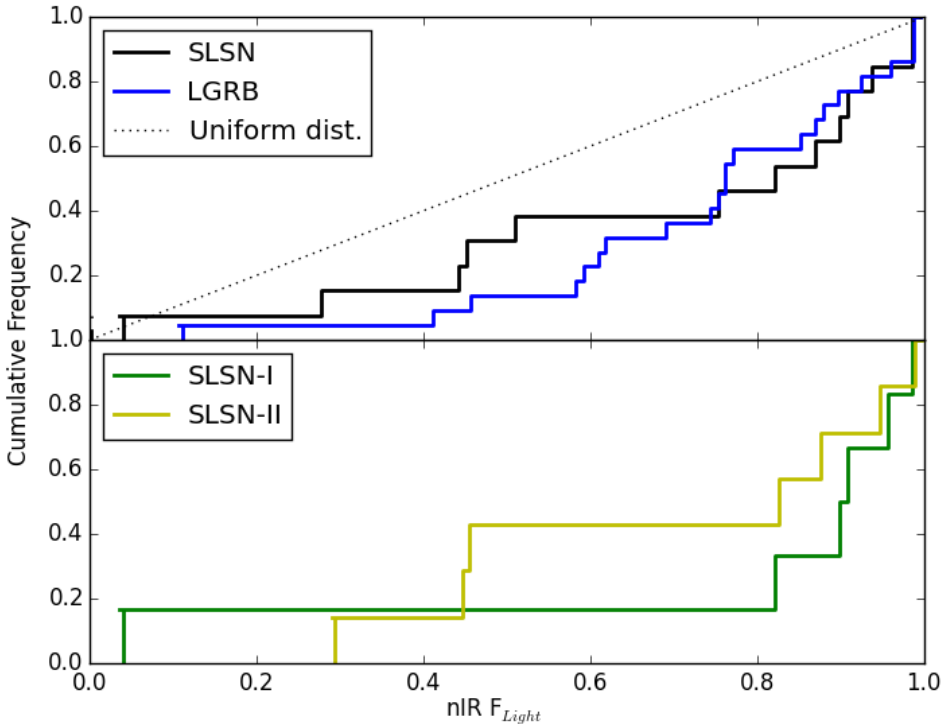

Figure 4.13: The cumulative distributions of nIR F_L parameters for SLSN and LGRB host galaxies observed within SNAPSHOT programme GO-12307 (upper panel), with an uniform distribution plotted to guide the eye. Again the SLSN host distribution is broken down by spectral subclass (lower panel). Both SLSN and LGRB events appear biased towards brighter nIR pixels within their host galaxies. However, given the compactness of both SLSN and LGRB hosts, this is likely a product of their morphologies rather than a progenitor bias.

SLSN-I appear to trace star formation within their hosts, and visually they seem to be less strongly correlated with these regions than LGRBs, a notion which seems to be supported by the lower surface luminosities of the pixels containing the SLSN explosion sites. These results are in agreement with those derived from a sample of PS1 SLSN-I host galaxies presented within the study of Lunnan et al. [2015], who achieve a typically higher level of astrometric precision in transient locations, largely due to the use of multi-epoch imaging of the SN event, which allows a weighted averaged, σ-clipped centroid of the SN to be determined, greatly improving the precision of the astrometric location within a *HST* image ($\sim$10-30 milliarcseconds). This increased precision results in much more robust estimations of the F_L parameter. Despite their poorer locational constraints, the apparent agreement between the independently derived results of this work and that of Lunnan et al. [2015] is encouraging, however, the lack of statistical distinction between SLSN-I and LGRB/CCSN populations makes it difficult to place constraints upon the relative ages and masses of stars local to SLSN explosion sites.

Incorporating the range of possible transient locations within the weighted F_L technique has revealed the extent to which the current locational constraints defocus the F_L distribution. As an intrinsically highly concentrated population will be scattered randomly by the astrometric errors, the probability of being located within a fainter pixel increases, and as such this resulting distribution can be considered a lower limit to the fractional flux under the current locational constraints.

However, the general shape of the distribution is still comparable to a normal F_L , which implied that, even when considering the uncertainties in their locations, we observe an association between SLSNe and UV bright regions within their hosts. Under the assumption of a location bias towards star formation within the error region, the weighted F_L distribution of SLSN visually seems to "recover" the normal F_L distribution fairly well, this similarity is most likely coincidence. This F_L distribution is strongly dependant upon the reality of this assumed bias, and at present can only be guessed at. Whilst the weighted F_L distributions have provided some additional confidence in the localisation of SLSNe events within their host galaxies, it is important to remember that the *measured* locations of transients within their hosts are already scattered from the "true" locations of the events, and the degree of additional scatter introduced via consideration of locational uncertainties cannot be known.

In light of the different progenitor models of SLSNe, whilst the locations alone of SLSNe within their host environments do not conclusively differentiate between the higher stellar masses of LGRB progenitors or the relatively less massive ones of

CCSNe, when put into context with the clear difference in global host properties that we observe, particularly between SLSNe and CCSNe (as shown within Chapter 3), it seems likely that there is some additional environmental factor which aids the production of their progenitors (rather than the progenitor mass alone).

A dependency upon more than just progenitor mass would seem to rule out PISN models, as this explosion mechanism relies more heavily upon the mass of the star prior to collapse in order to create the correct physical conditions to trigger instability. Such conclusions drawn from the results presented within this Chapter and within Lunnan et al. [2015] appear to be at odds with spectroscopic studies of SLSN host galaxies by Leloudas et al. [2015], who find the spectral properties of SLSN-I hosts to be comparable to those observed within Extreme Emission Line Galaxies (EELGs). The broad equivalent widths and strong emission lines of EELGs represent intense periods of starburst within these galaxies and as such, they are home to a young, massive stellar population. The authors suggest that the likeness of SLSN-I hosts to EELGs might possibly be evidence that these particular SLSNe represent the stellar deaths of the young stars produced within these bursts. However, given the observed relationship between cluster mass and the mass of the most massive star within it [Bonnell et al., 2001; Weidner and Kroupa, 2006], if SLSN progenitors were exceptionally young, and therefore massive, stars, it would seem logical then that their progenitors would be part of the most massive stellar cluster formed during this star burst, and therefore most likely to be located within the brightest pixels of their host galaxies. However, given that star formation within starburst galaxies has been shown to be clumpy at both local and moderate redshifts [e.g. Elmegreen et al., 2007; Tadaki et al., 2014; Guo et al., 2015; Hinojosa-Goñi et al., 2016b], it may be that perhaps these typically fainter locations are representative of unsmooth star formation on small scales within these host galaxies. Such behaviour is not atypical of local star forming galaxies, in which the compactness of the star forming clumps increases with increasing numbers of clumps within the galaxy [Hinojosa-Goñi et al., 2016b], which makes confidently discrediting a PISN model based upon the locations of SLSNe-I difficult.

Lunnan et al. [2015] have suggested that the lack of strong bias towards the brightest pixels could reflect instead a preference for low metallicity environments (but not necessarily linked with the production massive stars). Indeed, there is strong evidence that a large fraction of SLSN-I are located within hosts of low global metallicity [Chen et al., 2013; Lunnan et al., 2014; Leloudas et al., 2015], or located within the outskirts of more massive disk galaxies (e.g. see SN 1999as, PTF11rks from Chapter 3) for which a substantial metallicity gradient may exist. With regard

to the magnetar model of SLSNe production, an additional metallicity constraint may be compatible, if for a single progenitor the spin period of the magnetar is connected with it's metallicity [as has been suggested within Chen et al., 2016].

Another less explored option is a binary progenitor path for magnetar production of SLSNe, as such a system would provide a more natural mechanism for stripping a progenitor of it's hydrogen envelope and spinning up the star prior to it's collapse, and would not necessitate extremely massive progenitors (and so would not require SLSN events to occur coincident with the youngest, most massive stars within the host). Indeed, observations of Hα emission at late times within iPTF13ehe have been used to suggest that the SLSN shockwave collided with material stripped from a close companion star [Moriya et al., 2015]. However, at present it is not possible to comfortably differentiate between a single progenitor model with metallicity dependence and binary progenitor model for magnetar production for all SLSN-I events.

4.6.2 Locations of SLSN-II

Somewhat of a contrast are the locations of SLSN-II within their hosts. Within Chapter 3 I have already shown that hydrogen rich SLSN occupy the broadest range of host galaxy environments, ranging from massive spiral galaxies to the faintest transient host galaxies observed to date. This sample of SLSN-II hosts (to date, the only SLSN-II hosts with *HST* coverage) are amongst some of the earliest SLSNe to be identified [see Gal-Yam, 2012], and as a consequence suffer from a severe lack of available discovery imaging. Although the F_L parameters of SLSN-II events here appear to be generally lower than those of SLSN-I, with the absolute luminosities of these regions almost consistently fainter than both SLSN-I and CCSN events, the results derived here are hampered by small number statistics. Offset analysis including additional SLSN-II from ground based imaging suggests that the locations of SLSN-II within their hosts may be more comparable to those of SLSN-I, with many events located much closer to stronger star forming regions within their hosts (which in turn, would likely result in higher fractional flux values). Although the difference in resolution achieved between the *HST* and ground based samples leaves these results highly tenuous, it certainly highlights the need for an increased sample of SLSN-II hosts with high-resolution imaging, especially if we are to use the locations to begin to constrain the underlying progenitor populations. The tendency towards lower F_L values with larger uncertainty regions means the properties of SLSN-II locations are subject to a greater degree of scatter than SLSN-I, and as such the properties of their sub-galactic environments are less constrained. This

issue will only be solved with the acquisition of high resolution imaging of a larger sample of SLSN-II hosts.

With the dawn of the LSST era approaching, the number of observed SLSN events will themselves be plentiful, however it is important to note the importance of maintaining a similarly large sample of host galaxies with dedicated follow up, if we are to continue use these as a route to understanding SLSN progenitors created within them.

4.7 Conclusions

Using high resolution *HST* imaging, I have determined the locations of a sample of both hydrogen poor and hydrogen rich SLSN events within their host galaxies, and used their locations to determine the properties of the sub-galactic environments of SLSNe and UV and nIR wavelengths. The following conclusions can be drawn:

- In general, SLSN events trace star formation within their host galaxies; they are located within bright UV pixels and follow a host offset distribution similar to LGRB events. However, SLSN are less concentrated towards the brightest pixels within their hosts than LGRB events are, but are located typically close to regions of strong star formation within the host.

- When considered individually, the hydrogen poor and hydrogen rich subclasses of SLSN appear to occupy very different local environments within their hosts. SLSNe-I are typically located on brighter UV pixels than SLSNe-II, who appear to favour typically fainter regions of their host galaxies.

- The poor constraints upon the locations of SLSN acts to dilute their F_L distribution, as illustrated through application of a weighted fractional flux technique. The effects of this are particularly potent for SLSNe events at the faint end of this distribution, for which the current sample currently suffers from larger locational uncertainties. This behaviour may have consequences for SLSN-II events, whose low F_L values are thus subject to higher scatter.

The compact and irregular nature of SLSN host galaxies leaves them incredibly vulnerable to large scale fluctuations in sub-galactic environment properties when accounting for the positional uncertainty of the transient. Only with an increased sample size, particularly for SLSN-II hosts, will statistical study of the environments begin to constrain the properties of the stellar populations local to these exotic transients.

Chapter 5

Metallicity dependencies in SLSNe and LGRB host galaxies

"Whatever stars are made of, his and mine are the same"
— Emily Brönte, *Wuthering Heights*
(adapted by C.R. Angus)

5.1 Introduction

The host galaxies of SLSNe have been shown to possess a remarkable nature; they are some of the faintest galaxies to host a luminous transient event [c.f. Chapter 3, Lunnan et al., 2014; Perley et al., 2016], with the potential to produce extreme fields of ionising radiation within the local Universe [Leloudas et al., 2015]. The striking preference of SLSN events for low mass host galaxies has been emphasised within the near-IR photometric results of Chapter 3, and within other SLSN host galaxy studies [for instance Lunnan et al., 2013; Leloudas et al., 2015; Perley et al., 2016; Japelj et al., 2016], probing galaxy masses down as low as $10^6\,M_\odot$. From correlations established from local galaxies between stellar mass and chemical enrichment [e.g. Tremonti et al., 2004; Lee et al., 2006; Michel-Dansac et al., 2008; Salim et al., 2014], the observed low masses of SLSN host galaxies suggest that they are also low in metallicity. This appears to be complementary of the moderate-to-strong radiation-fields observed; as the production of numerous massive stars necessary to produce this ionising radiation becomes increasingly likely within lower metallicity environments [e.g. Stanway et al., 2016].

The comparison of SLSN host galaxies properties with those of other host

galaxy populations, allows further conclusions to be drawn; the systemically lower masses of SLSN hosts than LGRB hosts might imply that these environments are also typically less chemically enriched. LGRB host galaxies are now well established as low metallicity environments [Stanek et al., 2006; Modjaz et al., 2008; Levesque et al., 2010; Graham and Fruchter, 2013a], especially when compared to field galaxies and the host galaxies of core collapse supernovae. Such results have led to suggestions of a metallicity threshold, or cutoff, above which the rate of LGRB production sharply decreases [e.g. Wolf and Podsiadlowski, 2007; Kocevski et al., 2009]. Thus the presence of SLSN events in apparently less metal enriched hosts logically implies a similar effect at play within this host galaxy population, with the SLSN rate suppressed at a more extreme metallicity threshold.

Theoretically, a metallicity threshold has some credence in the production of massive core collapse events, particularly with the collapsar model of LGRBs [Woosley, 1993; MacFadyen and Woosley, 1999]. The production of a single massive progenitor which has maintained a significant fraction of it's original angular momentum [Yoon and Langer, 2005; Woosley and Heger, 2006], becomes increasingly likely within a less chemically enriched environment as the effects of stellar winds become less prominent in this regime [Kudritzki and Puls, 2000; Vink and de Koter, 2005]. Indeed, for models of SLSN production, low metallicity environments are also favourable; either for the production of exceptionally massive stellar cores (PISNe/PPISNe) or once again, for the retention of mass and angular momentum to produce a sufficiently rapidly spinning remnant at the heart of the star (the internal engine model).

However, testing whether the rate of transient production is heavily suppressed above a certain metallicity threshold within a sample of host galaxies is non trivial, particularly for the hosts of LGRBs and SLSNe. Given the intrinsic faintness of some members of these host populations, metallicity determinations at the faint end of their luminosity function become problematic, as such hosts can often only be photometrically detected within very deep imaging (c.f. the hosts of SN 2008es, SN 2008fz and SN 2009jh within Chapter 3). Alongside this, the typically high (z>0.5) redshifts of many transient hosts also becomes an issue, as even for more luminous galaxies, the increased luminosity distances make the acquisition of emission lines within spectra of adequate signal-to-noise for metallicity determination observationally expensive. This leaves only a select few galaxies (luminous, local galaxies) for which metallicity measurements are viable. As a result, the conclusions drawn through emission line metallicity estimates do so based upon a flux limited sample of hosts, although even for these hosts, the metallicity measured is typically

a global metallicity, and does not necessarily reflect the chemical enrichment of the population local to the transient.

To account for this, proxies have frequently been used in order to estimate metallicities over a more complete range of host luminosities (and masses). These proxies take the form of the aforementioned mass-metallicity (MZ) relationship; an established statistical correlation between the stellar mass of a galaxy and it's level of chemical enrichment [Tremonti et al., 2004]. Whilst the form of the MZ relationship is subject to variation dependant upon the metallicity calibration used [for further detail see Kewley and Ellison, 2008], this general correlation allows an approximate metallicity to be determined for galaxies of known mass. Since to first order the galaxy mass is directly proportional to the near-IR luminosity, such mass measurements are far more straightforward than spectroscopic metallicities, and can be attempted at a wide range of redshifts.

The employment of MZ proxies has led to conflicting results for the implied metallicities of LGRB environments. Recent studies of a uniformly selected sample of LGRB hosts (including host galaxies of GRBs without a detected afterglow, so called "dark" bursts) using near infrared *Spitzer* imaging to determine stellar masses, suggest that from the metallicities derived via MZ proves, the GRB rate only becomes heavily suppressed in environments above approximately solar metallicity [Perley et al., 2015b]. Whilst this metallicity threshold is notably higher than those observed spectroscopically [e.g. Fynbo et al., 2003; Modjaz et al., 2006; Fruchter et al., 2006; Graham and Fruchter, 2013a], it is significantly higher than thresholds predicted by single-progenitor models of LGRB production [e.g. $Z \lesssim 0.2 Z_{\odot}$ Yoon and Langer, 2005; Levan et al., 2016], and instead is highly suggestive of a binary progenitor path [for which metallicity becomes less of a restriction, Trenti et al., 2015].

Whilst this disagreement may cause some confusion for the progenitors of LGRB events, an explanation for this discrepancy may lie within the treatment of MZ proxies. The majority of studies which utilise this method utilise the numerical form of a given MZ relation, which itself describes an average metallicity for a given mass. Observationally, there is an intrinsic scatter to the MZ relation, which is a reflection of changes in the galaxy's star forming history and the inflow/outflow of gas [Ohta et al., 2012]. Although estimated to be fairly low within field galaxies in the local Universe (for relatively luminous/massive galaxies, this is estimated to typically be 0.1 dex, Tremonti et al. 2004), any source of scatter will act to naturally broaden the range of potential metallicities a galaxy may possess at a given stellar mass (and vice versa). Thus using a direct conversion of mass to metallicity using

an MZ relation will fail to account for this spread, which may lead to inaccurate metallicity threshold inference. This is demonstrated within Figure 5.1.

The lower panel of Figure 5.1 shows the masses and global metallicities a volume limited sample of SDSS galaxies from Tremonti et al. [2004] (within the redshift range $0.02<z<0.04$). The galaxy population which would arise upon the enforcement of a metallicity threshold of 12+log(O/H)=8.2 (or Z= 0.15 $Z_{\odot}$) are highlighted in blue. The middle panels shows the inferred mass functions for the SDSS galaxies and the metallicity restricted galaxies. At a metallicity threshold of Z= 0.15 $Z_{\odot}$, by number the majority of galaxies should lie at around $10^{8.5}\,M_{\odot}$. However, upon examination of the distribution of total galaxy mass for this threshold (in the mass-weighted cumulative mass functions shown within the upper panel of Figure 5.1), only about 25% of the total galaxy mass is contained within galaxies with less massive than $10^{8.5}\,M_{\odot}$. In this particular example galaxies with masses up to $10^{9.5}$ $M_{\odot}$may in fact be indicative of a metallicity threshold of 0.15 $Z_{\odot}$, which using a simple MZ relation would imply an upper limit on the galaxy mass an order of magnitude lower. Therefore the consideration of MZ scatter is important when determining progenitor metallicity thresholds.

Available emission line metallicity estimates of SLSN host galaxies have confirmed that SLSNe preferentially occur within hosts of typically low chemical enrichment [Lunnan et al., 2013; Leloudas et al., 2015; Perley et al., 2016]. Proxies derived from stellar mass estimates suggest that the level of chemical enrichment is even poorer than that observed within LGRB hosts [Chapter 3, Perley et al., 2016]. Given the discrepancies in LGRB metallicity threshold inferred between different studies [e.g. Graham and Fruchter, 2013a; Perley et al., 2015b], it is therefore important to ascertain whether these differences may be reconciled if the true spread in the distribution of galaxies in the mass-metallicity plane is taken into account.

As the thresholds based upon proxies are not frequently in agreement with those inferred from emission line diagnostics, it is important to understand the likely distribution of different metallicities around galaxies of a given mass, as discrepancies may have major ramifications for the likely progenitor populations for transients. In this chapter I will explore the use of MZ proxies and the impact of metallicity scatter upon them, and how this approach may lead to more robust conclusions for transient host populations for which spectroscopic observations are not feasible across a complete sample (in particular, LGRBs and SLSNe).

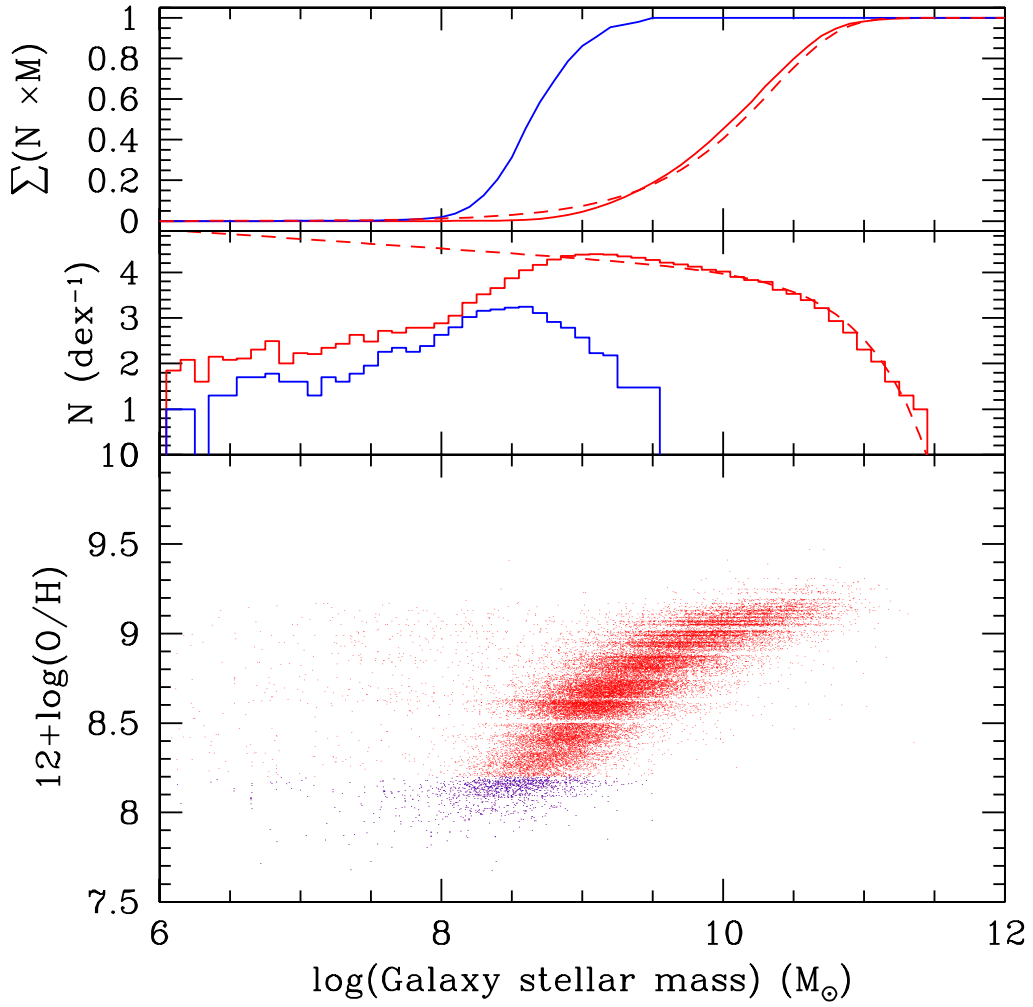

Figure 5.1: *Figure produced by Andrew Levan.* Bottom panel: the Tremonti et al. [2004] mass-metallicity relationship for SDSS galaxies (red), with the population of galaxies which would arise from the enforcement of a Z=0.15 $Z_{\odot}$ (12+log(O/H)=8.2) metallicity cut. Middle panel: the mass functions of the SDSS and metal-cut galaxy populations (dashed line shows the overall population). Top panel: the mass-weighted cumulative mass functions. The mass functions indicate that at a metallicity threshold of 12+log(O/H)=8.2, the majority of galaxies should possess masses of around $10^{8.5}\,M_{\odot}$, however, due to the large inherent scatter in the MZ relation, the majority of the mass budget for this metallicity threshold is dominated by rarer, but higher mass systems.

5.2 Host Galaxy Samples

Here I will utilise more complete samples of transient host galaxies which include those for which metallicity measurements are easily accessible, and those whose redshifts/luminosities make the direct determination of metallicities difficult, and thus necessitate the use of a mass metallicity proxy to explore their chemical enrichment. I will consider the mass distribution of SLSNe host galaxies studied within Chapter 3, whose masses have been determined through near-IR imaging and SED fitting, and compare the distribution of these hosts to the MZ model at different metallicity thresholds.

I shall also compare the distributions produced by the MZ model with LGRB host galaxies drawn from the SHOALS sample, which represents an unbiased sample of LGRB hosts [Perley et al., 2015a,b]. The study of Perley et al. [2015b] utilises deep 3.6 micron *Spitzer* imaging for stellar mass determinations of these host galaxies across a redshift range $0.1<z<\sim5$. At present, the metallicities inferred from the median of the Zahid et al. [2014] MZ relation conflict with the results of previous spectroscopic studies and theoretical models, as collectively they infer a metallicity threshold higher than previously observed [~1 $Z_{\odot}$ Perley et al., 2015b] (although recent spectroscopic studies such as [Graham and Fruchter, 2013a, 2017] suggest more modest metallicity thresholds of <0.3 $Z_{\odot}$).

As the sources of scatter which affect the spread of the MZ relation are best characterised within the local Universe, and the evolution of these parameters over cosmic time remains a complex problem, I will restrict the samples of transient hosts to those at relatively local ($z<1.0$) redshifts, where the MZ relation is better understood

5.3 Model Description

To investigate the how the effects of scatter within the MZ relation affect the conclusions drawn from mass-metallicity proxies, the simplest route to doing this is to consider the likely range of stellar masses which may arise under different metallicity cuts.

The MZ relationship was first statistically quantified by Tremonti et al. [2004] using 53,000 SDSS galaxies, showing a strong correlation between the galaxy's gas phase metallicity (which provides the chemical enrichment of the recent/younger stellar populations within the galaxy) and it's stellar mass. The empirical relationship derived from this correlation provides a direct map between the stellar mass of

a galaxy and it's effective chemical enrichment. However, SDSS samples are often incomplete at the faint end, and so direct use of these catalogs to infer the fraction of galaxies with a given metallicity cut may not provide a complete narrative over the whole luminosity function. This is clearly visible as the apparent turn-off in the mass function shown in Fig 5.1 below $\sim 10^9\,M_\odot$. SDSS fibre spectra also do not provide a detailed picture of any metallicity distribution *within* a galaxy.

Whilst it's specific form may be subject to change depending upon the metallicity calibration under consideration [Kewley and Ellison, 2008], the general correlation between stellar mass and metallicity holds over a variety of galaxy masses ($10^6\,M_\odot$- $10^{11}\,M_\odot$, Lee et al. 2006) and has been observed out to high redshifts [Savaglio et al., 2005; Ma et al., 2016].

The evolution of gas phase metallicities over a range of redshifts as a function of stellar mass has been parameterised by Ma et al. [2016] as;

$$\begin{aligned} log\left(\frac{Z}{Z_\odot}\right) &= 12 + \log\frac{O}{H} - 9.0 \\ &= 0.35\left(\log\frac{M_*}{M_\odot} - 10\right) + 0.93\left(\exp\left(-0.43z\right)\right) - 1.05 \end{aligned} \tag{5.1}$$

where z is the redshift under consideration. Whilst emission line gas phase metallicities obtained for the majority of transient host galaxies can only be reliably measured at very low redshifts (z<0.5), the photometric probing of stellar masses significantly increases the available redshift range of host galaxies. Therefore when considering the predicted distribution of masses under different metallicity cuts this relationship will be utilised at an appropriate redshift for the sample of transient host galaxies the models are being compared to.

In order to determine the likely range of stellar masses which may arise under different metallicity cuts, the total mass contained within each mass bin is obtained by weighting the galaxy mass by the number of galaxies expected to be found at this mass. The number of expected galaxies is determined by the galaxy luminosity function, which describes the density of galaxies within a given volume as a function of their luminosity. The luminosity function may be characterised by a Schechter function [Schechter, 1976]. When expressed in terms of stellar mass, this becomes the galaxy Stellar Mass Function (SMF), which provides an estimation of the number of galaxies at a given mass.

$$\phi(M)dM = \left(\frac{\phi^*}{M^*}\right)\left(\frac{M}{M^*}\right)^{\alpha} \exp\left(-\left(M/M^*\right)\right)dM \tag{5.2}$$

Here M^* represents a characteristic stellar mass of the Schechter function, ϕ^* is a normalisation factor for the density of galaxies, and α describes the slope of the power law distribution found at the low end of the mass function.

Although the SMF has been shown to evolve weakly with redshift (due to changes in feedback processes which inhibit star formation at lower redshift, Hopkins et al. 2014), as the transient samples to be examined within this work are at primarily low redshift (for SLSNe, the median redshift is 0.234 and the subset of the SHOALS LGRB sample used here has a median redshift of 0.776), I employ values of M^*, ϕ^*, α parameters determined for a sample of star forming galaxies at low redshift range $0.2<z<0.5$ as determined by Tomczak et al. [2014]. The evolution found by Tomczak et al. [2014] is relatively weak over the typical redshift range of transient hosts used within this thesis ($0.2\lesssim z\lesssim 1.5$), this should also provide an adequate approximation of the mass function over the redshift range of the transient hosts considered thus far. As such, I take M^*, α and ϕ^* to be $10^{10.72}\,\mathrm{M}_{\odot}$, -1.34 and $10^{-2.94}$ Mpc^{-3} respectively.

In order to track the total stellar mass (M_{Tot}) contained within each mass increment of the MZ relation, a mass weighted mass function is required. The Schecter function, $\phi\,(M)$ is therefore weighted at each point by the mass of the galaxies (M) under consideration within the interval M_a to M_b, providing the total galaxy mass contained within galaxies in this mass range,

$$M_{\mathrm{Tot}} = \int_{M_a}^{M_b} M\phi\,(M)\,dM. \tag{5.3}$$

Utilizing this with the M-Z relation then provides the total stellar mass at a given metallicity. There are several sources of scatter within the MZ relation which act to broaden the range of potential metallicities a galaxy mass may represent (and vice versa, increasing the range of galaxy masses stars of given metallicity may be located), and is therefore a key consideration in building these MZ population models. The key sources of scatter within the MZ model include:

- Intrinsic: there is some intrinsic scatter to the MZ relation, originally estimated by Tremonti et al. [2004] to be 0.1 dex for local galaxies, although more recent measurements have judged this level of scatter to be higher (0.16 dex, Lee et al. 2006) and revealed it's increase towards lower stellar masses, from $\sim$0.2 dex at $10^{11}\,\mathrm{M}_{\odot}$ out to $\sim$0.7 dex within low $\sim 10^{8}\,\mathrm{M}_{\odot}$ galaxies [Zahid

et al., 2012]. The physical origin of this intrinsic scatter has been attributed to variations in chemical enrichment resulting from the accretion/dispelling of gas with galactic winds at different timescales [Davé et al., 2011; Forbes et al., 2014].

- Internal: the presence of a metallicity dispersion within a galaxy may act to increase the range of possible stellar metallicities which may be observed within it, such that low metallicity stellar populations may be located within galaxies at much higher central metallicity.

- Environmental: the local environment to a galaxy has been observed to influence it's level of chemical enrichment. Additional inflows/outflows influenced by SNe in close neighbouring galaxies may act to increase or deplete gas within a galaxy, through tidal stripping [Farouki and Shapiro, 1982] or strangulation [Larson et al., 1980]. The influence of environment within dense galactic clusters or groups has been shown to affect approximately 15% of the scatter in the MZ relation Cooper et al. [2008].

An additional concern may be the metallicity calibration under consideration. Kewley and Ellison [2008] have shown that different strong line metallicity calibrations change the form of the MZ relation, which in turn also varies the level of observed scatter within the correlation, with some calibrations showing a tighter MZ correlation than others. However, to first order, as the metallicity calibrations within this model can be considered consistent, any change under different calibrations would only generate a systematic offset in the absolute metallicities inferred, not the general spread of host masses for which stars at a given metallicity may be located at.

For simplicity, I will account for the first two sources of scatter within this model (namely the intrinsic scatter and the scatter introduced by the presence of an internal metallicity dispersion).

Studies of the near-IR luminosity-metallicity relationship show a similar degree of observed scatter to the normal MZ relation [Salzer et al., 2005], which given the proxy between the near-IR luminosity of a galaxy and it's stellar mass, suggests that the scatter associated with stellar mass has significantly less impact upon the scatter within the MZ relation than metallicity does. Assuming that each stellar mass is fixed (i.e. there is negligible[1] error in the mass estimate of the host), I assume the probability is given by a Gaussian distribution, for which the mean is

[1] with respect to the uncertainty in the metallicity estimate

the predicted metallicity from the MZ fit and whose spread is a combination of the two different sources of scatter. However, it is worth noting that the galaxies used to characterise the MZ relation are local galaxies, for which their properties are typically better constrained than the more distant galaxies associated with SLSNe and LGRBs, and therefore these populations are likely subject to additional scatter due to their more poorly constrained nature.

Here I will consider the difference between a scenario with fixed level of intrinsic scatter, $\sigma_{\rm MZ}$ over all stellar masses, and a case when the scatter is allowed to evolve with the stellar mass. In the latter case, this will simply take the form of a linear interpolation of the level of scatter across stellar mass using the results of Zahid et al. [2012].

Metallicity gradients have shown to be common amongst local elliptical and spiral galaxies [e.g. Carollo et al., 1993; Greene et al., 2015], with the degree of variation across the galaxy dependant upon it's star forming history, level of local gas inflow/outflow and merger history [for instance; Chiappini et al., 2001; Mollá et al., 2006; Di Matteo et al., 2009]. The existence of an internal metallicity gradient allows for the presences of lower metallicity stellar populations within a globally more chemically enriched environment. Therefore, when considering the locations of stars below a particular metallicity threshold, the additional scatter generated by internal metallicity distributions must also be considered.

For simplicity, this additional scatter will also be modelled as a Gaussian, centred upon the global, average metallicity determined from MZ relation, and whose broadening is given by the degree of the internal metallicity dispersion within the host ($\sigma_{\rm grad}$). Whilst the study of metallicity dispersions within local disk galaxies have shown that there typically exists a negative trend in chemical enrichment as you move towards the outer regions of the galaxy [Searle, 1971], when galaxies are observed at higher redshifts, the observed "global" metallicity which is measured is approximately the median metallicity within the dispersion range, (based on MUSE observations of local galaxies; J. Lyman, private communication). Thus for the purposes of this work, it is reasonable to treat this internal dispersion scatter as a normal Gaussian, centred around the median metallicity of the galaxy, rather than a skewed distribution.

The level of additional scatter induced by the presence of a metallicity dispersion varies greatly from galaxy to galaxy. Spatially resolved spectroscopic observations of disc galaxies within the Calar Alto Legacy Integral Field Area (CALIFA) survey [Sánchez et al., 2012] have revealed a diverse range of metallicity gradients [covering a range of $\sim$ dex Marino et al., 2016]. Metallicity dispersions have also

been shown to be weakly dependant upon the stellar mass of the galaxy for galaxies $>10^9\,M_\odot$[Roig et al., 2015], with simulations revealing that gas phase metallicity gradients are greater within within galaxies more massive than $10^{10}\,M_\odot$, with less dispersion in lower mass galaxies (complete to $\sim 10^9\,M_\odot$, Tissera et al. 2016). The local environment of a galaxy may also affect it's internal metallicity dispersion; interacting systems have been identified as possessing shallower metallicity gradients than those found isolated systems, suggesting a connection between internal dispersion and merger/interaction driven gas dynamics [Kewley et al., 2010].

To accommodate this complex variation of metallicity scatter within a galaxy, the additional scatter induced through the presence of an internal metallicity dispersion will be approximated in a simple manner. Here I shall treat all internal dispersions as a normally distributed range of metallicities with a fixed level of scatter at all galaxy masses. This level of scatter will be fixed at an arbitrary 0.1 dex.

In order to determine the total scatter induced in stellar mass for a given metallicity within the MZ relation, these two Gaussians ($\sigma_{\rm MZ}$ and $\sigma_{\rm grad}$) are convolved, such that the final metallicity uncertainty is is a guassian centred on the mean of the MZ relation and whose scatter is given as $\sigma_{\rm Z} = \sqrt{\sigma_{\rm MZ}^2 + {\sigma_{\rm grad}}^2}$.

Therefore to determine the distribution of galaxy masses we could expect under a chosen metallicity threshold, the total mass of galaxies found at each mass bin within the MZ relation is also weighted by this Gaussian distribution (integrated up to the metallicity threshold). Thus for each mass interval, the total mass contained within galaxies in this interval is multiplied by the normalised integral of the Gaussian between 0 and the critical metallicity. This generates a final distribution of galaxy masses in which stars below the critical metallicity are located, which can then be compared to observed populations of transient host galaxies.

5.4 Results

5.4.1 Model Properties

To demonstrate the how the likely distribution of host galaxy masses will alter under the influence of different metallicity thresholds, I first present the results from modelling a variety of metallicity restrictions upon the MZ relation within the local Universe (z=0) , under a "standard" scatter of 0.2 dex within Figure 5.2. The modelled populations here are subject to metallicity thresholds within the range 0.1 $Z_\odot$<Z<3 $Z_\odot$, this latter threshold chosen to include essentially all stars and galaxies.

Contrary to what one may expect from using a direct translation from mass

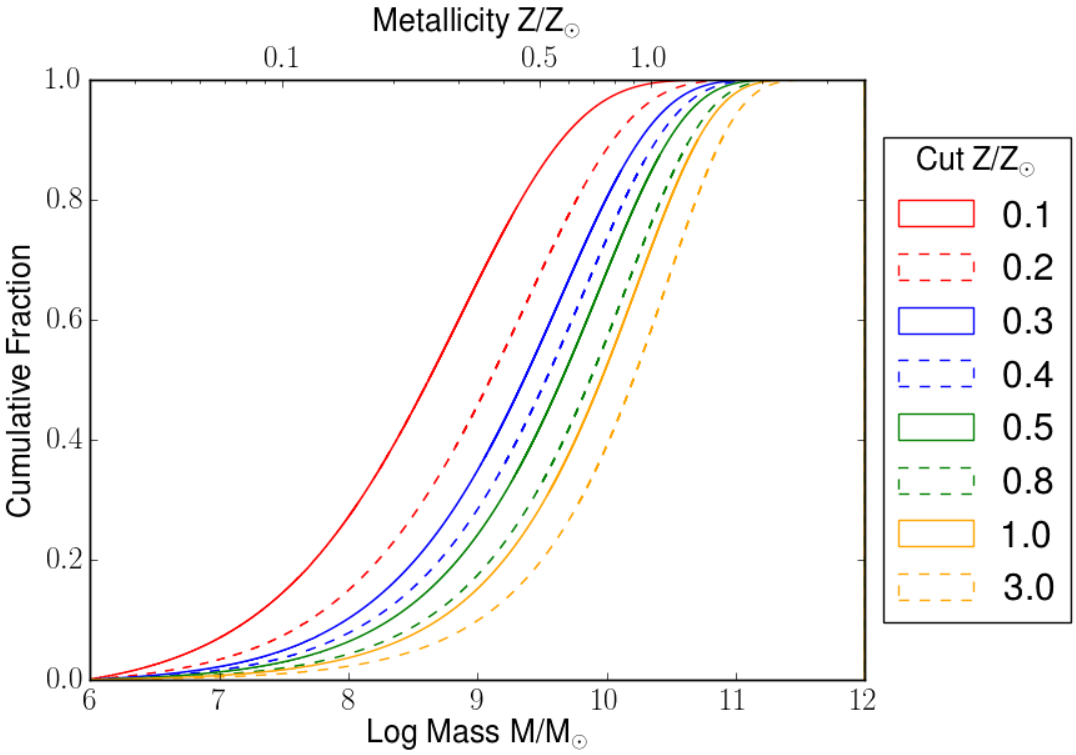

Figure 5.2: The cumulative galaxy mass functions (for local galaxies, z=0) which may be observed when the populations in question are subject to a variety of metallicity thresholds (within the range $0.1Z_{\odot}<Z<3Z_{\odot}$). The upper x-axis describes the metallicity which would be inferred from the median of the MZ relation for the given mass point. Here the scatter in likely metallicity measurement is a convolution of the intrinsic scatter in the MZ relation and the additional scatter induced by the presence of internal metallicity dispersions within the galaxy (with the degree of scatter dependant upon the mass of the galaxy).

to metallicity using an MZ proxy, when considering very low metallicity restrictions, the majority of the stars with metallicities below this threshold will be contained within galaxies substantially more massive than that implied by the proxy. For instance for a 0.1 $Z_{\odot}$ metallicity restriction, an MZ proxy using the Ma et al. [2016] relation in the local Universe would suggest a sharp truncation of the mass function at a limit of around $10^{7.485}\,M_{\odot}$, however, looking at Figure 5.2, we see more than ∼85% of the total stellar population at $Z<0.1_{\odot}$ are located within galaxies more massive than this.

However, this is easily explained by the form of the SMF. With increasing stellar mass, the observed SMF has a declining distribution with mass with a sharp cutoff at around M_{*}. When weighted by stellar mass, and for the modest faint end

slopes observed in the local Universe this means that a significant fraction of the stellar mass is contained within galaxies close to M_*. Hence, even accounting for only a small fraction of these galaxies (or their stellar population) having metallicities below the critical threshold set for the production of a transient, their contribution to the overall population can still be significant. Therefore for low metallicity cuts the majority of the transients are found within galaxies that (if using the MZ relation) would have significantly higher metallicities.

The effects of increased intrinsic scatter towards low stellar masses is visually demonstrated within Figure 5.2, which shows the likely distribution of galaxies containing stars of a given metallicity within MZ space. Looking at this map, it's clear that if one were to consider the locations of stars below a metallicity threshold of $0.1Z_{\odot}$, the increasing the scatter at low masses allows for the presences of stars within this threshold in much more massive hosts.

Measurements of the MZ relation, it's shape and scatter will ultimately provide important constraints upon models concerning galaxy formation and evolution [e.g. Davé et al., 2011]. It is therefore instructive to consider how the distribution of masses would vary under different assumptions about the intrinsic scatter of the MZ relation. Within Figure 5.3 I demonstrate the effects of increased scatter (fixed across all galaxy masses) on local (z=0.0) galaxy populations subject to a metallicity threshold of $Z = 0.3\ Z_{\odot}$. Here it is clear how the scatter of an MZ relation dramatically affects the range of host masses within which stars below this critical metallicity may be located. At this low metallicity threshold, the introduction of very high levels of scatter (0.6 dex) creates a distribution of galaxy masses/metallicities comparable to that observed with less scatter at a higher threshold (see Figure 5.2).

The strong influence of the much larger intrinsic scatter of the MZ relation is again highlighted within Figure 5.4, which demonstrates the expected distributions at metallicity thresholds of $Z = 0.1$, 0.3, 0.5 and $1.0\ Z_{\odot}$ where the intrinsic scatter (stellar mass-variable, and fixed at 0.2 dex over the mass range) are shown separately for each metallicity cut (solid and dashed lines respectively). Again, at low metallicity thresholds, when the scatter is allowed to vary with stellar mass, the increased level of scatter at low stellar masses dominates the form of the distribution. In this case, the presence of low mass galaxies with high chemical enrichment reduces the fraction of stellar mass below the critical metallicities which may be found within low mass galaxies, pushing the likely locations of low metallicity stars out to higher mass galaxies than achieved then the locations are scattered by the same about over all host masses. At higher metallicity cuts the difference between the two scenarios becomes less pronounced, as the majority of stars are located within more massive

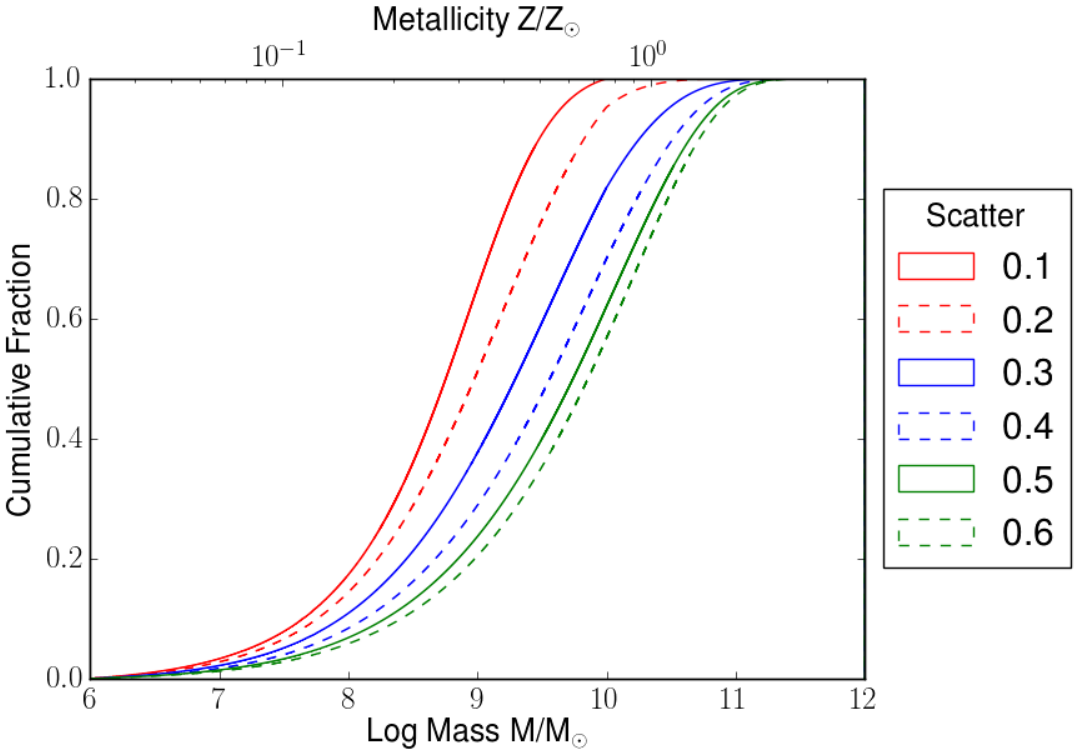

Figure 5.3: The cumulative galaxy mass functions for a Z = 0.3 $Z_\odot$ metallicity threshold under the influence of increasing intrinsic scatter (fixed at a set value over all galaxy masses) from the MZ relation (scatter range $0.1<\sigma_{MZ}<0.6$ dex). Scatter from metallicity gradients is still accounted for, although at higher values of scatter, it's influence becomes negligible. Here the influence of a large intrinsic scatter upon host galaxies within the same metallicity range acts to spread the observed population over a wider range of stellar masses.

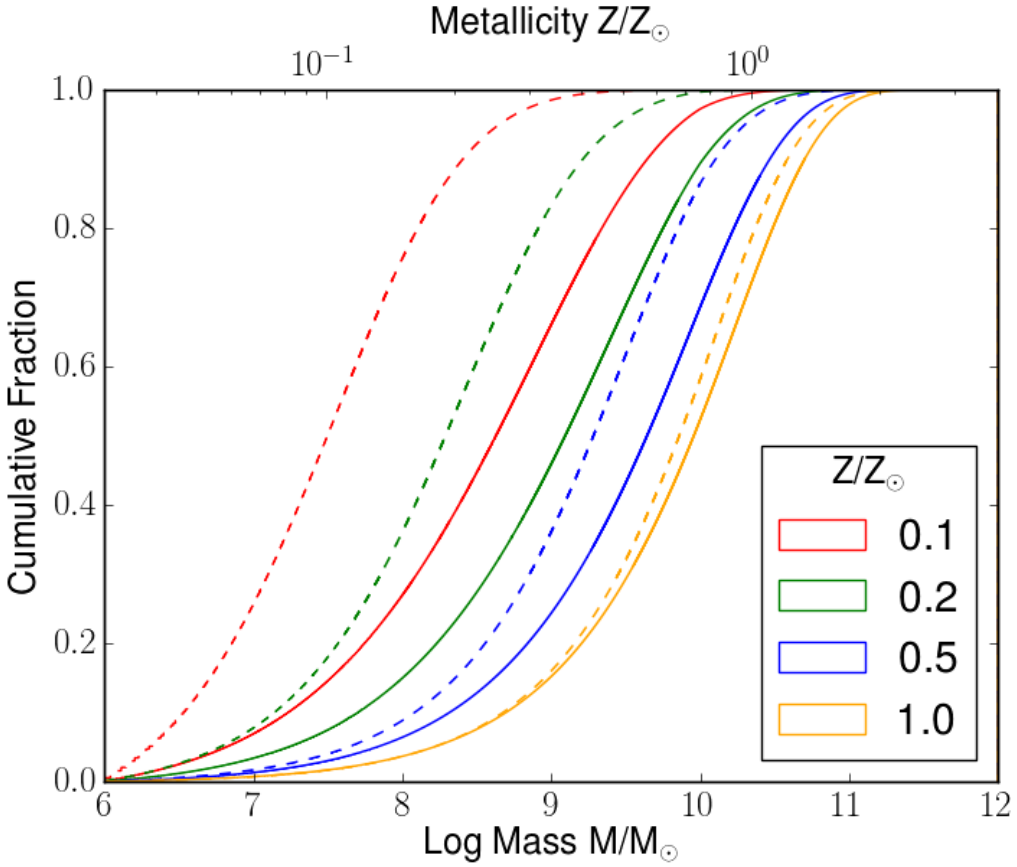

Figure 5.4: The cumulative galaxy mass functions at metallicity thresholds of Z = 0.1, 0.2, 0.5 and 1.0 $Z_\odot$ where the the intrinsic source of scatter is fixed at 0.2 dex (dashed lines) and allowed to evolve with the stellar mass of the galaxy (solid lines) as interpolated from the findings of Zahid et al. [2012]. The inclusion of higher levels of scatter at lower stellar masses forces the distribution to narrow in this range, as the increased scatter permits high metallicity environments (which exceed the threshold) within low mass galaxies.

galaxies, for which the mass-dependent scatter is significantly lower.

5.4.2 Constraining Transient Host Metallicities

Within this section I shall compare the MZ model to the LGRB and SLSN host galaxy populations outlined within Section 5.2. For each host galaxy sample, masses derived from SED fitting were used for comparison with the model output distributions. Iterations over the chosen metallicity threshold were performed (using incremental steps of $0.05Z_{\odot}$) such that the best fitting metallicity threshold could be found, with the prescription for scatter either fixed at 0.2 dex or determined via the mass variable method, but beyond this scatter was not variable. As the masses of the SLSN and LGRB hosts were determined via similar SED fitting routines, any discrepancies inherent to deriving their masses will affect both populations, thereby providing a reasonable like-for-like comparison when comparing chemical enrichment.

The model is first fit to the SHOALS LGRB host galaxies[2] located within the redshift range $0.5<z<1.0$ within Figure 5.5, using the median redshift from this sample of z=0.776 to characterise the form of the [Ma et al., 2016] MZ relation. The best fitting metallicity threshold of to this sample was identified to be 0.1 $Z_{\odot}$. Whilst such a low metallicity threshold is surprising, this is again a consequence of the distribution of galaxy mass within mass-metallicity space. Due to the large scatter in metallicities at the low mass end, the vast majority of stars below a critical metallicity of $Z_{\odot}$ are located within substantially more massive galaxies than one might expect from a standard MZ proxy.

The broadened distribution of likely host galaxy masses which results from the incorporation of increasing intrinsic scatter at lower stellar masses agrees well with the shape of the LGRB distribution at this redshift range. For all transient samples, statistical testing (two sample KS and AD testing) is performed between the output of the model and the observed host galaxy samples, the results of which are presented within Table 5.1. SHOALS LGRB hosts are statistically indistinguishable from model when a metallicity threshold of 0.1 $Z_{\odot}$ (p=0.556 and p=0.564 for KS and AD tests respectively).

This metallicity threshold is more consistent with the inferred metallicity thresholds from recent emission-line studies of Graham and Fruchter [2013a, 2017], which at present suggest low ($\sim 1/3$ $Z_{\odot}$) GRB metallicities. To assess how the effects of internal scatter due to metallicity dispersions may effect the inferred stellar

[2]Due to the low population numbers at $0.5<z$, this bin is not considered to prevent any additional biases introduced from small number statistics

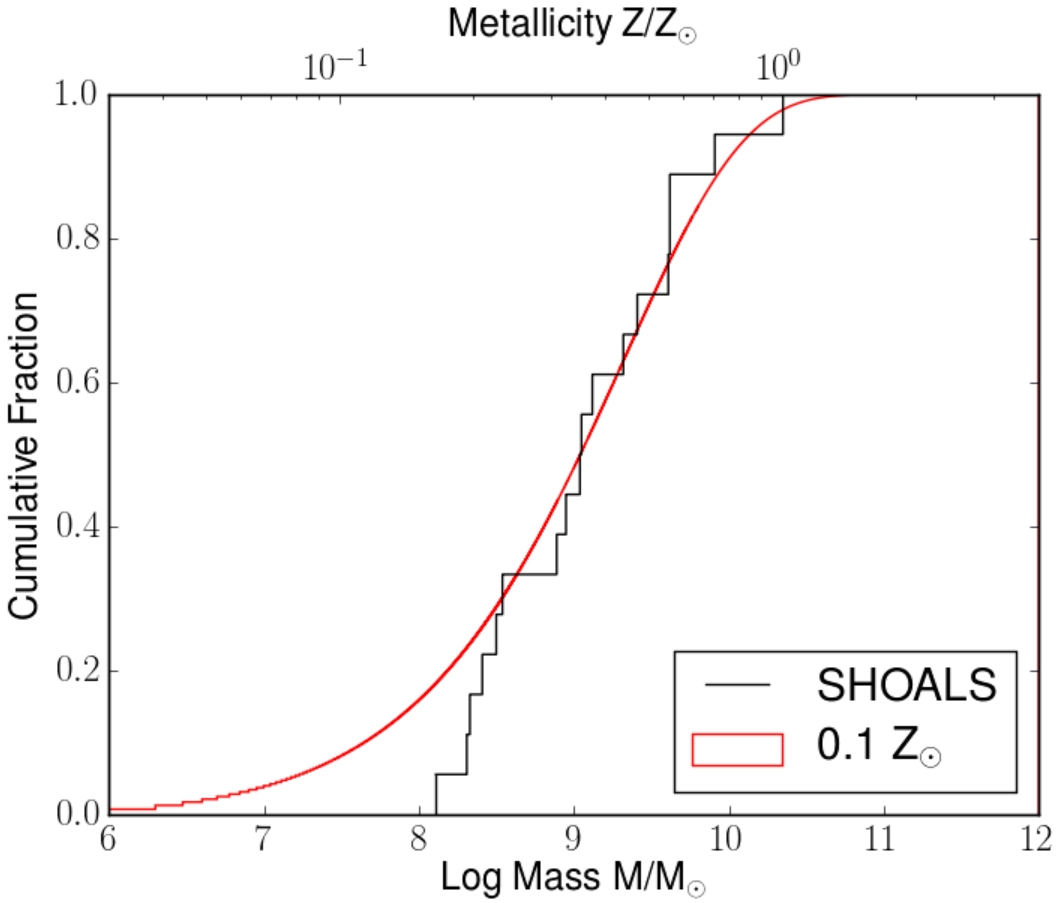

Figure 5.5: Comparison of an MZ model cumulative mass distribution subject to a metallicity threshold with the mass function of SHOALS LGRB host galaxies within the redshift range $0.5<z<1.0$. The best visual fit displayed here was found for the Ma et al. [2016] MZ relation (for a redsfhit of z=0.776, consistent with the mean of the SHOALS sample used here) when a metallicity cutoff of 0.1 $Z_{\odot}$ when the intrinsic scatter of the MZ relation is allowed to vary across the stellar mass range.

population metallicity thresholds inferred from emission line metallicities, I determine the likely *global* metallicities which would be measured when considering the locations of stellar populations below a metallicity cut within Figure 5.6. Here the only source of scatter in metallicity is that contributed by an internal dispersion (set at 0.1 dex), and this model is compared to the measured global metallicities of LGRB hosts from Graham and Fruchter [2013a] within the range $0.0<z<0.5$. Whilst previously the authors have suggested suppression above $\sim$1/3 $Z_{\odot}$ (below which $\sim$70% of their sample lie), when considering the scatter induced by a metallicity gradient, this sample is statistically consistent with tracing stellar populations below a threshold of 0.2 $Z_{\odot}$. Although these two thresholds are not drastically different, this highlights the importance of considering the effects of metallicity scatter by an internal gradient or dispersion when considering the chemical enrichment of transient populations.

A similar approach is applied to the host galaxies of SLSNe with masses determined from SED fitting within Chapter 3. The redshift distribution of this sample is heavily skewed towards low redshifts ($z<0.5$). Hence only host galaxies within the redshift range $0.0<z<0.5$ are compared to metallicity cut models (MZ relation using the median metallicity of $z=0.202$). This sample is compared to models of different metallicity thresholds, and the best fitting critical metallicity model is presented alongside the SLSN host mass distribution within Figure 5.7.

Here too, the general population of SLSN hosts appears to be consistent with a model population restricted to metallicities less than 0.1 $Z_{\odot}$, which is surprising given the differences observed in stellar mass within Chapter 3. Although here the sample of LGRB host galaxies has changed for like-for-like comparison with SLSN hosts, the general properties of the LGRB hosts used from [Svensson et al., 2010] within Chapter 3 and the SHOALS LGRB hosts here are consistent (KS result p=0.474).

However, the lack of SHOALS hosts at $z<0.5$ and the rapid evolution of the LGRB population in the near-IR between $0.5<z<1.5$ [Perley et al., 2015b], suggests this similarity may be due to the increased redshift range considered within the previous Chapters. There is also significant evolution of the Ma et al. [2016] MZ relation between the two median redshifts of $z=0.2$ to $z=0.7$ due to the exponential redshift term within the relation. The jump in metallicity which results from this is a decrease of 0.15 dex, or a factor of about 1.5 in metallicity for the same stellar mass, which may also account for this observed difference. To check this, the host galaxies LGRBs from Svensson et al. [2010][3] at $z<0.5$ are considered compared

[3]A sample whose mass distribution is statistically comparable to those of the SHOALS sample

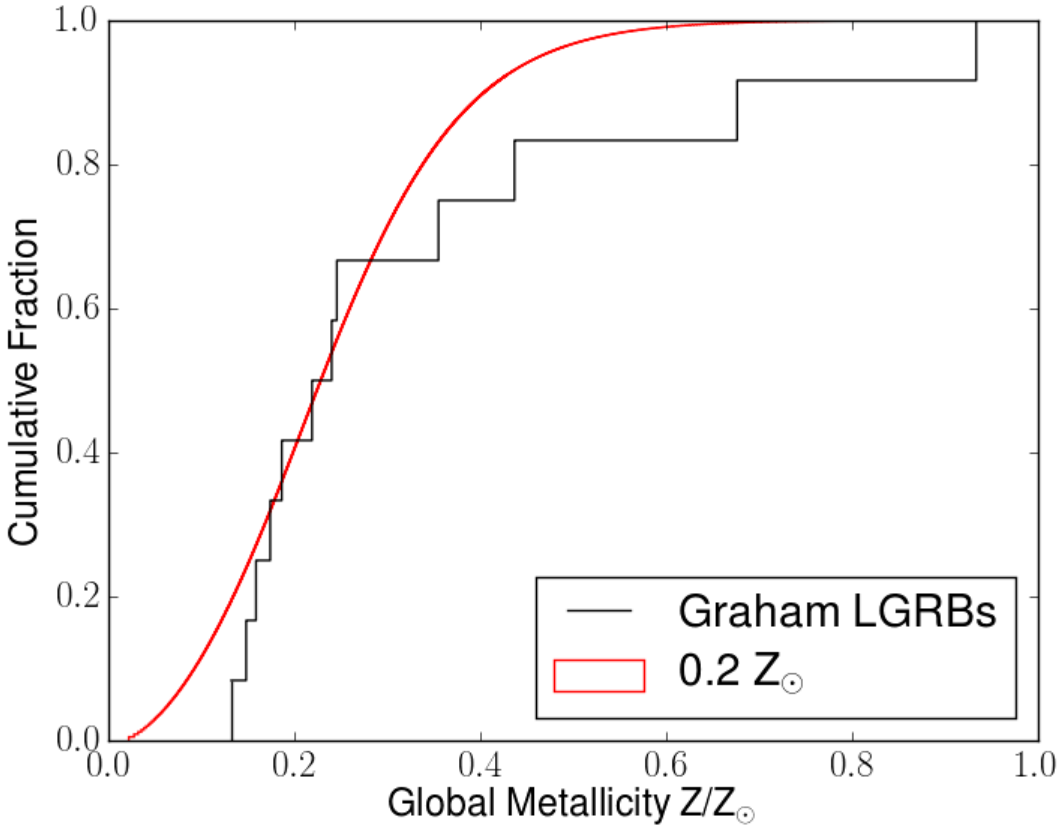

Figure 5.6: Comparison of the emission line global metallicites Graham and Fruchter [2013a] LGRB galaxies in the range $0.0<z<0.5$ with the expected distribution of global metallicities which might be observed when looking for stars below a metallicity threshold of 0.2 $Z_{\odot}$. Here the MZ model accounts only for the internal scatter in metallicities generated from an internal metallicity dispersion (set at 0.1 dex).

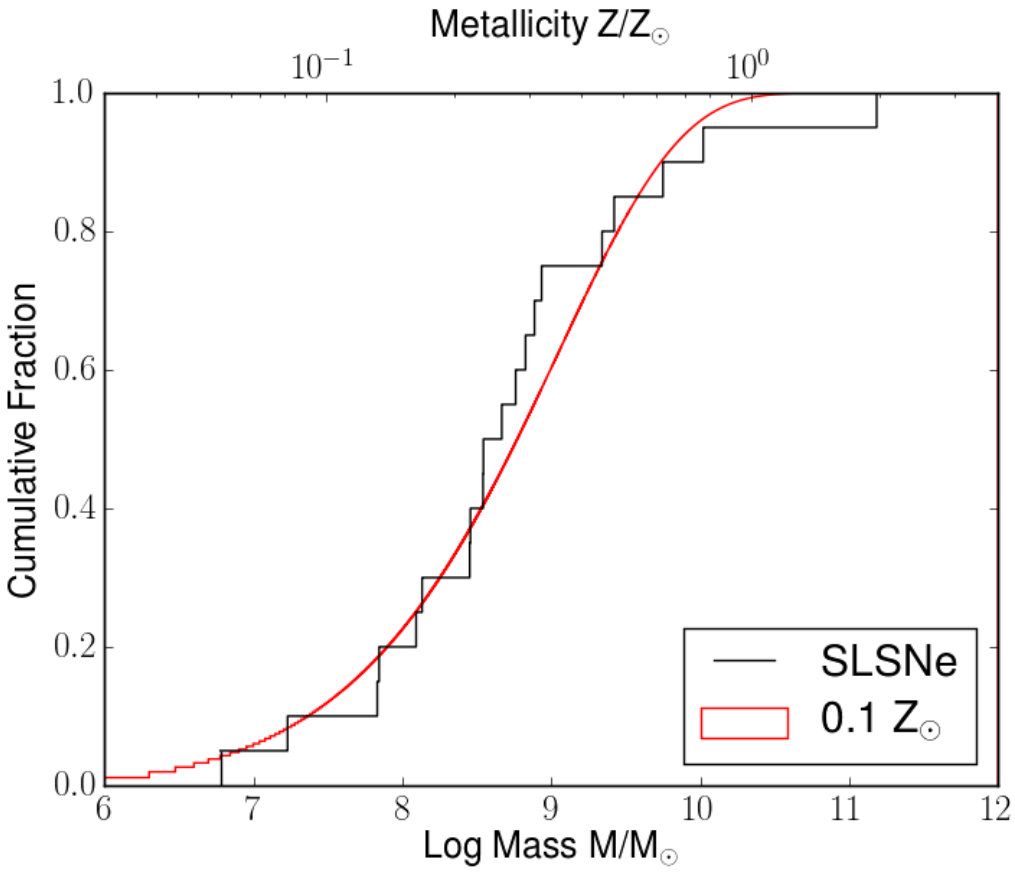

Figure 5.7: The mass function of the *HST* observed SLSN host galaxies from Chapter 3 within the redshift range $0.01<z<0.5$, compared to the best fitting model with a metallicity threshold of 0.1 $Z_{\odot}$ (with variable intrinsic scatter across the stellar mass range).

Table 5.1: Two sample Anderson-Darling probability and Kolmogorov-Smirnov test results between the mass distribution of SHOALS LGRB events and *HST* imaged SLSN events against metallicity thresholds imposed within the MZ model.

Host	Metallicity Threshold	KS Stat.	AD Stat.
SHOALS LGRBs $0.5<z<1.0$	0.1 $Z_{\odot}$	0.556	0.564
Svensson et al. [2010] LGRBs $0.0<z<0.5$	0.2 $Z_{\odot}$	0.982	0.885
SLSNe $0.0<z<0.5$	0.1 $Z_{\odot}$	0.531	0.490
SLSNe-I $0.0<z<0.5$	0.05 $Z_{\odot}$	0.232	0.206
SLSNe-II $0.0<z<0.5$	0.1 $Z_{\odot}$	0.398	0.073
	0.2 $Z_{\odot}$	0.722	0.155
	0.3 $Z_{\odot}$	0.516	0.105
Graham LGRBs $0.0<z<0.5$	0.2 $Z_{\odot}$ (internal scatter only)	0.717	0.114

to the MZ model within Figure 5.8, and found to agree well with an MZ model threshold of $Z<0.2$. Therefore this observed difference in metallicity threshold may be attributed to the evolution towards more massive galaxies with lower metallicities at higher redshifts.

As extensively highlighted shown within the literature and Chapter 3, the environments of SLSNe-I and SLSNe-II differ greatly, particularly in terms of stellar mass range. Thus I break the SLSN sample down by spectral subclass and display their comparisons to different metallicity cuts within Figures 5.9 and 5.10.

Whilst the statistically best fitting model for SLSN-I hosts of a threshold of 0.05 $Z_{\odot}$ does not appear to be too different from the $\sim$0.1/0.2 $Z_{\odot}$ threshold implied for the SHOALS/Svensson et al. [2010] LGRB hosts, when considering the form of the SLSN mass function in Figure 5.9, it's clear that this much tighter mass function of host galaxies is poorly recovered under mass-dependant scatter. Whilst this may be attributed to small number statistics, the much larger sample of SLSN-I host masses presented within the recent work of [Schulze et al., 2016] follows a similarly narrow mass distribution over the same redshift range. If this is indeed typical of SLSN-I hosts, it may be that some additional environmental factor plays some part in the production of their progenitor systems, which restricts these events to a

presented within Perley et al. [2015b]

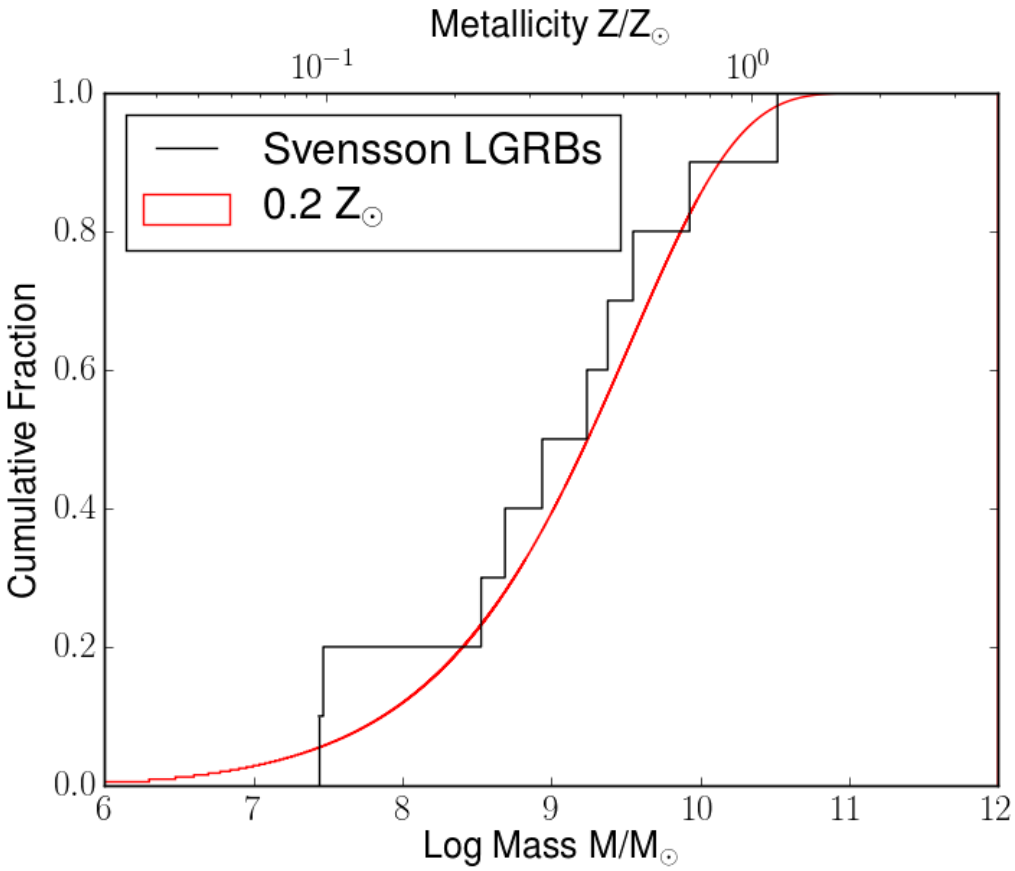

Figure 5.8: The mass function of the LGRB host galaxies from [Svensson et al., 2010] used within Chapter 3 with a redshift range matching the SLSNe hosts considered here. Using the MZ model at a median redshift of z=0.273, a strong similarity is found between these LGRB hosts and the results of the model at a metallicity threshold of 0.2 $Z_{\odot}$.

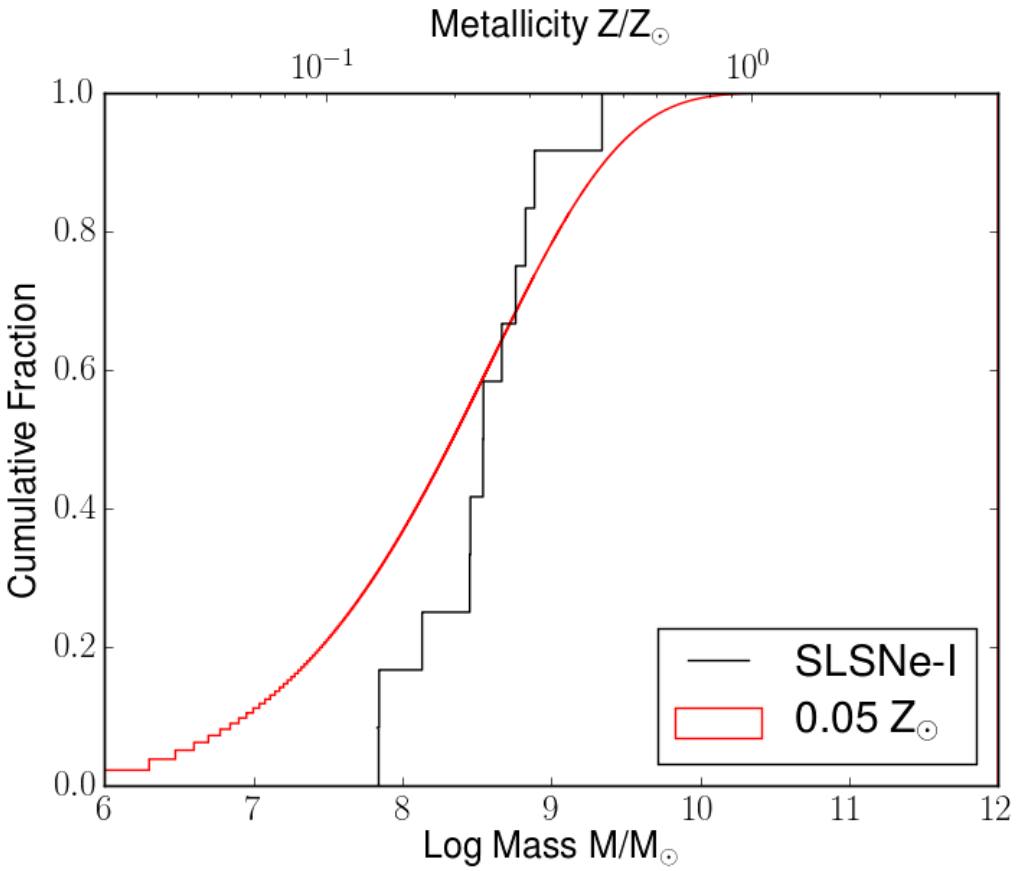

Figure 5.9: Comparison of the SLSN-I hosts against the MZ model output at a metallicity threshold of Z=0.05 $Z_\odot$ (using a median redshift of z=0.244 for the MZ relation). Although statistically this threshold provides the best fit to the observations (KS p= 0.232 and AD p= 0.206), the increased intrinsic scatter at low masses fails to fully account for the narrow observed distribution of SLSN-I host masses.

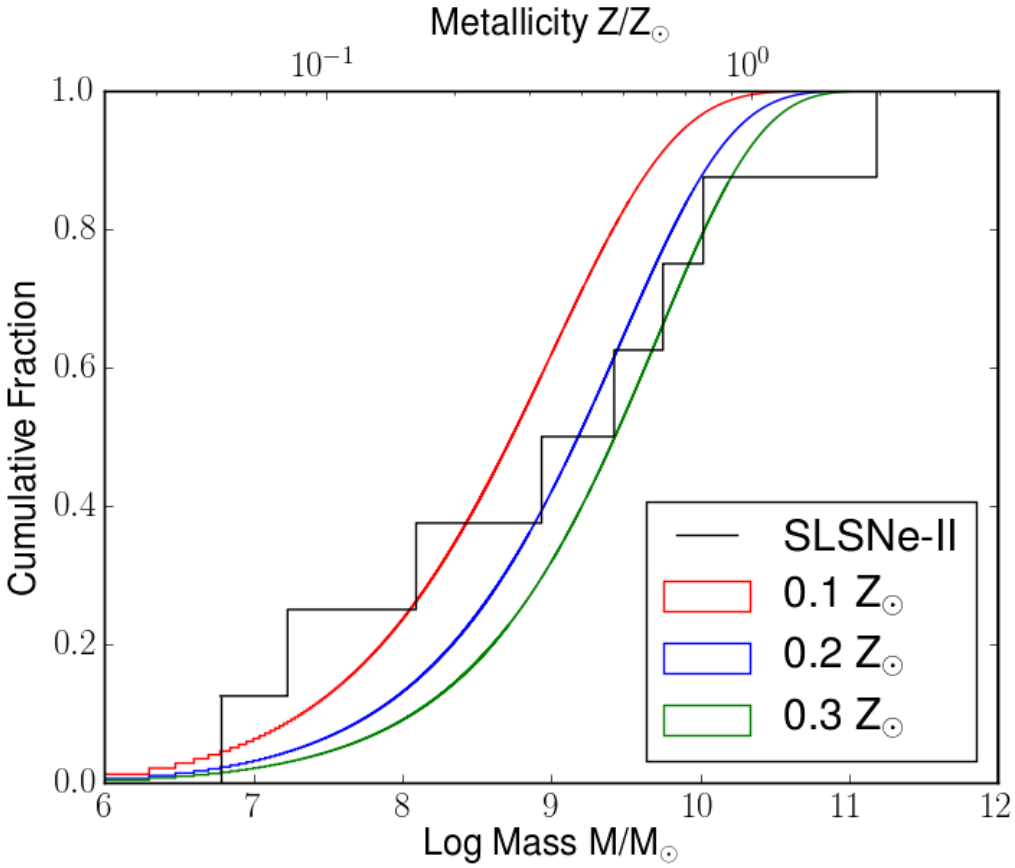

Figure 5.10: Model distributions (for a median redshift of z=0.151) at metallicity thresholds of 0.1, 0.2, 0.3 and 0.3 $Z_{\odot}$ with mass-dependant scatter compared to the mass function of SLSN-II host galaxies observed with HST. It is very difficult to distinguish between these three metallicity thresholds, as all provide comparable results from statistical testing. The inability to describe this broad range of host galaxy masses suggests that the dependance of SLSNe-II upon environmental metallicity is much weaker than LGRBs.

very exclusive sample of galaxies. However, the modest probabilities found with KS and AD testing (p=0.232 and p=0.206) does suggest there is a strong metallicity contingent for progenitor production.

Simultaneously, the broader mass distribution of SLSN-II host galaxies within Figure 5.10 allows multiple metallicity cuts to fit the observed host galaxy mass function (as seen statistically within Table 5.1). Indeed, none of the KS tests have sufficiently low probability (e.g.<5%) to offer moderately strong rejection that the host population is drawn from the underlying modelled distribution. Whilst the existence of satellites or strong metallicity dispersions cannot be ruled out for the larger hosts in this sample (which would result in a sample of generally lower chemical enrichment), at present the small sample size of hosts cannot be used to determine any of the underlying physics at work within this population. The statistical degeneracy of this sample with the suggested metallicity thresholds may be solved in future work with further exploration of the MZ model and an increased SLSNe-II sample size.

5.5 Discussion

These simple models provide a quick and effective tool to diagnose the presence of a metallicity threshold amongst a transient host galaxy population. When used appropriately, they provide a more robust approximation of the range of stellar metallicities traced by a host galaxy sample, under the assumption that metallicity is a key parameter in determining the production of a given transient population.

Through incorporating sources of scatter within the MZ relation, I have created a robust model which may be used for comparison with the mass functions/metallicity distributions of transient host populations such that the likely metallicity of the progenitor populations may be explored. This model provides a more reliable probe of the locations of stellar populations subject to a metallicity restriction than the more common use of the median value of the MZ relation to infer a metallicity threshold from approximate global metallicities. It should also be noted that the gas phase metallicities predicted are not always indicative of the chemical enrichment of the progenitor star itself, and cannot be used to accurately define an evolutionary pathway (as a stellar [Fe/H] ratio can). However, in the absence of spectroscopic metallicity estimates for galaxies drawn from the faint end of the host luminosity function, these models do provide a tool which may be utilised when the use of an MZ relation proxy is necessary.

Using these models, I have shown that differences observed between the

metallicity thresholds for LGRBs inferred from emission line metallicity diagnostics [Graham and Fruchter, 2013a] and previous inferences from the average of an MZ relation [Perley et al., 2015b] may be rendered more compatible. The high ($\sim$1 $Z_{\odot}$) critical metallicity inferred by Perley et al. [2015b] suggested that a binary pathway may be a more feasible route to producing an LGRB event, given the weaker dependance of producing such a progenitor system upon metallicity [Podsiadlowski et al., 2010; Trenti et al., 2015], unlike single star models, which require lower metallicity environments for the retention high mass and angular momentum prior to collapse. The MZ model has shown that the masses and global metallicities of local ($0.0<z<0.5$) LGRB hosts galaxies are consistent with a the likely distribution of hosts which may be observed when considering the locations of stars below a critical metallicity of $\sim$ 0.2 $Z_{\odot}$. This derived threshold does depend upon the assumption that the redshift-dependant MZ relation of Ma et al. [2016] reliably describes the correlation between mass and metallicity at the extreme end of the luminosity function. However, whilst utilising other forms of the MZ relation to describe the behaviour of mass and metallicity may change the detailed thresholds of transient samples, this will not alter the general description of the model.

This metallicity threshold is somewhat stricter than those estimated from spectroscopic observations [e.g. Graham and Fruchter, 2013a; Krühler et al., 2015], which predict more modest thresholds between $\sim$0.3-0.5 $Z_{\odot}$. It is, however, consistent with models LGRBs produced via chemically homogenous massive stars (whose rapid rotation induces strong chemical mixing which alters it's evolution), for which the rate of occurrence drops rapidly after a metallicity of 0.2 $Z_{\odot}$ [Yoon and Langer, 2005; Levan et al., 2016]. Whilst this still cannot distinguish between a binary or single progenitor route, the success of the MZ model in describing the observed populations of LGRB host galaxies does support the notion that LGRB progenitor production is highly dependant upon the metallicity of it's host environment.

The model has also shown that the host galaxies of SLSNe may also be described as tracing the locations of low ($Z<0.1$ $Z_{\odot}$) stellar populations, with a stronger metallicity thresholds for SLSNe-I events than SLSNe-II. Although degeneracies observed in metallicity threshold models for SLSN-II environments, combined with a small sample size doesn't allow us to place strong constraints upon the progenitors of these events, their hosts do generally appear to be tracing metal poor populations ($\lesssim$0.3 $Z_{\odot}$).

Although the model cannot rule out the possibility that SLSNe-I progenitors are drawn from a population of stars restricted to stars to low metallicities of $<$0.05 $Z_{\odot}$, the large levels of intrinsic scatter in the MZ relation does not recover

the narrow mass range occupied by SLSN-I hosts particularly well. This might suggest that there is some additional factor which governs the production of these transients, alongside a typically low progenitor metallicity. Leloudas et al. [2015] and Schulze et al. [2016] have suggested that the broad (>100Å), equivalent widths observed within emission lines of SLSN-I host galaxies suggest very young environments for SLSNe-I, given that these are highly dependant upon the star-formation history of the galaxy [Lee et al., 2009] and the time following the most recent burst [Leitherer et al., 1999]. Indeed, the narrow mass distribution of SLSN-I host galaxies limits them almost exclusively to dwarf galaxies, whose star forming histories tend to be bursty in nature [Guo et al., 2016]. These intense bursts of star formation are less frequently observed within more massive galaxies within the local Universe [Hinojosa-Goñi et al., 2016a], which may explain the narrower range of masses observed within the SLSN-I host galaxy population. If the star forming cycles of these dwarf galaxies are typically on the order of 1-2 Gyr [Lee et al., 2009], the chance of observing a SLSN event at the beginning of the star burst (whilst the population is young, as indicated by the strong equivalent widths) is very small, and as such the occurrence of a high fraction of SLSNe within such galaxies may not be coincidental [Schulze et al., 2016], and thus an additional requirement of a young stellar population does not seem an unreasonable suggestion.

The implications for progenitor models if this were the case are interesting. Massive stars exploding as PISNe provide the most obvious suggestion for a young population at typically low metallicity, which would fall in with the extreme radiation fields observed within local SLSN-I host galaxies [Leloudas et al., 2015]. Whilst this model has been somewhat downplayed due to the requirement of extreme ($\sim 10^{-4}$ $Z_{\odot}$) metallicities required to produce high mass progenitor cores of between $\sim$60 to $\sim$130 $M_{\odot}$ [Heger and Woosley, 2002; Chatzopoulos and Wheeler, 2012a], recent models have shown that massive ($\sim$200 $M_{\odot}$) stars at near solar metallicity are capable of producing PISNe in the presence of a dipolar surface magnetic field (which acts to suppress mass loss by stellar winds) [Georgy et al., 2017]. Therefore the low-to-modest metallicity population traced by SLSNe may still allow these massive stars to collapse as PISNe.

However, it is still possible to reconcile a similar progenitor path for SLSNe-I and LGRBs, even if the metallicity of progenitors were not a strict factor in SLSNe-I production. The magnetar model of SLSNe and LGRBs works based upon different spin down times releasing energy on different time scales, such that for a LGRB the energy is deposited quickly, allowing it to break out through the stellar envelope, whilst for SLSNe this release occurs over a more gradual time scale, trapping this

energy behind the SN shock wave [Metzger et al., 2015]. It may be possible to describe this distinction between more immediate/more gradual release in energy via a metallicity dependence, where the spin period of the resulting magnetar is tied to the metallicity of it's environment. Indeed, a correlation between modelled magnetar spin period and the chemical enrichment of the environment has been suggested using global metallicity studies of a small sample of local ($z \lesssim 0.3$) SLSN-I hosts by Chen et al. [2016]. However, given the large number of variables to magnetar-powered transient production (the magnetic field strength, mass and opacity of the ejecta), it seems unlikely that metallicity alone would provide such a strong influence in the environmental preference of magnetar-powered transients.

5.6 Conclusions

I have shown that through incorporating sources of scatter inherent to the mass metallicity relation within simple models, we may utilise the proxy from the mass-metallicity relationship more effectively than using the average value of chemical enrichment that this relationship predicts. These models have shown that:

- Sources of scatter within the MZ relation can explain the observed discrepancy between the metallicity threshold predicted by spectroscopic results and those which utilise an average of the MZ relation.
- The sources of scatter within the MZ relation may vastly change the likely distribution of low metallicity stars within the local Universe. It is important to understand the sources and origin of this scatter, such that we may more accurately account for its effects.
- These models have confirmed that LGRBs and SLSNe arise from low metallicity environments. When accounting for the different sources of scatter within spectroscopic metallicities and those inferred from an MZ proxy, they have successfully reconciled the apparent differences in inferred progenitor population metallicity threshold for LGRBs.

Whilst there is room for development within these models, to better account for evolution with redshift and the additional sources of scatter inherent to the MZ relation, they have proved a simple but powerful tool which may be used to better constraint the chemical enrichment of transient host galaxies across the luminosity function.

Chapter 6

Conclusions and Future Work

" I cannot be right all the time. Quite often I is left instead of right"

—Roald Dahl, *The BFG*
(also a sentiment of C.R. Angus)

SLSNe represent one of many new interesting classes of transient event uncovered due to the instigation of deep, wide field, high cadence transient surveys over the past decade. Their extreme luminosities, coupled with their longevity in the optical allow them to be probed out to high redshifts [Cooke et al., 2012], with the potential to trace the evolution of star formation, the IMF and chemical enrichment over cosmic time.

Their progenitors are at present, poorly characterised. Whilst believed to be associated with massive ($>8\,M_{\odot}$) stars, exactly how massive these stars are and the physical mechanisms through which their core collapse proceeds are unknown. As the results of spectral and light curve modelling leave are currently lack the necessary constraints to draw firm conclusions [Nicholl et al., 2013; Inserra et al., 2013], and the events themselves lie beyond the reach of direct progenitor detection methods, interest has turned to the host galaxies of the events, such that through their properties the underlying stellar populations may be deduced.

Prior to the commencement of the work undertaken for this thesis, the host galaxies of SLSNe were known to be faint and blue [Neill et al., 2011] with possibly low metallicities [Stoll et al., 2011; Lunnan et al., 2013; Chen et al., 2013]. The field of SLSNe host galaxy studies has shown much progress in recent years, with the sample of characterised hosts increasing from a variety of surveys [such as PanSTARRS and PTF, Lunnan et al., 2014; Perley et al., 2016], covering both their photometric and spectroscopic properties [Lunnan et al., 2015; Leloudas et al.,

2015].

The primary goal of this thesis has been to use high resolution *HST* WFC3 imaging at UV and nIR wavelengths to examine the global and sub galactic environments of a sample of SLSN host galaxies, such that their underlying stellar populations may be better characterised. In addition, I have also considered the implications different metallicity restrictions upon transient progenitors, and how such thresholds may be reflected within the host galaxy populations.

6.1 Summary of Results

6.1.1 Global Environment Properties

Within Chapter 3 I used the *HST* imaging to consider the global properties of SLSN host galaxies of all spectral types, comparing their UV and nIR properties to those of CCSNe and LGRB host galaxies to place constraints upon their stellar populations in terms of mass and age. This study has shown that the host galaxies of SLSNe are typically fainter in both wavelength regimes than other transient host galaxies, and also morphologically more compact. These observations have also drawn focus to the significant fraction of SLSN events which arise from exceptionally faint (M_V>-13) host galaxies. Using these photometric properties to better constrain the masses and star formation rates derived from SED fitting, these SLSN host galaxies have also been shown to be less massive than the comparison samples, with typically lower star formation rates.

The work undertaken within Chapter 3 was the first to highlight the observable differences between the environments of hydrogen-poor (Type-I and Type-R) and hydrogen-rich (Type II) SLSNe. The host galaxies of SLSN-I events are consistently fainter than CCSNe and LGRBs, which by extension implies lower masses, star formation rates and chemical enrichments for their environments. Given the proposed similarities between the collapsar model of LGRBs and the favoured internal engine model of SLSNe-I production, these differences are puzzling, as it would be logical for analogous progenitors to arise from similar environments. The systematic offset of SLSN-I towards fainter, lower mass host galaxies than those for within which an LGRB event has occurred suggests that some additional constraint within their host environment dictates their rate of production within the local Universe, (i.e. the as opposed to the production of an LGRB event if their progenitor masses are similar). Given the very narrow spread of host galaxy masses observed within the SLSN-I population, this additional factor may be a metallicity threshold, such that SLSN-I arise from lower metallicity environments than those observed for

LGRB events.

On the other hand, the work within this Chapter identified SLSNe-II events as arising from galaxies whose environmental properties span a much broader range than SLSNe-I. The presence of SLSNe-II within both extremely low mass ($\sim 10^6$ $M_\odot$) hosts and more massive galaxies (e.g. SN2006gy, $M_*=10^{11.18}$ $M_\odot$), suggests one of two scenarios. Either these particular SLSNe are produced within very specific sub galactic environments (whose properties become washed out by the global properties of the host), such as a very intense burst of star formation or a pocket of very low metallicity within a more generally metal rich host. Or this diversity in environment may simply reflect an equally diverse set of progenitor routes for SLSNe-II.

6.1.2 Subgalactic Environment Properties

The global properties of SLSNe host galaxies have revealed their extreme nature, and in doing so have implicated a strong connection between the properties of the environment and the progenitors of these transients. However, internal fluctuations in environmental conditions which are common within galaxies within the local Universe (metallicities gradients and pockets of small scale star formation) may change the inferred properties of the stellar populations local to the SN explosion, and thus change the inferred progenitor types (and so the resulting explosion mechanisms which produce the transient).

The high resolution imaging from the *HST* data set was used to study the sub-galactic environments of SLSNe within their host galaxies. For the redshift range of the sample, this imaging allows the local environments to be probed down to $\sim$0.1 kpc scales. The work of Chapter 4 uses the rest-frame UV imaging of the host galaxies to derive the star forming properties of the immediate environments of SLSNe. Through the use of the fractional flux parameter, the fraction of host light contained within pixels of a lower surface brightness than the one containing the transient, it was ascertained that SLSNe are typically associated with bright UV regions within their host galaxies, and thus show association with recent star formation. Whilst visually it would appear that the UV locations of SLSNe within their hosts are generally fainter than those of LGRB events, and brighter than those CCSNe, which in turn implies that they are associated with progenitors of intermediate age and mass to those of these two different transient populations, statistically they cannot be distinguished.

As the typical uncertainties associated with the localisation of SLSNe within this sample are relatively poor ($\sim$10's mas), I have implemented a weighted fractional flux technique to incorporate the range of possible transient locations within

the transient uncertainty region. As an intrinsically highly concentrated population would be scattered randomly by astrometric errors, which would naturally produce a distribution focused towards fainter pixels, this technique therefore allows us to place lower limits upon the concentration of a fractional flux distribution. For SLSNe hosts this still suggests an association with star forming regions within the host galaxy, even when the distribution is diluted by the inclusion of surrounding pixels.

At a subclass level, SLSN-II events seem to exhibit a preference for fainter regions of their host galaxies, although given the small sample size considered here, this is statistically inconclusive and motivates the need for an increased sample of SLSN-II hosts with high resolution imaging. For hydrogen poor SLSNe, whilst the constraints placed by the localisations do not at present allow us to distinguish whether their distribution is more analogous to LGRB of CCSN environments, they are consistent with previous study of SLSN-I environments by Lunnan et al. [2015], who find that the locations of SLSNe-I may statistically be similar to those of LGRBs, who exhibit a strong preference for bright UV regions. Whether this preference is a direct reflection upon the progenitor masses involved, or the result of some additional environmental preference when producing SLSN-I progenitors (such as local metallicity) is unknown.

6.1.3 Mass Metallicity Modelling

The observed differences in the photometric properties of SLSNe and LGRB host populations, particularly in terms of their stellar masses, suggest similar differences in their chemical enrichment, based upon our current understanding of the correlation between galaxy stellar mass and metallicity. Such differences in metallicity would provide key insight into any differences in their progenitors, and may help to constrain models of SLSNe production.

Problems in constraining this issue arise with the availability of spectroscopic observations of SLSN and LGRB hosts. A combination of low intrinsic brightness and typically high redshift makes the acquisition of spectroscopic observations for a complete sample of hosts across the luminosity function observationally expensive. This means that the conclusions drawn from the results of spectroscopic observations of more local populations (which suggest similar chemical enrichment, Lunnan et al. 2014) are biased against this faint end.

Many previous inferences of the presence of a metallicity threshold within a transient population do so based upon approximations from the median of the correlation observed between the mass and metallicity of a galaxy. However, as I

demonstrated within Chapter 5, there are multiple sources of scatter which act to broaden the likely range of galaxies stars below a given metallicity threshold may occur. Normal MZ proxies fail to account for this scatter, and as a consequence often over-estimate the true metallicity threshold being traced by progenitor populations.

Within Chapter 5 I have presented a model which accounts for the key sources of scatter within the mass-metallicity relationship; namely, the scatter introduced through the presence of an internal metallicity dispersion within a given galaxy, and the scatter intrinsic to the MZ relation, which evolves with the galaxy mass range under consideration. By utilising the redshift dependant MZ relation of Ma et al. [2016], I have created a model which can be used to approximate the locations of stars below a chosen metallicity threshold, which may then be compared with observed populations of transient host galaxies such that it may be ascertained whether these hosts do provide a representative sample of hosts to stars within this range.

Using these models I have shown that LGRB host galaxies are consistent with a population of galaxies host to stars below a metallicity threshold of 0.2 $Z_{\odot}$. This model has successfully reconciled differences between metallicity thresholds inferred from spectroscopic observations of local LGRB hosts [Graham and Fruchter, 2013a] and from metallicity thresholds inferred from the use of MZ-proxy for a more complete sample of LGRB hosts across their luminosity function [Perley et al., 2015b].

This model has also demonstrated that SLSNe originate from galaxies which are host to typically low metallicity ($<$0.1-0.2 $Z_{\odot}$) stellar populations, although larger sample sizes are required for confirmation. The similarity in populations at low metallicity within LGRB and SLSNe-I host galaxies may suggest progenitors of similar mass or explosion route. However, the narrow distribution of host galaxy masses observed within SLSN-I hosts suggests that there may be additional or more dominant factors which govern their production.

6.1.4 Impact of this thesis

This thesis has highlighted the unusual environments of SLSNe, on a global and sub-galactic scale. The typically extreme nature of SLSN-I environments, in luminosity, mass and star formation rate suggests that the production of a SLSN-I progenitor is highly tied to the properties of the environment in which it forms. Given the proposed similarities which have been suggested between the progenitors of LGRBs and SLSNe, (either between the collapsar model of LGRB production and a black hole-driven internal engine, or powered via magnetars at different spin down rates),

this thesis has examined the differences and similarities in their environments in a like-for-like manner, such that we may better understand whether there is any underlying connection in their progenitor systems.

As the poor constraints upon the locations of SLSN-I used within this thesis allow us only to place limits upon the likely distribution of sub-galactic environments traced by this population, it is at present unclear whether they exhibit the same preference for the brightest UV regions within their host galaxies that LGRB events do. The hosts of SLSNe-I are also typically of lower stellar mass, and although modelling of the underlying stellar metallicities suggests that both galaxy populations are consistent with hosting stars of low (0.1-0.2 $Z_{\odot}$) metallicity, the very narrow range of host masses occupied by SLSN-I may be a result of additional environmental constraints upon their progenitors.

This work has also shown that the hosts of SLSNe-II events are extremely diverse in nature, spanning an appreciably broad range of host galaxy masses and star formation rates, although at present the constraints upon their locations do not provide a clear indication of their preference for sub-galactic environment properties. Host galaxies of this SLSN subclass incorporate both the most luminous and the intrinsically faintest galaxies within the SLSN population. Such diversity in environment suggests that the production hydrogen rich SLSNe progenitors depends either very little upon the environments in which they are born.

The MZ model presented within this thesis has proven a simple but effective tool to trace to distribution of locations of stellar populations below a given metallicity throughout the Universe. It has successfully reconciled differences in metallicity thresholds inferred for populations of LGRB host galaxies determined spectroscopically and through a standard MZ proxy. Assuming that the metallicity of the progenitor is a key parameter in the production of any given transient, this model provides a more robust method of approximating the likely locations of stars of specified chemical enrichment, which may then be compared to the observed locations of transients and thus a metallicity threshold inferred if appropriate.

6.2 Future Work

Despite the progress in recent years towards a better understanding of SLSN events, there are still many outstanding issues surrounding these luminous transients.

The proposed standardisation of SLSN events [Inserra and Smartt, 2014; Papadopoulos et al., 2015; Scovacricchi et al., 2016] requires a much more detailed knowledge of their progenitors and the physical mechanisms behind the production

of their lightcurves. This information is likely to follow the anticipated numerous SLSN event discoveries which will accompany new generation telescopes such as LSST, Euclid and JWST. The increased sample size, coupled with higher redshift coverage from deeper imaging surveys such as DES, will allow statistical analysis of SLSN events across a broader redshift range[1], such that we may better understand their typical behaviour, and rule out atypical events from standardisation calculations. The detection of SLSN out to higher redshifts will also provide a probe of the top-heavy IMF at early cosmic times through comparison of the evolution of the SLSN rate and SFR density [Tanaka et al., 2013].

Although the environments of SLSNe have provided some interesting insight into the likely progenitors of these unusual transients, particularly in terms of their chemical enrichment (as indicated by their low mass galaxies, and concurrence with low metallicity populations within MZ modelling), there is still some difficulty in distinguishing between the different progenitor paths of SLSNe. Whilst the inferred local populations to SLSNe explosions are thought to be young, metal poor stars, determining whether such populations are more likely to explode as a PISN or produce a magnetar-powered transient is difficult, particularly given the large number of variables involved in magnetar production. In the absence of direct progenitor imaging of a very local event, which would allow us to place direct limits upon the mass of the progenitor, we must continue to rely upon the constraints introduced through the explosion parameter modelling. One key to deciphering the difference between these two models may lie within a better understanding of pre-explosion bumps which have been observed within several SLSN lightcurves [Leloudas et al., 2012; Nicholl et al., 2015; Piro, 2015; Smith et al., 2016]. Multi-colour, high cadence surveys such as DES, and in the future LSST and Euclid, will provide information to begin fitting the temperature (and subsequent evolution) of these bumps, which can be use to distinguish between different progenitor models. With the drastically increased sample of SLSN events which will result from these surveys, we will be able to place statistical limits not only upon the presence of bumps within the SLSN population, but also (if their behaviour is ubiquitous) upon the likely mechanisms which produce them.

The large internal diversity present within SLSN-II events, particularly with the presence of a growing subset of these events which do not display signs of interaction during their photospheric phase [Inserra et al., 2016], leaves much ambiguity to their progenitor systems. Whilst signatures of hydrogen indicate the existence of

[1] at present, the volume limited nature of many transient surveys, find events only out to redshift $z{\sim}1.5$

some form of extended stellar envelope surrounding the progenitor, how this envelope is produced and the ultimate driving force behind the SN is unknown. This ambiguity can really only be solved with an increased sample of Type II SLSNe with both detailed follow up observations of the transients and the host galaxies.

Whilst the strong radiation fields observed in many SLSNe-I host galaxies and metallicity thresholds inferred from MZ modelling are highly suggestive that the progenitors of SLSNe-I events arise from low metallicity massive stars formed within a recent burst of star formation, at present it is not clear whether SLSNe-I exclusively trace the brightest light within their hosts (which would be the logical progression from arising from the youngest stars within a star burst). Observationally the link between cluster mass and most massive member suggests that if SLSNe-I progenitors are the youngest (and therefore, most massive stars) formed within a recent starburst, they should be located within the most massive clusters in the galaxy (which would likely be the most star forming and therefore brightest in the UV).

One simple approach to test this is to model the likely fractional flux distributions which may arise under stochastic star formation with different assumptions about the level of star formation within the galaxy. Under the assumption that the transient is arising from the most massive star within a cluster, the form of the fractional flux distribution may be found under different cluster mass restrictions, and thus the form of the likely transient population's F_L distribution can be approximated under different assumptions about their progenitor mass. As demonstrated within Figure 6.1, when increasingly higher mass progenitors are required, the fractional flux distribution becomes more concentrated towards brighter regions (and higher fractional flux values).

Future work will also include detailed modelling of the affects of stochastic star formation upon SLSNe locations. By assessing how the concentration of a fractional flux for a given mass progenitor distribution alters under different assumptions about the level of star formation within the host galaxy sample, we may at last begin to assess how the nature of massive star formation may impacts the production of different stellar masses, and thus relate this to the rates of production of SLSNe.

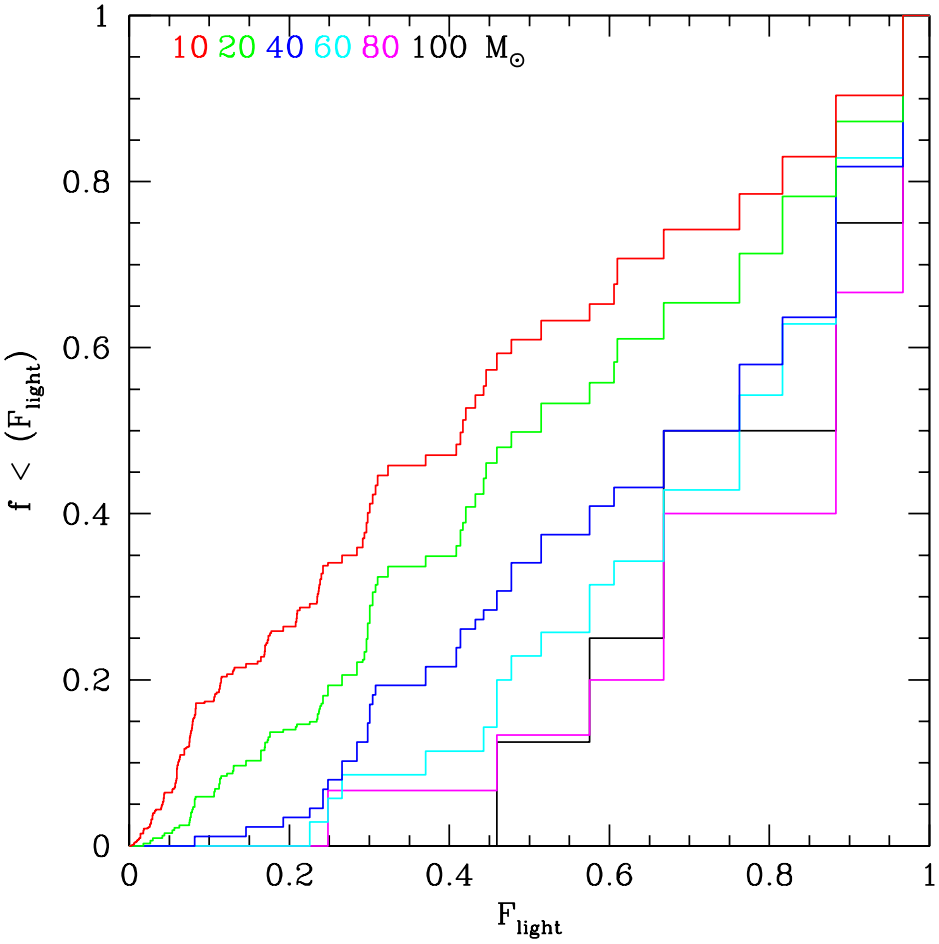

Figure 6.1: *Figure produced by Andrew Levan.* The likely distribution of fractional flux parameters which would arise from transients produced by stars with initial masses of 10, 20, 40, 60, 80 and 100 $M_\odot$. Naturally, as more massive stars are required, the concentration of the fractional flux distribution increases towards higher F_L values. By considering how this concentration changes under different star formation rates will provide an indication of how star formation may impact the rate of SLSN production within the local universe.

Appendix A

LGRB and CCSN Comparison Samples for Photometric and Location Comparison

Table A.1: CCSNe comparison sample selected from the GOODs survey, for which I carry out nIR photometric measurements for the work in Chapter 3. Here I report apparent magnitudes alongside redshifts and host co-ordinates. Within this sample, the affects of SExtractor's unrealistic uncertainty determination for all objects is apparent, particularly given the brighter nature of this sample of hosts. However, this does not impact the overall conclusions drawn from these results.

Event	z	RA (J2000)	Dec (J2000)	m_{nIR} AB mag
SN2006aj	0.03	03:21:39.670	+16:52:02.27	19.702 ± 0.002
SN2002hs	0.39	03:32:18.590	- 27:48:33.70	22.362 ± 0.009
SN2002fv	0.70	03:32:19.220	- 27:49:34.00	23.971 ± 0.016
SN2002hq	0.67	03:32:29.940	- 27:43:47.20	19.162 ± 0.001
SN2002kb	0.58	03:32:42.441	- 27:50:25.08	19.221 ± 0.0014
SN2002fz	0.84	03:32:48.598	- 27:54:17.14	20.385 ± 0.002
SN2003ba	0.29	12:36:15.925	+62:12:37.38	18.8852± 0.0009
SN2003bb	0.96	12:36:24.506	+62:08:34.84	19.3208± 0.0016
SN2003ew	0.58	12:36:27.828	+62:11:24.71	20.817 ± 0.005
SN2003dx	0.51	12:36:31.772	+62:08:48.25	22.223 ± 0.004
SN2003er	0.63	12:36:32.270	+62:07:35.20	19.1932± 0.0006
SN2003en	0.54	12:36:33.179	+62:13:47.34	21.91 ± 0.11
SN2003bc	0.51	12:36:38.130	+62:09:52.88	20.807 ± 0.0018
SN2003dz	0.48	12:36:39.967	+62:07:52.12	23.81 ± 0.03
SN2003N	0.43	12:37:09.140	+62:11:01.20	22.809 ± 0.008
SN2003ea	0.98	12:37:12.066	+62:12:38.04	22.870 ± 0.009
SN2002kl	0.41	12:37:49.350	+62:14:05.71	22.2 ± 0.2

Table A.2: Absolute magnitudes and sizes of CCSNe comparison sample selected from the GOODs survey, used for nIR photometric analysis within Chapter 3. Again, SExtractor produces unphysical photometric errors, although this does not impact the overall conclusions drawn from these results.

Event	M_{nIR} AB mag	r_{80} (nIR) kpc
SN2006aj	-16.250 ± 0.002	1.1 ± 0.4
SN2002hs	-18.897 ± 0.009	1.1 ± 0.3
SN2002fv	-18.608 ± 0.016	0.56 ± 0.13
SN2002hq	-23.323 ± 0.001	1.4± 0.5
SN2002kb	-22.9378 ± 0.0014	1.4 ± 0.5
SN2002fz	-22.600 ±0.002	0.9 ±0.3
SN2003ba	-21.7071 ±0.0009	1.2 ± 0.4
SN2003bb	-23.9609 ± 0.0016	1.3 ± 0.4
SN2003ew	-21.346 ± 0.005	1.3 ± 0.4
SN2003dx	-19.648 ± 0.004	0.56 ± 0.15
SN2003er	-23.1551 ± 0.0006	0.9 ± 0.3
SN2003en	-20.09 ± 0.11	0.60 ± 0.16
SN2003bc	-21.0661 ± 0.0018	0.8 ± 0.3
SN2003dz	-17.93 ± 0.03	0.63 ± 0.16
SN2003N	-18.677 ± 0.008	0.66 ± 0.18
SN2003ea	-20.457 ± 0.009	0.71 ±0.18
SN2002kl	-19.20 ± 0.2	0.57 ± 0.15

Table A.3: LGRB subsample from SNAPSHOT survey used for nIR photometric analysis within Chapter 3. Full details for these hosts can be found within Lyman et al. [2017]

heightEvent	Redshift	RA(J2000)	Dec(J2000)
GRB050824	0.828	00:48:56.260	+22:36:33.20
GRB051016B	0.9364	08:48:27.860	+13:39:19.60
GRB060218	0.0331	03:21:39.650	+16:52:01.30
GRB060505	0.089	22:07:03.380	-27:48:52.90
GRB060602A	0.787	16:03:42.500	+66:36:02.60
GRB060614	0.125	21:23:32.190	-53:01:36.50
GRB060729	0.54	06:21:31.840	-62:22:12.10
GRB060912A	0.937	00:21:08.110	+20:58:19.20
GRB061007	1.2622	03:05:19.59	-50:30:02.3
GRB061110A	0.758	22:25:09.850	-02:15:31.00
GRB070318	0.840	03:13:56.760	-42:56:46.80
GRB070521	1.3500	16:10:38.62	+30:15:22.1
GRB071010A	0.98	19:12:14.624	-32:24:07.16
GRB071010B	0.947	10:02:09.240	+45:43:49.70
GRB071112C	0.823	02:36:50.910	+28:22:16.80
GRB071112	1.1400	18:26:25.26	+47:04:30.00
GRB080430	0.767	11:01:14.660	+51:41:07.80
GRB080520	1.5457	18:40:46.37	-54:59:30.6
GRB080707	1.2322	02:10:28.41	+33:06:34.5
GRB080805	1.5042	20:56:53.47	-62:26:40.2
GRB080916A	0.689	22:25:06.360	-57:01:22.90
GRB081007	0.5295	22:39:50.500	-40:08:49.80
GRB090424	0.544	12:38:05.090	+16:50:15.70
GRB090618	0.54	19:35:58.400	+78:21:25.20
GRB091127	0.49	02:26:19.910	-18:57:08.90
GRB091208B	1.063	01:57:34.090	+16:53:22.70

Table A.4: Core Collapse SNe drawn the [1] GOODS sample and from [2] Sanders et al. [2012] and [3] Lennarz et al. [2012], used for UV photometric analysis within Chapter 3.

Event	Redshift	RA(J2000)	Dec(J2000)	
SN2002fz	0.841	03:32:48.598	-27:54:17.14	3
SN2002hq	0.669	03:32:29.94	-27:43:47.2	1
SN2002if	0.321	01:50:04.51	+00:00:26.4	3
SN2002kb	0.58	03:32:42.441	-27:50:25.08	3
SN2002ke	0.577	03:31:58.77	-27:45:00.7	1
SN2002kl	0.41	12:37:49.350	+62:14:05.71	3
SN2003ba	0.286	12:36:15.925	+62:12:37.38	3
SN2003bb	0.954	12:36:24.506	+62:08:34.84	3
SN2003bc	0.511	12:36:38.130	+62:09:52.88	1
SN2003dx	0.46	12:36:31.772	+62:08:48.25	3
SN2003ea	0.89	12:37:12.066	+62:12:38.04	3
SN2003ew	0.66	12:36:27.828	+62:11:24.71	3
HST04Geo	0.937	12:36:44.432	+62:10:53.19	1
HST04Riv	0.606	03:32:32.407	-27:44:52.84	1
HST05Bra	0.48	12:37:21.764	+62:12:25.67	1
HST05Den	0.971	12:37:14.773	+62:10:32.61	1
SN2005hm	0.035	21:39:00.65	-01:01:38.7	2
SN2005nb	0.023	12:13:37.61	+16:07:16.2	2
SN2006ip	0.030	23:48:31.68	-02:08:57.3	2
SN2006ir	0.02	23:04:35.68	+07:36:21.5	2
SN2006jo	0.076	01:23:14.72	-00:19:46.7	2
SN2006nx	0.137	03:33:30.63	-00:40:38.2	2
SN2006sg	0.44	02:08:13.041	-03:46:21.93	2
SN2006tq	0.26	02:10:00.698	-04:06:00.91	2
SN2007I	0.021	11:59:13.15	-01:36:18.9	2
SN2007ea	0.04	15:53:46.27	-27:02:15.5	2
SN2007ff	0.05	01:24:10.24	+09:00:40.5	2
SN2007gl	0.03	03:11:33.21	-00:44:46.7	2
SN2007hb	0.02	02:08:34.02	+29:14:14.3	2
SN2007hn	0.03	21:02:46.85	-04:05:25.2	2
SN2010ah	0.049	11:44:02.99	+55:41:27.6	2

Table A.5: LGRBs from Ghosts [4] Savaglio et al. [2009] (and references therein), [5] Resmi et al. [2012], [6]Hjorth et al. [2012],[7]Sollerman et al. [2007], [8]Perley et al. [2013],[9] Levan et al. [2007] , [10] Cool et al. [2007], [11] Tanvir et al. [2010], [12] Krühler et al. [2011], [13] McBreen et al. [2010],[14] Holland et al. [2010], [15] Vergani et al. [2011], [16] Starling et al. [2011], [17] Abazajian et al. [2009], [18]Pérez-Ramírez et al. [2013], [19] Elliott et al. [2013], [20] Levan et al. [2014a].

Event	Redshift	RA(J2000)	Dec(J2000)	ref.
GRB970228	0.695	05:01:46.7	+11:46:53	4
GRB970508	0.8350	06:53:49.2	+79:16:19	4
GRB970828	0.9580	18:08:31.6	+59:18:51	4
GRB980425	0.0085	19:35:03.2	-52:50:46	4
GRB980703	0.9660	23:59:06.7	+08:35:07	4
GRB990705	0.842	05:09:54.5	-72:07:53	4
GRB990712	0.434	22:31:53.061	-73:24:28.58	4
GRB991208	0.706	16:33:53.51	+46:27:21.5	4
GRB000210	0.846	01:59:15.6	-40:39:33	4
GRB010921	0.435	22:55:59.90	+40:55:52.9	4
GRB011121	0.360	11:34:26.67	-76:01:41.6	4
GRB020405	0.698	13:58:03.12	-31:22:22.2	4
GRB020819B	0.41	23:27:19.475	+06:15:55.95	4
GRB020903	0.25	22:48:42.34	-20:46:09.3	4
GRB030329	0.168	10:44:50.030	+21:31:18.15	4
GRB030528	0.782	17:04:00.3	-22:37:10	4
GRB031203	0.1055	08:02:30.4	-39:51:00	4
GRB040924	0.859	02:06:22.52	+16:08:48.8	4
GRB050525	0.606	18:32:32.560	+26:20:22.34	5
GRB050824	0.8278	00:48:56.100	+22:36:32.00	6,7
GRB050826	0.296	05:51:01.590	-02:38:35.40	4
GRB060202	0.785	02:23:22.940	+38:23:03.70	8
GRB060218	0.0335	03:21:39.670	+16:52:0	4
GRB060912A	0.937	00:21:08.11	+20:58:18.9	9
GRB070612	0.6710	08:05.4	+37:15	10
GRB080319B	0.93	14:31:41.04	+36:18:09.2	11
GRB081109	0.979	22:03:11.50	-54:42:40.5	12
GRB090328	0.7354	06:02:39.69	-41:52:55.1	13
GRB090417B	0.345	13:58:44.8	+47:00:55	14
GRB091127	0.49	02:26:19.87	-18:57:08.6	15
GRB100316D	0.0591	07:10:30.63	-56:15:19.7	16
GRB100418	0.6239	17:05:26.96	+11:27:41.9	17
GRB100621A	0.5420	21:01:13.12	-51:06:22.5	12
GRB100816A	0.8049	23:26:57.56	+26:34:42.6	18
GRB110918	0.984	02:10:09.39	-27:06:19.6	19
GRB101225A	0.85	00:00:47.48	+44:36:01.0	20
GRB111209A	0.67	00:57:22.700	-46:48:05.00	20
GRB120422A	0.28	09:07:38.38	+14:01:07.5	17
GRB130427A	0.35	11:32:32.63	+27:41:51.7	20

Table A.6: UV photometric properties of CCSNe used within Chapter 3.

Event	m_{UV} AB mag	M_{UV} AB mag
SN2002fz	22.36 ± 0.01	-20.636 ± 0.01
SN2002hq	22.455 ± 0.021	-20.074 ± 0.021
SN2002if	20.54 ± 0.044	-20.38 ± 0.044
SN2002kb	21.337 ± 0.007	-20.839 ± 0.007
SN2002ke	22.883 ± 0.019	-19.316 ± 0.019
SN2002kl	23.81 ± 0.01	-17.595 ± 0.01
SN2003ba	21.533 ± 0.197	-19.062 ± 0.197
SN2003bb	21.444 ± 0.007	-21.836 ± 0.007
SN2003bc	22.645 ± 0.008	-19.281 ± 0.008
SN2003dx	23.917 ± 0.343	-17.745 ± 0.343
SN2003ea	24.13 ± 0.023	-19.016 ± 0.023
SN2003ew	22.603 ± 0.193	-19.874 ± 0.193
HST04Geo	24.438 ± 0.03	-18.842 ± 0.03
HST04Riv	26.992 ± 0.175	-15.315 ± 0.175
HST05Bra	23.649 ± 0.023	-18.156 ± 0.023
HST05Den	25.949 ± 0.106	-17.408 ± 0.106
SN2005hm	21.5 ± 0.22	-14.599 ± 0.22
SN2005nb	15.966 ± 0.011	-19.215 ± 0.011
SN2006ip	17.263 ± 0.022	-18.459 ± 0.022
SN2006ir	17.347 ± 0.027	-17.491 ± 0.027
SN2006jo	18.073 ± 0.028	-19.676 ± 0.028
SN2006nx	21.119 ± 0.192	-18.285 ± 0.192
SN2006sg	22.991 ± 0.259	-18.608 ± 0.259
SN2006tq	22.855 ± 0.617	-17.576 ± 0.617
SN2007I	19.11 ± 0.07	-15.827 ± 0.07
SN2007ea	15.49 ± nan	-20.715 ± nan
SN2007ff	17.322 ± 0.027	-19.563 ± 0.027
SN2007gl	17.057 ± 0.026	-19.183 ± 0.026
SN2007hb	15.617 ± 0.009	-19.283 ± 0.009
SN2007hn	18.295 ± 0.036	-17.577 ± 0.036
SN2010ah	20.15 ± 0.12	-16.544 ± 0.12

Table A.7: UV photometric properties of LGRBs from Ghosts used within Chapter 3.

Event	m_{UV} AB mag	M_{UV} AB mag
GRB970228	25.1 ± 0.23	-18.2 ± 0.2
GRB970508	25.59 ±0.15	-17.56 ± 0.15
GRB970828	25.28 ± 0.29	-18.1 ± 0.3
GRB980425	15.77 ± 0.03	-17.46 ± 0.03
GRB980703	22.57 ±0.06	-20.86 ± 0.06
GRB990705	22.79 ± 0.18	-20.42 ± 0.18
GRB990712	23.15 ±0.08	-18.46 ± 0.08
GRB991208	24.51 ± 0.15	-18.15 ± 0.15
GRB000210	24.18 ±0.08	-18.89 ± 0.08
GRB010921	22.6 ± 0.1	-19.4 ± 0.1
GRB011121	24.1 ±0.1	-18.7 ± 0.1
GRB020405	22.6 ±0.05	-20.14 ± 0.05
GRB020819B	20.31 ±0.02	-21.33 ± 0.02
GRB020903	21.6 ± 0.09	-18.79 ± 0.09
GRB030329	23.33 ± 0.09	-16.16 ± 0.09
GRB030528	21.92 ± 0.18	-22.58 ± 0.18
GRB031203	18.23 ± 0.17	-24.70 ± 0.17
GRB040924	24.31 ± 0.28	-18.9 ± 0.3
GRB050525	≥24.0	≥-18.586
GRB050824	23.77 ± 0.14	-19.28 ± 0.14
GRB050826	21.37 ± 0.28	-21.34 ± 0.28
GRB060202	23.29 ± 0.07	-19.72 ± 0.07
GRB060218	20.5 ± 0.13	-15.85 ± 0.13
GRB060912A	22.72 ± 0.04	-20.63 ± 0.04
GRB070612	22.48 ± 0.17	-20.19 ± 0.17
GRB080319B	26.95 ± 0.12	-16.29 ± 0.12
GRB081109	22.69 ± 0.06	-20.69 ± 0.06
GRB090328	22.64 ± 0.13	-20.26 ± 0.13
GRB090417B	23.24 ± 0.53	-17.8 ± 0.5
GRB091127	24.14 ± 0.16	-17.79 ± 0.16
GRB100316D	18.73 ± 0.09	-18.97 ± 0.09
GRB100418	22.61 ± 0.16	-19.97 ± 0.16
GRB100621A	21.79 ± 0.06	-20.34 ± 0.06
GRB100816A	23.08 ± 0.15	-20.02 ± 0.15
GRB110918	22.04 ± 0.05	-21.35 ± 0.05
GRB101225A	26.75 ± 0.13	-16.60 ± 0.13
GRB111209A	25.75 ± 0.14	-16.82 ± 0.14
GRB120422A	22.17 ± 0.5	-18.5 ± 0.5

Table A.8: Astrometric uncertainties for locations of GOODS CCSN within HST WFC3 UVIS imaging. All discovery images used for matching were drawn from the original GOODS survey imaging using HST ACS images in the F450W, F606W, F814W and F850LP bands. The small errors computed within SExtractor for this sample does impact the overall conclusions drawn from these results.

CCSN	Redshift	UV X_{err} mas	UV Y_{err} mas
SN2002hq	0.67	23.97	30.85
SN2002kl	0.41	11.73	15.47
SN2003bc	0.51	23.69	22.04
SN2002hs	0.39	17.49	20.43
SN2002kb	0.58	17.83	17.09
SN2002ke	0.58	10.80	8.90
SN2003N	0.43	5.59	5.59
SN2003ea	0.98	9.13	13.19
SN2003en	0.54	5.89	3.00
HST04Bon	0.66	29.91	32.86
HST04Cay	0.8	9.86	11.75
HST04Con	0.84	26.98	24.21
HST04Cum	0.97	3.64	4.02
HST04Geo	0.94	122.61	122.25
HST04Hei	0.58	21.88	25.78
HST04Jef	0.96	15.07	9.27
HST04Ken	0.52	12.43	10.81
HST04Pol	0.56	44.48	56.50
HST04Riv	0.61	17.56	13.14
HST04Sos	0.55	37.93	38.04
HST05Bra	0.48	28.29	28.39
HST05Den	0.97	23.93	16.02
HST05Mob	0.68	21.94	20.82
HST05Pic	0.91	9.63	6.95
HST05Ton	0.78	37.88	32.06
K0405-005	0.68	10.57	17.91
K0405-007	0.5	3.11	4.82
K0405-008	0.88	12.23	12.02

Table A.9: Location properties of the GOODS CCSN within HST WFC3 UVIS imaging.

CCSN	F_L	UV r_{50} r_{50}	UV Host Offset (kpc)	UV Brightest Pix. Offset (kpc)	Offset Err (kpc)	Log L $L_{\odot}kpc^{-2}$
SN2002hq	0.561	4.76	13.49	20.39	0.27	8.41
SN2002kl	0.369	0.67	5.78	0.49	0.11	8.04
SN2003bc	0.179	2.24	8.23	7.09	0.20	8.03
SN2002hs	0.457	0.24	5.77	1.81	0.14	7.38
SN2002kb	0.995	4.19	8.68	0.05	0.16	8.86
SN2002ke	0.561	3.70	7.05	0.73	0.09	8.18
SN2003ea	0.08	1.79	8.50	3.75	0.13	7.49
SN2003en	0.007	0.63	6.47	0.73	0.04	6.13
HST04Bon	-	1.68	12.39	4.04	0.31	-
HST04Cay	-	0.66	8.19	1.58	0.12	-
HST04Con	0	2.59	8.12	0.68	0.28	7.12
HST04Cum	0.564	0.54	7.99	0.21	0.04	9.10
HST04Geo	0.865	2.65	7.95	0.45	1.37	8.72
HST04Hei	0.015	1.13	6.87	0.77	0.22	7.64
HST04Jef	0.498	1.32	8.07	0.15	0.14	8.34
HST04Ken	0.7	2.84	6.39	0.72	0.10	8.23
HST04Pol	0.528	4.75	8.59	8.91	0.47	7.76
HST04Riv	0.679	1.16	6.83	0.13	0.15	8.11
HST04Sos	0.539	1.84	7.07	0.06	0.34	7.72
HST05Bra	0.82	1.49	6.06	0.26	0.24	8.27
HST05Den	0.505	1.57	7.97	0.14	0.23	8.34
HST05Mob	0.603	1.08	7.21	0.53	0.21	7.92
HST05Pic	0.706	2.56	9.48	0.87	0.09	8.61
HST05Ton	0.511	1.12	7.51	0.72	0.37	8.05
K0405-005	0.062	1.39	7.88	1.26	0.15	7.65
K0405-007	0.52	0.91	6.12	0.13	0.04	7.58
K0405-008	0.175	1.05	7.98	1.81	0.13	7.87

Bibliography

K. N. Abazajian, J. K. Adelman-McCarthy, M. A. Agüeros, S. S. Allam, C. Allende Prieto, D. An, K. S. J. Anderson, S. F. Anderson, J. Annis, N. A. Bahcall, and et al. The Seventh Data Release of the Sloan Digital Sky Survey. , 182:543, June 2009. doi: 10.1088/0067-0049/182/2/543.

C. P. Ahn, R. Alexandroff, C. Allende Prieto, S. F. Anderson, T. Anderton, B. H. Andrews, É. Aubourg, S. Bailey, E. Balbinot, R. Barnes, and et al. The Ninth Data Release of the Sloan Digital Sky Survey: First Spectroscopic Data from the SDSS-III Baryon Oscillation Spectroscopic Survey. , 203:21, December 2012. doi: 10.1088/0067-0049/203/2/21.

J. Anderson and L. R. Bedin. An Empirical Pixel-Based Correction for Imperfect CTE. I. HST's Advanced Camera for Surveys. , 122:1035–1064, September 2010. doi: 10.1086/656399.

J. P. Anderson, S. M. Habergham, P. A. James, and M. Hamuy. Progenitor mass constraints for core-collapse supernovae from correlations with host galaxy star formation. , 424:1372–1391, August 2012. doi: 10.1111/j.1365-2966.2012.21324.x.

I. Appenzeller, K. Fricke, W. Fürtig, W. Gässler, R. Häfner, R. Harke, H.-J. Hess, W. Hummel, P. Jürgens, R.-P. Kudritzki, K.-H. Mantel, W. Meisl, B. Muschielok, H. Nicklas, G. Rupprecht, W. Seifert, O. Stahl, T. Szeifert, and K. Tarantik. Successful commissioning of FORS1 - the first optical instrument on the VLT. *The Messenger*, 94:1–6, December 1998.

I. Arcavi, A. Gal-Yam, M. M. Kasliwal, R. M. Quimby, E. O. Ofek, S. R. Kulkarni, P. E. Nugent, S. B. Cenko, J. S. Bloom, M. Sullivan, D. A. Howell, D. Poznanski, A. V. Filippenko, N. Law, I. Hook, J. Jönsson, S. Blake, J. Cooke, R. Dekany, G. Rahmer, D. Hale, R. Smith, J. Zolkower, V. Velur, R. Walters, J. Henning, K. Bui, D. McKenna, and J. Jacobsen. Core-collapse Supernovae from the Palo-

mar Transient Factory: Indications for a Different Population in Dwarf Galaxies. , 721:777–784, September 2010. doi: 10.1088/0004-637X/721/1/777.

W. D. Arnett. Type I supernovae. I - Analytic solutions for the early part of the light curve. , 253:785–797, February 1982. doi: 10.1086/159681.

I. K. Baldry, K. Glazebrook, T. Budavári, D. J. Eisenstein, J. Annis, N. A. Bahcall, M. R. Blanton, J. Brinkmann, I. Csabai, T. M. Heckman, H. Lin, J. Loveday, R. C. Nichol, and D. P. Schneider. The Sloan Digital Sky Survey u-band Galaxy Survey: luminosity functions and evolution. , 358:441–456, April 2005. doi: 10.1111/j.1365-2966.2005.08799.x.

K. Barbary, K. S. Dawson, K. Tokita, G. Aldering, R. Amanullah, N. V. Connolly, M. Doi, L. Faccioli, V. Fadeyev, A. S. Fruchter, G. Goldhaber, A. Goobar, A. Gude, X. Huang, Y. Ihara, K. Konishi, M. Kowalski, C. Lidman, J. Meyers, T. Morokuma, P. Nugent, S. Perlmutter, D. Rubin, D. Schlegel, A. L. Spadafora, N. Suzuki, H. K. Swift, N. Takanashi, R. C. Thomas, and N. Yasuda. Discovery of an Unusual Optical Transient with the Hubble Space Telescope. , 690:1358–1362, January 2009. doi: 10.1088/0004-637X/690/2/1358.

N. Bastian. On the star formation rate - brightest cluster relation: estimating the peak star formation rate in post-merger galaxies. , 390:759–768, October 2008. doi: 10.1111/j.1365-2966.2008.13775.x.

E. Berger, R. Chornock, R. Lunnan, R. Foley, I. Czekala, A. Rest, C. Leibler, A. M. Soderberg, K. Roth, G. Narayan, M. E. Huber, D. Milisavljevic, N. E. Sanders, M. Drout, R. Margutti, R. P. Kirshner, G. H. Marion, P. J. Challis, A. G. Riess, S. J. Smartt, W. S. Burgett, K. W. Hodapp, J. N. Heasley, N. Kaiser, R.-P. Kudritzki, E. A. Magnier, M. McCrum, P. A. Price, K. Smith, J. L. Tonry, and R. J. Wainscoat. Ultraluminous Supernovae as a New Probe of the Interstellar Medium in Distant Galaxies. , 755:L29, August 2012. doi: 10.1088/2041-8205/755/2/L29.

E. Bertin and S. Arnouts. SExtractor: Software for source extraction. , 117:393–404, June 1996.

H. A. Bethe. Energy Production in Stars. *Physical Review*, 55:434–456, March 1939. doi: 10.1103/PhysRev.55.434.

H. A. Bethe and J. R. Wilson. Revival of a stalled supernova shock by neutrino heating. , 295:14–23, August 1985. doi: 10.1086/163343.

P. K. Blanchard, E. Berger, and W.-f. Fong. The Offset and Host Light Distributions of Long Gamma-Ray Bursts: A New View From HST Observations of Swift Bursts. , 817:144, February 2016. doi: 10.3847/0004-637X/817/2/144.

M. R. Blanton, R. H. Lupton, D. J. Schlegel, M. A. Strauss, J. Brinkmann, M. Fukugita, and J. Loveday. The Properties and Luminosity Function of Extremely Low Luminosity Galaxies. , 631:208–230, September 2005. doi: 10.1086/431416.

J. S. Bloom, S. R. Kulkarni, and S. G. Djorgovski. The Observed Offset Distribution of Gamma-Ray Bursts from Their Host Galaxies: A Robust Clue to the Nature of the Progenitors. , 123:1111–1148, March 2002. doi: 10.1086/338893.

J. S. Bloom, D. A. Perley, W. Li, N. R. Butler, A. A. Miller, D. Kocevski, D. A. Kann, R. J. Foley, H.-W. Chen, A. V. Filippenko, D. L. Starr, B. Macomber, J. X. Prochaska, R. Chornock, D. Poznanski, S. Klose, M. F. Skrutskie, S. Lopez, P. Hall, K. Glazebrook, and C. H. Blake. Observations of the Naked-Eye GRB 080319B: Implications of Nature's Brightest Explosion. , 691:723–737, January 2009. doi: 10.1088/0004-637X/691/1/723.

J. S. Bloom, D. Kasen, K. J. Shen, P. E. Nugent, N. R. Butler, M. L. Graham, D. A. Howell, U. Kolb, S. Holmes, C. A. Haswell, V. Burwitz, J. Rodriguez, and M. Sullivan. A Compact Degenerate Primary-star Progenitor of SN 2011fe. , 744: L17, January 2012. doi: 10.1088/2041-8205/744/2/L17.

I. A. Bonnell, C. J. Clarke, M. R. Bate, and J. E. Pringle. Accretion in stellar clusters and the initial mass function. , 324:573–579, June 2001. doi: 10.1046/j.1365-8711.2001.04311.x.

M. Bourque, J. Anderson, S. M. Baggett, J. A. Biretta, S. E. Deustua, D. Hammer, K. Noeske, J. W. MacKenty, and WFC3 Team. Wide Field Camera 3: Trends in the UVIS Detector. In *American Astronomical Society Meeting Abstracts*, volume 222 of *American Astronomical Society Meeting Abstracts*, page 316.11, June 2013.

O. Bromberg, E. Nakar, T. Piran, and R. Sari. An Observational Imprint of the Collapsar Model of Long Gamma-Ray Bursts. , 749:110, April 2012. doi: 10.1088/0004-637X/749/2/110.

N. Bucciantini, E. Quataert, B. D. Metzger, T. A. Thompson, J. Arons, and L. Del Zanna. Magnetized relativistic jets and long-duration GRBs from magnetar spin-down during core-collapse supernovae. , 396:2038–2050, July 2009. doi: 10.1111/j.1365-2966.2009.14940.x.

Z. Cano. A new method for estimating the bolometric properties of Ibc supernovae. , 434:1098–1116, September 2013. doi: 10.1093/mnras/stt1048.

C. M. Carollo, I. J. Danziger, and L. Buson. Metallicity Gradients in Early Type Galaxies. , 265:553, December 1993. doi: 10.1093/mnras/265.3.553.

J. M. Castro Cerón, M. J. Michałowski, J. Hjorth, D. Watson, J. P. U. Fynbo, and J. Gorosabel. Star Formation Rates and Stellar Masses in z ˜ 1 Gamma-Ray Burst Hosts. , 653:L85–L88, December 2006. doi: 10.1086/510618.

E. Chatzopoulos and J. C. Wheeler. Effects of Rotation on the Minimum Mass of Primordial Progenitors of Pair-instability Supernovae. , 748:42, March 2012a. doi: 10.1088/0004-637X/748/1/42.

E. Chatzopoulos and J. C. Wheeler. Hydrogen-poor Circumstellar Shells from Pulsational Pair-instability Supernovae with Rapidly Rotating Progenitors. , 760: 154, December 2012b. doi: 10.1088/0004-637X/760/2/154.

E. Chatzopoulos, J. C. Wheeler, J. Vinko, R. Quimby, E. L. Robinson, A. A. Miller, R. J. Foley, D. A. Perley, F. Yuan, C. Akerlof, and J. S. Bloom. SN 2008am: A Super-luminous Type IIn Supernova. , 729:143, March 2011. doi: 10.1088/0004-637X/729/2/143.

T.-W. Chen, S. J. Smartt, F. Bresolin, A. Pastorello, R.-P. Kudritzki, R. Kotak, M. McCrum, M. Fraser, and S. Valenti. The Host Galaxy of the Super-luminous SN 2010gx and Limits on Explosive ^{56}Ni Production. , 763:L28, February 2013. doi: 10.1088/2041-8205/763/2/L28.

T.-W. Chen, S. J. Smartt, A. Jerkstrand, M. Nicholl, F. Bresolin, R. Kotak, J. Polshaw, A. Rest, R. Kudritzki, Z. Zheng, N. Elias-Rosa, K. Smith, C. Inserra, D. Wright, E. Kankare, T. Kangas, and M. Fraser. The host galaxy and late-time evolution of the superluminous supernova PTF12dam. , 452:1567–1586, September 2015. doi: 10.1093/mnras/stv1360.

T.-W. Chen, S. J. Smartt, R. M. Yates, M. Nicholl, T. Krühler, P. Schady, M. Dennefeld, and C. Inserra. A sub-solar metallicity is required for superluminous supernova progenitors. *ArXiv e-prints*, May 2016.

R. A. Chevalier and C. M. Irwin. Shock Breakout in Dense Mass Loss: Luminous Supernovae. , 729:L6, March 2011. doi: 10.1088/2041-8205/729/1/L6.

C. Chiappini, F. Matteucci, and D. Romano. Abundance Gradients and the Formation of the Milky Way. , 554:1044–1058, June 2001. doi: 10.1086/321427.

L. Chomiuk, R. Chornock, A. M. Soderberg, E. Berger, R. A. Chevalier, R. J. Foley, M. E. Huber, G. Narayan, A. Rest, S. Gezari, R. P. Kirshner, A. Riess, S. A. Rodney, S. J. Smartt, C. W. Stubbs, J. L. Tonry, W. M. Wood-Vasey, W. S. Burgett, K. C. Chambers, I. Czekala, H. Flewelling, K. Forster, N. Kaiser, R.-P. Kudritzki, E. A. Magnier, D. C. Martin, J. S. Morgan, J. D. Neill, P. A. Price, K. C. Roth, N. E. Sanders, and R. J. Wainscoat. Pan-STARRS1 Discovery of Two Ultraluminous Supernovae at z 0.9. , 743:114, December 2011. doi: 10.1088/0004-637X/743/2/114.

L. Christensen, J. Hjorth, and J. Gorosabel. UV star-formation rates of GRB host galaxies. , 425:913–926, October 2004. doi: 10.1051/0004-6361:20040361.

L. Christensen, P. M. Vreeswijk, J. Sollerman, C. C. Thöne, E. Le Floc'h, and K. Wiersema. IFU observations of the GRB 980425/SN 1998bw host galaxy: emission line ratios in GRB regions. , 490:45–59, October 2008. doi: 10.1051/0004-6361:200809896.

N. N. Chugai, S. I. Blinnikov, R. J. Cumming, P. Lundqvist, A. Bragaglia, A. V. Filippenko, D. C. Leonard, T. Matheson, and J. Sollerman. The Type IIn supernova 1994W: evidence for the explosive ejection of a circumstellar envelope. , 352: 1213–1231, August 2004. doi: 10.1111/j.1365-2966.2004.08011.x.

M. Cirasuolo, R. J. McLure, J. S. Dunlop, O. Almaini, S. Foucaud, I. Smail, K. Sekiguchi, C. Simpson, S. Eales, S. Dye, M. G. Watson, M. J. Page, and P. Hirst. The evolution of the near-infrared galaxy luminosity function and colour bimodality up to z ˜= 2 from the UKIDSS Ultra Deep Survey Early Data Release. , 380:585–595, September 2007a. doi: 10.1111/j.1365-2966.2007.12038.x.

M. Cirasuolo, R. J. McLure, J. S. Dunlop, O. Almaini, S. Foucaud, I. Smail, K. Sekiguchi, C. Simpson, S. Eales, S. Dye, M. G. Watson, M. J. Page, and P. Hirst. The evolution of the near-infrared galaxy luminosity function and colour bimodality up to z ˜= 2 from the UKIDSS Ultra Deep Survey Early Data Release. , 380:585–595, September 2007b. doi: 10.1111/j.1365-2966.2007.12038.x.

J. Cooke, M. Sullivan, A. Gal-Yam, E. J. Barton, R. G. Carlberg, E. V. Ryan-Weber, C. Horst, Y. Omori, and C. G. Díaz. Superluminous supernovae at redshifts of 2.05 and 3.90. , 491:228–231, November 2012. doi: 10.1038/nature11521.

R. J. Cool, D. J. Eisenstein, D. W. Hogg, M. R. Blanton, D. J. Schlegel, J. Brinkmann, D. Q. Lamb, D. P. Schneider, and D. E. vanden Berk. GRB070612 - SDSS pre-burst observations. *GRB Coordinates Network*, 6510:1, 2007.

M. C. Cooper, C. A. Tremonti, J. A. Newman, and A. I. Zabludoff. The role of environment in the mass-metallicity relation. , 390:245–256, October 2008. doi: 10.1111/j.1365-2966.2008.13714.x.

P. A. Crowther, O. Schnurr, R. Hirschi, N. Yusof, R. J. Parker, S. P. Goodwin, and H. A. Kassim. The R136 star cluster hosts several stars whose individual masses greatly exceed the accepted 150M$_{solar}$ stellar mass limit. , 408:731–751, October 2010. doi: 10.1111/j.1365-2966.2010.17167.x.

R. M. Cutri and et al. VizieR Online Data Catalog: AllWISE Data Release (Cutri+ 2013). *VizieR Online Data Catalog*, 2328:0, November 2013.

T. Dahlen, L.-G. Strolger, A. G. Riess, B. Mobasher, R. Chary, C. J. Conselice, H. C. Ferguson, A. S. Fruchter, M. Giavalisco, M. Livio, P. Madau, N. Panagia, J. L. Tonry, and GOODS Team. High Redshift Supernova Rates in the GOODS Fields. In *American Astronomical Society Meeting Abstracts*, volume 35 of *Bulletin of the American Astronomical Society*, page 1278, December 2003.

R. Davé, K. Finlator, and B. D. Oppenheimer. Galaxy evolution in cosmological simulations with outflows - II. Metallicities and gas fractions. , 416:1354–1376, September 2011. doi: 10.1111/j.1365-2966.2011.19132.x.

B. Davies, D. F. Figer, R.-P. Kudritzki, C. Trombley, C. Kouveliotou, and S. Wachter. The Progenitor Mass of the Magnetar SGR1900+14. , 707:844–851, December 2009. doi: 10.1088/0004-637X/707/1/844.

M. De Becker, G. Rauw, J. Manfroid, and P. Eenens. Early-type stars in the young open cluster IC 1805. II. The probably single stars HD15570 and HD15629, and the massive binary/triple system HD15558. , 456:1121–1130, September 2006. doi: 10.1051/0004-6361:20065300.

S. E. de Mink, O. R. Pols, and S.-C. Yoon. Binaries at Low Metallicity: Ranges For Case A, B and C Mass Transfer. In B. W. O'Shea and A. Heger, editors, *First Stars III*, volume 990 of *American Institute of Physics Conference Series*, pages 230–232, March 2008. doi: 10.1063/1.2905549.

J. Deng, K. S. Kawabata, Y. Ohyama, K. Nomoto, P. A. Mazzali, L. Wang, D. J. Jeffery, M. Iye, H. Tomita, and Y. Yoshii. Subaru Spectroscopy of the Interacting Type Ia Supernova SN 2002ic: Evidence of a Hydrogen-rich, Asymmetric Circumstellar Medium. , 605:L37–L40, April 2004. doi: 10.1086/420698.

L. Dessart, D. J. Hillier, R. Waldman, E. Livne, and S. Blondin. Superluminous supernovae: ^{56}Ni power versus magnetar radiation. , 426:L76–L80, October 2012. doi: 10.1111/j.1745-3933.2012.01329.x.

J. Dexter and D. Kasen. Supernova Light Curves Powered by Fallback Accretion. , 772:30, July 2013. doi: 10.1088/0004-637X/772/1/30.

P. Di Matteo, A. Pipino, M. D. Lehnert, F. Combes, and B. Semelin. On the survival of metallicity gradients to major dry-mergers. , 499:427–437, May 2009. doi: 10.1051/0004-6361/200911715.

M. Dickinson, M. Giavalisco, and GOODS Team. The Great Observatories Origins Deep Survey. In R. Bender and A. Renzini, editors, *The Mass of Galaxies at Low and High Redshift*, page 324, 2003. doi: 10.1007/10899892$_7$8.

A. J. Drake, S. G. Djorgovski, A. Mahabal, E. Beshore, S. Larson, M. J. Graham, R. Williams, E. Christensen, M. Catelan, A. Boattini, A. Gibbs, R. Hill, and R. Kowalski. First Results from the Catalina Real-Time Transient Survey. , 696: 870–884, May 2009a. doi: 10.1088/0004-637X/696/1/870.

A. J. Drake, S. G. Djorgovski, A. Mahabal, E. Beshore, S. Larson, M. J. Graham, R. Williams, E. Christensen, M. Catelan, A. Boattini, A. Gibbs, R. Hill, and R. Kowalski. First Results from the Catalina Real-Time Transient Survey. , 696: 870–884, May 2009b. doi: 10.1088/0004-637X/696/1/870.

A. J. Drake, S. G. Djorgovski, J. L. Prieto, A. Mahabal, D. Balam, R. Williams, M. J. Graham, M. Catelan, E. Beshore, and S. Larson. Discovery of the Extremely Energetic Supernova 2008fz. , 718:L127–L131, August 2010. doi: 10.1088/2041-8205/718/2/L127.

L. Dressel. *Wide Field Camera 3 Instrument Handbook for Cycle 21 v. 5.0*. December 2012.

M. R. Drout, A. M. Soderberg, A. Gal-Yam, S. B. Cenko, D. B. Fox, D. C. Leonard, D. J. Sand, D.-S. Moon, I. Arcavi, and Y. Green. The First Systematic Study of Type Ibc Supernova Multi-band Light Curves. , 741:97, November 2011. doi: 10.1088/0004-637X/741/2/97.

R. C. Duncan and C. Thompson. Formation of very strongly magnetized neutron stars - Implications for gamma-ray bursts. , 392:L9–L13, June 1992. doi: 10.1086/186413.

J. J. Eldridge, R. G. Izzard, and C. A. Tout. The effect of massive binaries on stellar populations and supernova progenitors. , 384:1109–1118, March 2008. doi: 10.1111/j.1365-2966.2007.12738.x.

J. Elliott, T. Krühler, J. Greiner, S. Savaglio, F. Olivares, E. A. Rau, A. de Ugarte Postigo, R. Sánchez-Ramírez, K. Wiersema, P. Schady, D. A. Kann, R. Filgas, M. Nardini, E. Berger, D. Fox, J. Gorosabel, S. Klose, A. Levan, A. Nicuesa Guelbenzu, A. Rossi, S. Schmidl, V. Sudilovsky, N. R. Tanvir, and C. C. Thöne. The low-extinction afterglow in the solar-metallicity host galaxy of γ-ray burst 110918A. , 556:A23, August 2013. doi: 10.1051/0004-6361/201220968.

D. M. Elmegreen, B. G. Elmegreen, S. Ravindranath, and D. A. Coe. Resolved Galaxies in the Hubble Ultra Deep Field: Star Formation in Disks at High Redshift. , 658:763–777, April 2007. doi: 10.1086/511667.

R. T. Farouki and S. L. Shapiro. Simulations of merging disk galaxies. , 259:103–115, August 1982. doi: 10.1086/160151.

J. C. Forbes, M. R. Krumholz, A. Burkert, and A. Dekel. On the origin of the fundamental metallicity relation and the scatter in galaxy scaling relations. , 443: 168–185, September 2014. doi: 10.1093/mnras/stu1142.

W. A. Fowler and F. Hoyle. Neutrino Processes and Pair Formation in Massive Stars and Supernovae. , 9:201, December 1964. doi: 10.1086/190103.

O. D. Fox, N. Smith, S. M. Ammons, J. Andrews, K. A. Bostroem, S. B. Cenko, G. C. Clayton, E. Dwek, A. V. Filippenko, J. S. Gallagher, P. L. Kelly, J. C. Mauerhan, A. A. Miller, and S. D. Van Dyk. What powers the 3000-day light curve of SN 2006gy? , 454:4366–4378, December 2015. doi: 10.1093/mnras/stv2270.

A. Fruchter and et al. *HST MultiDrizzle Handbook*. January 2009.

A. S. Fruchter and R. N. Hook. Drizzle: A Method for the Linear Reconstruction of Undersampled Images. , 114:144–152, February 2002. doi: 10.1086/338393.

A. S. Fruchter, A. J. Levan, L. Strolger, P. M. Vreeswijk, S. E. Thorsett, D. Bersier, I. Burud, J. M. Castro Cerón, A. J. Castro-Tirado, C. Conselice, T. Dahlen, H. C. Ferguson, J. P. U. Fynbo, P. M. Garnavich, R. A. Gibbons, J. Gorosabel, T. R. Gull, J. Hjorth, S. T. Holland, C. Kouveliotou, Z. Levay, M. Livio, M. R. Metzger, P. E. Nugent, L. Petro, E. Pian, J. E. Rhoads, A. G. Riess, K. C. Sahu, A. Smette,

N. R. Tanvir, R. A. M. J. Wijers, and S. E. Woosley. Long γ-ray bursts and core-collapse supernovae have different environments. , 441:463–468, May 2006. doi: 10.1038/nature04787.

H. O. U. Fynbo, C. A. Diget, U. C. Bergmann, M. J. G. Borge, J. Cederkäll, P. Dendooven, L. M. Fraile, S. Franchoo, V. N. Fedosseev, B. R. Fulton, W. Huang, J. Huikari, H. B. Jeppesen, A. S. Jokinen, P. Jones, B. Jonson, U. Köster, K. Langanke, M. Meister, T. Nilsson, G. Nyman, Y. Prezado, K. Riisager, S. Rinta-Antila, O. Tengblad, M. Turrion, Y. Wang, L. Weissman, K. Wilhelmsen, J. Äystö, and ISOLDE Collaboration. Revised rates for the stellar triple-α process from measurement of ^{12}C nuclear resonances. , 433:136–139, January 2005.

J. P. U. Fynbo, P. Jakobsson, P. Møller, J. Hjorth, B. Thomsen, M. I. Andersen, A. S. Fruchter, J. Gorosabel, S. T. Holland, C. Ledoux, H. Pedersen, J. Rhoads, M. Weidinger, and R. A. M. J. Wijers. On the Lyalpha emission from gamma-ray burst host galaxies: Evidence for low metallicities. , 406:L63–L66, July 2003. doi: 10.1051/0004-6361:20030931.

J. P. U. Fynbo, P. Jakobsson, J. X. Prochaska, D. Malesani, C. Ledoux, A. de Ugarte Postigo, M. Nardini, P. M. Vreeswijk, K. Wiersema, J. Hjorth, J. Sollerman, H.-W. Chen, C. C. Thöne, G. Björnsson, J. S. Bloom, A. J. Castro-Tirado, L. Christensen, A. De Cia, A. S. Fruchter, J. Gorosabel, J. F. Graham, A. O. Jaunsen, B. L. Jensen, D. A. Kann, C. Kouveliotou, A. J. Levan, J. Maund, N. Masetti, B. Milvang-Jensen, E. Palazzi, D. A. Perley, E. Pian, E. Rol, P. Schady, R. L. C. Starling, N. R. Tanvir, D. J. Watson, D. Xu, T. Augusteijn, F. Grundahl, J. Telting, and P.-O. Quirion. Low-resolution Spectroscopy of Gamma-ray Burst Optical Afterglows: Biases in the Swift Sample and Characterization of the Absorbers. , 185:526–573, December 2009. doi: 10.1088/0067-0049/185/2/526.

A. Gal-Yam. Luminous Supernovae. *Science*, 337:927, August 2012. doi: 10.1126/science.1203601.

A. Gal-Yam, P. Mazzali, E. O. Ofek, P. E. Nugent, S. R. Kulkarni, M. M. Kasliwal, R. M. Quimby, A. V. Filippenko, S. B. Cenko, R. Chornock, R. Waldman, D. Kasen, M. Sullivan, E. C. Beshore, A. J. Drake, R. C. Thomas, J. S. Bloom, D. Poznanski, A. A. Miller, R. J. Foley, J. M. Silverman, I. Arcavi, R. S. Ellis, and J. Deng. Supernova 2007bi as a pair-instability explosion. , 462:624–627, December 2009. doi: 10.1038/nature08579.

B. T. Gänsicke, A. J. Levan, T. R. Marsh, and P. J. Wheatley. SCP 06F6: A Carbon-

rich Extragalactic Transient at Redshift z sime 0.14? , 697:L129–L132, June 2009. doi: 10.1088/0004-637X/697/2/L129.

P. M. Garnavich, B. E. Tucker, A. Rest, E. J. Shaya, R. P. Olling, D. Kasen, and A. Villar. Shock Breakout and Early Light Curves of Type II-P Supernovae Observed with Kepler. , 820:23, March 2016. doi: 10.3847/0004-637X/820/1/23.

C. Georgy, G. Meynet, S. Ekström, G. A. Wade, V. Petit, Z. Keszthelyi, and R. Hirschi. Possible pair-instability supernovae at solar metallicity from magnetic stellar progenitors. *ArXiv e-prints*, February 2017.

L. M. Germany, D. J. Reiss, E. M. Sadler, B. P. Schmidt, and C. W. Stubbs. SN 1997CY/GRB 970514: A New Piece in the Gamma-Ray Burst Puzzle? , 533: 320–328, April 2000. doi: 10.1086/308639.

S. Gezari, J. P. Halpern, D. Grupe, F. Yuan, R. Quimby, T. McKay, D. Chamarro, M. D. Sisson, C. Akerlof, J. C. Wheeler, P. J. Brown, S. B. Cenko, A. Rau, J. O. Djordjevic, and D. M. Terndrup. Discovery of the Ultra-Bright Type II-L Supernova 2008es. , 690:1313–1321, January 2009. doi: 10.1088/0004-637X/690/2/1313.

S. Ginzburg and S. Balberg. Superluminous Light Curves from Supernovae Exploding in a Dense Wind. , 757:178, October 2012. doi: 10.1088/0004-637X/757/2/178.

E. Glebbeek, E. Gaburov, S. E. de Mink, O. R. Pols, and S. F. Portegies Zwart. The evolution of runaway stellar collision products. , 497:255–264, April 2009. doi: 10.1051/0004-6361/200810425.

S. Gonzaga and et al. *The DrizzlePac Handbook*. June 2012.

S. González-Gaitán, N. Tominaga, J. Molina, L. Galbany, F. Bufano, J. P. Anderson, C. Gutierrez, F. Förster, G. Pignata, M. Bersten, D. A. Howell, M. Sullivan, R. Carlberg, T. de Jaeger, M. Hamuy, P. V. Baklanov, and S. I. Blinnikov. The rise-time of Type II supernovae. , 451:2212–2229, August 2015. doi: 10.1093/mnras/stv1097.

J. F. Graham and A. S. Fruchter. The Metal Aversion of Long-duration Gamma-Ray Bursts. , 774:119, September 2013a. doi: 10.1088/0004-637X/774/2/119.

J. F. Graham and A. S. Fruchter. The Metal Aversion of Long-duration Gamma-Ray Bursts. , 774:119, September 2013b. doi: 10.1088/0004-637X/774/2/119.

J. F. Graham and A. S. Fruchter. The Relative Rate of LGRB Formation as a Function of Metallicity. , 834:170, January 2017. doi: 10.3847/1538-4357/834/2/170.

J. E. Greene, R. Janish, C.-P. Ma, N. J. McConnell, J. P. Blakeslee, J. Thomas, and J. D. Murphy. The MASSIVE Survey. II. Stellar Population Trends Out to Large Radius in Massive Early-type Galaxies. , 807:11, July 2015. doi: 10.1088/0004-637X/807/1/11.

J. Greiner, P. A. Mazzali, D. A. Kann, T. Krühler, E. Pian, S. Prentice, F. Olivares E., A. Rossi, S. Klose, S. Taubenberger, F. Knust, P. M. J. Afonso, C. Ashall, J. Bolmer, C. Delvaux, R. Diehl, J. Elliott, R. Filgas, J. P. U. Fynbo, J. F. Graham, A. N. Guelbenzu, S. Kobayashi, G. Leloudas, S. Savaglio, P. Schady, S. Schmidl, T. Schweyer, V. Sudilovsky, M. Tanga, A. C. Updike, H. van Eerten, and K. Varela. A very luminous magnetar-powered supernova associated with an ultra-long γ-ray burst. , 523:189–192, July 2015. doi: 10.1038/nature14579.

J. H. Groh, C. Georgy, and S. Ekström. Progenitors of supernova Ibc: a single Wolf-Rayet star as the possible progenitor of the SN Ib iPTF13bvn. , 558:L1, October 2013. doi: 10.1051/0004-6361/201322369.

Y. Guo, H. C. Ferguson, E. F. Bell, D. C. Koo, C. J. Conselice, M. Giavalisco, S. Kassin, Y. Lu, R. Lucas, N. Mandelker, D. M. McIntosh, J. R. Primack, S. Ravindranath, G. Barro, D. Ceverino, A. Dekel, S. M. Faber, J. J. Fang, A. M. Koekemoer, K. Noeske, M. Rafelski, and A. Straughn. Clumpy Galaxies in CANDELS. I. The Definition of UV Clumps and the Fraction of Clumpy Galaxies at 0.5 z 3. , 800: 39, February 2015. doi: 10.1088/0004-637X/800/1/39.

Y. Guo, M. Rafelski, S. M. Faber, D. C. Koo, M. R. Krumholz, J. R. Trump, S. P. Willner, R. Amorín, G. Barro, E. F. Bell, J. P. Gardner, E. Gawiser, N. P. Hathi, A. M. Koekemoer, C. Pacifici, P. G. Pérez-González, S. Ravindranath, N. Reddy, H. I. Teplitz, and H. Yesuf. The Bursty Star Formation Histories of Low-mass Galaxies at 0.4 z 1 Revealed by Star Formation Rates Measured From Hβ and FUV. , 833:37, December 2016. doi: 10.3847/1538-4357/833/1/37.

V. V. Gvaramadze, A. Y. Kniazev, A.-N. Chené, and O. Schnurr. Two massive stars possibly ejected from NGC 3603 via a three-body encounter. , 430, March 2013.

S. M. Habergham, J. P. Anderson, P. A. James, and J. D. Lyman. Environments of interacting transients: impostors and Type IIn supernovae. , 441:2230–2252, July 2014. doi: 10.1093/mnras/stu684.

R. Hainich, U. Rühling, H. Todt, L. M. Oskinova, A. Liermann, G. Gräfener, C. Foellmi, O. Schnurr, and W.-R. Hamann. The Wolf-Rayet stars in the Large

Magellanic Cloud. A comprehensive analysis of the WN class. , 565:A27, May 2014. doi: 10.1051/0004-6361/201322696.

F. Hammer, H. Flores, D. Schaerer, M. Dessauges-Zavadsky, E. Le Floc'h, and M. Puech. Detection of Wolf-Rayet stars in host galaxies of gamma-ray bursts (GRBs): are GRBs produced by runaway massive stars ejected from high stellar density regions? , 454:103–111, July 2006. doi: 10.1051/0004-6361:20064823.

M. Hamuy, M. M. Phillips, N. B. Suntzeff, J. Maza, L. E. González, M. Roth, K. Krisciunas, N. Morrell, E. M. Green, S. E. Persson, and P. J. McCarthy. An asymptotic-giant-branch star in the progenitor system of a type Ia supernova. , 424:651–654, August 2003.

W. E. Harris. A Catalog of Parameters for Globular Clusters in the Milky Way. , 112: 1487, October 1996. doi: 10.1086/118116.

K. Hatano, D. Branch, K. Nomoto, J. S. Deng, K. Maeda, P. Nugent, and G. Aldering. The Type Ic Hypernova SN 1999as. In *American Astronomical Society Meeting Abstracts #198*, volume 33 of *Bulletin of the American Astronomical Society*, page 838, May 2001.

A. Heger and S. E. Woosley. The Nucleosynthetic Signature of Population III. , 567: 532–543, March 2002. doi: 10.1086/338487.

A. Heger, N. Langer, and S. E. Woosley. Presupernova Evolution of Rotating Massive Stars. I. Numerical Method and Evolution of the Internal Stellar Structure. , 528: 368–396, January 2000. doi: 10.1086/308158.

R. Hinojosa-Goñi, C. Muñoz-Tuñón, and J. Méndez-Abreu. Starburst galaxies in the COSMOS field: clumpy star-formation at redshift 0 z 0.5. , 592:A122, August 2016a. doi: 10.1051/0004-6361/201527066.

R. Hinojosa-Goñi, C. Muñoz-Tuñón, and J. Méndez-Abreu. Starburst galaxies in the COSMOS field: clumpy star-formation at redshift 0 z 0.5. , 592:A122, August 2016b. doi: 10.1051/0004-6361/201527066.

J. Hjorth, D. Malesani, P. Jakobsson, A. O. Jaunsen, J. P. U. Fynbo, J. Gorosabel, T. Krühler, A. J. Levan, M. J. Michałowski, B. Milvang-Jensen, P. Møller, S. Schulze, N. R. Tanvir, and D. Watson. The Optically Unbiased Gamma-Ray Burst Host (TOUGH) Survey. I. Survey Design and Catalogs. , 756:187, September 2012. doi: 10.1088/0004-637X/756/2/187.

P. W. Hodge. Distribution of H II Regions in Irregular Galaxies. , 156:847, June 1969. doi: 10.1086/150018.

S. T. Holland, B. Sbarufatti, R. Shen, P. Schady, J. R. Cummings, E. Fonseca, J. P. U. Fynbo, P. Jakobsson, E. Leitet, S. Linné, P. W. A. Roming, M. Still, and B. Zhang. GRB 090417B and its Host Galaxy: A Step Toward an Understanding of Optically Dark Gamma-ray Bursts. , 717:223–234, July 2010. doi: 10.1088/0004-637X/717/1/223.

P. F. Hopkins, D. Kereš, J. Oñorbe, C.-A. Faucher-Giguère, E. Quataert, N. Murray, and J. S. Bullock. Galaxies on FIRE (Feedback In Realistic Environments): stellar feedback explains cosmologically inefficient star formation. , 445:581–603, November 2014. doi: 10.1093/mnras/stu1738.

P. Hudelot, J.-C. Cuillandre, K. Withington, Y. Goranova, H. McCracken, F. Magnard, Y. Mellier, N. Regnault, M. Betoule, H. Aussel, J. J. Kavelaars, P. Fernique, F. Bonnarel, F. Ochsenbein, and O. Ilbert. VizieR Online Data Catalog: The CFHTLS Survey (T0007 release) (Hudelot+ 2012). *VizieR Online Data Catalog*, 2317:0, September 2012.

C. Inserra and S. J. Smartt. Superluminous Supernovae as Standardizable Candles and High-redshift Distance Probes. , 796:87, December 2014. doi: 10.1088/0004-637X/796/2/87.

C. Inserra, S. J. Smartt, A. Jerkstrand, S. Valenti, M. Fraser, D. Wright, K. Smith, T.-W. Chen, R. Kotak, A. Pastorello, M. Nicholl, F. Bresolin, R. P. Kudritzki, S. Benetti, M. T. Botticella, W. S. Burgett, K. C. Chambers, M. Ergon, H. Flewelling, J. P. U. Fynbo, S. Geier, K. W. Hodapp, D. A. Howell, M. Huber, N. Kaiser, G. Leloudas, L. Magill, E. A. Magnier, M. G. McCrum, N. Metcalfe, P. A. Price, A. Rest, J. Sollerman, W. Sweeney, F. Taddia, S. Taubenberger, J. L. Tonry, R. J. Wainscoat, C. Waters, and D. Young. Super-luminous Type Ic Supernovae: Catching a Magnetar by the Tail. , 770:128, June 2013. doi: 10.1088/0004-637X/770/2/128.

C. Inserra, S. J. Smartt, E. E. E. Gall, G. Leloudas, T.-W. Chen, S. Schulze, A. Jerkstarnd, M. Nicholl, J. P. Anderson, I. Arcavi, S. Benetti, R. A. Cartier, M. Childress, M. Della Valle, H. Flewelling, M. Fraser, A. Gal-Yam, C. P. Gutierrez, G. Hosseinzadeh, D. A. Howell, M. Huber, E. Kankare, E. A. Magnier, K. Maguire, C. McCully, S. Prajs, N. Primak, R. Scalzo, B. P. Schmidt, K. W. Smith, B. E. Tucker, S. Valenti, M. Wilman, D. R. Young, and F. Yuan. On the nature of Hydrogen-rich Superluminous Supernovae. *ArXiv e-prints*, April 2016.

P. Jakobsson, A. Levan, J. P. U. Fynbo, R. Priddey, J. Hjorth, N. Tanvir, D. Watson, B. L. Jensen, J. Sollerman, P. Natarajan, J. Gorosabel, J. M. Castro Cerón, K. Pedersen, T. Pursimo, A. S. Árnadóttir, A. J. Castro-Tirado, C. J. Davis, H. J. Deeg, D. A. Fiuza, S. Mikolaitis, and S. G. Sousa. A mean redshift of 2.8 for Swift gamma-ray bursts. , 447:897–903, March 2006. doi: 10.1051/0004-6361:20054287.

P. Jakobsson, J. Hjorth, D. Malesani, R. Chapman, J. P. U. Fynbo, N. R. Tanvir, B. Milvang-Jensen, P. M. Vreeswijk, G. Letawe, and R. L. C. Starling. The Optically Unbiased GRB Host (TOUGH) Survey. III. Redshift Distribution. , 752:62, June 2012. doi: 10.1088/0004-637X/752/1/62.

P. A. James and J. P. Anderson. The Hα Galaxy Survey . III. Constraints on supernova progenitors from spatial correlations with Hα emission. , 453:57–65, July 2006. doi: 10.1051/0004-6361:20054509.

A. Janiuk and D. Proga. Low Angular Momentum Accretion in the Collapsar: How Long Can a Long GRB Be? , 675:519-527, March 2008. doi: 10.1086/526511.

H.-T. Janka, F. Hanke, L. Hüdepohl, A. Marek, B. Müller, and M. Obergaulinger. Core-collapse supernovae: Reflections and directions. *Progress of Theoretical and Experimental Physics*, 2012(1):01A309, December 2012. doi: 10.1093/ptep/pts067.

J. Japelj, S. D. Vergani, R. Salvaterra, L. K. Hunt, and F. Mannucci. Taking stock of superluminous supernovae and long gamma-ray burst host galaxy comparison using a complete sample of LGRBs. , 593:A115, October 2016. doi: 10.1051/0004-6361/201628603.

N. Kaiser and Pan-STARRS Team. The Pan-STARRS Survey Telescope Project. In *American Astronomical Society Meeting Abstracts*, volume 37 of *Bulletin of the American Astronomical Society*, page 150.04, December 2005.

D. Kasen and L. Bildsten. Supernova Light Curves Powered by Young Magnetars. , 717:245–249, July 2010. doi: 10.1088/0004-637X/717/1/245.

D. Kasen, S. E. Woosley, and A. Heger. Pair Instability Supernovae: Light Curves, Spectra, and Shock Breakout. , 734:102, June 2011. doi: 10.1088/0004-637X/734/2/102.

D. Kasen, B. D. Metzger, and L. Bildsten. Magnetar-driven Shock Breakout and Double-peaked Supernova Light Curves. , 821:36, April 2016. doi: 10.3847/0004-637X/821/1/36.

P. L. Kelly and R. P. Kirshner. Core-collapse Supernovae and Host Galaxy Stellar Populations. , 759:107, November 2012. doi: 10.1088/0004-637X/759/2/107.

P. L. Kelly, R. P. Kirshner, and M. Pahre. Long γ-Ray Bursts and Type Ic Core-Collapse Supernovae Have Similar Locations in Hosts. , 687:1201–1207, November 2008. doi: 10.1086/591925.

P. L. Kelly, M. Hicken, D. L. Burke, K. S. Mandel, and R. P. Kirshner. Hubble Residuals of Nearby Type Ia Supernovae are Correlated with Host Galaxy Masses. , 715:743–756, June 2010. doi: 10.1088/0004-637X/715/2/743.

P. L. Kelly, A. V. Filippenko, M. Modjaz, and D. Kocevski. The Host Galaxies of Fast-ejecta Core-collapse Supernovae. , 789:23, July 2014. doi: 10.1088/0004-637X/789/1/23.

R. C. Kennicutt, Jr. Star Formation in Galaxies Along the Hubble Sequence. , 36: 189–232, 1998. doi: 10.1146/annurev.astro.36.1.189.

L. J. Kewley and S. L. Ellison. Metallicity Calibrations and the Mass-Metallicity Relation for Star-forming Galaxies. , 681:1183-1204, July 2008. doi: 10.1086/587500.

L. J. Kewley, W. R. Brown, M. J. Geller, S. J. Kenyon, and M. J. Kurtz. SDSS 0809+1729: Connections Between Extremely Metal-Poor Galaxies and Gamma-Ray Burst Hosts. , 133:882–888, March 2007. doi: 10.1086/509135.

L. J. Kewley, D. Rupke, H. J. Zahid, M. J. Geller, and E. J. Barton. Metallicity Gradients and Gas Flows in Galaxy Pairs. , 721:L48–L52, September 2010. doi: 10.1088/2041-8205/721/1/L48.

M. Kiewe, A. Gal-Yam, I. Arcavi, D. C. Leonard, J. Emilio Enriquez, S. B. Cenko, D. B. Fox, D.-S. Moon, D. J. Sand, A. M. Soderberg, and T. CCCP. Caltech Core-Collapse Project (CCCP) Observations of Type IIn Supernovae: Typical Properties and Implications for Their Progenitor Stars. , 744:10, January 2012. doi: 10.1088/0004-637X/744/1/10.

R. Knop, G. Aldering, S. Deustua, G. Goldhaber, M. Kim, P. Nugent, E. Helin, S. Pravdo, D. Rabinowitz, and K. Lawrence. Supernovae 1999as and 1999at in Anonymous Galaxies. , 7128:1, March 1999.

D. Kocevski, A. A. West, and M. Modjaz. Modeling the GRB Host Galaxy Mass Distribution: Are GRBs Unbiased Tracers of Star Formation? , 702:377–385, September 2009. doi: 10.1088/0004-637X/702/1/377.

C. S. Kochanek. Failed Supernovae Explain the Compact Remnant Mass Function. , 785:28, April 2014. doi: 10.1088/0004-637X/785/1/28.

A. Kozyreva, S. Blinnikov, N. Langer, and S.-C. Yoon. Observational properties of low-redshift pair instability supernovae. , 565:A70, May 2014. doi: 10.1051/0004-6361/201423447.

A. Kozyreva, M. Gilmer, R. Hirschi, C. Fröhlich, S. Blinnikov, R. T. Wollaeger, U. M. Noebauer, D. R. van Rossum, A. Heger, W. P. Even, R. Waldman, A. Tolstov, E. Chatzopoulos, and E. Sorokina. Fast evolving pair-instability supernova models: evolution, explosion, light curves. , 464:2854–2865, January 2017. doi: 10.1093/mnras/stw2562.

R. G. Kron. Photometry of a complete sample of faint galaxies. , 43:305–325, June 1980. doi: 10.1086/190669.

P. Kroupa. On the variation of the initial mass function. , 322:231–246, April 2001. doi: 10.1046/j.1365-8711.2001.04022.x.

T. Krühler, J. Greiner, P. Schady, S. Savaglio, P. M. J. Afonso, C. Clemens, J. Elliott, R. Filgas, D. Gruber, D. A. Kann, S. Klose, A. Küpcü-Yoldaş, S. McBreen, F. Olivares, D. Pierini, A. Rau, A. Rossi, M. Nardini, A. Nicuesa Guelbenzu, V. Sudilovsky, and A. C. Updike. The SEDs and host galaxies of the dustiest GRB afterglows. , 534:A108, October 2011. doi: 10.1051/0004-6361/201117428.

T. Krühler, D. Malesani, J. P. U. Fynbo, O. E. Hartoog, J. Hjorth, P. Jakobsson, D. A. Perley, A. Rossi, P. Schady, S. Schulze, N. R. Tanvir, S. D. Vergani, K. Wiersema, P. M. J. Afonso, J. Bolmer, Z. Cano, S. Covino, V. D'Elia, A. de Ugarte Postigo, R. Filgas, M. Friis, J. F. Graham, J. Greiner, P. Goldoni, A. Gomboc, F. Hammer, J. Japelj, D. A. Kann, L. Kaper, S. Klose, A. J. Levan, G. Leloudas, B. Milvang-Jensen, A. Nicuesa Guelbenzu, E. Palazzi, E. Pian, S. Piranomonte, R. Sánchez-Ramírez, S. Savaglio, J. Selsing, G. Tagliaferri, P. M. Vreeswijk, D. J. Watson, and D. Xu. GRB hosts through cosmic time. VLT/X-Shooter emission-line spectroscopy of 96 γ-ray-burst-selected galaxies at 0.1 z 3.6. , 581:A125, September 2015. doi: 10.1051/0004-6361/201425561.

R.-P. Kudritzki and J. Puls. Winds from Hot Stars. , 38:613–666, 2000. doi: 10.1146/annurev.astro.38.1.613.

N. Langer, A. J. van Marle, A. J. T. Poelarends, and S.-C. Yoon. Massive Stars, Supernovae and long GRBs. In A. de Koter, L. J. Smith, and L. B. F. M. Waters,

editors, *Mass Loss from Stars and the Evolution of Stellar Clusters*, volume 388 of *Astronomical Society of the Pacific Conference Series*, page 37, June 2008.

D. Larson, J. Dunkley, G. Hinshaw, E. Komatsu, M. R. Nolta, C. L. Bennett, B. Gold, M. Halpern, R. S. Hill, N. Jarosik, A. Kogut, M. Limon, S. S. Meyer, N. Odegard, L. Page, K. M. Smith, D. N. Spergel, G. S. Tucker, J. L. Weiland, E. Wollack, and E. L. Wright. Seven-year Wilkinson Microwave Anisotropy Probe (WMAP) Observations: Power Spectra and WMAP-derived Parameters. , 192:16, February 2011. doi: 10.1088/0067-0049/192/2/16.

R. B. Larson, B. M. Tinsley, and C. N. Caldwell. The evolution of disk galaxies and the origin of S0 galaxies. , 237:692–707, May 1980. doi: 10.1086/157917.

J. Larsson, A. J. Levan, M. B. Davies, and A. S. Fruchter. A new constraint for gamma-ray burst progenitor mass. , 376:1285–1290, April 2007. doi: 10.1111/j.1365-2966.2007.11523.x.

N. M. Law, S. Kulkarni, E. Ofek, R. Quimby, M. Kasliwal, and Palomar Transient Factory Collaboration. The Palomar Transient Factory (PTF): Overview. In *American Astronomical Society Meeting Abstracts #213*, volume 41 of *Bulletin of the American Astronomical Society*, page 469.01, January 2009.

H. Lee, E. D. Skillman, J. M. Cannon, D. C. Jackson, R. D. Gehrz, E. F. Polomski, and C. E. Woodward. On Extending the Mass-Metallicity Relation of Galaxies by 2.5 Decades in Stellar Mass. , 647:970–983, August 2006. doi: 10.1086/505573.

J. C. Lee, R. C. Kennicutt, Jr., S. J. J. G. Funes, S. Sakai, and S. Akiyama. Dwarf Galaxy Starburst Statistics in the Local Volume. , 692:1305-1320, February 2009. doi: 10.1088/0004-637X/692/2/1305.

B. Leibundgut. Type Ia Supernovae. , 10:179–209, 2000. doi: 10.1007/s001590000009.

C. Leitherer, D. Schaerer, J. D. Goldader, R. M. G. Delgado, C. Robert, D. F. Kune, D. F. de Mello, D. Devost, and T. M. Heckman. Starburst99: Synthesis Models for Galaxies with Active Star Formation. , 123:3–40, July 1999. doi: 10.1086/313233.

G. Leloudas, J. Sollerman, A. J. Levan, J. P. U. Fynbo, D. Malesani, and J. R. Maund. Do Wolf-Rayet stars have similar locations in hosts as type Ib/c supernovae and long gamma-ray bursts? , 518:A29, July 2010. doi: 10.1051/0004-6361/200913753.

G. Leloudas, E. Chatzopoulos, B. Dilday, J. Gorosabel, J. Vinko, A. Gallazzi, J. C. Wheeler, B. Bassett, J. A. Fischer, J. A. Frieman, J. P. U. Fynbo, A. Goobar,

M. Jelínek, D. Malesani, R. C. Nichol, J. Nordin, L. Östman, M. Sako, D. P. Schneider, M. Smith, J. Sollerman, M. D. Stritzinger, C. C. Thöne, and A. de Ugarte Postigo. SN 2006oz: rise of a super-luminous supernova observed by the SDSS-II SN Survey. , 541:A129, May 2012. doi: 10.1051/0004-6361/201118498.

G. Leloudas, S. Schulze, T. Krühler, J. Gorosabel, L. Christensen, A. Mehner, A. de Ugarte Postigo, R. Amorín, C. C. Thöne, J. P. Anderson, F. E. Bauer, A. Gallazzi, K. G. Hełminiak, J. Hjorth, E. Ibar, D. Malesani, N. Morell, J. Vinko, and J. C. Wheeler. Spectroscopy of superluminous supernova host galaxies. A preference of hydrogen-poor events for extreme emission line galaxies. , 449:917–932, May 2015. doi: 10.1093/mnras/stv320.

D. Lennarz, D. Altmann, and C. Wiebusch. A unified supernova catalogue. , 538: A120, February 2012. doi: 10.1051/0004-6361/201117666.

A. Levan, P. Crowther, R. de Grijs, N. Langer, D. Xu, and S.-C. Yoon. Gamma-Ray Burst Progenitors. , 202:33–78, December 2016. doi: 10.1007/s11214-016-0312-x.

A. J. Levan, P. Jakobsson, C. Hurkett, N. R. Tanvir, J. Gorosabel, P. Vreeswijk, E. Rol, R. Chapman, N. Gehrels, P. T. O'Brien, J. P. Osborne, R. S. Priddey, C. Kouveliotou, R. Starling, D. vanden Berk, and K. Wiersema. A case of mistaken identity? GRB060912A and the nature of the long-short GRB divide. , 378:1439–1446, July 2007. doi: 10.1111/j.1365-2966.2007.11879.x.

A. J. Levan, A. M. Read, B. D. Metzger, P. J. Wheatley, and N. R. Tanvir. Superluminous X-Rays from a Superluminous Supernova. , 771:136, July 2013. doi: 10.1088/0004-637X/771/2/136.

A. J. Levan, N. R. Tanvir, A. S. Fruchter, J. Hjorth, E. Pian, P. Mazzali, R. A. Hounsell, D. A. Perley, Z. Cano, J. Graham, S. B. Cenko, J. P. U. Fynbo, C. Kouveliotou, A. Pe'er, K. Misra, and K. Wiersema. Hubble Space Telescope Observations of the Afterglow, Supernova, and Host Galaxy Associated with the Extremely Bright GRB 130427A. , 792:115, September 2014a. doi: 10.1088/0004-637X/792/2/115.

A. J. Levan, N. R. Tanvir, R. L. C. Starling, K. Wiersema, K. L. Page, D. A. Perley, S. Schulze, G. A. Wynn, R. Chornock, J. Hjorth, S. B. Cenko, A. S. Fruchter, P. T. O'Brien, G. C. Brown, R. L. Tunnicliffe, D. Malesani, P. Jakobsson, D. Watson, E. Berger, D. Bersier, B. E. Cobb, S. Covino, A. Cucchiara, A. de Ugarte Postigo, D. B. Fox, A. Gal-Yam, P. Goldoni, J. Gorosabel, L. Kaper, T. Krühler, R. Karjalainen, J. P. Osborne, E. Pian, R. Sánchez-Ramírez, B. Schmidt, I. Skillen, G. Tagliaferri, C. Thöne, O. Vaduvescu, R. A. M. J. Wijers, and B. A. Zauderer.

A New Population of Ultra-long Duration Gamma-Ray Bursts. , 781:13, January 2014b. doi: 10.1088/0004-637X/781/1/13.

E. M. Levesque, L. J. Kewley, E. Berger, and H. J. Zahid. The Host Galaxies of Gamma-ray Bursts. II. A Mass-metallicity Relation for Long-duration Gamma-ray Burst Host Galaxies. , 140:1557–1566, November 2010. doi: 10.1088/0004-6256/140/5/1557.

L.-X. Li. Shock breakout in Type Ibc supernovae and application to GRB 060218/SN 2006aj. , 375:240–256, February 2007. doi: 10.1111/j.1365-2966.2006.11286.x.

S. Lim, N. Hwang, and M. G. Lee. The Star Cluster System in the Nearby Starburst Galaxy M82. , 766:20, March 2013. doi: 10.1088/0004-637X/766/1/20.

R. Lunnan, R. Chornock, E. Berger, D. Milisavljevic, M. Drout, N. E. Sanders, P. M. Challis, I. Czekala, R. J. Foley, W. Fong, M. E. Huber, R. P. Kirshner, C. Leibler, G. H. Marion, M. McCrum, G. Narayan, A. Rest, K. C. Roth, D. Scolnic, S. J. Smartt, K. Smith, A. M. Soderberg, C. W. Stubbs, J. L. Tonry, W. S. Burgett, K. C. Chambers, R.-P. Kudritzki, E. A. Magnier, and P. A. Price. PS1-10bzj: A Fast, Hydrogen-poor Superluminous Supernova in a Metal-poor Host Galaxy. , 771: 97, July 2013. doi: 10.1088/0004-637X/771/2/97.

R. Lunnan, R. Chornock, E. Berger, T. Laskar, W. Fong, A. Rest, N. E. Sanders, P. M. Challis, M. R. Drout, R. J. Foley, M. E. Huber, R. P. Kirshner, C. Leibler, G. H. Marion, M. McCrum, D. Milisavljevic, G. Narayan, D. Scolnic, S. J. Smartt, K. W. Smith, A. M. Soderberg, J. L. Tonry, W. S. Burgett, K. C. Chambers, H. Flewelling, K. W. Hodapp, N. Kaiser, E. A. Magnier, P. A. Price, and R. J. Wainscoat. Hydrogen-poor Superluminous Supernovae and Long-duration Gamma-Ray Bursts Have Similar Host Galaxies. , 787:138, June 2014. doi: 10.1088/0004-637X/787/2/138.

R. Lunnan, R. Chornock, E. Berger, A. Rest, W. Fong, D. Scolnic, D. O. Jones, A. M. Soderberg, P. M. Challis, M. R. Drout, R. J. Foley, M. E. Huber, R. P. Kirshner, C. Leibler, G. H. Marion, M. McCrum, D. Milisavljevic, G. Narayan, N. E. Sanders, S. J. Smartt, K. W. Smith, J. L. Tonry, W. S. Burgett, K. C. Chambers, H. Flewelling, R.-P. Kudritzki, R. J. Wainscoat, and C. Waters. Zooming In on the Progenitors of Superluminous Supernovae With the HST. , 804:90, May 2015. doi: 10.1088/0004-637X/804/2/90.

R. Lunnan, R. Chornock, E. Berger, D. Milisavljevic, D. O. Jones, A. Rest, W. Fong, C. Fransson, R. Margutti, M. R. Drout, P. K. Blanchard, P. Challis, P. S. Cowperth-

waite, R. J. Foley, R. P. Kirshner, N. Morrell, A. G. Riess, K. C. Roth, D. Scolnic, S. J. Smartt, K. W. Smith, V. A. Villar, K. C. Chambers, P. W. Draper, M. E. Huber, N. Kaiser, R.-P. Kudritzki, E. A. Magnier, N. Metcalfe, and C. Waters. PS1-14bj: A Hydrogen-poor Superluminous Supernova With a Long Rise and Slow Decay. , 831:144, November 2016. doi: 10.3847/0004-637X/831/2/144.

J. Lyman, D. Bersier, P. James, P. Mazzali, J. Eldridge, M. Fraser, and E. Pian. Bolometric light curves and explosion parameters of 38 stripped-envelope core-collapse supernovae. *arXiv:1406.3667*, June 2014.

J. D. Lyman, A. J. Levan, N. R. Tanvir, J. P. U. Fynbo, J. T. W. McGuire, D. A. Perley, C. R. Angus, J. S. Bloom, C. J. Conselice, . S. Fruchter, J. Hjorth, P. Jakobsson, and R. L. C. Starling. The host galaxies and explosion sites of long-duration gamma ray bursts: Hubble Space Telescope near-infrared imaging. , January 2017. doi: 10.1093/mnras/stx220.

X. Ma, P. F. Hopkins, C.-A. Faucher-Giguère, N. Zolman, A. L. Muratov, D. Kereš, and E. Quataert. The origin and evolution of the galaxy mass-metallicity relation. , 456:2140–2156, February 2016. doi: 10.1093/mnras/stv2659.

A. I. MacFadyen and S. E. Woosley. Collapsars: Gamma-Ray Bursts and Explosions in "Failed Supernovae". , 524:262–289, October 1999. doi: 10.1086/307790.

A. Maeder. The most massive stars evolving to red supergiants - Evolution with mass loss, WR stars as post-red supergiants and pre-supernovae. , 99:97–107, June 1981.

P. Marchant, N. Langer, P. Podsiadlowski, T. M. Tauris, and T. J. Moriya. A new route towards merging massive black holes. , 588:A50, April 2016. doi: 10.1051/0004-6361/201628133.

R. A. Marino, A. Gil de Paz, S. F. Sánchez, P. Sánchez-Blázquez, N. Cardiel, A. Castillo-Morales, S. Pascual, J. Vílchez, C. Kehrig, M. Mollá, J. Mendez-Abreu, C. Catalán-Torrecilla, E. Florido, I. Perez, T. Ruiz-Lara, S. Ellis, A. R. López-Sánchez, R. M. González Delgado, A. de Lorenzo-Cáceres, R. García-Benito, L. Galbany, S. Zibetti, C. Cortijo, V. Kalinova, D. Mast, J. Iglesias-Páramo, P. Papaderos, C. J. Walcher, and J. Bland-Hawthorn. Outer-disk reddening and gas-phase metallicities: The CALIFA connection. , 585:A47, January 2016. doi: 10.1051/0004-6361/201526986.

P. A. Mazzali, A. I. McFadyen, S. E. Woosley, E. Pian, and M. Tanaka. An upper limit to the energy of gamma-ray bursts indicates that GRBs/SNe are powered by magnetars. , 443:67–71, September 2014. doi: 10.1093/mnras/stu1124.

P. A. Mazzali, M. Sullivan, E. Pian, J. Greiner, and D. A. Kann. Spectrum formation in superluminous supernovae (Type I). , 458:3455–3465, June 2016. doi: 10.1093/mnras/stw512.

S. McBreen, T. Krühler, A. Rau, J. Greiner, D. A. Kann, S. Savaglio, P. Afonso, C. Clemens, R. Filgas, S. Klose, A. Küpcü Yoldaş, F. Olivares E., A. Rossi, G. P. Szokoly, A. Updike, and A. Yoldaş. Optical and near-infrared follow-up observations of four Fermi/LAT GRBs: redshifts, afterglows, energetics, and host galaxies. , 516: A71, June 2010. doi: 10.1051/0004-6361/200913734.

A. W. McConnachie. The Observed Properties of Dwarf Galaxies in and around the Local Group. , 144:4, July 2012. doi: 10.1088/0004-6256/144/1/4.

M. McCrum, S. J. Smartt, R. Kotak, A. Rest, A. Jerkstrand, C. Inserra, S. A. Rodney, T.-W. Chen, D. A. Howell, M. E. Huber, A. Pastorello, J. L. Tonry, F. Bresolin, R.-P. Kudritzki, R. Chornock, E. Berger, K. Smith, M. T. Botticella, R. J. Foley, M. Fraser, D. Milisavljevic, M. Nicholl, A. G. Riess, C. W. Stubbs, S. Valenti, W. M. Wood-Vasey, D. Wright, D. R. Young, M. Drout, I. Czekala, W. S. Burgett, K. C. Chambers, P. Draper, H. Flewelling, K. W. Hodapp, N. Kaiser, E. A. Magnier, N. Metcalfe, P. A. Price, W. Sweeney, and R. J. Wainscoat. The superluminous supernova PS1-11ap: bridging the gap between low and high redshift. , 437:656–674, January 2014. doi: 10.1093/mnras/stt1923.

M. McCrum, S. J. Smartt, A. Rest, K. Smith, R. Kotak, S. A. Rodney, D. R. Young, R. Chornock, E. Berger, R. J. Foley, M. Fraser, D. Wright, D. Scolnic, J. L. Tonry, Y. Urata, K. Huang, A. Pastorello, M. T. Botticella, S. Valenti, S. Mattila, E. Kankare, D. J. Farrow, M. E. Huber, C. W. Stubbs, R. P. Kirshner, F. Bresolin, W. S. Burgett, K. C. Chambers, P. W. Draper, H. Flewelling, R. Jedicke, N. Kaiser, E. A. Magnier, N. Metcalfe, J. S. Morgan, P. A. Price, W. Sweeney, R. J. Wainscoat, and C. Waters. Selecting superluminous supernovae in faint galaxies from the first year of the Pan-STARRS1 Medium Deep Survey. , 448:1206–1231, April 2015. doi: 10.1093/mnras/stv034.

S. Mereghetti, J. A. Pons, and A. Melatos. Magnetars: Properties, Origin and Evolution. , March 2015. doi: 10.1007/s11214-015-0146-y.

B. D. Metzger, D. Giannios, T. A. Thompson, N. Bucciantini, and E. Quataert. The protomagnetar model for gamma-ray bursts. , 413:2031–2056, May 2011. doi: 10.1111/j.1365-2966.2011.18280.x.

B. D. Metzger, B. Margalit, D. Kasen, and E. Quataert. The diversity of transients from magnetar birth in core collapse supernovae. , 454:3311–3316, December 2015. doi: 10.1093/mnras/stv2224.

L. Michel-Dansac, D. G. Lambas, M. S. Alonso, and P. Tissera. The mass-metallicity relation of interacting galaxies. , 386:L82–L86, May 2008. doi: 10.1111/j.1745-3933.2008.00466.x.

A. A. Miller, R. Chornock, D. A. Perley, M. Ganeshalingam, W. Li, N. R. Butler, J. S. Bloom, N. Smith, M. Modjaz, D. Poznanski, A. V. Filippenko, C. V. Griffith, J. H. Shiode, and J. M. Silverman. The Exceptionally Luminous Type II-Linear Supernova 2008es. , 690:1303–1312, January 2009. doi: 10.1088/0004-637X/690/2/1303.

A. A. Miller, N. Smith, W. Li, J. S. Bloom, R. Chornock, A. V. Filippenko, and J. X. Prochaska. New Observations of the Very Luminous Supernova 2006gy: Evidence for Echoes. , 139:2218–2229, June 2010. doi: 10.1088/0004-6256/139/6/2218.

R. Minkowski. Spectra of Supernovae. , 53:224, August 1941. doi: 10.1086/125315.

M. Modjaz, K. Z. Stanek, P. M. Garnavich, P. Berlind, S. Blondin, W. Brown, M. Calkins, P. Challis, A. M. Diamond-Stanic, H. Hao, M. Hicken, R. P. Kirshner, and J. L. Prieto. Early-Time Photometry and Spectroscopy of the Fast Evolving SN 2006aj Associated with GRB 060218. , 645:L21–L24, July 2006. doi: 10.1086/505906.

M. Modjaz, L. Kewley, R. P. Kirshner, K. Z. Stanek, P. Challis, P. M. Garnavich, J. E. Greene, P. L. Kelly, and J. L. Prieto. Measured Metallicities at the Sites of Nearby Broad-Lined Type Ic Supernovae and Implications for the Supernovae Gamma-Ray Burst Connection. , 135:1136–1150, April 2008. doi: 10.1088/0004-6256/135/4/1136.

M. Modjaz, L. Kewley, J. S. Bloom, A. V. Filippenko, D. Perley, and J. M. Silverman. Progenitor Diagnostics for Stripped Core-collapse Supernovae: Measured Metallicities at Explosion Sites. , 731:L4, April 2011. doi: 10.1088/2041-8205/731/1/L4.

M. Modjaz, S. Blondin, R. P. Kirshner, T. Matheson, P. Berlind, F. B. Bianco, M. L. Calkins, P. Challis, P. Garnavich, M. Hicken, S. Jha, Y. Q. Liu, and G. H. Marion. Optical Spectra of 73 Stripped-envelope Core-collapse Supernovae. , 147:99, May 2014. doi: 10.1088/0004-6256/147/5/99.

M. Modjaz, Y. Q. Liu, F. B. Bianco, and O. Graur. The Spectral SN-GRB Connection: Systematic Spectral Comparisons between Type Ic Supernovae, and broad-lined Type Ic Supernovae with and without Gamma-Ray Bursts. *ArXiv e-prints*, September 2015.

M. Mollá, J. M. Vílchez, M. Gavilán, and A. I. Díaz. The nitrogen-to-oxygen evolution in galaxies: the role of the star formation rate. , 372:1069–1080, November 2006. doi: 10.1111/j.1365-2966.2006.10892.x.

T. Moriya, N. Tominaga, M. Tanaka, K. Maeda, and K. Nomoto. A Core-collapse Supernova Model for the Extremely Luminous Type Ic Supernova 2007bi: An Alternative to the Pair-instability Supernova Model. , 717:L83–L86, July 2010. doi: 10.1088/2041-8205/717/2/L83.

T. J. Moriya and N. Tominaga. Diversity of Luminous Supernovae from Non-steady Mass Loss. , 747:118, March 2012. doi: 10.1088/0004-637X/747/2/118.

T. J. Moriya, Z.-W. Liu, J. Mackey, T.-W. Chen, and N. Langer. Revealing the binary origin of Type Ic superluminous supernovae through nebular hydrogen emission. , 584:L5, December 2015. doi: 10.1051/0004-6361/201527515.

D. K. Nadyozhin. The properties of NI to CO to Fe decay. , 92:527–531, June 1994. doi: 10.1086/192008.

E. Nakar and R. Sari. Early Supernovae Light Curves Following the Shock Breakout. , 725:904–921, December 2010. doi: 10.1088/0004-637X/725/1/904.

J. D. Neill, M. Sullivan, A. Gal-Yam, R. Quimby, E. Ofek, T. K. Wyder, D. A. Howell, P. Nugent, M. Seibert, D. C. Martin, R. Overzier, T. A. Barlow, K. Foster, P. G. Friedman, P. Morrissey, S. G. Neff, D. Schiminovich, L. Bianchi, J. Donas, T. M. Heckman, Y.-W. Lee, B. F. Madore, B. Milliard, R. M. Rich, and A. S. Szalay. The Extreme Hosts of Extreme Supernovae. , 727:15, January 2011. doi: 10.1088/0004-637X/727/1/15.

M. Nicholl and S. J. Smartt. Seeing double: the frequency and detectability of double-peaked superluminous supernova light curves. , 457:L79–L83, March 2016. doi: 10.1093/mnrasl/slv210.

M. Nicholl, S. J. Smartt, A. Jerkstrand, C. Inserra, M. McCrum, R. Kotak, M. Fraser, D. Wright, T.-W. Chen, K. Smith, D. R. Young, S. A. Sim, S. Valenti, D. A.

Howell, F. Bresolin, R. P. Kudritzki, J. L. Tonry, M. E. Huber, A. Rest, A. Pastorello, L. Tomasella, E. Cappellaro, S. Benetti, S. Mattila, E. Kankare, T. Kangas, G. Leloudas, J. Sollerman, F. Taddia, E. Berger, R. Chornock, G. Narayan, C. W. Stubbs, R. J. Foley, R. Lunnan, A. Soderberg, N. Sanders, D. Milisavljevic, R. Margutti, R. P. Kirshner, N. Elias-Rosa, A. Morales-Garoffolo, S. Taubenberger, M. T. Botticella, S. Gezari, Y. Urata, S. Rodney, A. G. Riess, D. Scolnic, W. M. Wood-Vasey, W. S. Burgett, K. Chambers, H. A. Flewelling, E. A. Magnier, N. Kaiser, N. Metcalfe, J. Morgan, P. A. Price, W. Sweeney, and C. Waters. Slowly fading super-luminous supernovae that are not pair-instability explosions. , 502: 346–349, October 2013. doi: 10.1038/nature12569.

M. Nicholl, S. J. Smartt, A. Jerkstrand, S. A. Sim, C. Inserra, J. P. Anderson, C. Baltay, S. Benetti, K. Chambers, T.-W. Chen, N. Elias-Rosa, U. Feindt, H. A. Flewelling, M. Fraser, A. Gal-Yam, L. Galbany, M. E. Huber, T. Kangas, E. Kankare, R. Kotak, T. Krühler, K. Maguire, R. McKinnon, D. Rabinowitz, S. Rostami, S. Schulze, K. W. Smith, M. Sullivan, J. L. Tonry, S. Valenti, and D. R. Young. LSQ14bdq: A Type Ic Super-luminous Supernova with a Double-peaked Light Curve. , 807:L18, July 2015. doi: 10.1088/2041-8205/807/1/L18.

M. Nicholl, E. Berger, S. J. Smartt, R. Margutti, A. Kamble, K. D. Alexander, T.-W. Chen, C. Inserra, I. Arcavi, P. K. Blanchard, R. Cartier, K. C. Chambers, M. J. Childress, R. Chornock, P. S. Cowperthwaite, M. Drout, H. A. Flewelling, M. Fraser, A. Gal-Yam, L. Galbany, J. Harmanen, T. W.-S. Holoien, G. Hosseinzadeh, D. A. Howell, M. E. Huber, A. Jerkstrand, E. Kankare, C. S. Kochanek, Z.-Y. Lin, R. Lunnan, E. A. Magnier, K. Maguire, C. McCully, M. McDonald, B. D. Metzger, D. Milisavljevic, A. Mitra, T. Reynolds, J. Saario, B. J. Shappee, K. W. Smith, S. Valenti, V. A. Villar, C. Waters, and D. R. Young. SN 2015BN: A Detailed Multi-wavelength View of a Nearby Superluminous Supernova. , 826:39, July 2016. doi: 10.3847/0004-637X/826/1/39.

Y. Niino. Revisiting the metallicity of long-duration gamma-ray burst host galaxies: the role of chemical inhomogeneity within galaxies. , 417:567–572, October 2011. doi: 10.1111/j.1365-2966.2011.19299.x.

P. E. Nugent, M. Sullivan, S. B. Cenko, R. C. Thomas, D. Kasen, D. A. Howell, D. Bersier, J. S. Bloom, S. R. Kulkarni, M. T. Kandrashoff, A. V. Filippenko, J. M. Silverman, G. W. Marcy, A. W. Howard, H. T. Isaacson, K. Maguire, N. Suzuki, J. E. Tarlton, Y.-C. Pan, L. Bildsten, B. J. Fulton, J. T. Parrent, D. Sand, P. Podsiadlowski, F. B. Bianco, B. Dilday, M. L. Graham, J. Lyman, P. James, M. M.

Kasliwal, N. M. Law, R. M. Quimby, I. M. Hook, E. S. Walker, P. Mazzali, E. Pian, E. O. Ofek, A. Gal-Yam, and D. Poznanski. Supernova SN 2011fe from an exploding carbon-oxygen white dwarf star. , 480:344–347, December 2011. doi: 10.1038/nature10644.

E. O. Ofek, P. B. Cameron, M. M. Kasliwal, A. Gal-Yam, A. Rau, S. R. Kulkarni, D. A. Frail, P. Chandra, S. B. Cenko, A. M. Soderberg, and S. Immler. SN 2006gy: An Extremely Luminous Supernova in the Galaxy NGC 1260. , 659:L13–L16, April 2007. doi: 10.1086/516749.

E. O. Ofek, I. Rabinak, J. D. Neill, I. Arcavi, S. B. Cenko, E. Waxman, S. R. Kulkarni, A. Gal-Yam, P. E. Nugent, L. Bildsten, J. S. Bloom, A. V. Filippenko, K. Forster, D. A. Howell, J. Jacobsen, M. M. Kasliwal, N. Law, C. Martin, D. Poznanski, R. M. Quimby, K. J. Shen, M. Sullivan, R. Dekany, G. Rahmer, D. Hale, R. Smith, J. Zolkower, V. Velur, R. Walters, J. Henning, K. Bui, and D. McKenna. Supernova PTF 09UJ: A Possible Shock Breakout from a Dense Circumstellar Wind. , 724: 1396–1401, December 2010. doi: 10.1088/0004-637X/724/2/1396.

K. Ohta, K. Yabe, F. Iwamuro, S. Yuma, M. Akiyama, N. Tamura, and FMOS Team. Stellar-Mass Metallicity Relation at z
1.4. In W. Aoki, M. Ishigaki, T. Suda, T. Tsujimoto, and N. Arimoto, editors, *Galactic Archaeology: Near-Field Cosmology and the Formation of the Milky Way*, volume 458 of *Astronomical Society of the Pacific Conference Series*, page 87, August 2012.

J. B. Oke, J. G. Cohen, M. Carr, J. Cromer, A. Dingizian, F. H. Harris, S. Labrecque, R. Lucinio, W. Schaal, H. Epps, and J. Miller. The Keck Low-Resolution Imaging Spectrometer. , 107:375, April 1995. doi: 10.1086/133562.

T. Pan, A. Loeb, and D. Kasen. Pair-instability supernovae via collision runaway in young dense star clusters. , 423:2203–2208, July 2012. doi: 10.1111/j.1365-2966.2012.21030.x.

T. Pan, D. Patnaude, and A. Loeb. Superluminous X-ray emission from the interaction of supernova ejecta with dense circumstellar shells. , 433:838–848, July 2013. doi: 10.1093/mnras/stt780.

A. Papadopoulos, C. B. D'Andrea, M. Sullivan, R. C. Nichol, K. Barbary, R. Biswas, P. J. Brown, R. A. Covarrubias, D. A. Finley, J. A. Fischer, R. J. Foley, D. Goldstein, R. R. Gupta, R. Kessler, E. Kovacs, S. E. Kuhlmann, C. Lidman, M. March, P. E. Nugent, M. Sako, R. C. Smith, H. Spinka, W. Wester, T. M. C. Abbott, F. Abdalla,

S. S. Allam, M. Banerji, J. P. Bernstein, R. A. Bernstein, A. Carnero, L. N. da Costa, D. L. DePoy, S. Desai, H. T. Diehl, T. Eifler, A. E. Evrard, B. Flaugher, J. A. Frieman, D. Gerdes, D. Gruen, K. Honscheid, D. James, K. Kuehn, N. Kuropatkin, O. Lahav, M. A. G. Maia, M. Makler, J. L. Marshall, K. W. Merritt, C. J. Miller, R. Miquel, R. Ogando, A. A. Plazas, N. A. Roe, A. K. Romer, E. Rykoff, E. Sanchez, B. X. Santiago, V. Scarpine, M. Schubnell, I. Sevilla, M. Soares-Santos, E. Suchyta, M. Swanson, G. Tarle, J. Thaler, L. D. Tucker, R. H. Wechsler, and J. Zuntz. DES13S2cmm: the first superluminous supernova from the Dark Energy Survey. , 449:1215–1227, May 2015. doi: 10.1093/mnras/stv174.

A. Pastorello, S. J. Smartt, M. T. Botticella, K. Maguire, M. Fraser, K. Smith, R. Kotak, L. Magill, S. Valenti, D. R. Young, S. Gezari, F. Bresolin, R. Kudritzki, D. A. Howell, A. Rest, N. Metcalfe, S. Mattila, E. Kankare, K. Y. Huang, Y. Urata, W. S. Burgett, K. C. Chambers, T. Dombeck, H. Flewelling, T. Grav, J. N. Heasley, K. W. Hodapp, N. Kaiser, G. A. Luppino, R. H. Lupton, E. A. Magnier, D. G. Monet, J. S. Morgan, P. M. Onaka, P. A. Price, P. H. Rhoads, W. A. Siegmund, C. W. Stubbs, W. E. Sweeney, J. L. Tonry, R. J. Wainscoat, M. F. Waterson, C. Waters, and C. G. Wynn-Williams. Ultra-bright Optical Transients are Linked with Type Ic Supernovae. , 724:L16–L21, November 2010. doi: 10.1088/2041-8205/724/1/L16.

D. Pérez-Ramírez, J. P. Norris, J. Gorosabel, A. J. Castro-Tirado, L. Hernández-García, A. de Ugarte Postigo, S. Guziy, J. C. Tello, R. Sánchez-Ramírez, and P. Ferrero. A GTC study of the afterglow and host galaxy of the short-duration GRB 100816A. In A. J. Castro-Tirado, J. Gorosabel, and I. H. Park, editors, *EAS Publications Series*, volume 61 of *EAS Publications Series*, pages 345–349, July 2013. doi: 10.1051/eas/1361055.

D. A. Perley, A. J. Levan, N. R. Tanvir, S. B. Cenko, J. S. Bloom, J. Hjorth, T. Krühler, A. V. Filippenko, A. Fruchter, J. P. U. Fynbo, P. Jakobsson, J. Kalirai, B. Milvang-Jensen, A. N. Morgan, J. X. Prochaska, and J. M. Silverman. A Population of Massive, Luminous Galaxies Hosting Heavily Dust-obscured Gamma-Ray Bursts: Implications for the Use of GRBs as Tracers of Cosmic Star Formation. , 778:128, December 2013. doi: 10.1088/0004-637X/778/2/128.

D. A. Perley, R. A. Perley, J. Hjorth, M. J. Michałowski, S. B. Cenko, P. Jakobsson, T. Krühler, A. J. Levan, D. Malesani, and N. R. Tanvir. Connecting GRBs and ULIRGs: A Sensitive, Unbiased Survey for Radio Emission from Gamma-Ray Burst Host Galaxies at 0 z 2.5. , 801:102, March 2015a. doi: 10.1088/0004-637X/801/2/102.

D. A. Perley, N. R. Tanvir, J. Hjorth, T. Laskar, E. Berger, R. Chary, A. de Ugarte Postigo, J. P. U. Fynbo, T. Krühler, A. J. Levan, M. J. Michałowski, and S. Schulze. The Swift GRB Host Galaxy Legacy Survey - II. Rest-Frame NIR Luminosity Distribution and Evidence for a Near-Solar Metallicity Threshold. *arXiv:1504.02479*, April 2015b.

D. A. Perley, R. Quimby, L. Yan, P. Vreeswijk, A. De Cia, R. Lunnan, A. Gal-Yam, O. Yaron, A. V. Filippenko, M. L. Graham, and P. E. Nugent. Host-Galaxy Properties of 32 Low-Redshift Superluminous Supernovae from the Palomar Transient Factory. *ArXiv e-prints*, April 2016.

A. L. Piro. Using Double-peaked Supernova Light Curves to Study Extended Material. , 808:L51, August 2015. doi: 10.1088/2041-8205/808/2/L51.

A. E. Piskunov, N. V. Kharchenko, E. Schilbach, S. Röser, R.-D. Scholz, and H. Zinnecker. Why simple stellar population models do not reproduce the colours of Galactic open clusters. , 507:L5–L8, November 2009. doi: 10.1051/0004-6361/200913270.

P. Podsiadlowski, P. C. Joss, and J. J. L. Hsu. Presupernova evolution in massive interacting binaries. , 391:246–264, May 1992. doi: 10.1086/171341.

P. Podsiadlowski, N. Ivanova, S. Justham, and S. Rappaport. Explosive common-envelope ejection: implications for gamma-ray bursts and low-mass black-hole binaries. , 406:840–847, August 2010. doi: 10.1111/j.1365-2966.2010.16751.x.

S. F. Portegies Zwart and E. P. J. van den Heuvel. A runaway collision in a young star cluster as the origin of the brightest supernova. , 450:388–389, November 2007. doi: 10.1038/nature06276.

S. F. Portegies Zwart, S. L. W. McMillan, and M. Gieles. Young Massive Star Clusters. , 48:431–493, September 2010. doi: 10.1146/annurev-astro-081309-130834.

S. Prajs, M. Sullivan, M. Smith, A. Levan, N. V. Karpenka, T. D. P. Edwards, C. R. Walker, W. M. Wolf, C. Balland, R. Carlberg, A. Howell, C. Lidman, R. Pain, C. Pritchet, and V. Ruhlmann-Kleider. The Volumetric Rate of Superluminous Supernovae at z
1. , August 2016. doi: 10.1093/mnras/stw1942.

N. Prantzos and S. Boissier. On the relative frequencies of core-collapse supernovae sub-types: The role of progenitor metallicity. , 406:259–264, July 2003. doi: 10.1051/0004-6361:20030717.

D. Prialnik. *An Introduction to the Theory of Stellar Structure and Evolution*. July 2000.

J. L. Prieto, K. Z. Stanek, and J. F. Beacom. Characterizing Supernova Progenitors via the Metallicities of their Host Galaxies, from Poor Dwarfs to Rich Spirals. , 673: 999–1008, February 2008. doi: 10.1086/524654.

R. M. Quimby, G. Aldering, J. C. Wheeler, P. Höflich, C. W. Akerlof, and E. S. Rykoff. SN 2005ap: A Most Brilliant Explosion. , 668:L99–L102, October 2007. doi: 10.1086/522862.

R. M. Quimby, S. Kulkarni, E. Ofek, M. M. Kasliwal, A. Gal-Yam, S. Ben-Ami, C. Badenes, A. Sternberg, J. Botyanszki, P. E. Nugent, and D. A. Howell. Discovery of a Luminous Supernova, PTF10vqv. *The Astronomer's Telegram*, 2979:1, October 2010.

R. M. Quimby, S. B. Cenko, O. Yaron, D. Xu, A. Horesh, J. Silverman, A. V. Filippenko, J. W. Derose, and P. Nugent. Discovery of a Luminous Supernova, PTF11dsf. *The Astronomer's Telegram*, 3465:1, June 2011a.

R. M. Quimby, S. R. Kulkarni, M. M. Kasliwal, A. Gal-Yam, I. Arcavi, M. Sullivan, P. Nugent, R. Thomas, D. A. Howell, E. Nakar, L. Bildsten, C. Theissen, N. M. Law, R. Dekany, G. Rahmer, D. Hale, R. Smith, E. O. Ofek, J. Zolkower, V. Velur, R. Walters, J. Henning, K. Bui, D. McKenna, D. Poznanski, S. B. Cenko, and D. Levitan. Hydrogen-poor superluminous stellar explosions. , 474:487–489, June 2011b. doi: 10.1038/nature10095.

R. M. Quimby, S. R. Kulkarni, M. M. Kasliwal, A. Gal-Yam, I. Arcavi, M. Sullivan, P. Nugent, R. Thomas, D. A. Howell, E. Nakar, L. Bildsten, C. Theissen, N. M. Law, R. Dekany, G. Rahmer, D. Hale, R. Smith, E. O. Ofek, J. Zolkower, V. Velur, R. Walters, J. Henning, K. Bui, D. McKenna, D. Poznanski, S. B. Cenko, and D. Levitan. Hydrogen-poor superluminous stellar explosions. , 474:487–489, June 2011c. doi: 10.1038/nature10095.

J. L. Racusin, E. W. Liang, D. N. Burrows, A. Falcone, T. Sakamoto, B. B. Zhang, B. Zhang, P. Evans, and J. Osborne. Jet Breaks and Energetics of Swift Gamma-Ray Burst X-Ray Afterglows. , 698:43–74, June 2009. doi: 10.1088/0004-637X/698/1/43.

C. Raskin, E. Scannapieco, J. Rhoads, and M. Della Valle. Using Spatial Distributions to Constrain Progenitors of Supernovae and Gamma-Ray Bursts. , 689:358–370, December 2008. doi: 10.1086/592495.

G. Rauw and M. De Becker. Early-type stars in the young open cluster IC 1805. I. The SB2 system BD+60deg497 and the probably single stars BD +60deg 501$andBD+$ 60deg513., 421 : 693 − −702, $July$2004.doi : 10.1051/0004 − 6361 : 20040255.

N. Rea, M. Gullón, J. A. Pons, R. Perna, M. G. Dainotti, J. A. Miralles, and D. F. Torres. Constraining the GRB-Magnetar Model by Means of the Galactic Pulsar Population. , 813:92, November 2015. doi: 10.1088/0004-637X/813/2/92.

L. Resmi, K. Misra, G. Jóhannesson, A. J. Castro Tirado, J. Gorosabel, M. Jelínek, D. Bhattacharya, P. Kubánek, G. C. Anupama, A. Sota, D. K. Sahu, A. de Ugarte Postigo, S. B. Pandey, R. Sánchez Ramírez, M. Bremer, and R. Sagar. Comprehensive multiwavelength modelling of the afterglow of GRB 050525A. , 427:288–297, November 2012. doi: 10.1111/j.1365-2966.2012.21713.x.

D. Richardson, D. Branch, D. Casebeer, J. Millard, R. C. Thomas, and E. Baron. A Comparative Study of the Absolute Magnitude Distributions of Supernovae. , 123: 745–752, February 2002. doi: 10.1086/338318.

A. G. Riess, A. V. Filippenko, P. Challis, A. Clocchiatti, A. Diercks, P. M. Garnavich, R. L. Gilliland, C. J. Hogan, S. Jha, R. P. Kirshner, B. Leibundgut, M. M. Phillips, D. Reiss, B. P. Schmidt, R. A. Schommer, R. C. Smith, J. Spyromilio, C. Stubbs, N. B. Suntzeff, and J. Tonry. Observational Evidence from Supernovae for an Accelerating Universe and a Cosmological Constant. , 116:1009–1038, September 1998. doi: 10.1086/300499.

A. G. Riess, L.-G. Strolger, S. Casertano, H. C. Ferguson, B. Mobasher, B. Gold, P. J. Challis, A. V. Filippenko, S. Jha, W. Li, J. Tonry, R. Foley, R. P. Kirshner, M. Dickinson, E. MacDonald, D. Eisenstein, M. Livio, J. Younger, C. Xu, T. Dahlén, and D. Stern. New Hubble Space Telescope Discoveries of Type Ia Supernovae at z = 1: Narrowing Constraints on the Early Behavior of Dark Energy. , 659:98–121, April 2007. doi: 10.1086/510378.

B. Roig, M. R. Blanton, and R. Yan. Stellar Metallicity Gradients in SDSS Galaxies. , 808:26, July 2015. doi: 10.1088/0004-637X/808/1/26.

W. R. J. Rolleston, S. J. Smartt, P. L. Dufton, and R. S. I. Ryans. The Galactic metallicity gradient. , 363:537–554, November 2000.

W. R. J. Rolleston, C. Trundle, and P. L. Dufton. The present-day chemical composition of the LMC. , 396:53–64, December 2002. doi: 10.1051/0004-6361:20021088.

S. Salim, J. C. Lee, C. Ly, J. Brinchmann, R. Davé, M. Dickinson, J. J. Salzer, and S. Charlot. A Critical Look at the Mass-Metallicity-Star Formation Rate Relation in the Local Universe. I. An Improved Analysis Framework and Confounding Systematics. , 797:126, December 2014. doi: 10.1088/0004-637X/797/2/126.

E. E. Salpeter. The Luminosity Function and Stellar Evolution. , 121:161, January 1955. doi: 10.1086/145971.

J. J. Salzer, J. C. Lee, J. Melbourne, J. L. Hinz, A. Alonso-Herrero, and A. Jangren. Metal Abundances of KISS Galaxies. IV. Galaxian Luminosity-Metallicity Relations in the Optical and Near-Infrared. , 624:661–679, May 2005. doi: 10.1086/429386.

S. F. Sánchez, R. C. Kennicutt, A. Gil de Paz, G. van de Ven, J. M. Vílchez, L. Wisotzki, C. J. Walcher, D. Mast, J. A. L. Aguerri, S. Albiol-Pérez, A. Alonso-Herrero, J. Alves, J. Bakos, T. Bartáková, J. Bland-Hawthorn, A. Boselli, D. J. Bomans, A. Castillo-Morales, C. Cortijo-Ferrero, A. de Lorenzo-Cáceres, A. Del Olmo, R.-J. Dettmar, A. Díaz, S. Ellis, J. Falcón-Barroso, H. Flores, A. Gallazzi, B. García-Lorenzo, R. González Delgado, N. Gruel, T. Haines, C. Hao, B. Husemann, J. Iglésias-Páramo, K. Jahnke, B. Johnson, B. Jungwiert, V. Kalinova, C. Kehrig, D. Kupko, Á. R. López-Sánchez, M. Lyubenova, R. A. Marino, E. Mármol-Queraltó, I. Márquez, J. Masegosa, S. Meidt, J. Mendez-Abreu, A. Monreal-Ibero, C. Montijo, A. M. Mourão, G. Palacios-Navarro, P. Papaderos, A. Pasquali, R. Peletier, E. Pérez, I. Pérez, A. Quirrenbach, M. Relaño, F. F. Rosales-Ortega, M. M. Roth, T. Ruiz-Lara, P. Sánchez-Blázquez, C. Sengupta, R. Singh, V. Stanishev, S. C. Trager, A. Vazdekis, K. Viironen, V. Wild, S. Zibetti, and B. Ziegler. CALIFA, the Calar Alto Legacy Integral Field Area survey. I. Survey presentation. , 538:A8, February 2012. doi: 10.1051/0004-6361/201117353.

N. E. Sanders, A. M. Soderberg, E. M. Levesque, R. J. Foley, R. Chornock, D. Milisavljevic, R. Margutti, E. Berger, M. R. Drout, I. Czekala, and J. A. Dittmann. A Spectroscopic Study of Type Ibc Supernova Host Galaxies from Untargeted Surveys. , 758:132, October 2012. doi: 10.1088/0004-637X/758/2/132.

M. A. Sandoval, R. P. Vo, A. J. Romanowsky, J. Strader, J. Choi, Z. G. Jennings, C. Conroy, J. P. Brodie, C. Foster, A. Villaume, M. A. Norris, J. Janz, and D. A. Forbes. Hiding in Plain Sight: Record-breaking Compact Stellar Systems in the Sloan Digital Sky Survey. , 808:L32, July 2015. doi: 10.1088/2041-8205/808/1/L32.

S. Savaglio, K. Glazebrook, D. Le Borgne, S. Juneau, R. G. Abraham, H.-W. Chen, D. Crampton, P. J. McCarthy, R. G. Carlberg, R. O. Marzke, K. Roth, I. Jørgensen,

and R. Murowinski. The Gemini Deep Deep Survey. VII. The Redshift Evolution of the Mass-Metallicity Relation. , 635:260–279, December 2005. doi: 10.1086/497331.

S. Savaglio, K. Glazebrook, and D. Le Borgne. The Galaxy Population Hosting Gamma-Ray Bursts. , 691:182–211, January 2009. doi: 10.1088/0004-637X/691/1/182.

K. Schawinski, S. Justham, C. Wolf, P. Podsiadlowski, M. Sullivan, K. C. Steenbrugge, T. Bell, H.-J. Röser, E. S. Walker, P. Astier, D. Balam, C. Balland, R. Carlberg, A. Conley, D. Fouchez, J. Guy, D. Hardin, I. Hook, D. A. Howell, R. Pain, K. Perrett, C. Pritchet, N. Regnault, and S. K. Yi. Supernova Shock Breakout from a Red Supergiant. *Science*, 321:223–226, July 2008. doi: 10.1126/science.1160456.

P. Schechter. An analytic expression for the luminosity function for galaxies. , 203: 297–306, January 1976. doi: 10.1086/154079.

E. F. Schlafly and D. P. Finkbeiner. Measuring Reddening with Sloan Digital Sky Survey Stellar Spectra and Recalibrating SFD. , 737:103, August 2011. doi: 10.1088/0004-637X/737/2/103.

B. Schmidt, J. Tonry, B. Barris, P. Garnavich, S. Holland, A. Riess, N. B. Suntzeff, R. A. Schommer, R. C. Smith, P. Candia, P. Challis, S. Jha, L. Strolger, A. Clocchiatti, B. Leibundgut, and J. Sollerman. Supernovae. , 7516:1, November 2000.

S. C. Schuler, J. R. King, and L.-S. The. Stellar Nucleosynthesis in the Hyades Open Cluster. , 701:837–849, August 2009. doi: 10.1088/0004-637X/701/1/837.

S. Schulze, R. Chapman, J. Hjorth, A. J. Levan, P. Jakobsson, G. Björnsson, D. A. Perley, T. Krühler, J. Gorosabel, N. R. Tanvir, A. de Ugarte Postigo, J. P. U. Fynbo, B. Milvang-Jensen, P. Møller, and D. J. Watson. The Optically Unbiased GRB Host (TOUGH) Survey. VII. The Host Galaxy Luminosity Function: Probing the Relationship between GRBs and Star Formation to Redshift $\sim 6.$, $808: 73, July 2015. doi: 10.1088/0004 - 637X/808/1/73$.

S. Schulze, T. Krühler, G. Leloudas, J. Gorosabel, A. Mehner, J. Buchner, S. Kim, E. Ibar, R. Amorín, R. Herrero-Illana, J. P. Anderson, F. E. Bauer, L. Christensen, M. de Pasquale, A. de Ugarte Postigo, A. Gallazzi, J. Hjorth, N. Morrell, D. Malesani, M. Sparre, B. Stalder, A. A. Stark, C. C. Thöne, and J. C. Wheeler. Cosmic evolution and metal aversion in super-luminous supernova host galaxies. *ArXiv e-prints*, December 2016.

D. Scovacricchi, R. C. Nichol, D. Bacon, M. Sullivan, and S. Prajs. Cosmology with superluminous supernovae. , 456:1700–1707, February 2016. doi: 10.1093/mnras/stv2752.

L. Searle. Evidence for Composition Gradients across the Disks of Spiral Galaxies. , 168:327, September 1971. doi: 10.1086/151090.

F. H. Shu, F. C. Adams, and S. Lizano. Star formation in molecular clouds - Observation and theory. , 25:23–81, 1987. doi: 10.1146/annurev.aa.25.090187.000323.

S. J. Smartt. Progenitors of Core-Collapse Supernovae. , 47:63–106, September 2009. doi: 10.1146/annurev-astro-082708-101737.

M. Smith, M. Sullivan, C. B. D'Andrea, F. J. Castander, R. Casas, S. Prajs, A. Papadopoulos, R. C. Nichol, N. V. Karpenka, S. R. Bernard, P. Brown, R. Cartier, J. Cooke, C. Curtin, T. M. Davis, D. A. Finley, R. J. Foley, A. Gal-Yam, D. A. Goldstein, S. González-Gaitán, R. R. Gupta, D. A. Howell, C. Inserra, R. Kessler, C. Lidman, J. Marriner, P. Nugent, T. A. Pritchard, M. Sako, S. Smartt, R. C. Smith, H. Spinka, R. C. Thomas, R. C. Wolf, A. Zenteno, T. M. C. Abbott, A. Benoit-Lévy, E. Bertin, D. Brooks, E. Buckley-Geer, A. Carnero Rosell, M. Carrasco Kind, J. Carretero, M. Crocce, C. E. Cunha, L. N. da Costa, S. Desai, H. T. Diehl, P. Doel, J. Estrada, A. E. Evrard, B. Flaugher, P. Fosalba, J. Frieman, D. W. Gerdes, D. Gruen, R. A. Gruendl, D. J. James, K. Kuehn, N. Kuropatkin, O. Lahav, T. S. Li, J. L. Marshall, P. Martini, C. J. Miller, R. Miquel, B. Nord, R. Ogando, A. A. Plazas, K. Reil, A. K. Romer, A. Roodman, E. S. Rykoff, E. Sanchez, V. Scarpine, M. Schubnell, I. Sevilla-Noarbe, M. Soares-Santos, F. Sobreira, E. Suchyta, M. E. C. Swanson, G. Tarle, A. R. Walker, W. Wester, and DES Collaboration. DES14X3taz: A Type I Superluminous Supernova Showing a Luminous, Rapidly Cooling Initial Pre-peak Bump. , 818:L8, February 2016. doi: 10.3847/2041-8205/818/1/L8.

N. Smith and R. McCray. Shell-shocked Diffusion Model for the Light Curve of SN 2006gy. , 671:L17–L20, December 2007. doi: 10.1086/524681.

N. Smith, R. D. Gehrz, P. M. Hinz, W. F. Hoffmann, J. L. Hora, E. E. Mamajek, and M. R. Meyer. Mass and Kinetic Energy of the Homunculus Nebula around η Carinae. , 125:1458–1466, March 2003. doi: 10.1086/346278.

N. Smith, W. Li, R. J. Foley, J. C. Wheeler, D. Pooley, R. Chornock, A. V. Filippenko, J. M. Silverman, R. Quimby, J. S. Bloom, and C. Hansen. SN 2006gy: Discovery of the Most Luminous Supernova Ever Recorded, Powered by the Death

of an Extremely Massive Star like η Carinae. , 666:1116–1128, September 2007. doi: 10.1086/519949.

J. Sollerman, J. P. U. Fynbo, J. Gorosabel, J. P. Halpern, J. Hjorth, P. Jakobsson, N. Mirabal, D. Watson, D. Xu, A. J. Castro-Tirado, C. Féron, A. O. Jaunsen, M. Jelínek, B. L. Jensen, D. A. Kann, J. E. Ovaldsen, A. Pozanenko, M. Stritzinger, C. C. Thöne, A. de Ugarte Postigo, S. Guziy, M. Ibrahimov, S. P. Järvinen, A. Levan, V. Rumyantsev, and N. Tanvir. The nature of the X-ray flash of August 24 2005. Photometric evidence for an on-axis z = 0.83 burst with continuous energy injection and an associated supernova? , 466:839–846, May 2007. doi: 10.1051/0004-6361:20066683.

K. Z. Stanek, O. Y. Gnedin, J. F. Beacom, A. P. Gould, J. A. Johnson, J. A. Kollmeier, M. Modjaz, M. H. Pinsonneault, R. Pogge, and D. H. Weinberg. Protecting Life in the Milky Way: Metals Keep the GRBs Away. , 56:333–345, December 2006.

E. R. Stanway, A. J. Levan, N. Tanvir, K. Wiersema, A. van der Horst, C. G. Mundell, and C. Guidorzi. GRB 080517: a local, low-luminosity gamma-ray burst in a dusty galaxy at z = 0.09. , 446:3911–3925, February 2015. doi: 10.1093/mnras/stu2286.

E. R. Stanway, J. J. Eldridge, and G. D. Becker. Stellar population effects on the inferred photon density at reionization. , 456:485–499, February 2016. doi: 10.1093/mnras/stv2661.

R. L. C. Starling, K. Wiersema, A. J. Levan, T. Sakamoto, D. Bersier, P. Goldoni, S. R. Oates, A. Rowlinson, S. Campana, J. Sollerman, N. R. Tanvir, D. Malesani, J. P. U. Fynbo, S. Covino, P. D'Avanzo, P. T. O'Brien, K. L. Page, J. P. Osborne, S. D. Vergani, S. Barthelmy, D. N. Burrows, Z. Cano, P. A. Curran, M. de Pasquale, V. D'Elia, P. A. Evans, H. Flores, A. S. Fruchter, P. Garnavich, N. Gehrels, J. Gorosabel, J. Hjorth, S. T. Holland, A. J. van der Horst, C. P. Hurkett, P. Jakobsson, A. P. Kamble, C. Kouveliotou, N. P. M. Kuin, L. Kaper, P. A. Mazzali, P. E. Nugent, E. Pian, M. Stamatikos, C. C. Thöne, and S. E. Woosley. Discovery of the nearby long, soft GRB 100316D with an associated supernova. , 411:2792–2803, March 2011. doi: 10.1111/j.1365-2966.2010.17879.x.

D. S. Stevenson. *Extreme Explosions: Supernovae, Hypernovae, Magnetars and Other Unusual Cosmoc Blasts*. 2014.

R. Stoll, J. L. Prieto, K. Z. Stanek, R. W. Pogge, D. M. Szczygieł, G. Pojmański, J. Antognini, and H. Yan. SN 2010jl in UGC 5189: Yet Another Luminous Type

IIn Supernova in a Metal-poor Galaxy. , 730:34, March 2011. doi: 10.1088/0004-637X/730/1/34.

L.-G. Strolger, R. C. Smith, N. B. Suntzeff, M. M. Phillips, G. Aldering, P. Nugent, R. Knop, S. Perlmutter, R. A. Schommer, L. C. Ho, M. Hamuy, K. Krisciunas, L. M. Germany, R. Covarrubias, P. Candia, A. Athey, G. Blanc, A. Bonacic, T. Bowers, A. Conley, T. Dahlén, W. Freedman, G. Galaz, E. Gates, G. Goldhaber, A. Goobar, D. Groom, I. M. Hook, R. Marzke, M. Mateo, P. McCarthy, J. Méndez, C. Muena, S. E. Persson, R. Quimby, M. Roth, P. Ruiz-Lapuente, J. Seguel, A. Szentgyorgyi, K. von Braun, W. M. Wood-Vasey, and T. York. The Type Ia Supernova 1999aw: A Probable 1999aa-like Event in a Low-Luminosity Host Galaxy. , 124:2905–2919, November 2002. doi: 10.1086/343058.

L.-G. Strolger, T. Dahlen, and A. G. Riess. Empirical Delay-time Distributions of Type Ia Supernovae from the Extended Goods/Hubble Space Telescope Supernova Survey. , 713:32–40, April 2010. doi: 10.1088/0004-637X/713/1/32.

K. M. Svensson, A. J. Levan, N. R. Tanvir, A. S. Fruchter, and L.-G. Strolger. The host galaxies of core-collapse supernovae and gamma-ray bursts. , 405:57–76, June 2010. doi: 10.1111/j.1365-2966.2010.16442.x.

K.-i. Tadaki, T. Kodama, I. Tanaka, M. Hayashi, Y. Koyama, and R. Shimakawa. The Nature of Hα-selected Galaxies at z 2. II. Clumpy Galaxies and Compact Star-forming Galaxies. , 780:77, January 2014. doi: 10.1088/0004-637X/780/1/77.

F. Taddia, J. Sollerman, G. Leloudas, M. D. Stritzinger, S. Valenti, L. Galbany, R. Kessler, D. P. Schneider, and J. C. Wheeler. Early-time light curves of Type Ib/c supernovae from the SDSS-II Supernova Survey. , 574:A60, February 2015. doi: 10.1051/0004-6361/201423915.

M. Tanaka, T. J. Moriya, N. Yoshida, and K. Nomoto. Detectability of high-redshift superluminous supernovae with upcoming optical and near-infrared surveys. , 422: 2675–2684, May 2012. doi: 10.1111/j.1365-2966.2012.20833.x.

M. Tanaka, T. J. Moriya, and N. Yoshida. Detectability of high-redshift superluminous supernovae with upcoming optical and near-infrared surveys - II. Beyond z = 6. , 435:2483–2493, November 2013. doi: 10.1093/mnras/stt1469.

N. R. Tanvir and P. Jakobsson. Observations of GRBs at high redshift. *Philosophical Transactions of the Royal Society of London Series A*, 365:1377–1384, May 2007. doi: 10.1098/rsta.2006.1992.

N. R. Tanvir, E. Rol, A. J. Levan, K. Svensson, A. S. Fruchter, J. Granot, P. T. O'Brien, K. Wiersema, R. L. C. Starling, P. Jakobsson, J. Fynbo, J. Hjorth, P. A. Curran, A. J. van der Horst, C. Kouveliotou, J. L. Racusin, D. N. Burrows, and F. Genet. Late-time Observations of GRB 080319B: Jet Break, Host Galaxy, and Accompanying Supernova. , 725:625–632, December 2010. doi: 10.1088/0004-637X/725/1/625.

The Dark Energy Survey Collaboration. The Dark Energy Survey. *ArXiv Astrophysics e-prints*, October 2005.

C. C. Thöne, A. de Ugarte Postigo, R. García-Benito, G. Leloudas, S. Schulze, and R. Amorín. A young stellar environment for the superluminous supernova PTF12dam. , 451:L65–L69, July 2015. doi: 10.1093/mnrasl/slv051.

P. B. Tissera, S. E. Pedrosa, E. Sillero, and J. M. Vilchez. The gas metallicity gradient and the star formation activity of disc galaxies. , 456:2982–2992, March 2016. doi: 10.1093/mnras/stv2736.

A. R. Tomczak, R. F. Quadri, K.-V. H. Tran, I. Labbé, C. M. S. Straatman, C. Papovich, K. Glazebrook, R. Allen, G. B. Brammer, G. G. Kacprzak, L. Kawinwanichakij, D. D. Kelson, P. J. McCarthy, N. Mehrtens, A. J. Monson, S. E. Persson, L. R. Spitler, V. Tilvi, and P. van Dokkum. Galaxy Stellar Mass Functions from ZFOURGE/CANDELS: An Excess of Low-mass Galaxies since z = 2 and the Rapid Buildup of Quiescent Galaxies. , 783:85, March 2014. doi: 10.1088/0004-637X/783/2/85.

C. A. Tremonti, T. M. Heckman, G. Kauffmann, J. Brinchmann, S. Charlot, S. D. M. White, M. Seibert, E. W. Peng, D. J. Schlegel, A. Uomoto, M. Fukugita, and J. Brinkmann. The Origin of the Mass-Metallicity Relation: Insights from 53,000 Star-forming Galaxies in the Sloan Digital Sky Survey. , 613:898–913, October 2004. doi: 10.1086/423264.

M. Trenti, R. Perna, and R. Jimenez. The Luminosity and Stellar Mass Functions of GRB Host Galaxies: Insight Into the Metallicity Bias. , 802:103, April 2015. doi: 10.1088/0004-637X/802/2/103.

M. Ugliano, H.-T. Janka, A. Marek, and A. Arcones. Progenitor-explosion Connection and Remnant Birth Masses for Neutrino-driven Supernovae of Iron-core Progenitors. , 757:69, September 2012. doi: 10.1088/0004-637X/757/1/69.

S. van den Bergh and G. A. Tammann. Galactic and extragalactic supernova rates. , 29:363–407, 1991. doi: 10.1146/annurev.aa.29.090191.002051.

S. van den Bergh, W. Li, and A. V. Filippenko. Classifications of the Host Galaxies of Supernovae, Set III. , 117:773–782, August 2005. doi: 10.1086/431435.

S. D. Vergani, H. Flores, S. Covino, D. Fugazza, J. Gorosabel, A. J. Levan, M. Puech, R. Salvaterra, J. C. Tello, A. de Ugarte Postigo, P. D'Avanzo, V. D'Elia, M. Fernández, J. P. U. Fynbo, G. Ghirlanda, M. Jelínek, A. Lundgren, D. Malesani, E. Palazzi, S. Piranomonte, M. Rodrigues, R. Sánchez-Ramírez, V. Terrón, C. C. Thöne, L. A. Antonelli, S. Campana, A. J. Castro-Tirado, P. Goldoni, F. Hammer, J. Hjorth, P. Jakobsson, L. Kaper, A. Melandri, B. Milvang-Jensen, J. Sollerman, G. Tagliaferri, N. R. Tanvir, K. Wiersema, and R. A. M. J. Wijers. GRB 091127/SN 2009nz and the VLT/X-shooter spectroscopy of its host galaxy: probing the faint end of the mass-metallicity relation. , 535:A127, November 2011. doi: 10.1051/0004-6361/201117726.

J. S. Vink and A. de Koter. On the metallicity dependence of Wolf-Rayet winds. , 442:587–596, November 2005. doi: 10.1051/0004-6361:20052862.

J. S. Vink, A. de Koter, and H. J. G. L. M. Lamers. Mass-loss predictions for O and B stars as a function of metallicity. , 369:574–588, April 2001. doi: 10.1051/0004-6361:20010127.

P. M. Vreeswijk, S. Savaglio, A. Gal-Yam, A. De Cia, R. M. Quimby, M. Sullivan, S. B. Cenko, D. A. Perley, A. V. Filippenko, K. I. Clubb, F. Taddia, J. Sollerman, G. Leloudas, I. Arcavi, A. Rubin, M. M. Kasliwal, Y. Cao, O. Yaron, D. Tal, E. O. Ofek, J. Capone, A. S. Kutyrev, V. Toy, P. E. Nugent, R. Laher, J. Surace, and S. R. Kulkarni. The Hydrogen-poor Superluminous Supernova iPTF 13ajg and its Host Galaxy in Absorption and Emission. , 797:24, December 2014. doi: 10.1088/0004-637X/797/1/24.

E. Waxman and B. Katz. Shock breakout theory. *ArXiv e-prints*, July 2016.

J.-J. Wei, X.-F. Wu, and F. Melia. Testing Cosmological Models with Type Ic Super Luminous Supernovae. , 149:165, May 2015. doi: 10.1088/0004-6256/149/5/165.

C. Weidner and P. Kroupa. The maximum stellar mass, star-cluster formation and composite stellar populations. , 365:1333–1347, February 2006. doi: 10.1111/j.1365-2966.2005.09824.x.

C. Weidner, P. Kroupa, and I. A. D. Bonnell. The relation between the most-massive star and its parental star cluster mass. , 401:275–293, January 2010. doi: 10.1111/j.1365-2966.2009.15633.x.

S. Wellstein and N. Langer. Implications of massive close binaries for black hole formation and supernovae. , 350:148–162, October 1999.

M. Wittkowski, P. H. Hauschildt, B. Arroyo-Torres, and J. M. Marcaide. Fundamental properties and atmospheric structure of the red supergiant VY Canis Majoris based on VLTI/AMBER spectro-interferometry. , 540:L12, April 2012. doi: 10.1051/0004-6361/201219126.

C. Wolf and P. Podsiadlowski. The metallicity dependence of the long-duration gamma-ray burst rate from host galaxy luminosities. , 375:1049–1058, March 2007. doi: 10.1111/j.1365-2966.2006.11373.x.

S. E. Woosley. SN 1987A - After the peak. , 330:218–253, July 1988. doi: 10.1086/166468.

S. E. Woosley. Gamma-ray bursts from stellar mass accretion disks around black holes. , 405:273–277, March 1993. doi: 10.1086/172359.

S. E. Woosley. Pulsational-Pair Instability Supernovae. *ArXiv e-prints*, August 2016.

S. E. Woosley and A. Heger. The Progenitor Stars of Gamma-Ray Bursts. , 637: 914–921, February 2006. doi: 10.1086/498500.

S. E. Woosley, S. Blinnikov, and A. Heger. Pulsational pair instability as an explanation for the most luminous supernovae. , 450:390–392, November 2007. doi: 10.1038/nature06333.

L. Yan, R. Quimby, E. Ofek, A. Gal-Yam, P. Mazzali, D. Perley, P. M. Vreeswijk, G. Leloudas, A. De Cia, F. Masci, S. B. Cenko, Y. Cao, S. R. Kulkarni, P. E. Nugent, U. D. Rebbapragada, P. R. Woźniak, and O. Yaron. Detection of Broad Hα Emission Lines in the Late-time Spectra of a Hydrogen-poor Superluminous Supernova. , 814:108, December 2015. doi: 10.1088/0004-637X/814/2/108.

L. Yan, R. Lunnan, D. Perley, A. Gal-Yam, O. Yaron, R. Roy, R. Quimby, J. Sollerman, C. Fremling, G. Leloudas, S. B. Cenko, P. Vreeswijk, A. De Cia, E. O. Ofek, S. R. Kulkarni, F. Masci, U. D. Rebbapragada, and P. Woźniak. Hydrogen-poor Superluminous Supernovae With Late-time H-alpha Emission: Three Events From the Intermediate Palomar Transient Factory. *ArXiv e-prints*, April 2017.

S.-C. Yoon and N. Langer. Evolution of rapidly rotating metal-poor massive stars towards gamma-ray bursts. , 443:643–648, November 2005. doi: 10.1051/0004-6361:20054030.

S.-C. Yoon, S. E. Woosley, and N. Langer. Type Ib/c Supernovae in Binary Systems. I. Evolution and Properties of the Progenitor Stars. , 725:940–954, December 2010. doi: 10.1088/0004-637X/725/1/940.

L. R. Yungelson, E. P. J. van den Heuvel, J. S. Vink, S. F. Portegies Zwart, and A. de Koter. On the evolution and fate of super-massive stars. , 477:223–237, January 2008. doi: 10.1051/0004-6361:20078345.

N. Yusof, R. Hirschi, G. Meynet, P. A. Crowther, S. Ekström, U. Frischknecht, C. Georgy, H. Abu Kassim, and O. Schnurr. Evolution and fate of very massive stars. , 433:1114–1132, August 2013. doi: 10.1093/mnras/stt794.

H. J. Zahid, F. Bresolin, L. J. Kewley, A. L. Coil, and R. Davé. The Metallicities of Low Stellar Mass Galaxies and the Scatter in the Mass-Metallicity Relation. , 750: 120, May 2012. doi: 10.1088/0004-637X/750/2/120.

H. J. Zahid, G. I. Dima, R.-P. Kudritzki, L. J. Kewley, M. J. Geller, H. S. Hwang, J. D. Silverman, and D. Kashino. The Universal Relation of Galactic Chemical Evolution: The Origin of the Mass-Metallicity Relation. , 791:130, August 2014. doi: 10.1088/0004-637X/791/2/130.